Development and Characterization of Advanced FO Membranes using Exfoliated 2D Nanomaterials for Energy Generation and Separation Processes

Thesis submitted in partial fulfilment of

the requirements for the degree

of

DOCTOR OF PHILOSOPHY

Priyamjeet Deka

(Roll No: 186151006)

School of Energy Science and Engineering

Indian Institute of Technology, Guwahati

Guwahati-781039, Assam, India

July 2023

TH-3195_186151006

Dedicated to family for their unconditional

love, support and encouragement

TH-3195_186151006

Indian Institute of Technology Guwahati, India

Guwahati-781039, Assam, India

School of Energy Science and Engineering

STATEMENT

I hereby declare that the work presented in this thesis entitled **"Development and Characterization of Advanced FO Membranes using Exfoliated 2D Nanomaterials for Energy Generation and Separation Processes"** is the results of the investigations carried out by me at the School of Energy Science and Engineering, Indian Institute of Technology Guwahati, Assam, India under the supervisions of **Prof. Senthilmurugan Subbiah** and **Dr. Kalyan Raidongia**.

In keeping with the general practice of reporting scientific observations, due acknowledgement has been made whenever the work described is based on the findings of other investigators.

Priyamjeet Deka

Roll No: 186151006

School of Energy Science and Engineering

Indian Institute of Technology, Guwahati

Guwahati-781039, Guwahati, Assam, India

July 2023

TH-3195_186151006

Indian Institute of Technology Guwahati, India

Guwahati-781039, Assam, India

School of Energy Science and Engineering

CERTIFICATE

This is to certify that the work embodied in this thesis **"Development and Characterization of Advanced FO Membranes using Exfoliated 2D Nanomaterials for Energy Generation and Separation Processes"** has been carried out by Mr. Priyamjeet Deka for the award of Ph.D. degree at the School of Energy Science and Engineering, Indian Institute of Technology Guwahati, Assam, India, under the guidance and supervision of mine and Dr. Kalyan Raidongia. The work embodied in this thesis has not been submitted to any other university or institute for the award of any degree or diploma.

(Prof. Senthilmurugan Subbiah and Dr. Kalyan Raidongia)

Thesis Supervisors

Department of Chemical Engineering and Department of Chemistry

Indian Institute of Technology Guwahati

Guwahati-781039, Guwahati, Assam, India

July 2023

TH-3195_186151006

ACKNOWLEDGEMENTS

It is a pleasant duty to convey my special thanks to many people who have supported and accompanied me during my Ph.D. tenure.

First and foremost, I would like to express my sincere gratitude to my supervisors, **Prof. Senthilmurugan Subbiah** and **Dr. Kalyan Raidongia** for giving me an opportunity to work under their expert supervisions. This thesis would not have been possible without their limitless efforts, expert guidance, valuable suggestions, boundless support and freedom to work. He has been a continuous source of encouragement throughout my Ph.D. life and it is my good fortune to have them as my supervisors.

I convey my special thanks to my doctoral committee members, **Prof. Kaustubha Mohanty** (Chairperson), **Prof. G. Pugazhenthi** and **Dr. Uttam Manna** and former committee member **Dr. Anki Reddy katha** for their valuable advices, suggestions, constant engouragement, and constructive inputs of my work progress, which helped a lot in improving my thesis.

I am grateful to all the faculty members of School of Energy Science and Engineering, IIT Guwahati for their encouragements and also the technical staff of School of Energy Science and Engineering, Department of Chemical Engineering, and Department of Chemistry for their valuable supports. I am thankful to the Central Instrument Facility (CIF) and Department of Chemistry of IIT Guwahati for various instrument facilities and IIT Guwahati for the scholarship.

With two thesis supervisors, I got the opportunity to be part of two research groups. I would like to take these opportunities to thank all my seniors and lab mates from each research group. Firstly, from Prof. Senthilmurugan's research group (Water-and-Energy Nexus Lab), I would

TH-3195_186151006

like to thank Dr. Vishal Kumar Verma, Dr. Vigneshwaran K, Dr. Habtom Teklu Aseffa, Dr. Arunkumar Chandrasekaran, Dr. Senthil Selva, Dr. Aanisha Akhtar, Dr. Nivedhitha S, Dr. Viswanth Ramba, Dr. Muniraja Tippa, Dr. Ananya Bardhan, Ms. Seema Bharati, Ms. Neelam Dutta, Mr. Surendhar G, Mr. Munubarthi Kranthi K, Mr. Dinesh K. Gautam, Mr. Balakumara Vignesh, Mr. Shanmugam, Mr. Bijoyendr, Mr. Venkatesh and Mr. Bedanta Chakraborty for their constant support, laughter and motivations. I would also like to thank Dr. Rajkumar Gogoi, Dr. Kundan Saha, Dr. Jumi Deka, Dr. Tukhar Jyoti Konch, Mr. Arindom Bikash Neog, Ms. Trisha Dutta, Mr. Madhurjya Buragohain, Mr. Raktim Gogoi, Ms. Barsha Rani Bora, Ms. Bipasha Saikia, Ms. Kiran Mayawad, Mr. Deepak Jyoti Deuri, Mr. Bikash K. Das, Ms. Sonali Roy, Ms. Nabamallika Nath, Ms. Parijat Pratim Das, Mr. Mrityunjoy Dey, Mr. Priyanku Garg, Mr. Gouri S. Mandal, Mr. Monotosh Mondol, Mr. Arnab Ghosh, Mr. Krishnaraajan Sundararajan, Mr. Harshan Madeshwaran and Mr. Ahitagni Das from Dr. Kalyan's research group (Nanofluidic Lab). I would like to thank our lab asistants Mr. Banajit Saloi, Mr. Bishnu and Mr. Rupam for their timely assistance.

Finally, I would like to express my sincere gratitude with great honour to my family members for their limitless love, absolute support, sincere encouragement and inspiration for lifting me uphill in this phase of my life. I am fortunate and blessed to have such a caring and supportive family starting from papa (Binanda Deka), maa (Mandira Deka), my elder sister (Priyanka Deka Das) and my brother-in-law (Rahul Das), who sacrificed and struggled to make my life smooth going for this big achievement.

Thank you very much, everyone for your endless supports and encouragements.

(Priyamjeet Deka)

School of Energy Science and Engineering

Indian Institute of Technology Guwahati

TH-3195_186151006

ABSTRACT

Water shortage has become a global problem due to the high human consumption, rapid industrialization and low availability of freshwater resources. Extensive efforts have been put forward by researchers to overcome the freshwater crisis by exploring new desalination techniques, and wastewater reuse without damaging the natural freshwater ecosystems. One such pivotal technology for purifying water was the membrane technology. Membrane technology is an emerging and advanced process that can provide a sustainable solution to desalination and wastewater treatment. Although pressure-driven membrane separation processes were used for producing freshwater, its high energy consumption prevent them from further employment. Hence, modification of existing membrane-based separation technology is required to overcome its demerits.

Forward osmosis (FO) is an emerging membrane-based separation technology that can replace the existing pressure-driven membrane-based separation processes without compromising the energy consumption. Compared to thermal processes and pressure-driven membrane separation processes, the FO allows the concentrating solution with higher concentration while maintaining the product quality. Advantages like low fouling propensity and availability of energy-efficient draw solution regeneration technology may enable FO as one of the energy- efficient technology for desalination and wastewater treatment. However, commercial and polymeric FO membranes still lack in some areas like providing high water flux, low reverse solute flux (RSF) and low anti-fouling properties. Hence, there was an apparent requirement for the commercial FO membranes to be modified with nanomaterials that can render anti-fouling properties together with attaining high water and low RSF. Therefore, the practical utility of the FO process in critical applications like desalination, energy harvesting, wastewater

TH-3195_186151006

treatment and resource recovery relies on the availability of robust and effective fouling-resistant FO membranes. Therefore, the thesis has addressed certain identified research gaps in the fundamental aspects of the existing membrane.

Based on the prior knowledge of the FO membranes and its working principle, this thesis focuses on the development of existing membranes with the incorporation of different compositions of two-dimensional (2D) nanomaterials as active layer for enhancing the performance in various applications in the FO process. The long-term stability of the fabricated membranes in ideal as well as real conditions was investigated in this thesis.

To enhance the membrane quality and performance in FO process, fabrication of FO membrane with reduced graphene oxide (rGO) nanosheets doped with polystyrene sulfonic acid (PSS) was done. The practical application of the FO process depends on high water permeability and low RSF. Therefore, we have reported the use of rGO and PSS to enhance the water permeation properties and selectivity of the as-prepared FO membranes. After the fabrication process, the membrane was tested in ideal conditions with 1M NaCl and DI water as draw and feed solutions, respectively. Subsequent addition of PSS layer onto rGO laminates improved the hydrophilicity and surface charge of the membrane rendering excellent water flux (34 L m^{-2} h^{-1}) and lower specific reverse solute flux (SRSF) (0.18 g/L), thus enhancing the FO performance for longer duration also.

Once the fabricated membrane showed promising result in ideal conditions, other fabricated membranes were tested in real conditions to validate the feasibility of the membranes to sustain in harsh conditions. Therefore, a novel FO membrane consisting of sericin and reduced graphene oxide nanosheets was fabricated for antibiotic recovery application using membrane crystallization forward osmosis process. The use of

TH-3195_186151006

hydrophilic natural protein named sericin was used to enhance the FO performance and resolve the trade-off between permeability and selectivity of FO membrane also improving the membrane stability during the antibiotic's recovery process. The sericin doped rGO membrane achieved an outstanding water flux of 54 L m^{-2} h^{-1} while maintaining the SRSF of 0.12 g/L as compared to commercial FO membranes (0.5-6 g/L). The as-prepared membrane also showed higher stability FO performance for 30 hrs of continuous operation without compromising the water flux and RSF, thus confirming the anti- fouling properties of sericin-doped rGO membranes. Moreover, the application with batch FO process yielded continuous crystalline rifaximin antibiotics without consuming higher energy.

After analysing the performance of fabricated FO membranes in real conditions, the balance between the FO process and simultaneous energy harvesting using lamellar bilayer FO membrane was investigated to resolve water-energy nexus issues. Here, we have fabricated a novel amorphous silicon oxide crosslinked vanadium pentoxide (VO) and rGO membrane using a vacuum assisted filtration process. The ion-selective membrane showed superior nanofluidic properties in salinity gradient energy conversion technology with high powder output of 4.72 W.m^{-2}. Finally, the fabricated membrane was used for simultaneous energy harvesting and FO process and it was observed that with 1M KCl as draw solution and DI water as feed solution, the membrane achieved output voltage and current of 300 mV and 35 µA, respectively, at lowest flow rate of 0.5 L/h. With the pumping power output of 0.1 W.m^{-2} at lowest flow rate, the extracted energy from FO process was able to save an overall 26% of energy. Hence, the ease of coupling FO and concentration gradient-driven energy harvesting processes in novel platform can resolve highly entangled issues in water-energy nexus.

TH-3195_186151006

Overall, the results discussed in the given thesis provides a better insight into the development of forward osmosis membrane and its various applications.

Keywords: 2D nanomaterials, Forward osmosis, Membranes, Crystallization, Nanofluidic

भारतीय प्रौद्योगिकी संस्थान गुवाहाटी • Indian Institute of Technology Guwahati •

TH-3195_186151006

Table of Contents

TH-3195_186151006

TH-3195_186151006

TH-3195_186151006

TH-3195_186151006

TH-3195_186151006

TH-3195_186151006

LIST OF FIGURE

TH-3195_186151006

TH-3195_186151006

TH-3195_186151006

TH-3195_186151006

TH-3195_186151006

TH-3195_186151006

TH-3195_186151006

NOMENCLATURE

L_p	Pure water permeability (L m^{-2} h^{-1} bar^{-1})
B	Solute permeability coefficient (L m^{-2} h^{-1})
S	Structural parameter (nm)
D	Diffusion Coefficient (m h^{-1})
J_w	Water flux (L m^{-2} h^{-1})
J_s	Reverse solute flux (g m^{-2} h^{-1})
Q	Flow rate (L h^{-1})
k	Mass transfer coefficient (m s^{-1})
K	Solute resistivity (m^{-1})
A_m	Membrane area (m^2)
M	Mass (kg)
M_w	Molecular weight
R	Gas constant (J K^{-1} mol^{-1})
C_{db}	Draw solution concentration on bulk phase (g L^{-1})
C_{dm}	Draw solution concentration on membrane surface (g L^{-1})
C_{fb}	Feed solution concentration on bulk phase (g L^{-1})
C_{fm}	Feed solution concentration on membrane surface (g L^{-1})
π	Osmotic Pressure (bar)
P	Power density (W m^{-2})
t	Time
T	Temperature

TH-3195_186151006

Abbreviations

AEM: Anion Exchange Membrane

AFM: Atomic Force Microscopy

ALDS: Active Layer Facing Draw Solution

ALFS: Active Layer Facing Feed Solution

AQP: Aquaporin

ASiO: Amorphous Silicon Oxide

CA: Cellulose Acetate

CECP: Concentrative External Concentration Polarization

CICP: Concentrative Internal Concentration Polarization

CNT: Carbon Nanotube

COD: Chemical Oxygen Demand

COF: Covalent Organic Framework

CP: Concentration Polarization

CTA: Cellulose Triacetate

DECP: Dilutive External Concentration Polarization

DICP: Dilutive Internal Concentration Polarization

DI: De-ionized water

DS: Draw Solution

ECP: External Concentration Polarization

EDX: Energy-dispersive X-ray

FESEM: Field Emission Scanning Electron Microscopy

FETEM: Field Emission Transmission Electron Microscopy

TH-3195_186151006

FO: Forward Osmosis

FRR: Flux Recovery Ratio

FS: Feed Solution

FTIR: Fourier-transform infrared spectroscopy

GO: Graphene Oxide

HF: Hollow Fibre

HPLC: High-performance Liquid Chromatography

ICP: Internal Concentration Polarization

IEM: Ion Exchanged Membrane

KCl: Potassium Chloride

KH_2PO_4: Potassium Dihydrogen Phosphate

MBR: Membrane Bioreactor

MD: Membrane Distillation

MF: Microfiltration

$MgCl_2$: Magnesium Chloride

NaCl: Sodium Chloride

NF: Nanofiltration

NTU: Nephelometric Turbidity Unit

PAA: Polyacrylic Acid

PAN: Polyacrylonitrile

PEI: Polyetherimide

PEG: Polyethylene Glycol

PES: Polyethersulfone

TH-3195_186151006

PSS: Polystyrene Sulfonic Acid

PTFE: Polytetrafluoroethylene

PVDF: Polyvinylidene fluoride

PRO: Pressure Retarded Osmosis

RED: Reverse Electrodialysis

RGO: Reduced Graphene Oxide

RO: Reverse Osmosis

RSF: Reverse Solute Flux

SD: Solution Diffusion

SRSF: Specific Reverse Solute Flux

TDS: Total Dissolved Solids

TFC: Thin-film Composite

TFN: Thin-film Nanocomposite

TOC: Total Organic Carbon

TSS: Total Soluble Solids

UF: Ultrafiltration

UV: Ultraviolet

VO: Vanadium Pentoxide

TH-3195_186151006

CHAPTER 1

1 Introduction

Abstract: This chapter provides a general overview of membrane processes and discusses the fundamentals of the forward osmosis process in aqueous concentration and energy generation applications, followed by the importance of 2D nanomaterials in membrane technology, followed by motivation associated with studies conducted in this thesis.

TH-3195_186151006

1.1 Introduction to membrane process

Membrane technology has been extensively employed for a wide range of separation applications, including water purification, wastewater treatment, desalination, and industrial separation processes. Since the 1980s, membrane processes such as microfiltration (MF), ultrafiltration (UF), nanofiltration (NF), and reverse osmosis (RO) have been studied and implemented in commercial-scale applications.

Meanwhile, osmotic membrane separation processes such as forward osmosis (FO), pervaporation, and membrane distillation have gained attraction since the 2000s, and their potential for various applications, including desalination[1], aqueous solution concentration[2], and crystallization[3], was explored by industries and academic researchers. Although Aquaporin Ltd.'s biomimetic membrane technology demonstrates the promising potential for FO/RO-based desalination, it's widespread adoption and commercial success in this field have yet to be fully achieved. Factors contributing to this situation include the conservative nature of the water treatment industry, the challenges associated with large-scale, low-cost production of biomimetic membranes, and regulatory barriers.

In addition, the FO process has historically been limited in desalination applications due to the lack of energy-efficient draw solute regeneration processes. However, FO membranes have subsequently been adapted for smaller-capacity NF and RO systems in Point-of-Use (POU) water treatment systems. These systems typically have less stringent requirements than large-scale desalination plants, making it easier for companies to meet production demands and find immediate commercial applications.

Furthermore, FO applications have proven to be more attractive in high-value resource recovery, food and beverage industry, and pharmaceutical applications. These industries benefit from the FO process because it operates at lower temperatures and enables nucleation

TH-3195_186151006

at the concentration polarization layer. As a result, FO has emerged as a potentially viable and economically competitive technology for resource recovery and concentration applications.

1.2 Aqueous solution concentration applications

The development of robust, effective, and safe concentration methods that can be operated at low temperatures was indeed crucial across many fields. Below were some examples of processes that necessitate such techniques and why these are needed:

Fruit Juice Concentration: Fruit juices were typically concentrated to reduce transport costs and increase shelf life. However, traditional heat-based concentration methods like evaporation can lead to loss of volatile flavours and nutrients, degradation of colour, and possible formation of off-flavours due to Maillard reactions or caramelization. A low-temperature process would help to retain these vital qualities of the juice. Membrane processes like Reverse Osmosis (RO) and Forward Osmosis (FO) are explored for this purpose.

Extraction and Concentration of Pharmaceuticals and Nutraceuticals: Many bioactive compounds were heat sensitive and can degrade or denature when exposed to high temperatures, reducing their effectiveness. For example, antibiotics, vitamins, and omega-3 fatty acids were often damaged by heat. Using low-temperature concentration methods can help preserve these molecules' integrity and functionality. Techniques such as Supercritical Fluid Extraction (SFE), Freeze Concentration, FO and Pervaporation are currently being researched for these applications.

Concentration of Dairy Products: High-temperature methods can affect the flavor, texture, and nutritional content of dairy products. Low-temperature evaporators, membrane filtration (like RO, FO, and Ultrafiltration), and freeze concentration are employed to concentrate milk or whey while preserving quality.

TH-3195_186151006

Biological and Biomedical Applications: For concentration of biological samples, such as blood plasma, cell cultures, or protein solutions, heat can cause severe damage, leading to coagulation, denaturation, or cell death. Low-temperature methods are thus crucial. Ultrafiltration, Tangential Flow Filtration (TFF), and FO are techniques often utilized in these cases.

Wastewater Treatment: Many industrial effluents contain heat-sensitive compounds that can be valuable if recovered or hazardous if not properly treated. Also, high-temperature treatments can be energy-intensive and expensive. Low-temperature concentration and separation techniques can enable the recovery of valuable materials and reduce the energy cost of treatment. Membrane processes like RO, FO, and Membrane Distillation (MD) are often employed.

In summary, low-temperature concentration processes are essential for preserving heat-sensitive compounds, enhancing product quality, and reducing energy costs and environmental impacts. However, energy efficiency and easy operation are key factors enabling these technologies to commercialization.

1.3 Forward Osmosis

In the membrane-based concentration process, the choice of membrane technology depends on the application's specific requirements. Process engineers must consider factors such as the nature of solutes, desired concentration levels, membrane material compatibility, operating conditions and fouling propensity during process selection and design for concentration applications. Different types of membrane technologies are adopted for concentration processes, including forward osmosis (FO), reverse osmosis (RO), nanofiltration (NF) and membrane distillation (MD). However, apart from the FO process, the other processes possess

TH-3195_186151006

several technical and economic limitations, such as severe fouling, high energy requirement, high-temperature operation and low selectivity[4,5]. In the traditional FO process, a draw solution with high osmotic pressure is used to create the driving force for water transport through the membrane. This process can be energy-efficient or energy-intensive depending upon the operating parameters for the concentration process. For example, the FO can be termed an energy-efficient process for low-temperature concentration applications of heat-sensitive products. However, the regeneration of conventional draw solutions is energy intensive and typically requires high pressure or thermal energy to separate water from the draw solute. To achieve energy-efficient draw solute recovery, following two approaches are explored by the researchers (i) the use of heat/electrical sensitive hydrogels as draw solutes[6] and (ii) the use of high molecular weight polymer solution as draw solute[7]. In the first approach, the draw solute is concentrated by applying a high temperature or electric field. In the second approach, diluted DS is concentrated by using UF and NF processes.

The FO process is suitable for low-temperature concentration applications because the feed and draw solution is not heated during the FO process. Unlike membrane distillation or evaporation processes where high-temperature difference is required for higher water flux, the FO process requires a higher salinity gradient to achieve high water flux while maintaining low temperature profile and simultaneously concentrating heat-sensitive products such as fruit juices and pharmaceutical resources by preserving the final product quality. Therefore, the concentration of various products using the FO process offers several advantages, including energy efficiency, reduced fouling, scalability and the ability to operate at lower temperatures compared to conventional concentration methods

FO is a concentration gradient process where a higher concentration draw solution was separated by a lower concentration feed solution using a semi-permeable membrane. As a

TH-3195_186151006

result, the water is drawn from the feed solution (FS) to the draw solution (DS), while most of the dissolved solutes or ions are rejected by the membrane and are concentrated in the feed. The process flow diagram of the FO process for concentration application is illustrated in Fig. 1.

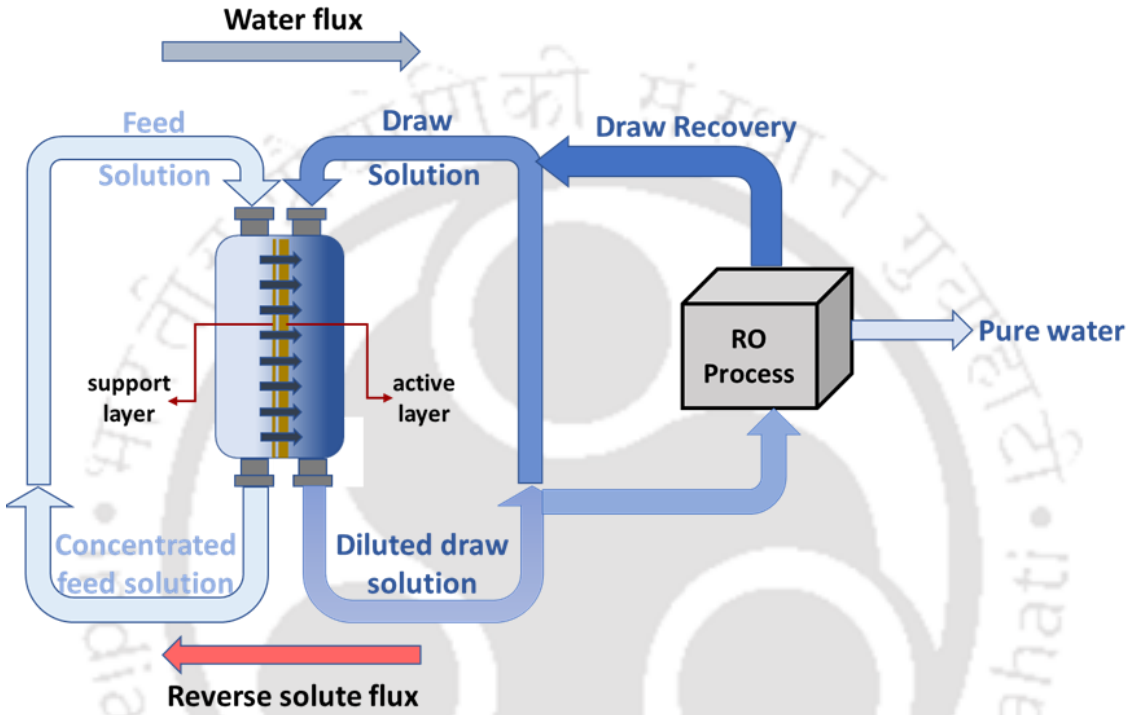

Fig. 1: Process flow diagram of FO process for concentration application

The driving force was the osmotic pressure difference across the membrane, which tends to extract water from lower concentration to higher-concentration regions [8]. Some of the unique properties of the FO process like (a) dense membrane with high selectivity and rejection that can enable to extract of only water from the feed leading to high concentration, (b) low pressure operation and does not require expensive high pressure pump and stainless steel pipe, (c) low fouling rate which increases the life span of FO membrane [9–11]. Therefore, the FO process can emerge as an innovative technology that can concentrate the streams like liquid food, dairy products, and pharmaceutical resources and address global challenges like desalination, power

TH-3195_186151006

generation and wastewater treatment [12–14]. However, the FO faced some limitations, like the low water flux, membrane fouling, draw solution recovery, high concentration polarization and low stability in harsh conditions [15–17]. Some of these limitations can be alleviated by developing novel FO membranes for given applications.

Conventional FO membranes are semi-permeable membranes that allow water to pass through them while rejecting dissolved solutes. The membrane structure comprises a porous support layer that provides mechanical support and a thin active layer for water permeability and selectivity purposes. The active layer was generally made of polymers such as cellulose acetate (CA), cellulose triacetate (CTA), Polyethersulfone (PES), polyvinylidene fluoride (PVDF) and many more [18]. However, conventional FO membranes face several challenges that limit their performance in practical applications. Some of these challenges include[19]:

a. Membrane fouling: Conventional FO membranes are susceptible to fouling due to their loose structure and large pore size, which allows foulants to deposit quickly on the membrane surface.

b. Reverse solute flux: Conventional FO membranes often suffer from high reverse solute flux (RSF) that limits the applicability of the FO process for concentration applications due to cross-contamination of feed by draw solution.

c. Low flux: Conventional FO membranes possess low water flux while using conventional support and separation layers, which increases operational time and energy consumption.

d. Concentration polarization: Due to higher RSF across the conventional FO membrane, the concentration of solutes at the membrane surface becomes significantly high, drastically decreasing the water flux.

TH-3195_186151006

e. Stability: Conventional FO membranes are unstable at higher pressure or temperature conditions and often prone to physical damage, limiting their performance.

1.3.1 Importance of novel FO membrane

Since conventional FO membranes have several limitations that restrict their applications, using novel membranes with properties that can address these limitations will revolutionize the FO process by increasing its efficiency, reducing its environmental impact and improving its overall sustainability. One of the primary advantages of using novel FO membranes is that they can attain a higher water flux rate than conventional membranes. Such a high flux membrane may enable reduced membrane cost and footprint of the FO plant. Moreover, these novel membranes can be engineered to be highly selective that can reject unwanted solutes from the feed stream. Another important advantage of novel FO membrane is their increased durability, high solute rejection, high water flux and fouling resistance characteristics. These membranes were often designed to withstand harsh conditions such as high temperatures, extreme pH and exposure to harsh chemicals, which can increase the lifespan of the membrane. The novel membranes also possess lower fouling properties that can increase the overall efficiency of the FO process. With the advantage of tuning and tailoring the physical and chemical properties, the novel FO membrane can allow greater flexibility in specific applications. Some of the novel membranes that are currently used are aquaporin (AQP) proteins [20], carbon-based materials such as carbon nanotubes (CNT)[21] and graphene-based materials like graphene oxide (GO)[22]. One key requirement in concentration application is that cross-contamination is not allowed. Due to the reverse solute flux, draw solute may contaminate with feed while concentrating by the FO process. Therefore, these novel membranes have the potential to significantly reduce reverse solute flux to an acceptable limit and make it a viable option for aqueous solution concentration applications.

TH-3195_186151006

1.3.2 Role of 2D nanomaterials in membrane technology

The 2D nanomaterials serve as key components for membrane separation layers, finding diverse applications like desalination, wastewater treatment, and energy generation These ultrathin membranes effectively eliminate contaminants due to their substantial surface area, mechanical strength, and stability. Their adjustable pore size and surface chemistry enable precise separation control, ensuring desired efficiency. Moreover, their high electrical conductivity lets 2D nanomaterial-based membranes convert chemical energy to electricity, bolstering system sustainability. Recent research focuses on enhancing commercial membranes with various 2D nanoporous materials like graphene, graphene oxide (GO) [26], molybdenum disulfide (MoS_2)[27], Mxene[28], and carbon nanotube (CNT)[29] and vanadium pentoxide (V_2O_5)[30]. These 2D nanocomposite materials have tremendous potential for various applications like wastewater treatment, desalination, the concentration of valuable resources and energy harvesting due to their unique properties like high hydrophilic nature, high anti-fouling, high rejection rate, longer stability, high electrical conductivity and high mechanical strength compared to conventional polymer membranes[31]. Therefore, this thesis explores innovative engineered nanomaterials integrated into energy-efficient forward osmosis to enhance permeability, selectivity, and energy generation mechanisms.

1.4 Simultaneous FO and energy generation

The standalone FO process was operated at low pressure and was less energy intensive, but when DS regeneration comes into scope, the integrated FO process was expected to consume equal or higher energy than other equivalent technologies like RO, MD. Under this circumstance, any additional energy generated by the FO process may help to reduce the net energy supply to the FO process. Therefore, electricity generation from the concentration gradient of FO process could reduce the operational cost and expand its application possibilities

TH-3195_186151006

into diverse areas. The viability of simultaneous electricity generation in the RO process was reported to be viable from laboratory studies[32].

The salinity gradient is projected to fulfil more than 15% of global energy needs. However, the unavailability of suitable membranes hinders progress in areas like pressure retarded osmosis (PRO)[33], and reverse electrodialysis (RED)[34]. Fabrication of ideal membranes for these processes requires exotic techniques/instrumentations, which were not widely available until recently. However, the recent escalation in the research related to the fabrication of novel membranes/materials uncovered several new ways of preparing well-packed perm-selective nanofluidic channels in high density. These new developments in membrane technology are leading to a resurgence in the concentration gradient-driven energy harvesting processes.

The concentration gradient-driven energy harvesting process involves the transport of ions across a selective membrane from a higher concentration to a lower concentration chamber, while the FO process involves the transport of water molecules across a semi-permeable membrane from a lower concentration to a higher concentration chamber[35]. The basic requirements of the membrane for both these processes are different; for example, a FO membrane needs to have high water flux and low salt permeability, while a RED membrane requires to have high ion selectivity and low resistance to ionic transport for the concentration gradient energy generation process. However, features like permselectivity, high porosity, high charge density, and higher stability are desired in both kinds of membranes. Due to their non-ion-specific transport properties, commercial FO membranes were not suitable for electrochemical-based energy harvesting processes. Coating of nanomaterials on conventional FO membranes was found to enhance the water flux and ion selectivity by increasing the charge density.

TH-3195_186151006

1.5 Research Motivation

1.5.1 Need for novel 2D nanomaterial-based FO membrane

High water flux and stable membrane with reduced RSF are critical aspects of achieving an energy-efficient FO process for concentration application. FO membranes made of conventional polymeric membranes have limitations on further increasing water flux without affecting reverse solute flux. Further, the FO membrane separation layer made of novel 2D nanomaterial were reported to enable high water flux, reduced RSF and fouling rate. Therefore, the development of a 2D nanomaterial-based FO membrane is essential to tackle the issues of conventional membranes. Some of the key benefits of using 2D nanomaterials in FO membranes are[36–38] namely: (i) enhanced permeability (ii) improved selectivity (iii) chemical and thermal stability (iv) potential for functionalization and (v) environmental sustainability

One of the most salient features of using these 2D nanomaterials in membrane is their enhanced permeability. This benefit is largely attributed to their atomic thickness and large surface areas. With uniform nanopores, whose sizes can be meticulously controlled, the resistance to fluid flow within these membranes is dramatically reduced, thereby improving the water flux. Together with the heightened porosity facilitated by their expansive surface area, the overall permeability of these membranes is significantly enhanced, boosting their efficiency in filtration processes.

Furthermore, the atomic-scale thickness of these materials, along with their uniformly distributed nanopores, results in improved selectivity. This precise molecular sieving leads to exceptional selectivity, an attribute that is paramount in improving the overall effectiveness of filtration processes by allowing the passage of desirable molecules while efficiently filtering out unwanted ones.

TH-3195_186151006

Another critical feature of these 2D nanomaterials is their inherent hydrophilic nature. When combined with their smooth surface topology, this property greatly reduces fouling tendencies, enhancing membrane longevity and sustaining their performance over time. The hydrophilicity also improves the wettability of these membranes, leading to a reduction in the contact angle and an increase in the rate of water permeation.

Furthermore, graphene and graphene oxide provide superior chemical and thermal stability. The robust lattice structure and covalent bonds within these materials provide strong resistance to chemical degradation and thermal stress, ensuring the durability and long-term performance of the membrane under a wide range of operational conditions.

These 2D nanomaterials also offer significant potential for functionalization. The presence of chemically active sites on their surface can be exploited to modify or tailor specific properties. This adaptability enhances the compatibility of these materials with a diverse range of applications, thus broadening their utility in various membrane technologies like selective separation and energy generation applications.

Finally, the use of these 2D nanomaterials like GO contributes to environmental sustainability. Their potential for synthesis using less energy-intensive methods, coupled with their durability, reduces waste over time. This not only aids in the preservation of the environment but also aligns with the growing global emphasis on sustainable development.

In summary, the cumulative advantages of 2D nanomaterials, including their hydrophilic nature, the potential for functionalization, exceptional selectivity, enhanced permeability, resistance to fouling, and thermal and chemical stability, collectively make them a promising and highly sought-after material in the advancement of membrane technologies.

1.5.2 Need of energy generation in FO process

TH-3195_186151006

At present, the FO process's adaptability in commercial applications is under progress, and their viability to deploy in high commercial value product applications such as pharma and food applications is under exploration. One hindrance is high energy consumption when DS regeneration comes into scope. Therefore, any reduction in energy consumption by improving water flux and simultaneous energy generation while the FO process can improve the overall economy of the FO process and its adaptability in other low commercial value product applications.

For example, the salinity gradient energy (SGE) has gained a lot of attention as a potential candidate for producing effective energy without compromising its resources[39]. Pressure retarded osmosis (PRO) and RED are two different SGE process explored for energy generation, where a semi-permeable membrane is used to separate the two salinity compartments and the difference in chemical potential between the two compartments lead to the energy conversion from chemical energy to electrical energy.

Similarly, simultaneous energy production during RO was proven on a lab-scale system and proven to reduce overall energy consumption in the RO process. Further, the energy harvesting from the FO process also ensures no emission of greenhouse gases, which positively impacts the environment. Therefore, the primary and most important reason for coupling energy and FO process together was to make the overall system more self-sustainable and economically viable in terms of costs and time.

Simultaneous FO and energy generation require smart membranes that enable high water flux and selective ion transportation. Such membranes can be developed by using innovative 2D nanomaterials like graphene oxide (GO), reduced graphene oxide (rGO). Vanadium pentoxide (VO), carbon nanotube (CNT), etc.

TH-3195_186151006

1.6 Research Objectives

This thesis aims to develop a FO membrane with novel 2D functionalized nanomaterials for forward osmosis and energy generation applications. The detailed objectives are:

1. Development of stable 2D functionalized nanomaterial-based FO membranes to achieve enhanced permeability, separation and anti-fouling performance
2. Performance analysis of developed novel FO membrane for antibiotic recovery from pharma effluent by adopting membrane crystallization concept
3. Studying the performance of novel FO membrane for simultaneous FO and energy generation process for concentration application was lab scale experiments

1.7 Thesis Organization

The thesis has been organized into six chapters. A brief synopsis of the chapters was presented as follows:

1. Chapter 1 starts with the general information about membrane technology and osmotic driven membrane processes and then presents the research motivation for the entire work. The objectives were also listed in this thesis.
2. Chapter 2 reviews the literatures on FO system and FO membranes and current progress on 2D nanomaterials for FO membranes. This chapter also presents the possible research gaps.
3. Chapter 3 demonstrates the development of polystyrene sulfonic acid doped reduced graphene oxide (PSS-rGO) FO membranes at different operating conditions. The fabricated membranes enhanced the FO performance with higher water flux and lower reverse solute flux for longer operation period.

TH-3195_186151006

4. Chapter 4 presents the development of a novel sericin doped reduced graphene oxide (rGO-S) bilayer FO membranes and used it to enhance the FO performance. The as-prepared membranes also showed superior anti-fouling properties and yielded a continuous antibiotic recovery in the membrane crystallization application.
5. Chapter 5 demonstrates the fabrication of novel amorphous silicon oxide crosslinked vanadium pentoxide and reduced graphene oxide (VO-aSiO-rGO) membrane for enhanced FO performance. The fabricated membranes showed outstanding long-term stability in acidic and basic conditions as well as during prolong operational hours of the FO process. Finally, the fabricated membranes were also tested for simultaneous energy generation and FO process in a self-sustain system for longer period and yielded 26% energy saving.
6. Chapter 6 summarizes the outcomes of the thesis work and provides a pathway for future scope.

TH-3195_186151006

भारतीय प्रौद्योगिकी संस्थान गुवाहाटी
Indian Institute of Technology Guwahati

CHAPTER 2

2 Review of Literature

Abstract: This chapter is aimed to provide a detailed literature review on the fundamentals of the FO process along with the current status on the use of FO membrane in aqueous solution concentration and energy generation applications. The challenges and perspectives of the FO process parameters are reported in this chapter. From the outcome of the literature survey, the prominent research gaps were identified to frame the objectives of the present research work at the end of this chapter.

TH-3195_186151006

2.1 FO Applications

2.2 Aqueous solution concentration

Concentration processes play a crucial role in diverse industries such as food, pharmaceuticals, beverages, and chemicals. While widely adopted, traditional concentration methods like evaporation and distillation were energy-intensive and may lead to thermal degradation of the product. More recently, membrane processes like ultrafiltration (UF), nanofiltration (NF), and reverse osmosis (RO) have gained traction in this field. However, these pressure-driven processes were constrained when the aqueous solution's osmotic pressure exceeds the module's design pressure, roughly around 80 bar.

To circumvent this limitation, forward osmosis (FO) is being investigated as a sophisticated membrane separation method for concentration and crystallization applications. The advantages of using FO are manifold: it can function at lower temperatures, it can be potentially integrated with crystallization processes, and it was more energy-efficient when draw solute (DS) energy-efficient regeneration is feasible.

This literature reviews summarize critique relevant research studies on FO processes for various concentration applications, using a highly selective thin-film composite membrane (TFC). The aim is to pinpoint the gaps in current technology and guide the scope of further research.

Wang et al.[40] investigated the preservation of apple juice by employing the FO process using CTA-FO membrane. The total soluble solids (TSS) in the apple juice was increased from 11° Brix to 60° Brix with a concentration fold of 5.45 in a single stage 48hrs batch FO process. The FO process efficiency was also enhanced by optimizing the operational conditions, membrane module and draw solute concentrations. This research indicates that the FO process has great potential for a thermal concentration of fruit juice in the food industry.

TH-3195_186151006

Cui et al.[41] demonstrated and evaluated an organic solvent forward osmosis (OSFO) process for concentration of active pharmaceutical ingredients (API) and recovery of organic solvents. The OSFO shows 98% rejection when recovering organic solvents from different feed solutions. When the feed solution was replaced with ethanol, a positive ethanol flux was observed with higher value in PRO mode as compared to FO mode and simultaneously low reverse solute flux was achieved.

Bardhan et al.[42] investigated the concentration of tea solution using energy-efficient FO process. During the FO experiment, tea components such as epigallocatechin-gallate (EGCg), epigallocatechin (EGC) and caffeine was extracted with increased concentration without compromising and losing the reverse solute flux and aroma, respectively. This process was considered a feasible solution for the treatment of waste effluent generated by tea processing industries.

Wu et al.[43] demonstrated the application of sewage concentration using GO modified TFN membrane in FO process. During the long-term experiment, the fabricated membrane exhibited good rejection of potassium (K^+), ammonia nitrogen (NH_4^+-N), and total organic carbon (TOC) present in sewage sludge and the final concentration of the total dissolved solids (TDS) and K^+ ions increased. This work reveals sewage wastewater concentration as a potential application in FO process.

Madhumala et al.[44] studied the feasibility of an aqueous fructose concentration using FO technique. It was observed when NaCl was chosen as draw solution, the concentration of fructose was increased from 16% to 21%, thus producing sugar crystals in the process.

Overall, the FO has several advantages over traditional methods for various concentration applications without compromising the quality and energy resources. The schematic diagram of FO process was illustrated in Fig. 2.

TH-3195_186151006

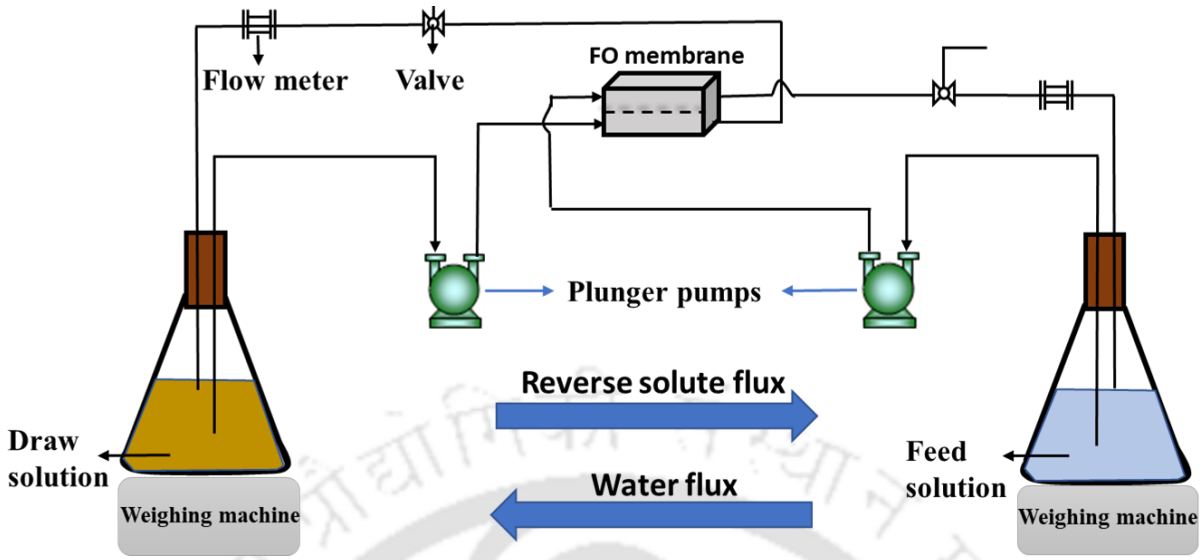

Fig. 2: Schematic diagram of FO process

2.2.1 Energy generation

Osmotic energy, sometimes referred to as salinity gradient power or blue energy, has emerged as a promising renewable energy source, leveraging the energy potential from the difference in the salt concentration between seawater and river water. This literature review will focus on key technologies such as Pressure Retarded Osmosis (PRO), Reverse Electrodialysis (RED), Capacitive mixing (CapMix), Hydrogel-based Osmotic Power, and Salinity Gradient Solar Ponds (SGSP), the literature related osmotic energy generation technology and viability of integrating both osmotic based separation energy generation process was brief bellow.

PRO is one of the most researched techniques for osmotic power generation. The fundamental premise lies in the movement of freshwater across a semipermeable membrane towards a high-salinity solution, generating pressure that can be converted into mechanical energy, typically via a turbine [33]. However, achieving a high power density requires specific conditions, such as optimal operating pressure and high-performance membranes[45]. Moreover, the significant

TH-3195_186151006

challenge of membrane fouling, leading to decreased performance and increased operational costs, has been highlighted in the literature[46].

Gonzales et al.[47] reported a TFC membrane fabricated with the melamine-based covalent organic framework (COF) and polyamide layer that increased the osmotic PRO performance in terms of water flux and exhibited a power density of 12.1 $W.m^{-2}$ at 24 bar.

She et al.[48] tested the fabric reinforcement materials by using different types of fabric for PRO TFC membranes, and it was observed that the TFC membrane made with tricot fabric material exhibited a power density of 7.1 $W.m^{-2}$ at 18.4 bar.

Son et al.[49] incorporated functionalized CNT in the Polyethersulfone (PES) support to increase the water flux and anti-fouling property in the PRO process. The prepared membrane was also used to harvest energy from saline water and exhibited a power density of 12.1 $W.m^{-2}$ at 21 bar using 1M NaCl as draw solution.

Fu et al.[50] developed a mixed matrix hollow fiber (HF) membrane for PRO and osmotic power generation. The fabricated membrane exhibited a maximum power density of 2.47 $W.m^{-2}$ at 7 bar pressure using 1M NaCl as draw solution.

RED exploits the movement of ions across ion-exchange membranes under the influence of a salinity gradient, generating an electric current. While RED offers advantages, such as a less complex process compared to PRO and the absence of moving parts, it faces challenges regarding membrane efficiency and the control of internal resistance, impacting the net power output. Despite this, the researchers have found promising ways to enhance RED performance, such as by using bipolar membranes[51].

Moreno et al.[52] studied the effect of flow velocity, membrane stack size and membrane type on reverse electrodialysis (RED) process. It was observed that a smaller stack induces high

TH-3195_186151006

pumping power density, which reduces the net power density as compared to a larger stack. Moreover, with increasing flow velocity, the power density also increases and reached up to 1.2 $W.m^{-2}$.

Tedesco et al.[53] studied the laboratory RED test with brackish water (0.1M NaCl) and brine water (5M NaCl). Under these conditions, a power density of 12 $W.m^{-2}$ was achieved of cell pair. The effect of feed concentrations, temperature and flowrate on the process parameters were also investigated with two different sets of ions exchanged membranes (IEMs).

Capacitive Mixing (CapMix), an osmotic energy recovery technique, operates on the principle of variable salinity to create a potential difference across capacitors[54]. Although the simplicity of CapMix technology and its material requirements were advantageous, its practical efficiency for large-scale implementation was a considerable challenge, necessitating further research.

Hydrogel-based Osmotic Power is a relatively new approach to osmotic power generation that leverages the swelling energy of hydrogels in contact with freshwater[55]. While this technology has shown promise in laboratory experiments, the translation to large-scale applications and the environmental impact of using hydrogels are areas that require more research.

SGSPs utilize both solar and osmotic power, thereby increasing energy yield per unit area[56]. While SGSPs offer the benefit of dual renewable energy sources, they require significant surface areas that are geographically dependent, and must account for evaporation losses and potential environmental impacts.

Numerous studies have questioned the osmotic process's economic feasibility for power generation. For example, FO is mainly applied to desalination or concentration processes as a

TH-3195_186151006

standalone method due to its energy efficiency[8]. However, it faces several economic challenges, including the need for expensive specialty chemicals as draw solutions and the cost of subsequent recovery of these draw solutions. Additionally, the durability and fouling of FO membranes can lead to high maintenance and replacement costs[57].

On the other hand, RED avoids some of the challenges related to FO; the current state of the technology presents its economic hurdles. The efficiency of RED is highly dependent on the quality and performance of ion exchange membranes, which have a substantial cost factor in the RED process. Furthermore, the costs related to pumping and maintaining a constant flow of fresh and saltwater add to the overall operation and maintenance costs[58].

The economic case for simultaneously using an osmotic-driven process for simultaneous concentration and energy generation can be more substantial. This is because each process can complement the other, increasing the overall efficiency and reducing the total costs.

2.2.2 Simultaneous energy generation and concentration of the aqueous solution

In recent years, hybrid applications consisting of simultaneous separation and energy generation have attracted significant attention due to their potential ability to address both energy and environmental challenges. It has been reported earlier that microbial desalination cell and electrochemical RO for the hybrid applications.

Microbial Desalination Cells (MDCs) are an innovative technology capable of wastewater treatment, seawater desalination, and eco-energy production. The system functions by leveraging the bio-electrochemical oxidation of organics in wastewater, which generates electricity and drives ion migration for desalination and value-added by-product creation[59].

One identified obstacle with MDCs is maintaining pH balance and managing high internal resistance[59,60]. This challenge has been addressed in part by the creation of a two-chamber

TH-3195_186151006

tubular MDC (TTMDC) that balances pH through a self-generated control mechanism[61]. Furthermore, to combat high internal resistance, the innovative design of a quadruple microbial desalination cell (QMDC) has been proposed and tested. Of the various connection configurations tested, parallel connections demonstrated the lowest internal resistance and highest power recovery, thus proving to be the most effective[60].

The concept of coupling the reverse osmosis process with MDCs has also been suggested to enhance the desalination process, particularly in arid areas like the UAE, thus combining the strengths of two powerful technologies. This coupled system demonstrates the potential for simultaneous energy generation and concentration processes. Furthermore, the performance of MDCs is found to vary significantly with different operating temperatures, emphasizing the need for careful operational control[62].

The integration of biocathode-microbial desalination cell technology with microalgae cultivation has shown promise, specifically when utilizing Chlorella vulgaris. The presence of microalgae in the cathode chamber significantly increased power density and salinity removal rate[63].

The sustainable development and scalability of MDC technology remain to be crucial factors for widespread application. MDC technology has already shown promise when using dewatered sludge as an anodic substrate, enhancing stability for desalination and electricity generation[64,65].

Lastly, the development of a pressure-driven ion-selective nanomembrane for desalination, known as the electrochemical energy-generating desalination system (EC-desalination), shows potential for simultaneous desalination and energy generation. This system demonstrates up to

TH-3195_186151006

51% energy savings compared to traditional reverse osmosis systems, illustrating the advantage of the combined process[32].

2.3 Summary and research gaps of energy generation and separation application

Similar MDC and EC-desalination, the FO process has shown great potential for both separation and energy generation applications. For separation applications, FO can process high salinity feed solutions without the need for extensive pre-treatment, reducing the overall energy consumption. It can also concentrate feed solutions to higher levels than conventional technologies like RO and NF without compromising the fouling parameters, thus reducing the size and cost of downstream separation process. Regarding the energy generation applications, the FO has shown great potential to provide a sustainable alternative to traditional power generation technologies through PRO and MD processes, such as low environmental impact, high efficiency, low operating costs, and low energy consumption. Overall, the novel FO process has the potential to revolutionize both separation and energy generation applications in a sustainable manner. Hence, further research and development in this area could lead to its widespread adoption in various industries. Some of the focus research area for developing FO process for concentration and energy generation applications as follows.

- Development of novel Membrane materials that will be facilitated both ion transport and high water flux with minimal reverse solute flux.
- Development of novel membrane module design than can facilitated both FO and electrochemical process with appropriate membrane and electrode.
- Techno economic analysis of combined system.

2.4 Novel membrane for FO applications

2.4.1 Membrane for standalone FO

TH-3195_186151006

The FO process was a promising technology for various applications like separation, concentration process, water treatment and sustainable energy generation. One of the critical components in the FO process was the fabrication of a suitable FO membrane that should have high water permeability, selectivity, stability, and anti-fouling properties under various operating conditions. In recent years, many researchers have focused on developing new membranes for FO that can improve its performance and reduce its energy consumption [66]. This literature review summarises some of the recent developments in membrane technology for standalone FO processes. According to the literature, there were mainly three different types of FO membranes:

a. Thin-film composite (TFC) membrane: TFC membranes consist of a thin polyamide layer on top of a microporous support layer. The polyamide layer was responsible for the membrane's selectivity, and the support layer provided mechanical strength to the polyamide layer. Some of the reported articles on the TFC FO membranes were:

Gonzales et al.[67] fabricated a polyvinylidene fluoride (PVDF) nanofiber supported TFC membrane using the electrospun technique. The negatively charged polyacrylic acid (PAA) nanofibers were deposited onto the PVDF layer to increase the hydrophilicity and selectivity. The fabricated membranes achieved a high water flux of 32 L m^{-2} h^{-1} and low SRSF of 0.16 g/L for 1M NaCl and DI water as DS and FS solutions.

Widjojo et al.[68] developed a TFC FO membrane via interfacial polymerization technique with 50% sulphonated content for enhancing performance and anti-fouling properties. The membranes exhibit 33 L m^{-2} h^{-1} and 21 L m^{-2} h^{-1} water flux under PRO and FO modes. The ICP was also alleviated with the increase in sulphonated materials in the membrane substrate.

TH-3195_186151006

Chowdhury et al.[69] demonstrated a TFC FO membrane composed of a PES nanofiber support layer and a polyamide layer using an interfacial polymerization technique. The fabricated membrane exhibits a good water flux of 27 L m^{-2} h^{-1} and low RSF of 4 g m^{-2} h^{-1} for 1M NaCl and DI water as DS and FS. The inherent properties of nanofiber enabled high water flux, low RSF, and high mechanical strength to the overall TFC membrane.

b. Cellulose-based membrane (CA): Cellulose-based membranes were derived from natural sources, such as wood pulp or cotton linter. These membranes exhibit high water permeability but lower salt rejection than TFC membranes. Some of the reported literature were:

Sairam et al.[70] synthesized CA flat sheet composite membrane for the FO process. The CA thin layer was casted on a nylon fabric support using phase inversion. The membrane achieved a water flux 6.8 L m^{-2} h^{-1} and NaCl rejection of 95%.

Wang et al.[71] developed a FO membrane consisting of a porous sublayer sandwiched between two CA selective layers via phase inversion. The double-skinned CA membrane exhibited a water flux of 48.2 L m^{-2} h^{-1} and low SRSF of 0.134 g/L using 5M $MgCl_2$ as DS.

Su et al.[72] first fabricated CA NF HF membrane for FO process. The membranes exhibited a water flux and RSF of 7.3 L m^{-2} h^{-1} and 0.5 g m^{-2} h^{-1}, respectively with 2M $MgCl_2$ and DI water as DS and FS, respectively.

Su et al.[73] designed novel dual-layer HF FO membrane fabricated from proprietary cellulose acetate propionate (CAP) polymer for wastewater reclamation through FO-MD hybrid system. The fabricated membrane has a higher water permeation rate of 13.7 L m^{-2} h^{-1} using only 0.5M $MgCl_2$ as DS.

TH-3195_186151006

c. 2D nanomaterials-based membrane: These membranes were composed of 2D nanomaterials, which have a thickness of only a few atoms and possess unique properties like high mechanical strength, high surface area, high anti-fouling, high hydrophilicity, excellent thermal and chemical stability and high selectivity, making them ideal candidates for use in FO membranes. Some of the reported literature were:

He et al.[74] fabricated a novel highly selective and hydrophilic FO membrane using sulfonated covalent organic frameworks (COFs). The negatively charged membrane enhanced the water flux (36 L m^{-2} h^{-1}) and maintained lower RSF (9 g m^{-2} h^{-1}) in PRO mode with 1M NaCl and DI water as DS and FS, respectively. The optimized membrane overcame the trade-off between water permeability and selectivity.

Tian et al.[75] embedded silica nanoparticles onto polyetherimide (PEI) nanofibrous support for making thin-film nanocomposite (TFN) FO membrane. The fabricated membrane exhibited a higher water flux of 72 L m^{-2} h^{-1} and low SRSF of 0.1 g/L with a lower structural parameter of 174 µm. The low structural parameter helped in mitigating the ICP.

Sun et al.[76] fabricated a novel TFN membrane featuring an interlayer of $Ti_3C_2T_x$ Mxene and intercalated with carbon nanotube (CNT) for municipal wastewater concentration. The membranes achieved a high-water flux and low SRSF of 63 L m^{-2} h^{-1} and 0.15 g/L, respectively with 1M NaCl and DI water as DS and FS. When FS was replaced with municipal wastewater, the membrane exhibited stable 22 L m^{-2} h^{-1} water flux and a water recovery of 50%.

Faria et al.[77] fabricated a TFC composite membrane functionalized with graphene oxide-silver nanocomposites for biofouling control in FO process. The fabricated membrane achieved a stable water flux of 20 L m^{-2} h^{-1} while simultaneously inhibiting the attachment of Pseudomonas aeruginosa cells, thus showing high anti-microbial property and reduce the flux

TH-3195_186151006

decline up to 30%. Summary of lab fabricated and commercial FO membrane performance details are summarised in Table 1.

Table 1: Different types of FO membrane at its performance comparison

Membranes	Feed Solution	Draw Solution	Water Flux (L m^{-2} h^{-1})	RSF (g m^{-2} h^{-1})	References
PP-HTI	DI water	2M NaCl	7	2.8	[78]
CTA-HTI	DI water	1M NaCl	11	17.52	[79]
Aquaporin	DI water	1M NaCl	14	5	[80]
Aquaporin	DI water	1M NaCl	20	4	[81]
PA-TFC	DI water	1M NaCl	40	12	[82]
PA-GO/PSf	DI water	2M NaCl	22.4	9	[83]
CNT/GO	DI water	1M NaCl	5.8	1.75	[84]
PDA-GO	DI water	1M NaCl	24.2	3.8	[85]
Ag-PDA/GO	DI water	1M NaCl	27	20	[86]
TFC (GO-CS)	DI water	1M NaCl	27.2	8.15	[87]
GO/MWCNT	DI water	1M NaCl	26.7	3.8	[88]
TFN (Cu-Al LDH-WS_2)	DI water	1M NaCl	40	18	[89]

Commercial FO membranes: PP-HTI, CTA-HTI, Aquaporin and PA-TFC

Lab fabricated FO membranes: PA-GO/PSf, CNT/GO, PDA-GO, Ag-PDA/GO, TFC (GO-CS), GO/MWCNT and TFN (Cu-Al LDH-WS_2)

TH-3195_186151006

2.4.2 Membrane for energy generation and concentration of the aqueous solution

Membrane-based technologies have been widely explored for simultaneous separation and energy generation, potentially addressing challenges like water treatment, concentration applications and energy production. In recent years, significant progress has been made in developing novel membrane materials, configurations and processes that can enhance separation efficiency, reduce energy consumption, and generate energy from waste streams. This literature review summarizes some of the different types of membranes used for separation and energy production applications.

a. Microbial desalination cell membranes: Microbial desalination cell technology uses ion-exchange membranes that can specifically allow particular type of ions to permeate while retaining others. The cation and anion exchange membranes can be used for desalination and removal of contaminants from water while creating a potential difference across the two compartments containing different salt concentrations by separating specific types of ions based on the surface charge of the membrane. These membranes were used in applications like RED, MFCs, and redox flow batteries for the separation of ions and new energy conversion[90]. Some of the reported literature on these membranes were:

Samsudin et al.[91] fabricated series of composite anion exchange membranes (AEMs) comprising quaternary ammonium poly (vinyl alcohol) electrospun nanofiber and different PDDA/QPVA matrix filler ratios by solution casting. The membranes exhibited good alkaline stability for a longer duration, greater mechanical strength, and higher water uptake of 57.6%. Their membranes achieved a power density of 24 $mW.cm^{-2}$ and a current density of 131 $mA.cm^{-2}$.

Zhang et al.[92] developed a system consisting of two membrane-based biochemical reactors that can simultaneously generate energy and desalinate saline water. The two membrane-based

TH-3195_186151006

biochemical reactors consist of osmotic microbial fuel cell coupled with microbial desalination cell. The coupled system significantly showed high desalination performance (96% conductivity reduction) and generated a highest power density of 12.45 W. m^{-3}.

Hong et al.[93] studied a new RED model to quantify power generation using ion exchange membranes. They also investigated the impact of saline and freshwater flow rate on the power density. It was observed that monovalent ions like NaCl induce higher power density than divalent ions like Na_2SO_4 and $MgCl_2$ due to the lower internal stack resistance of the multivalent ions. Moreover, higher power density was observed at higher flow rates in the saline water compartment than in the freshwater compartment.

Rahimnejad et al.[94] investigated the production of bioelectricity from pure glucose in air-cathode MFCs using proton exchange membranes. Potassium permanganate ($KMnO_4$) was used as oxidizing agent in the cathode chamber to enhance the voltage. The system generated the highest stable voltage of 760 mV for 72 hours while producing power output of 283 $mW.m^{-2}$.

b. Composite membranes: Composites membranes were multi-layered structures that consist of two or more different materials with distinct properties. Some of the examples were TFC membranes, nanocomposite membranes and mixed matrix membranes. The selective layer in composite membrane can be used for separation purposes while transport of specific ions from one side to another can be used for energy generation, such as in PRO system. Some of the reported literature on these membranes were:

Jang et al.[95] developed a sandwich-like composite membrane consisting of a commercial filtration membrane and conductive PEDOT:PSS/CNT layer for simultaneous water purification and energy generation applications. When polluted water was passed through it,

TH-3195_186151006

the membrane was able to reject 80% Mg^{2+} ions and 80% PFOA contaminants present in polluted groundwater while simultaneously generating high power of 15 µW.

Yang et al.[96] prepared the functionalized PDDA-MXene composite membrane for simultaneous electrokinetic energy conversion and organic molecular sieving applications. The positively charged membrane displayed good rejection (99%) for positively charged methylene blue (MB) dye molecules. By connecting with loading resistors, the maximum power output was reach over 500 mW.

Li et al.[97] developed a composite membrane comprising of natural biopolymer K-Carrageenan and metal organic framework ZIF-8 for simultaneous recovery of metal ions and electricity harvesting. The prepared membrane displayed good selectivity of Li^{+}/Co^{2+} ions with a separation factor of 8.29 and a good Li^{+} flux of 0.34 $mol.m^{-2}.h^{-1}$. The membrane also exhibited a good energy conversion rate with a power output of 3.54 µW during the separation process.

Ghaffar et al.[98] demonstrated graphene oxide-melanin (GOM) composite photothermal membrane for simultaneous solar water desalination and energy generation. The membrane showed excellent solar-thermal efficiency of 93.4% as compared to traditional carbon-based membrane. The water evaporation rate in presence of mixed salts ranges in between 1.05 and 1.35 kg m^{-2} h^{-1} with 66–86 % efficiency and achieved a maximum power density of 0.9 $W.m^{-2}$ at relative humidity of 60%.

2.5 Summary and literature gaps of membranes used in various applications

One of the key parameters in the sustainable FO process for separation and energy generation process is the development of novel FO membranes to improve efficiency, durability and scalability. Some common membranes including TFC and cellulose membranes are often used

TH-3195_186151006

for FO applications. However, low salt rejection rate, high fouling propensity and low mechanical stability have limited their usage for the longer run. To resolve the trade-off between water permeability and selectivity, the FO membranes are fabricated with 2D nanomaterials. 2D nanomaterials containing FO membranes have gained a lot of attention due to its unique properties like high hydrophilicity, high selectivity, high anti-fouling and high mechanical and chemical stability. In addition to the FO process, the novel membranes used for separation and energy generation simultaneously include ion-selective membranes and composite membranes. These have great potential to apply FO processes in water, wastewater treatment, pharma, and food industries. Therefore, with the ongoing research and development, the advancements in FO membranes have the potential to revolutionize the technology and make it more efficient, cost-effective and environmentally sustainable for various applications.

Although there have been significant improvements in the development of FO membranes, some literature gaps still need to be addressed.

- Development of FO membrane that can facilitate high water flux, low RSF and ion-selective transport
- Development of novel devices that achieve simultaneous FO process and energy generation
- Development of fouling-resistant membrane while using high fouling potential feed solution in food and pharma applications

2.6 FO process parameters

To evaluate the effectiveness of the FO, it's important to consider that its efficiency relies not only on the separation layer but also on several other factors. These factors encompass the appropriate choice of the support layer, the characteristics of the feed solution (FS) and draw

TH-3195_186151006

solution (DS), the configuration of the FO module, and the specific operating conditions of the process.

The efficiency of the FO process is largely determined by the operational conditions, which include the flow, pressure, and temperature of both the FS and DS. Careful control of these variables can have a substantial impact on the overall effectiveness of the osmotic process. For example, the flow rate of the solutions directly affects the transport rate of solutes and solvents, consequently influencing the concentration gradient. Likewise, the operational pressure influences the osmotic pressure, while temperature affects the diffusion rates and viscosity of the solutions.

Moreover, the configuration of the FO module plays a crucial role in its application both at the laboratory and commercial levels. Some standard configurations are the spiral-wound and the hollow-fibre modules. Each of these configurations offers unique benefits, with spiral-wound modules providing a high packing density and hollow-fibre modules offering a high surface-area-to-volume ratio.

However, the performance of the FO process can be adversely affected by challenges such as concentration polarization, membrane fouling, and suboptimal operational conditions. Concentration polarization can lead to a reduction in the effective osmotic driving force, while membrane fouling can cause pore blockage, thereby decreasing water flux. Suboptimal operational conditions, on the other hand, can lead to inefficient energy usage or lower separation efficiencies.

In the following section, a detailed analysis of these parameters is summarised, and the implications of not managing them appropriately as shown in Fig. 3.

TH-3195_186151006

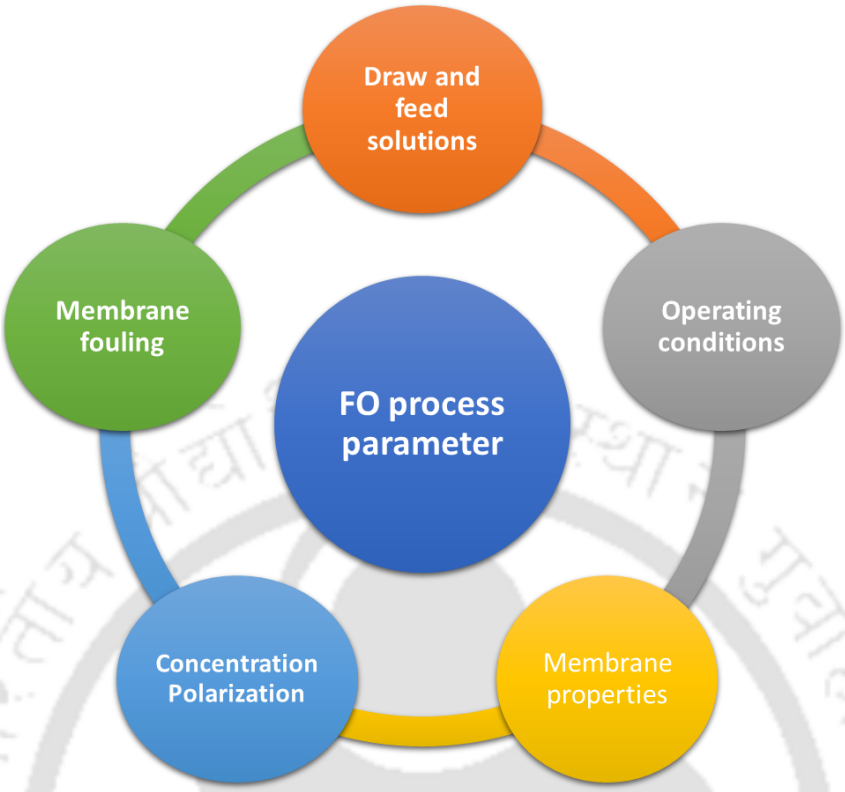

Fig. 3: Factors affecting the FO performance

2.6.1 Importance of Draw and Feed solution

The draw and feed solutions play a crucial role in driving the FO process. It's concentration and solute type are paramount as they directly affect the osmotic pressure gradient across the membrane. The higher the osmotic pressure gradient across the membrane, the higher will be the water flux. Research has involved a range of draw solutes such as salts, organic compounds, and nanoparticles[99,100]. In selecting the DS, one needs to consider its potential for reverse solute flux (RSF), ease of recovery, and environmental impact.

However, there's a caveat; excessively high concentrations can lead to increased osmotic pressure back-diffusion and potentially increases the reverse solute flux from draw solution to feed solution. It is undesirable because it reduces the water flux and can also contaminate the feed solution, thus reducing the process's efficiency and longevity[101,102]. Moreover,

TH-3195_186151006

recovering and regenerating the draw solution can be a challenging task as it increases the overall cost of production[103]. Also, a high concentrated feed solution can reduce the osmotic pressure drastically due to the presence of foulants which can exacerbate issues like concentration polarization and fouling, thus chemically degrading the FO membrane under certain conditions like pH and temperature. Many studies reported the foulants like macromolecules such as alginate, humic acid, and proteins are present in natural waters and wastewater effluents, which are commonly used as feed water [99,100]. Therefore, optimizing the draw solution and feed solution concentrations along with the membrane properties is crucial to achieve a balance between maximizing water flux and minimizing potential fouling aggregates. Moreover, the cost of preparing, recovering, and disposing of the draw and feed solutions is a key factor in the economic feasibility of FO processes.

2.6.2 FO Operating Conditions

The operating conditions of FO process significantly affect the process performance. Temperature is a key operating condition that can affect the efficiency of the FO process. Higher temperatures can enhance the diffusion rate and increase the water flux across the membrane by decreasing the liquid viscosity. However, elevated temperatures can also speed up fouling and scaling rates, posing a challenge to membrane longevity[104]. Similarly, the FO operates under different pressure conditions depending on the application. High-pressure FO might offer greater efficiency, but could also lead to more membrane fouling and higher energy consumption. Applying pressure on the feed side can improve the FO process performance by increasing the water flux, but excessive pressure may damage the membrane and reduce its efficiency due to negative transmembrane pressure[105]. Another important FO operating condition that can influence the performance is the flow rates of both draw and feed solutions. Increasing both the flow rates lead to an increase in FO performance (water flux)

TH-3195_186151006

due to higher osmotic pressure gradient achieve across the membrane. However, it can adversely affect other performance parameters of FO systems such as feed recovery and operating pressure[105]. Therefore, maintaining the optical temperature, pressure and cross-flow velocity across the membrane are pivotal for a higher overall performance while also sustaining the structural integrity of the membrane.

2.6.3 Membrane properties

The FO membrane is another crucial parameter, as its properties directly impact the process's efficiency and effectiveness. Factors such as the membrane's material, pore size, thickness, and hydrophilicity can greatly affect its performance. For instance, membranes with larger pores can facilitate higher water fluxes but may also allow more impurities to pass through, compromising the permeate quality. Also, the structure of the porous substrate determines the effect of ICP on the FO membrane[106]. For example, a low structural parameter (S) value of the support layer helps in mitigating the ICP to a large extent and subsequently enhances the water flux. Similarly, the active layer plays a crucial role in determining the overall performance and durability of the FO membrane[107]. The incorporation of organic or inorganic nanomaterials not only enhance the chemical and mechanical stability but also provides resistance to fouling[108,109]. Another parameter of the membrane that affects the performance in the FO process is the thickness. Thicker membranes generally have lower permeability but possess higher mechanical strength[110]. Therefore, the optimal thickness would be a balance between permeability and mechanical strength. Additionally, the cost of the membrane and its associated operational and maintenance costs will be a significant factor to consider. A cheaper membrane might not provide the desired efficiency or lifespan, while a more expensive one might offer superior performance but be prohibitively costly. Therefore,

TH-3195_186151006

selecting the right membrane with desired features without compromising the cost and efficiency is vital to ensure optimal FO process performance.

2.6.4 Concentration polarization

In the FO process, concentration polarization (CP) is a phenomenon that occurs and has implications for the overall efficiency and performance of the process. CP refers to the build-up of solutes on the membrane surface during the FO operation, resulting in a concentration gradient across the membrane that can impede water transport and reduce the water flux[111]. The CP layer affects the FO process in several ways. First, it increases the osmotic pressure on the feed solution side, opposing the natural osmotic flow of water. This resistance to water transport reduces the water flux through the membrane, limiting the overall efficiency of the FO process. Additionally, CP contributes to the membrane fouling. The concentrated solutes in the polarization layer promote the attachment and deposition of particles, colloids, and other foulants on the membrane surface, thus impeding water transport and reducing the membrane performance. The FO and PRO processes, defined by their membrane configurations as active layer facing feed solution (ALFS) and active layer facing draw solution (ALDS) respectively, have unique impacts on membrane fouling and concentration polarization phenomena[112]. The polarization occurring inside the porous support layer is referred as internal concentration polarization (ICP), whereas the polarization occurring on the membrane surface is referred as external concentration polarization (ECP)[113,114]. Furthermore, the ECP and ICP can be classified into concentrative and dilutive based on the orientation of the active layer and support layer[115]. The polarization that happens on the feed side is of a concentrative nature and differs from the dilutive polarization on the draw side caused by the incoming permeate flux. The concentrative polarization is referred to as concentrative external concentration polarization (CECP), while the polarization occurring on the draw side is termed dilutive

TH-3195_186151006

external concentration polarization (DECP)[116]. Similarly, dilutive internal concentration polarization (DICP) occurs on the draw side of the membrane due to the incoming permeate flux whereas concentrative internal concentration polarization (CICP) occurs on the feed side of the membrane when the feed solution concentration is high[117]. In the FO mode, CECP of the feed solute and DICP of the draw solute are observed. The active layer of the membrane interfaces directly with the feed solution in this setup, encouraging a continuous renewal of the solution at the membrane surface, which can aid in reducing foulant accumulation. However, this configuration has inherent challenges. Specifically, CECP can lead to an increase in the solute concentration at the membrane-feed interface, thereby reducing the osmotic pressure gradient that drives water transport across the membrane. Furthermore, DICP can cause a dilution of the draw solution within the porous support layer of the membrane, further reducing the effective osmotic pressure difference and, therefore, the overall water flux[117]. Thus, while the FO mode may exhibit lower fouling tendencies due to the constant renewal of the feed solution on the active layer, the overall effective osmotic pressure available for driving water flux could be lower than in the PRO mode, particularly when high fouling potential feeds such as liquid food or pharmaceutical effluent are used. Contrastingly, the PRO mode is characterized by the occurrence of dilutive external concentration polarization (DECP) of the draw solute and concentrative internal concentration polarization (CICP) of the feed solute[117]. The orientation of the active layer towards the draw solution reduces its exposure to potential feed foulants, mitigating the risk of fouling. However, this orientation exposes the porous support layer of the membrane to the feed solution, which can lead to severe fouling due to the deposition of feed foulants within the support layer. This fouling can decrease the porosity of the support layer, increase its hydraulic resistance, and ultimately lead to a decrease in the overall water flux. In particular, the flux in PRO mode may decrease more rapidly than

TH-3195_186151006

in FO mode due to the severity of CICP in the support layer, even though the initial water flux might be higher in PRO mode[118]. Notably, cleaning strategies can potentially be implemented to remove foulants from the support layer and mitigate these effects. Moreover, DECP in the PRO mode can result in the dilution of the draw solution near the membrane surface, decreasing the osmotic pressure difference and hence the driving force for water transport. However, due to the active layer's orientation towards the draw solution in PRO mode, a relatively high initial effective osmotic pressure can be achieved, potentially resulting in an elevated initial water flux compared to FO mode[119].

In summary, both the FO and PRO modes present unique advantages and challenges with respect to fouling mitigation and maintenance of effective water flux. While the FO mode offers a beneficial reduction in fouling, it may struggle with a lower initial water flux, particularly with high fouling potential feeds. In contrast, the PRO mode can provide a high initial water flux due to a higher effective osmotic pressure but could face a more rapid decrease in efficiency over time due to severe fouling within the support layer, even though cleaning strategies can potentially mitigate these effects.

2.6.5 Membrane fouling

One of the most important parameters that influence the FO system is the aggregation of foulants on the membrane surface. The fouling arises due to the accumulation of solutes (foulants) near the membrane surface during the separation process, which causes a blockage to the membrane pores, thus forming a gel layer on the membrane surface[120]. This can lead to reduced water flux, increased energy consumption and shortened membrane lifespan. The foulants or contaminants such as colloidal matter, inorganic compounds, dissolved organics and microorganisms present in the feed water are responsible for the biofouling of the membrane[121,122]. FO membrane fouling intensity is reduced by adopting appropriate pre-

TH-3195_186151006

treatment of the feed solution and chemical cleaning, which increases the costs and energy consumption of the overall membrane operation. It was imperative to understand the fouling behaviour in the FO process because both sides of the FO membrane were in contact with either feed water facing the active or support layer or natural DS solution facing the active or support layer[123]. Hence, the fouling behaviour can be classified into four categories (i) organic fouling, (ii) inorganic fouling, (iii) biofouling and (iv) colloidal fouling[16].

Moreover, this fouling can also be sub-classified as external and internal fouling. The primary factors influencing the fouling are operating conditions, feedwater characteristics, draw solution concentration, membrane properties and membrane orientation. Some reported literature showed that membrane fouling became more severe at higher water flux levels[124,125]. She et al. observed higher RSF with specific ions (i.e. Ca^{2+} or Mg^{2+}) in the feed solution at higher DS concentration, which caused additional organic fouling[101]. However, it was observed that fouling is not noticeable below the critical DS concentration.

Regarding membrane structural properties, it was observed that the membranes with smaller structural parameter deliver higher water flux which may lead to potential membrane fouling due to enhanced hydrodynamic drag force. The effect of fouling is also considered in membrane orientations. Many studies reported that the membrane was more prone to fouling in active layer facing draw solution (ALDS) orientation compared to active layer facing feed solution (ALFS) orientation due to severe pore clogging of the support layer by feed foulants and that enhances the CICP in ALDS orientation when fouling causing solution is used as FS[126,127]. Therefore, the occurrence of internal fouling by depositing foulants inside the pores of the support layer in ALDS orientation was more severe and irreversible. Moreover, frequent fouling can increase the intensity of cleaning cycles for maintaining the membrane performance, indirectly leading to more fouling, as aggressive cleaning can damage the

TH-3195_186151006

membrane and make it more susceptible to foulant deposition. Therefore, it is imperative to mitigate the fouling during the FO process to increase the efficiency and lifespan of the membranes.

2.6.6 Mitigation plan for fouling reduction

The occurrence of fouling during the FO process is inevitable; hence, mitigation of the same is imperative to increase the overall efficiency and membrane lifespan. Therefore, several strategies were employed to alleviate the fouling propensity. Physical and chemical cleaning can remove the deposited foulants on the membrane surface by enhancing the shear force[128]. However, chemical cleaning with sodium hydroxide (NaOH), biocides, acids and surfactants are required when concentrating pharma effluents and wastewater because of the irreversible fouling caused by complicated foulants in wastewater. However, these methods must be used judiciously as they can damage the membrane.

Moreover, hydrodynamic conditions like increasing the cross-flow velocity on both sides of the membrane can significantly reduce the external fouling on the membrane surfaces. The high shear force exerted on the membrane surface moves away the foulants on the membrane surface, thus reducing the membrane fouling and increasing the mass transport across the membrane[129]. However, the high flowrates on both sides enhance the pumping energy, which increases the energy consumption of the system. Also, pressure drop across the FO module at high flow rates is expected to increase without improving water flux. Another approach to mitigate fouling is integrating the FO process with other technologies, such as pressure retarded osmosis and reverse osmosis. This hybrid process can lower the fouling propensity by employing hydrodynamic control strategies in the osmotic dilution process[129,130]. Finally, the optimized strategy used to mitigate any fouling without compromising the energy and costs of the system was the development of the FO membrane

TH-3195_186151006

with desired properties. Membranes with inferior separation properties (i.e., lower water permeability and selectivity) could result in more solute diffusing from DS into FS and from FS into DS, which may increase the risk of fouling. Therefore, along with the membrane separation properties, the membrane surface properties (such as roughness, surface charge, hydrophilicity and specific functional groups) also influence the foulant-membrane interaction and play a pivotal role in alleviating the fouling[131]. Membranes with a hydrophilic surface and high surface charge density can reduce organic fouling and repel similarly charged foulants. In recent years, novel advanced nanomaterials have been developed and used for surface modifications and coatings to address the permeability-selectivity trade-off by increasing the water flux without compromising the salt rejection rates. Due to the high hydrophilic nature of the 2D nanomaterials, there is a thin hydration layer of water molecules on the membrane surface, which weakens the binding of other organic foulants or molecules on the membrane surface, thus preventing the fouling propensity to a great extend[132]. For example, Qui et al, developed a zwitterion-silver nanocomposite-modified film composite membrane that showed anti-fouling properties, improving both water flux and biofouling resistance for long-term operation[133]. Li et al. modified the FO membrane with hydrophilic polydopamine (PD) coating, which increased water flux and improved anti-fouling ability[134]. Therefore, 2D nanomaterials are expected to show a promising influence on the next generation of nanocomposite membranes for various separation applications. Considering recent developments, the field of membrane technology using nanomaterials is highly innovative and subject to rapid development.

2.7 Summary and literature gaps of FO process parameters

FO optimization involves selecting the appropriate draw and feed solutions, suitable FO membrane, fouling mitigation strategies to achieve the desired separation performance. The

TH-3195_186151006

selection of a suitable draw solution was crucial, as it determines the driving force for water flux and the membrane's selectivity. The FO membrane should exhibit high water permeability, high selectivity, high anti-fouling properties, and good mechanical and chemical stability for enhancing the FO process without compromising energy and cost. Finally, the effective fouling mitigation strategies like membrane surface modification, pre-treatment of the feed solution and physical and chemical cleaning can be applied to achieve a completely feasible FO system. Therefore, successful FO optimization requires careful consideration of the draw solution, FO membrane and fouling mitigation process to achieve the desired separation performance sustainably and cost-effectively. Although there have been significant improvements in the development of FO membranes, some literature gaps still need to be addressed.

- Development of novel stratagies to recover energy wasted in liquid pumping to minize the over all energy requirements
- Performance analysis of high flux and fouling-resistant membranes with respect to the orientation of the separation layer
- A detailed study on separation layer coating methods and their implications on membrane performance and production economics

2.8 Scope of the thesis

This thesis aims to investigate the potential of using exfoliated 2D nanomaterials to enhance the efficiency of forward osmosis process. The introduction provides an explanation of membrane technologies for concentration applications, along with its limitations. The importance of 2D nanomaterials in membrane technology and its application for simultaneous FO and energy generation is also discussed. Moreover, the purpose of the research motivations is also presented along with the research objectives. The literature reviews examine the previous research on novel FO process and FO membranes for separation and energy

TH-3195_186151006

applications, setting the stage for the merits and demerits of it. The outline of the FO process optimization along with the limitations is also being discussed. The remaining chapters describe the results and discussions for the development of novel FO membranes for various applications and presents the experimental work and observations and comparing the results to previous research. Finally, the conclusion summarizes the findings, discusses their implications in the field of FO membrane development and forward osmosis process and suggests avenues for further research.

TH-3195_186151006

TH-3195_186151006

CHAPTER 3

3 Synthesis and performance evaluation of reduced graphene oxide membrane doped with polystyrene sulfonic acid for forward osmosis process

Abstract: This chapter reports the use of graphene oxide (GO) and polystyrene sulfonic acid (PSS) polymer to enhance the permeation properties and selectivity of the FO-membrane. Size fractionization of GO flakes reveal the membrane coated with medium flakes (MF) showed optimum water flux and reverse solute flux for the FO application. The PSS-rGO membrane coated with MF performed better than that of the rGO membrane and commercially available cellulose triacetate membrane.

This part of the thesis is published in Sustainable Energy Technologies and Assessments. 44 (2021) 101093. (https://doi.org/https://doi.org/10.1016/j.seta.2021.101093).

TH-3195_186151006

3.1 Introduction

Forward osmosis has evolved as a low-cost and energy-efficient membrane separation technology for various applications like power generation[135], desalination[136], resource recovery[137], wastewater treatment[138] and concentration of aqueous products like tea and fruit juices[139,140]. The difference in chemical potential between the DS and FS drives the water from FS to DS through a semi-permeable membrane without the need of hydraulic pressure[141]. As a result, the FO process exhibits various desirable characteristics like low fouling propensity, less energy consumption and high water recovery that can be applied to different applications[142].

One of the key parameters for successful FO process is the suitability of FO membrane. A standard FO membrane should demonstrate low structural parameter, high water permeability, low salt rejection, high anti-fouling property and high mechanical and chemical stability[143]. However, the conventional FO membranes lack in providing some of these qualities like higher water permeability, low RSF. Moreover, the frequently used FO membranes are prone to severe fouling which limits their practical usage in various applications. Therefore, fabrication of robust and highly selective FO membranes is among the most critical research areas in the field of FO process.

Recently, researchers have focused on the modification of membrane surface for higher water permeability, high salt rejection and better fouling mitigation. In the last decade, atomically thin 2D nanomaterials like GO, rGO, titanium dioxide (TiO_2) and carbon nanotubes (CNT) have gained a lot of interest in membrane modification owing to its tunable hydrophilicity and high density of oxygen functional groups[144–146]. Out of these, GO based membranes have drawn researcher's attention because of its distinct structure, high hydrophilicity, high mechanical and chemical stability and low production cost[147]. Moreover, due to its high

TH-3195_186151006

water permeability, high salt rejection and superior anti-fouling properties, GO and rGO membranes are widely used in seawater desalination and wastewater treatment[148,149]. However, the stability of GO membranes in aqueous solution is still a challenging issue, which eventually becomes the bottleneck in its application. Due to this reason, the GO based membranes cannot be applied for long term stability performance which increases the cost of membrane production. Therefore, functionalization of GO based membranes with different polymers can enhanced the water permeability and selectivity without compromising the mechanical stability and cost of production for longer duration.

3.2 Scope of this investigation

The main motive of this investigation is to practically utilize a suitable FO membrane for the FO application. Recent studies have shown that hydrophilicity and mechanical stability of the GO based membranes can be enhanced by substituting the hydroxyl groups of GO with sulfonic groups[150,151]. Herein, in this study, the surface of the rGO membrane was directly doped with an aqueous solution of poly (4-styrene sulfonic) acid (PSS) polymer to enhance the water permeability, salt rejection along with mechanical stability for longer operational run. The linkage of SO_3H group of PSS with the carboxyl or hydroxyl groups of GO via hydrogen bonding, increases the hydrophilicity and mechanical strength of the overall membrane. Moreover, the surface charge of PSS-rGO membrane becomes more negative due to the presence of additional oxygen atom of PSS, thus increasing the salt rejection rate due to high electrostatic repulsion. However, the application of the as-prepared FO membranes hasn't been explored in FO process. Therefore, this work investigates the performance of the membrane in the FO process at various operating conditions like operating time and temperature, different GO flake sizes and stability test for continuous 25 long hours.

TH-3195_186151006

3.3 Experimental section

3.3.1 Synthesis of GO solutions

The GO nanosheets were prepared by using the modified Hummer method[152]. Typically, 250 mg of graphite powder was dispersed in an ice-cold solution of concentrated H_2SO_4 (12 ml) followed by slow addition of $KMnO_4$ (2 g) under continuous stirring conditions. The prepared solution was moved to a water bath maintained at 35 °C and continued with the stirring for 2 hours. After that, the ready solution was transferred to an ice bath. 100 ml of de-ionized (DI) water was added very slowly, maintaining the temperature below 35 °C until the temperature was stabilized. 10 ml H_2O_2 was added dropwise to the solution under ice-cold stirring conditions. The yellow solution obtained as such was mixed with 20 wt% HCl solution (500 ml) and repeatedly washed and filtered. After filtration, the solid GO sample was out inside a desiccator and cleaned with acetone. Finally, a required amount of GO sample was added to DI water to prepare GO solutions.

3.3.2 Preparation of large, medium and small-sized GO dispersion

The GO dispersion prepared by the modified Hummers method contains flakes with a wide range of lateral dimensions. The prepared GO dispersion (1mg/ml) was centrifuged at 2000 rpm for 10 minutes to separate the flakes of varying size ranges. Post-centrifugation, the solution was segregated into two categories, the supernatant solution as medium-sized GO flakes (MF) and the pellet as large-sized GO flakes (LF). The color of the aqueous dispersion of medium-sized GO flakes was observed to be light brown. A required amount of sample from medium GO flakes solution was sonicated for 6 hrs in a water bath to break them into further smaller flakes, and the obtained solution was considered as a sample of small-sized flakes (SF). After sonication, the SF GO-dispersion appeared light yellow.

TH-3195_186151006

3.3.3 Preparation method for rGO membrane and PSS coated rGO membrane

The aqueous dispersion (at 1mg/ml) of separated GO flakes (with respect to different size-range (LF, MF, and SF)) GO were passed through (i.e., vacuum filtered) the nylon microfiltration membranes (mean pore size = ~0.220 µm and thickness = 100 µm) to deposit a uniform layer on the exposed surface. The GO/nylon membranes were dried inside a desiccator for 24 hours and heated under vacuum conditions (pressure- 0.8 bar) at different temperatures (130 °C, 150 °C, and 180 °C for a definite time-period to prepare rGO/nylon membranes. Before conducting the FO experiment, the membranes were dipped in de-ionized water for 24 hours.

The dilute solution of PSS (100 µL in 40 ml DI water) was vacuum-filtered (0.8 bar) through the GO-coated nylon membranes of different flake sizes. The PSS-doped GO membranes were then heat-treated at optimized conditions of 150 °C temperature for 2.5 hrs heating duration inside a vacuum oven. The schematic diagram of the fabrication process was clearly illustrated in Fig. 4.

TH-3195_186151006

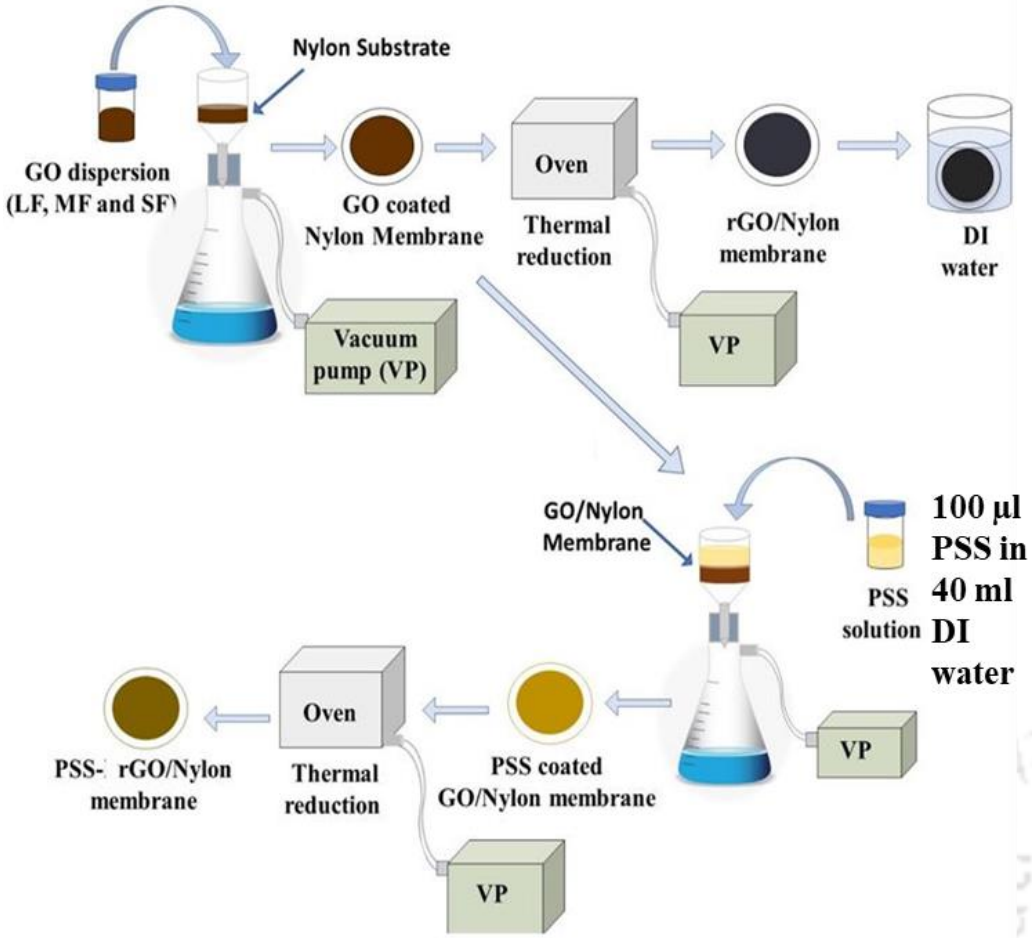

Fig. 4: The fabrication method for rGO and PSS-rGO membranes

3.3.4 Membrane Characterization

Field emission scanning electron microscope (FESEM, Sigma, India) and an atomic force microscope (AFM, Cypher, India) were used to study the morphology of the membrane samples. The pore size of the GO coated nylon and uncoated nylon membranes were analysed using a porometer machine (model: TECHPORO-AL-500). The water contact angle of the membrane samples was measured via the sessile drop method using a goniometer (Holmarc Opto-Mechatronics Pvt. Ltd.). X-ray diffractometer (XRD, Micromax-007HF, India) was used to determine the interlayer spacings of the lamellar membranes. The changes in the surface

TH-3195_186151006

functional group were evaluated using the FTIR spectrometer (PerkinElmer, Spectrum two, India). The presence of GO/rGO and PSS coated layer was confirmed through FESEM and energy dispersive x-ray (EDX) analysis.

3.3.5 FO experimental setup for performance evaluation

The performance of the rGO and PSS-rGO coated membrane was evaluated in a lab-scale FO experimental system, as shown in Fig. 5. The FO experimental setup consists of systemic connection of integrating FO test cell, feed & draw solution tank, pumps, conductivity sensor, and digital weighing balance. FO test cell (fabricated and supplied by Yantrabot Tech, Guwahati, India) separates the draw and the feed solution with an active membrane area of 4 cm^2. The weighing balance (model-XD/XR)) can measure and store the weight changes in both the draw and feed solution tank with an accuracy of ± 0.01g (supplied by Weighing solution Pvt. Ltd., New Delhi, India). The NaCl concentration in feed and draw tank was measured continuously using the Hanna conductivity meter (model-HI5321) with an accuracy of ± 0.1 ppm. The FO experiments were performed by facing the active layer to the draw solution. The draw and feed solutions were circulated through the FO test cell with a flow rate of 650 ml/min using respective water pumps, and the outlet from the FO test cell was recirculated back to individual solution tanks. 1M NaCl was used as a draw solution, while DI water was used as a feed solution. The feed and draw solutions in the respective tank were maintained at room temperature of 25ºC using temperature regulators. The water flux was calculated by measuring the change in weight of the draw solution tank. The feed & draw tank was sealed entirely throughout the process with a parafilm sheet to avoid evaporation loss from feed and draw solution tanks.

TH-3195_186151006

The water flux (Jv) was calculated by using equation 1:

$$J_v = \left(\frac{\Delta V}{A \times \Delta t}\right) \quad 1$$

$$\Delta V = V_{D_{at,t=0}} - V_{D_{at,t=\Delta t}} \quad 2$$

where ΔV was the change in volume of draw solution (l) with time Δt (hrs.), and A was the active membrane we (m^2). The SI unit of water flux has been used throughout the manuscript and denoted as (L m^{-2} h^{-1})

Similarly, the reverse solute flux was measured using measured NaCl concentration and volume in the feed tank with respect to time. The SI unit of reverse solute flux has been used throughout the manuscript and denoted as (g m^{-2} h^{-1}).

The reverse solute flux (J_s) was calculated using equation 3:

$$J_S = \frac{C_{F_{at,t=0}} V_{F_{at,t=0}} - C_{F_{at,t=\Delta t}} V_{F_{at,t=\Delta t}}}{A \times \Delta t}$$

3

Where, $C_{F.\ at\ t=0}$ was the concentration of feed tank at time = 0, $C_{F.\ at\ t=\Delta t}$ was the concentration of feed tank at time = Δt, $V_{F.\ at\ t=0}$ was the volume of feed tank at time = 0, $V_{F.\ at\ t=\Delta t}$ was the volume of feed tank at time = Δt. Both J_v & J_S was the average of triplicate measurements.

The specific reverse solute flux (SRSF) was calculated by dividing the RSF with the water flux using equation 4.

$$SRSF = \frac{Js}{Jv} \quad 4$$

Where J_s was the reverse solute flux (g m^{-2} h^{-1}), *Jv* was the water flux (L m^{-2} h^{-1})

TH-3195_186151006

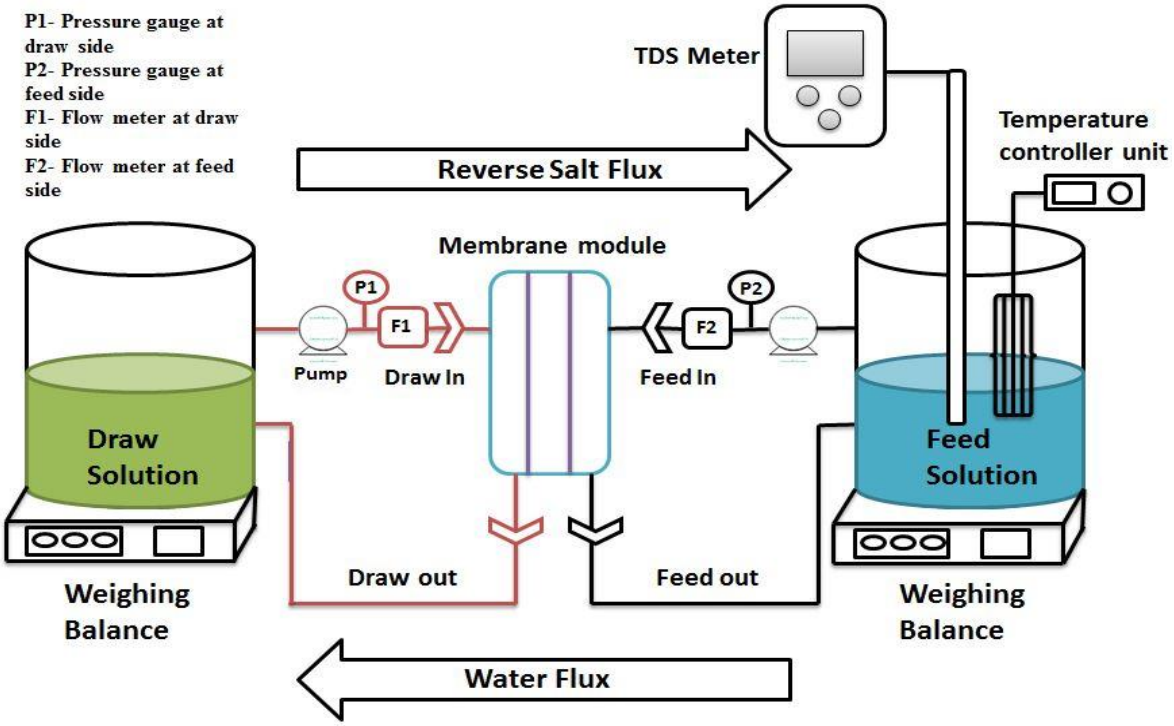

Fig. 5: Schematics of FO experimental setup used for evaluating the performance of rGO membrane and PSS-rGO membrane (active membrpane surface area ~4 cm^2)

3.4 Results and Discussions

3.4.1 Characterization of GO flakes

As discussed in the experimental section 3.2.1, the GO sample prepared by modified Hummer's method was separated into three categories based on different flakes dimensions as SF, MF, and LF. The digital photos of the aqueous dispersions of the samples of different flake size ranges are shown in Fig. 6a. With decreasing average flake sizes, the color of the GO dispersion gradually changed from dark brown to light brown. Different GO flake size dispersion of 0.1 g/L concentration was individually drop-cast on freshly prepared silicon wafers by dropping 4 µl of the solutions to examine their nanoscale morphology in FESEM and AFM. The nylon membranes coated with GO flakes of different sizes (LF, MF, and SF), 1mg of loading are shown in Fig. 6b. The rGO-coated membranes obtained after the thermal reduction of the

TH-3195_186151006

respective GO coated nylon membrane can be observed in Fig. 6c. The color of the rGO membrane changed from dark brown to black color due to the partial elimination of functional groups like epoxy, carboxyl, and hydroxyl groups[153]. Once the conditions were optimized for coating GO on the nylon support layer, the PSS solution was coated on the optimized rGO-coated membrane to fabricate the PSS-rGO membrane.

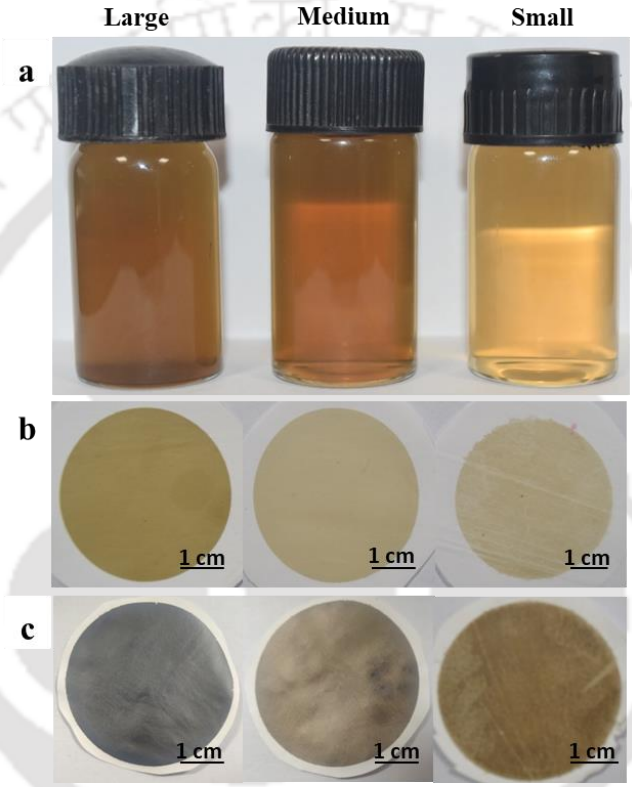

Fig. 6: Digital photos of (a) GO dispersion of different flake sizes, (LF, MF, and SF from left to right), (b) nylon membranes coated with GO flakes of different sizes-ranges (LF, MF, and SF), 1mg of loading, and (c) rGO coated membranes obtained after thermal

The height and lateral dimensions of segregated different-sized GO flakes were analysed using AFM analysis. Fig. 7a reveal the FESEM analysis of large-sized graphene oxide flake (5 µm) obtained via the modified Hummer method. Fig. 7b-d show the lateral dimensions and height for LF, MF, and SF single flakes, respectively. The lateral dimension for LF, MF, and SF was

TH-3195_186151006

3 µm, 1.5 µm, and 0.6 µm, respectively, as evident from AFM images. The average height of GO flakes (large, medium, and small) was found to be in the range of ~3-1 nm.

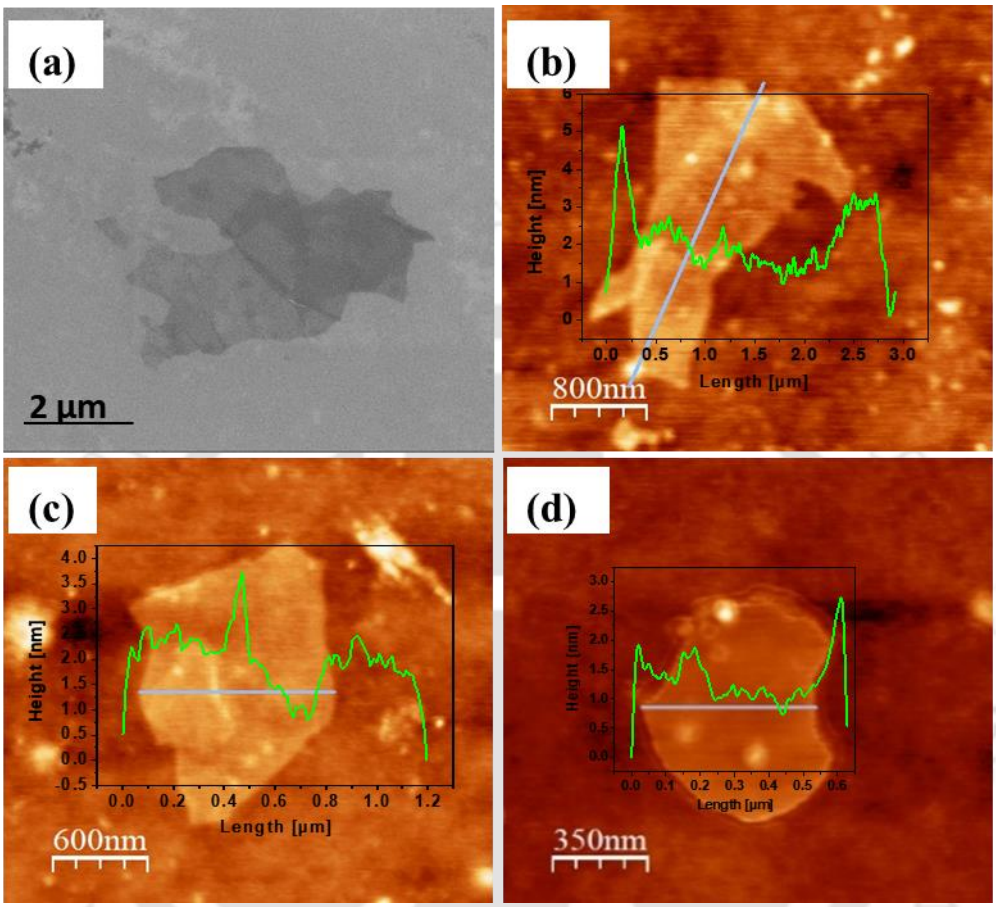

Fig. 7: (a) FESEM image of large-sized GO flake; AFM analysis of LF, MF, and SF with corresponding height profile (b) large-sized GO flake (c) medium-sized flake (d) small-sized flake

3.4.2 FESEM images of fabricated membranes

Fig. 8a show the surface morphology of the used flat sheet nylon microfiltration membrane. It illustrates micro-void space in overlapped sponge-like morphology with large pores of 0.22 µm. The surface morphology of the GO membrane in Fig. 8b shows a uniform deposition of GO flakes on the nylon membrane surface, entirely covering the void spaces of the support layer with few thin shallow cracks appearing on the outer surface of the GO coating. After

TH-3195_186151006

thermal annealing, the presence of small cracks and a grain-like structure of size around 2-3 nm was noticed on the surface of the uniformly deposited rGO layer (see Fig. 8c). The cracks on the GO layer appeared slightly denser than the rGO layer; this must-have happened due to the heat treatment process. The FESEM images revealed that vacuum filtration of the PSS solution smoothens the surface of the rGO membrane coated on the nylon support layer (see Fig. 8d). However, a few shallow cracks were still visible on the PSS-coated surface. The pore coverage by GO deposition on the nylon membrane was further confirmed through the cross-sectional FESEM examination of the rGO membrane on nylon support (see Fig. 8e). The thickness of the rGO layer loaded with 1 mg large GO flakes in 4 cm^2 membrane was calculated using cross-sectional FESEM analysis and was found to be ~1 µm (see Fig. 8f). The same was also confirmed by comparing the thickness of the rGO coated nylon membrane with that of a pristine nylon membrane (100 µm) by using an electronic micrometer.

TH-3195_186151006

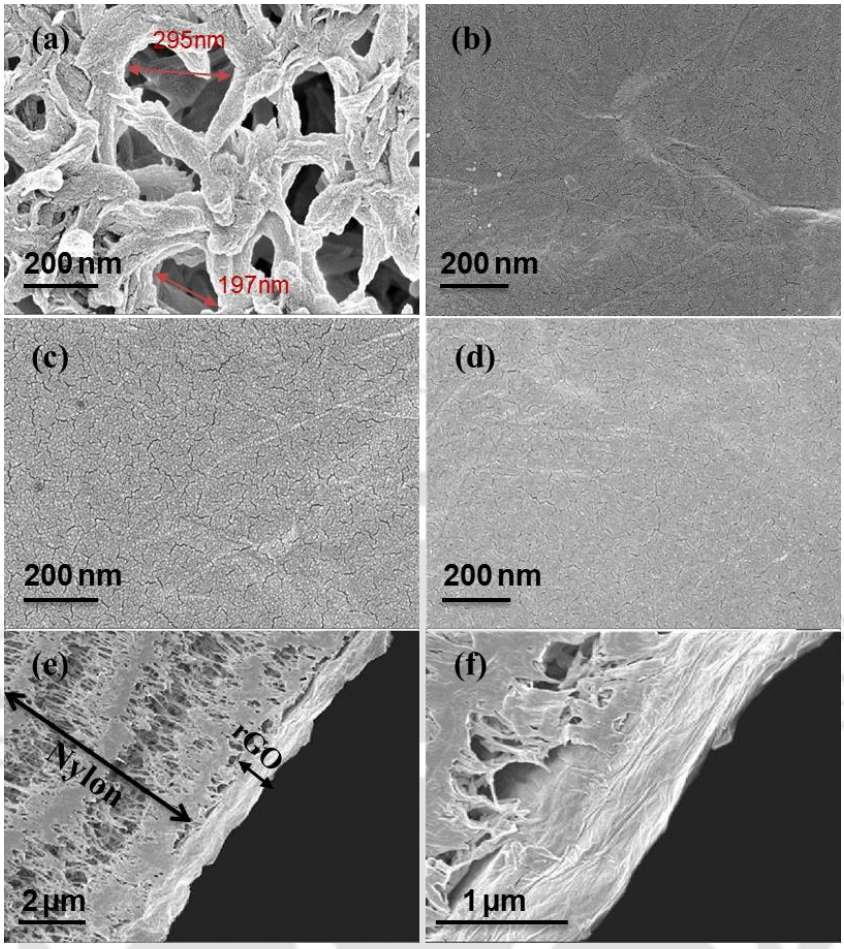

Fig. 8: FESEM image of (a) nylon substrate; surface morphology of (b) GO membrane (c) rGO membrane (d) PSS doped rGO membrane (e) cross-section of rGO membrane on nylon support (f) rGO layer at a higher resolution

3.4.3 EDX analysis of the fabricated membranes

Fig. 9a-d show the EDX analysis of the GO, rGO, PSS-GO, and PSS-rGO coated nylon membranes. The study shows that the C/O ratio in the rGO membrane has increased to 3.79 from 2.35 in the GO membrane. This increment can be attributed to the partial loss of some oxygen-containing functional groups in the rGO layer due to thermal reduction. The increase in sulfur content from 0.4 wt% to 3.7 wt% after PSS doping on GO membrane and 3 wt% on the rGO membrane confirms the coating of the PSS. Similarly, the oxygen content was found

TH-3195_186151006

to be reduced for rGO (from 29.7 wt% to 20.8 wt%), and PSS-rGO (from 27.3 wt% to 19.3 wt%) post thermal reduction.

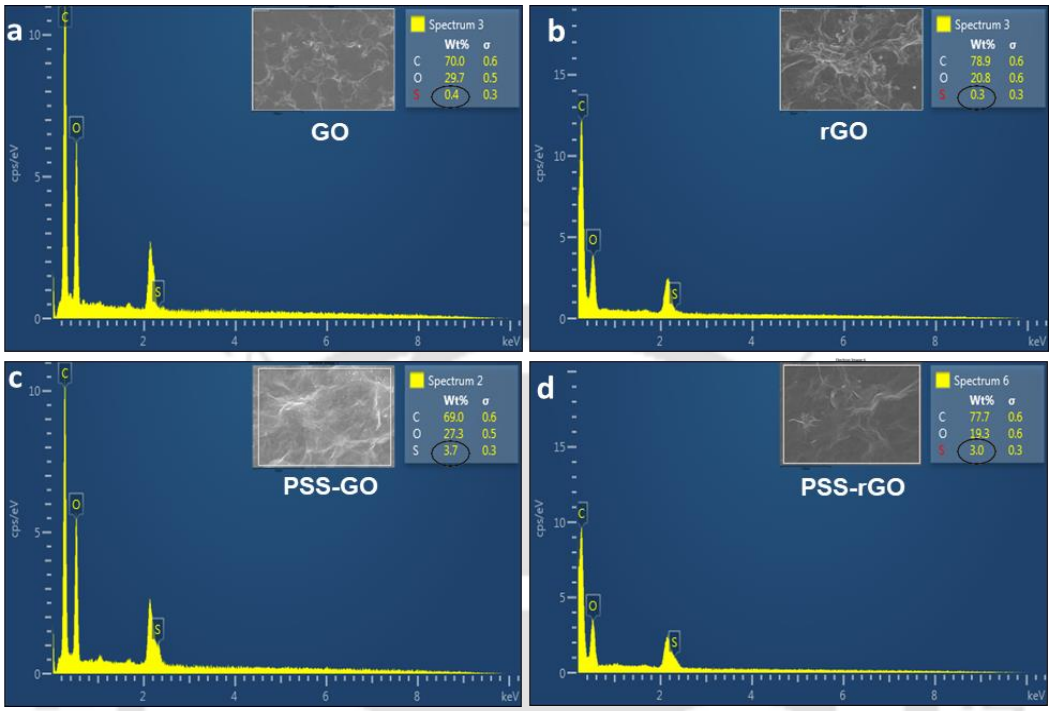

Fig. 9: EDX analysis for (a) GO membrane (b) rGO membrane (c) PSS-GO membrane and (d) PSS-rGO membrane

3.4.4 XRD, FTIR and contact angle analysis of the fabricated membranes

The interlayer spacing of the nanochannels between GO layers was calculated by determining the d-spacing from XRD characterization. Fig. 10a show the XRD pattern for GO, rGO, and PSS-GO membranes. The GO membrane exhibited a sharp peak at 10.2° with a corresponding d-spacing of 9Å, which was consistent with the previous study[154]. Upon heat treatment, the position of the XRD reflection changed to 11.2°, which corresponds to an interlayer spacing of 7.7Å. The slight shift in the interlayer spacing was also attributed to the partial removal of the functional groups by the heat treatment process at 150 °C. Further functionalization of PSS showed a negligible change in d-spacing, which indicates that the sulfonated acid group had

TH-3195_186151006

no effect on the crystal structure of GO. In principle, a uniform coating of reconstructed 2D GO flakes with smaller interlayer space should possess better salt-rejection efficiency.

Fig. 10b shows the FTIR spectrogram for GO coated on the nylon substrate, rGO membrane, and PSS-GO membrane. The peaks at 3390 cm^{-1}, 1720 cm^{-1}, 1570 $cm^{-1,}$ and 1060 cm^{-1} correspond to OH, C=O, C=C, and C-O functional groups, respectively[155]. After thermal reduction (rGO membrane), the broad peaks for the OH stretching at 3410 cm^{-1} and C=O stretching at 1720 cm^{-1} were completely removed. While the peak intensity for other functional groups (C=C) was diminished in magnitude as compared to GO membrane confirming the partial removal of oxygen-containing groups due to the annealing process. Further functionalization with PSS exhibits a peak at 790 cm^{-1}, which corresponds to the aromatic ring and additional peaks at 1050 cm^{-1} and 1100 cm^{-1} corresponding to the sulfonated acid group[156].

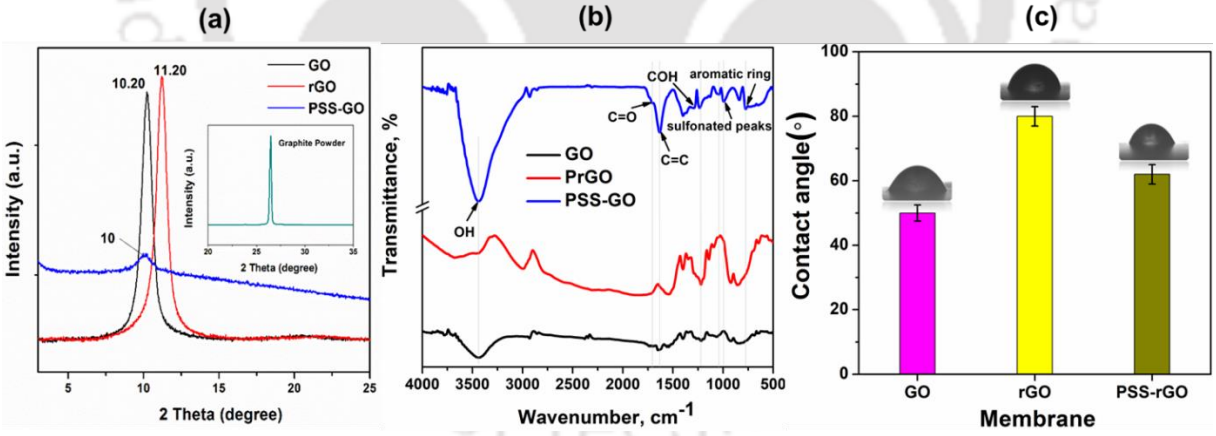

Fig. 10: (a) XRD analysis of GO/Nylon, rGO and PSS-GO membranes (inset shows XRD of graphite powder), (b) FTIR spectra of GO membrane, rGO membrane, and PSS-GO membrane and (c) contact angles of GO membrane, rGO membrane and PSS-rGO membrane

Fig. 10c shows the water contact-angles of GO, rGO, and PSS-rGO membranes. The water contact-angle for GO coated membrane before the thermal reduction was found to be 50°. The

TH-3195_186151006

contact-angle for thermally reduced rGO membrane increased to 80°. The contact angle must have increased due to partial removal of hydrophilic functional groups (i.e., carboxyl, epoxy, and hydroxyl groups), and hence exhibited reduced hydrophilicity. However, the rGO membrane still had some GO content as the contact angle was less than 90°. Interestingly, the deposition of the PSS drastically reduced the contact angle to 62°. The decreased contact angle (or strong hydrophilicity) of the PSS-rGO membrane compared to the rGO membrane can be attributed to the higher surface energy of the sulfonic groups[157]. Membranes with such high surface energy should be ideal for FO applications.

3.4.5 Effect of heating conditions on membrane performance

The membrane processing temperature and heating time were optimized to achieve the desired GO reduction and annealing of rGO on the nylon substrate. The membranes were fabricated at different temperatures (130 °C, 150 °C, and 180 °C) with fixed heating time (2 hrs.) and then with different heating time (1, 2, 2.5, and 3 hrs.) at a constant temperature of 150 ºC.

The process temperature was expected to control the GO reduction rate, and the time of heating was expected to enable better binding between nylon and rGO. Before optimizing temperature and heating time, original GO dispersion (mixed flakes) of 1mg/ml concentration was coated on the nylon membrane with constant GO loading to achieve ~1µm GO layer thickness. The GO coated membrane was then heated at different temperatures (130 °C, 150 °C, and 180 °C) for a fixed duration of 2 hrs. The membranes fabricated at different temperatures were then tested for its efficiency in a FO process experimental setup for 2 hrs duration (see section 3.3.4). During the FO experiment, both water and reverse solute flux decreased at a different ratio, with an increase in reduction-temperature for membrane fabrication. The water flux reduced with an increase in membrane fabrication temperature. The reduction of GO on heating, which narrowed the nanochannels for water passage, must have led to the decline in water flux. The

TH-3195_186151006

RSF values also simultaneously decreased with an increase in temperature due to narrower inter-layer spacing distance between nanosheets. Although RSF was found to be constant for 150 °C and 180 °C, the water flux was a little higher for 150 °C (see Fig. 11a). Therefore, 150 °C was considered as the optimum temperature for the next level of experiments.

Once the heating temperature was fixed at 150ºC, the rGO membranes were fabricated by varying heating time (1, 2, 2.5, and 3 hrs.) and evaluated for performance efficiency. It was noticed that with the increase in the heating period, the rGO membrane exhibited a decline in the water flux as well as the RSF (see Fig. 11b). Since, with every 1-hour increment of the heating period, the GO gets slightly reduced further, resulting in narrower GO nanochannels, which hinder the water flow as well as salt ions. However, when the membrane was heated for 3 hrs duration, there was a sudden rise in RSF, which indicates probable damage to the membrane layer when heated at high temperature for a longer-term. The RSF was higher for corresponding water flux for rGO membranes fabricated at 1, 1.5, 2 hrs of the heating period. The best possible result in terms of RSF was obtained at the heating time of 2.5 hrs at 150 °C. Hence, the optimum temperature and heating period for the rGO membrane fabrication were fixed at 150 °C and 2.5 hours, respectively.

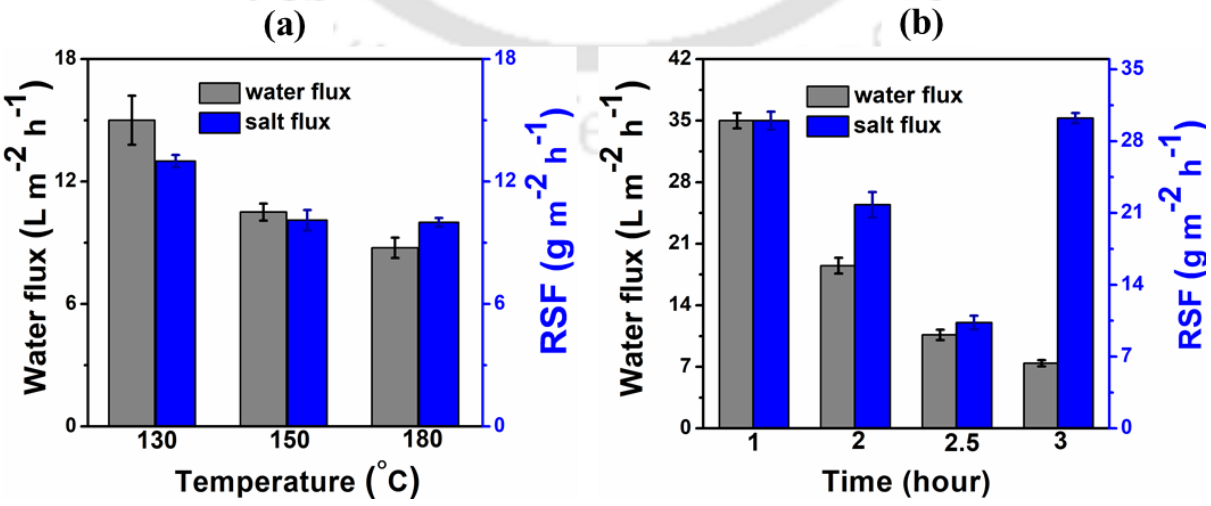

TH-3195_186151006

Fig. 11: Water flux and RSF profile with time for rGO membranes prepared with 1 µm thickness at (a) constant heating time (2 hrs.) with variable temperature (b) constant heating temperature (150ºC) with variable heating time

3.4.6 Effect of GO flake-size and thickness on membrane performance

The rGO membranes prepared using different size-range GO flakes were tested for their performance in a FO process setup. The rGO membranes with different amount of GO loading (i.e., 1, 2, and 5 µm thickness) were used to evaluate the rGO membrane performance. Fig. 12a-b show the water flux and RSF profile with respect to rGO thickness and flake size. The highest water flux was observed for SF (36 L m^{-2} h^{-1}) followed by MF (26.3 L m^{-2} h^{-1}), and then LF (19 L m^{-2} h^{-1}) coated rGO membrane. However, the RSF was also higher (150 g m^{-2} h^{-1}) in the case of membranes coated with SF. While the RSF decreased for both MF (5.5 g m^{-2} h^{-1}) and LF (4.2 g m^{-2} h^{-1}) coated rGO membranes. The decrease in interlayer space, together with the reduction in flake size, creates a low-friction hydrophobic channel in-between the GO layers, which assist in the movement of water molecules[158] and hence comparatively high water and reverse solute flux was observed in SF coated membrane. For the rGO membrane coated with LF, when loading was increased, the water flux decreased from 19 L m^{-2} h^{-1} to 8.6 L m^{-2} h^{-1} while for membrane coated with MF, the water flux dropped from 26.3 L m^{-2} h^{-1} to 11.2 L m^{-2} h^{-1}. However, for rGO membranes coated with SF, the water flux comparatively declined more from 36 to 12.5 L m^{-2} h^{-1}. Similarly, an increment in GO loading resulted in low RSF for the rGO membrane coated with LF (dropped from 4.2 g m^{-2} h^{-1} to 3 g m^{-2} h^{-1}) and MF (dropped from 5.5 to 3.7 g m^{-2} h^{-1}). This was due to the stacking of more GO flakes on top of each other, which provided higher resistance to water and salt ions to pass through it. However, for rGO membranes coated with SF, the RSF decreased drastically (~77%) from 150 to 33.4 g m^{-2} h^{-1}. This must-have happened due to the non-uniform deposition of SF for 1ml loading of

TH-3195_186151006

GO. Since the size of small GO flakes (0.4-0.8µm) was comparatively in the same range of nylon-membrane support pore size (~0.220 µm). However, as the loading of small-sized GO solution was increased to 2 ml and 5 ml, more GO flakes were deposited, which resulted in the uniform coating, thus reducing the RSF to 72.4 g m^{-2} h^{-1} and 33.4 g m^{-2} h^{-1}, respectively. The lowest salt flux (3 g m^{-2} h^{-1}) was observed for the rGO membrane with large-sized GO flakes and with 5 ml loading. The rGO membrane exhibited low SRSF for MF (0.2 g/L), and LF (0.22 g/L) in comparison to SF (4.16 g/L) with 1 ml GO loading (see Fig. 12c). With the increment in GO loading from 1 to 2 and 5 µm, the SRSF for SF coated rGO membranes decreased by 12% and 35%, respectively. However, the SRSF increased for both MF (by 36% for 2 µm and 54% for 5 µm), and LF (by 45% for 2 µm and 60% for 5 µm) coated rGO membranes. This is due to the drastic reduction of RSF values than water flux of SF compared to MF and LF while increasing the GO loading. Therefore, based on the permeation and SRSF results, the optimized condition for rGO membrane fabrication for high selectivity and water permeability would be coating with medium-sized GO flakes with a GO loading of 1µm thickness. The water transport mechanism in different sized GO flake layers was determined by measuring the offset distance between two inter-layers spacing, shown in Fig. 12d-f. In large-sized GO flakes, the offset distance was comparatively higher than medium and small-sized GO flakes. Due to this reason, the water transport through large-sized GO flake layer tends to be relatively time-consuming and hence results in low water flux compared to medium and small-sized GO flake membranes. Therefore, the least water flux was observed in membranes with large-sized GO flake membranes. Similarly, the reverse solute flux also tends to increase with the decrease in offset distance between two graphene layers.

TH-3195_186151006

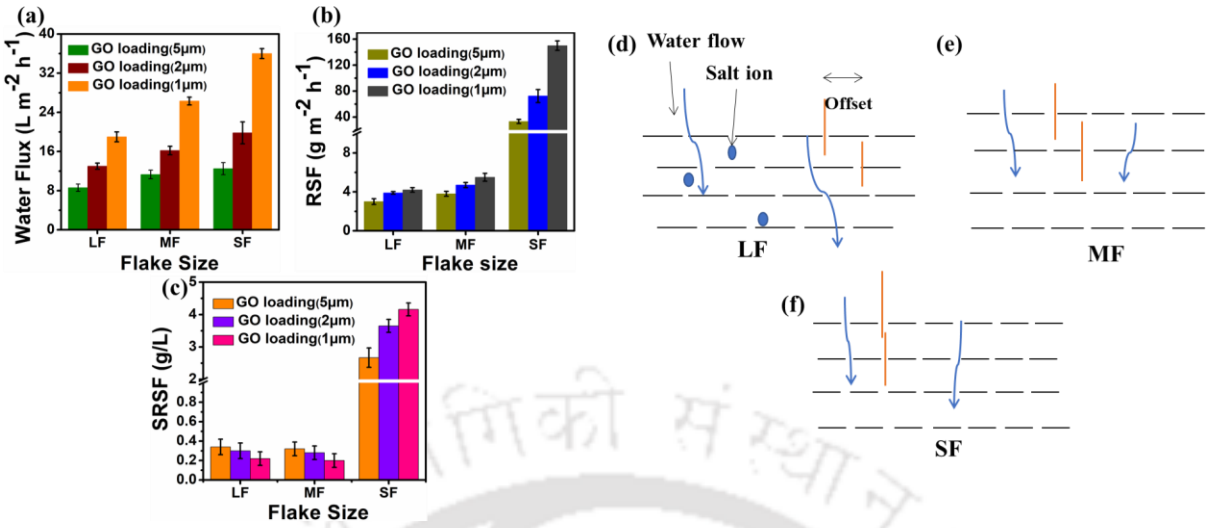

Fig. 12: (a) Water flux with LF. MF, and SF (b) RSF with LF, MF, and SF at different GO loading (5μm, 2 μm, and 1μm thickness) (c) specific reverse solute flux (SRSF) with LF, MF, and SF at different GO loading; Schematic illustration of water transport for (d) large-sized GO flakes layer (e) medium-sized GO flakes layer and (f) small-sized GO flake layer

3.4.7 Effect of PSS coating on the rGO membrane performance

Fig. 13a-c show the comparative performance of the rGO membrane and the PSS-rGO membrane in the FO process. The sulfonic group (SO_3H) present in PSS helps in improved water permeation properties as they assist in hydrogen bonding with water molecules[159]. The higher water flux was attributed to the large surface energy of the sulfonic acid group (SO_3H) (i.e., 25.1 L m^{-2} h^{-1}, 34 L m^{-2} h^{-1}, and 47.2 L m^{-2} h^{-1} for LF, MF, and SF, respectively) as compared to rGO membranes. Moreover, the XRD pattern reveals the interlayer d-spacing of the rGO membrane to be 7.7 Å, which was bigger than the kinetic diameter of water (~ 0.29 nm). Hence, the water molecules can easily pass through the membrane. However, the RSF for PSS incorporated membrane was almost the same as compared to rGO membranes (5 g m^{-2} h^{-1} for LF, 6.8 g m^{-2} h^{-1} for MF, and 162.2 g m^{-2} h^{-1} for SF). The hydrated sizes of Na^+ (0.72 nm) and Cl^- (0.66 nm) were in the same range of the interlayer d-spacing of rGO membrane[160].

TH-3195_186151006

Therefore, the flow of hydrated ions was restricted by the confinement of the rGO nanofluidic channels. Due to this reason, the PSS-rGO membrane exhibited even lower SRSF than the rGO membrane. With the addition of PSS, the SRSF further decreased to 9% for LF (0.20 g/L), 10% for MF (0.18 g/L) and 17.5% for SF (3.43 g/L) for 1µm thickness. The obtained results concluded that the medium-sized GO flake coated membrane doped with PSS showed the best possible performance compared to other flake sizes.

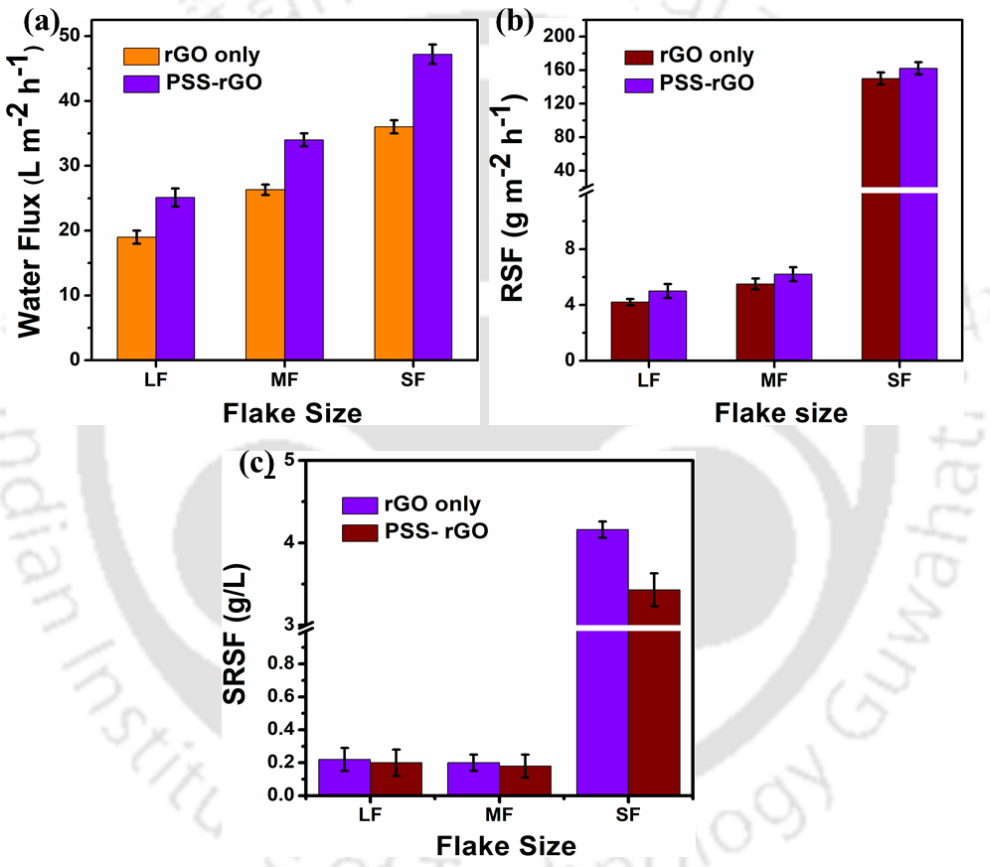

Fig. 13: (a) Comparative water flux with LF, MF, and SF for rGO and PSS-rGO membrane (b) Comparative RSF with LF, MF, and SF GO flakes for rGO and PSS-rGO membrane (with GO loading of 1µm thickness) (c) Comparative SRSF with LF, MF, and SF GO flakes for rGO and PSS-rGO membrane

TH-3195_186151006

3.4.8 Comparative performance analysis and stability test

For comparison of performance analysis, a commercial CTA-FO membrane was also operated under similar conditions. Since it was earlier observed that the MF-coated membrane provided the best performance for the FO process. In this case, only MF-coated membranes were used for comparing the membrane performance. Fig. 14a shows the water flux across each membrane, where the rGO membrane was seen to achieve a higher water flux (26.3 LMH) than the commercial CTA-FO membrane (7 LMH). Moreover, the water flux for the PSS-rGO membrane is found to be further higher by around five times (34 LMH) when compared to the CTA-FO membrane (7 LMH). Fig. 14b-c shows the RSF and SRSF values for the PSS-rGO and CTA-FO membrane. In contrast to water flux, the RSF values for rGO (5.5 gMH) and PSS-rGO membrane (6.2 gMH) was always lower than the CTA FO membrane (8.7 gMH). All the values reported are the average of three measurements for an initial 2 hrs of operation. The SRSF value for the PSS-rGO membrane was the lowest (0.18 g/L), followed by the rGO membrane (0.20 g/L) and the commercial CTA FO membrane (1.2 g/L). Though the RSF values of rGO and PSS-rGO membranes were almost the same, the difference between their water flux made a huge impact in distinguishing the SRSF values, which is termed as an essential factor for determining the best FO membrane.

The stability performance of rGO and PSS-rGO membranes coated with medium-sized GO flake, and CTA-FO membrane was evaluated for 24 long hours until it attained saturation. Initially, both PSS-rGO and rGO membranes exhibited a water flux of 33 LMH and 25 LMH, respectively, for the first 2 hrs of operation (see Fig. 14d). Though there was a decline in water flux for both membranes with increasing operation time, the PSS-rGO membrane exhibited comparatively high water flux (22.5 LMH) even after one day of continuous operation. In comparison, the rGO membrane showed relatively very less water flux (14 LMH) after

TH-3195_186151006

attaining saturation. Similarly, the PSS-rGO (6.5 gMH) and rGO (5.8 gMH) membranes exhibited low RSF in comparison to the CTA-FO membrane (8.5 gMH) for the initial period of operation. However, with the increase in operation time, the RSF increased gradually with time and reached saturation (see Fig. 14e). Upon reaching saturation (around 24 hrs), it was found that water flux of PSS-rGO was 1.5 times higher than the rGO membrane also the RSF value of the PSS-rGO membrane (26.8 gMH) was lower by ~22% than rGO membrane (35.8 gMH). However, the RSF value for the CTA-FO membrane remained more or less constant with a slight increment (12-15%) for the early 10 hours of operation. The presence of sulfonic groups in the PSS-rGO membrane resulted in electrostatic repulsion, which helped to lower the RSF values than the rGO membrane.

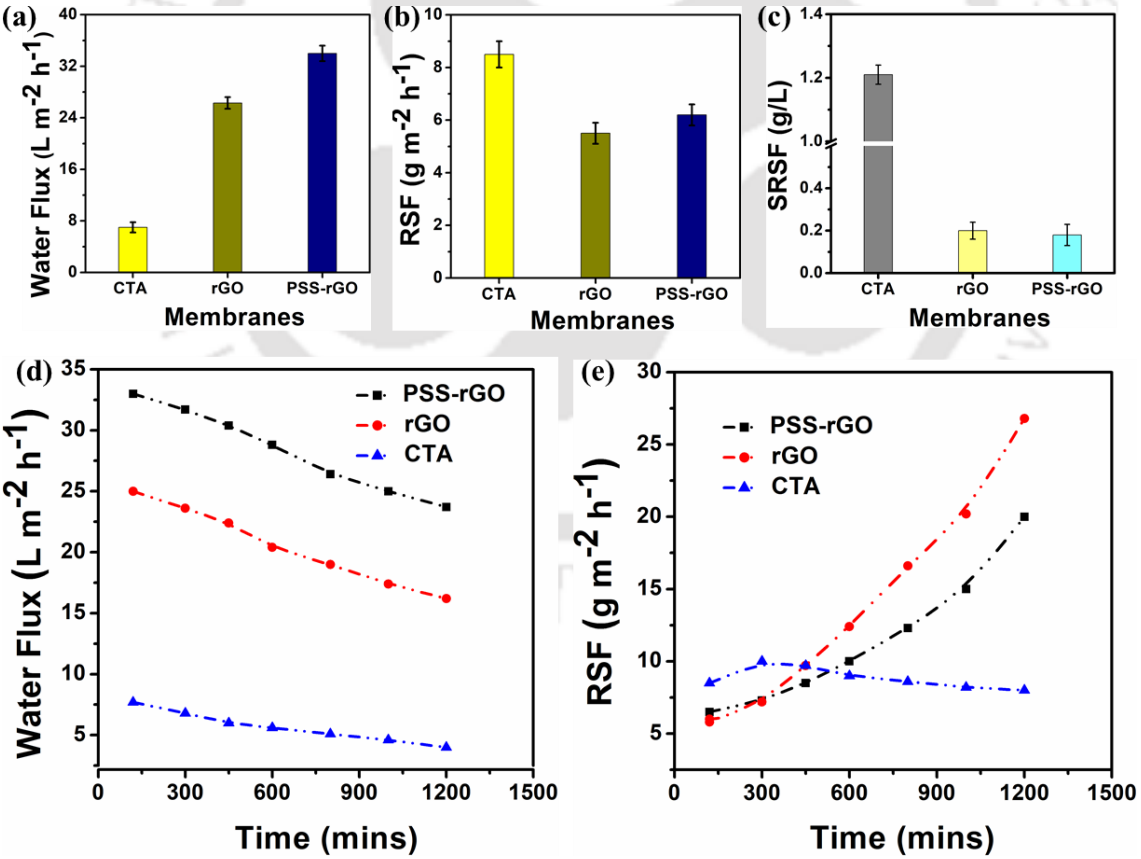

Fig. 14: Comparative study of (a) water flux with only MF for CTA-FO, rGO and PSS-rGO membranes (b) RSF with only MF for CTA-FO, rGO and PSS-rGO membranes (c) SRSF with

TH-3195_186151006

MF for CTA-FO, rGO, and PSS-rGO membranes; Stability test for the PSS-rGO, rGO and CTA membranes for (d) water flux vs time (e) RSF vs time; FESEM images of the PSS-rGO membranes for life cycle (f) after 2 hrs, (g) after 6 hrs, (h) after 24 hrs

3.5 Summary

In this study, GO coated membranes were fabricated via a simple vacuum filtration method followed by thermal reduction on nylon support. In the early stage, the effect of GO-flake size and process parameters (i.e., temperature and heating-time) were evaluated on membrane performance for FO-based operation. Size fractionation of GO flakes revealed medium-sized flakes with 1µm thickness exhibited the best possible outcome for optimized FO performance. Increment of GO loading in the SF coated membrane showed a reduction of SRSF value due to a drastic decrease in water flux and RSF values simultaneously. In contrast, LF and MF coated membrane showed an increase in SRSF values due to a relatively smaller decrease in water flux and RSF values. The optimum temperature and heating period for the rGO membrane fabrication were found to be 150 °C and 2.5 hours, respectively. The membrane properties were further enhanced via the addition of the PSS layer over rGO coated membranes. The performance analysis and stability test revealed that the PSS-rGO membrane was giving better performance than the rGO and CTA-FO membrane in terms of higher water flux and low SRSF values. These results confirm that GO flake sizes, temperature, and heating duration can manipulate the membrane properties and holds a pivotal influence in its FO performance. The incorporation of the PSS layer on the fabricated rGO membrane further enhanced its FO performance. This study established the excellent potential of PSS doped rGO membrane for application in FO based separation process, which has immense potential for use in desalination and wastewater treatment.

TH-3195_186151006

TH-3195_186151006

CHAPTER 4

4 Synthesis and performance evaluation of sericin doped reduced graphene oxide membrane for FO based membrane crystallization application

Abstract: This chapter reports the application of a hydrophilic natural protein named sericin as the doping material to r-GO-based dense layer to solve the trade-off between permeability and selectivity of FO membranes, and demonstrates the antibiotics recovery process using crystallization concept.

This part of the thesis is published in Journal of Membrane Science. 660 (2022) 120884. (https://doi.org/https://doi.org/10.1016/j.memsci.2022.120884).

TH-3195_186151006

4.1 Introduction

Antibiotics are comprised of a significant number of pharmaceutical compounds that can be used as human and veterinary treatment[161]. In recent years, the presence of pharmaceutical compounds in wastewater effluents have garnered a lot of attention as emerging contaminants. The isolation of these antibiotics from the fermentation broth using the membrane technology has gained importance due to its various advantages over traditional separation processes[162]. Among such antibiotics, rifaximin, is a semi-synthetic and non-absorbable antibiotic that is used to treat traveller's diarrhoea and hepatic encephalopathy[163]. It is reported that forward osmosis[41] and membrane distillation[164] processes are the two technologies that can be used to concentrate the pharmaceutical traces at lower energy consumption. The low temperature conditions in MD process can yield the recovery process, which in turn reduces the water flux as the temperature is the driving force, hence not economically feasible. However, in the FO process, increasing the draw solution concentrations can simultaneously increase the water flux and concentrate the resources to its crystallization point without compromising the energy consumption. The feed crystallization process can be achieved by processing the feed stream into multiple series connection. Hence, the FO-based crystallization process is a suitable process for low-temperature crystallization application.

The practical utility of a FO process depends on the suitability of FO membrane. An ideal FO membrane should possess properties like high water flux, low SRSF, low fouling and low ICP effect. However, the commercial FO membranes lack some of these properties which limit their practical usage[165]. Recently, researchers have focused on the modification of membrane surface with suitable nanomaterials for improving water flux and better fouling mitigation[143,166]. The incorporation of the nanomaterials not only enhances the water permeability and anti-fouling properties, but also increases the chemical and mechanical

TH-3195_186151006

strength. Hegab et al.[167] developed a composite TFC FO membrane by incorporating polydopamine onto GO nanosheets. The fabricated membrane improved the water flux and reverse solute flux compared to unmodified membrane by 21.5% and 80%, respectively. Moreover, the surface morphology and smoothness of the membrane are improved, thus enhancing the biofouling resistance. Unfortunately, these membranes exhibit moderate water flux and fouling resistance without the long-term stability performance. Therefore, incorporation of more than two hydrophilic nanomaterials with multifunctional groups can facilitate better fouling mitigation, more water flux and improved stability performance without compromising the cost of production [[168].

In recent decades, GO has been widely explored as active layer of the FO membrane due to its nano-scale thickness, high hydrophilicity and better anti-fouling properties[169]. However, due to its hydrophilic nature, the membrane swells in the aqueous solution and disintegrates which limits its mechanical and chemical durability. The annealing process of rGO membrane results in decrease of the inter-layer spacing between two nanosheets, thus increasing the stability and salt rejection rate, but at the cost of water permeability. Therefore, systematic investigation of doping various materials onto the rGO layer are required to overcome the trade-off between water permeability and selectivity without compromising the mechanical durability of the membrane.

4.2 Scope of this investigation

The primary objective of this study is to investigate the effectiveness of the sericin-doped rGO membranes for antibiotic recovery using FO-based membrane crystallization process. The isolation of antibiotics from the fermentation broth using a low-temperature membrane separation technology has gained importance due to its numerous advantages compared to the traditional separation and purification processes. Hence, the FO-based membrane

TH-3195_186151006

crystallization process could be an ideal tool for the low-temperature crystallization process. However, the practical utility of the FO process in critical applications like desalination, resource recovery, and wastewater treatment relies on the availability of robust, effective, and fouling-resistant FO membranes. Therefore, this study incorporates sericin, a silk protein with excellent biocompatibility and hydrophilicity, into the rGO membrane matrix, to enhance its FO performance in terms of water flux, selectivity, and crystal formation efficiency. Moreover, the fouling propensity of the fabricated sericin doped rGO membranes drastically reduces due to the anti-fouling properties of sericin, thus increasing the life cycle of the FO membrane. The findings of this research can provide valuable insights into the FO-based membrane crystallization application by enabling fouling-resistant energy efficient operation.

4.3 Experimental section

4.3.1 Theory

A mathematical model of the FO process was used to estimate membrane transport parameters, and it was developed by combining membrane transport and concentration polarization model equations. The water flux (J_w, $L\ m^{-2}\ h^{-1}$) and solute flux (J_s, $g\ m^{-2}\ h^{-1}$) across the membrane was represented by solution diffusion (SD) model in equations 5 and 6.

$$J_w = L_p\left[\left(\pi_{dm,NaCl} - \pi_{fm,NaCl}\right) - \left(P_d - P_f\right)\right] \quad 5$$

$$J_{s,NaCl} = B\left(C_{dm} - C_{fm}\right) \quad 6$$

where, the L_p, B, P_d, and P_f represents the pure water permeability coefficient ($L\ m^{-2}\ h^{-1} bar^{-1}$), solute (NaCl) permeability coefficient ($L\ m^{-2}\ h^{-1}$), and transmembrane pressure (bar) between DS and FS, respectively. The π_{dm}, π_{fm}, $C_{dm}$and C_{fm} represents the osmotic pressure

TH-3195_186151006

and concentration at the active layer of the membrane surface on the draw and feed sides, respectively. Here, the osmotic pressure (π, *bar*) was calculated using van't hoff equation.

In the given study, the experiments were conducted using ALDS (or PRO-mode). The steady state solute mass balance equations for the DECP (dilutive external concentration polarization) and CICP (concentrative internal concentration polarization)[170], were as follows in equations 7 and 8.

$$C_{fm} = C_{fb} \exp\left[J_w\left(\frac{1}{k_f} + \frac{S}{D}\right)\right] + \left(\frac{J_s}{J_w}\right)\exp\left[J_w\left(\frac{1}{k_f} + \frac{S}{D}\right)\right] - 1 \quad (7)$$

$$C_{dm} = \left(\frac{J_s}{J_w}\right)\exp\left[\left(\frac{-J_w}{k_d}\right) - 1\right] + C_{db}\exp\left(\frac{-J_w}{k_d}\right) \quad (8)$$

where, C_{fb}, C_{db}, C_{fm}, and C_{dm} represents the concentration ($g\ L^{-1}$) of the FS and DS at bulk and on the membrane surface, respectively. The k_f, and k_d represents the mass transfer coefficient ($m\ h^{-1}$) for the FS and DS, respectively. The S and D represent the structural parameter (nm) and diffusion coefficient ($m\ h^{-2}$).

4.3.2 Synthesis of GO nanosheets

GO was prepared by following modified Hummer's method. Typically, 250 mg of graphite and 1.5 g of $KMnO_4$ were slowly added into 12 ml of H_2SO_4 solution in an ice bath under continuous stirring conditions. The solution was then transferred into a water bath maintained at 35 °C. After 2 hours, the solution was transferred back to the ice bath and 100 ml of deionized (DI) water was added very slowly, maintaining the temperature below 30 °C. Which was followed by dropwise addition of H_2O_2 solution (10 ml). The addition of H_2O_2 changed the color of the solution from black to light yellow. The solution was repeatedly washed with HCl solution (20 wt.%, 500 ml) through filtration. After washing with HCl, the GO sample was

TH-3195_186151006

dried in a desiccator followed by washing with excess acetone. An aqueous dispersion of thus prepared GO (1 mg/ml) was centrifuged for 10 minutes (at 2000 rpm) to separate the large aggregates and the supernatant solution was preserved for further experiments.

4.3.3 Preparation method of sericin solution

The commercially available sericin powder (600 mg) with a molecular weight of 50~250 KDa was added to 30 ml DI water (20 mg/ml concentration) and stirred for 10 mins.

4.3.4 Fabrication of GO membrane

GO membrane was fabricated by using the vacuum filtration method. An aqueous 30 ml GO dispersion of 0.033 mg/ml concentration was vacuum filtered onto a nylon membrane (pore size 0.22 µm).

4.3.5 Facile fabrication of sericin doped r-GO membranes (S-r-GO and r-GO-S)

S-r-GO membranes were fabricated using two different approaches to modify the position of sericin and r-GO on the support layer. In the first approach, an aqueous GO dispersion of volume and concentration (30 ml, 0.033 mg/ml) was vacuum filtered through the commercial nylon membrane (pore size 0.22 µm), forming a layer of GO flakes on top of the nylon membrane. After coating GO layers, the sericin solution (30 ml, 20 mg/ml) was vacuum filtered through the nylon membrane (nylon 6,6) coated with GO layers. The tri-layered membrane was then dried inside a desiccator for 24 hours and followed by heating under a vacuum at 150 °C for 2 hours. The membrane prepared as such (by depositing GO as the first layer and sericin as the second layer on top of a commercial nylon membrane) was termed as S-r-GO membrane. The schematic illustration of the membrane fabrication technique is shown in Fig. 15a.

In the second method, a sericin solution of similar concentration and volume (30 ml, 20 mg/ml) was deposited on a nylon membrane through a gravitation-assisted filtration method without applying any external vacuum pressure. Once the sericin layer appeared to be dried, an aqueous

TH-3195_186151006

dispersion of GO (30 ml, 0.033 mg/ml) was vacuum filtered through the sericin-coated nylon membrane. The membrane prepared as such (sericin first, and GO second) is termed an r-GO-S membrane. Similar to S-r-GO, r-GO-S was dried inside a desiccator for 24 hours and heated under a vacuum at 150 °C for 2 hours. The schematic diagram of the membrane fabrication process is shown in Fig. 15b. In both the cases, the purpose of heat treatment was to eliminate some of the functional groups from GO flakes, reducing its affinity toward aqueous mediums.

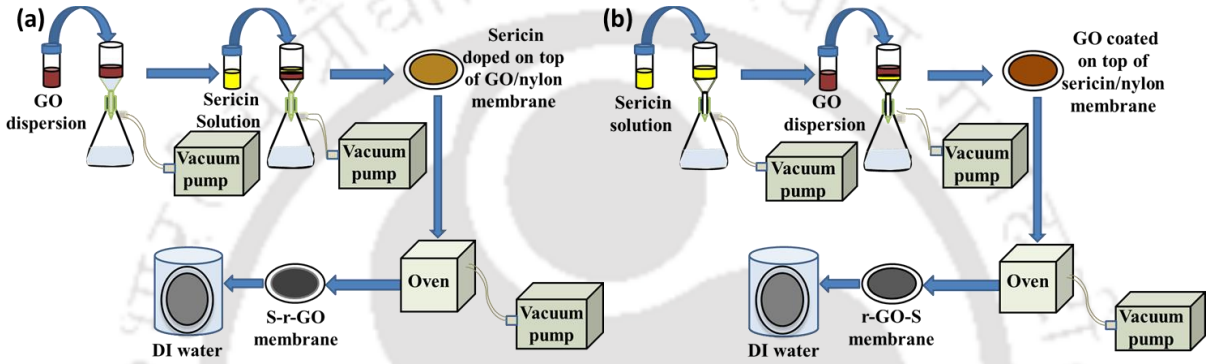

Fig. 15: Schematic diagram of the fabrication method of (a) S-r-GO/nylon membrane, (b) r-GO-S/nylon membrane

4.3.6 Membrane Characterization

The morphology of the samples was examined by using a field emission scanning electron microscope (FESEM, Sigma, India), field emission transmission electron microscope (FETEM, JEOL, India), and atomic force microscope (AFM, Cypher, India). The contact angle measurement was analysed by using a Holmarc goniometer. X-ray diffractometer (XRD, Micromax-007HF) was used for inter-layer spacing measurement of membranes. The presence of chemical functional groups was determined by using Fourier-transform infrared spectroscopy (FTIR). The elemental analysis of the samples was examined by using an energy dispersive x-ray (EDX). The surface charge and leachability of the samples were analysed by

TH-3195_186151006

zeta sizer instrument and UV spectroscopy, respectively. The pore size measurement was examined by Tech Porometer (TECH INC).

4.3.7 Characterization of Rifaximin effluent

The recovered product from the effluent as rifaximin was evident with the help of characterization analysis such as XRD, FTIR, High-performance liquid chromatography (HPLC), and FESEM analysis of the crystals produced by rifaximin. The osmolarity of the effluent solution was characterized by using an osmometer instrument. The osmotic pressure was calculated by putting the values of osmolality measured by the osmometer into the van't Hoff equation 9. Osmolality measures the total number of dissolved particles per kilogram of solvent. The SI unit of osmotic pressure was bar.

$$Posm = c * R * T \quad (9)$$

Where P_{osm} is the osmotic pressure, c is osmolality in (mOsmol/kg water), R is the universal gas constant (0.082054 in atm/mol*K) and T is the temperature in Kelvin (K). The osmotic pressure of different draw solutions is shown in Table 2.

Table 2: Osmotic pressure of different solutions

Solutions	**Molarity (M)**	**Osmolality (mOsmol/kg H_2O)**	**Universal Gas Constant, R (atm/mol*K)**	**Temp, T (K)**	**Osmotic Pressure (Bar)**
NaCl	1	2000	0.082054	298	48.8
KCl	1	2050	0.082054	298	50.6
KH_2PO_4	1	1450	0.082054	298	34.6

TH-3195_186151006

Further, rifaximin samples were analysed using HPLC connected with a UV-vis detector (Shimadzu, Prominence UFLC, SPD-20A, Singapore) at the maximum absorption wavelength of 236 nm. The mobile phase prepared for rifaximin concentration with Merck Chromolith® High-Resolution C-18 reverse phase column (1.5 μm, 4.6mm×100mm) as follows: 70% of Acetonitrile and 30% of 0.05 M Ammonium Acetate (CH_3COONH_4) was mixed with 500 ml in total volume. To maintain the pump pressure, the flow rate of the mobile phase solution was kept at 1.0 ml/min, and the retention time of the samples was obtained at 1.876 min.

4.3.8 Membrane performance evaluation in FO process

The performance of the fabricated r-GO and sericin doped r-GO membranes was investigated by using a lab-scale FO system under a controlled environment. The schematic FO setup was shown in Fig. 16. The FO test cell was placed between draw and feed tanks with an effective membrane area of 4 cm^2. The test cell was fabricated and supplied by Yantrabot Tech, Guwahati, India. The volume change in the tanks was recorded by using a weighing balance (model-XD/XR) with an accuracy of ± 0.01g and supplied by weighing solution ltd, New Delhi. The NaCl concentration on both the tanks was measured by using Hanna conductivity meter (model-HI5321) with an accuracy of ±0.1ppm. While experimenting, the performance was obtained in both active layers facing draw solution (ALDS) and active layer facing feed solution (ALFS). Using two pumps, the draw and feed solutions were circulated through a nylon-made FO test cell with 50 and 70 L/h flow rates, respectively. The solutions used in the draw and feed tanks were 1M NaCl and DI water in each 500 ml volume, respectively, and maintained at 25 °C. However, for crystallization application, the draw and feed tanks were replaced with 4M NaCl and effluent solutions in each 400 ml volume, respectively, and maintained at 25 °C and 40 °C, respectively. Both the tanks were completely sealed with a parafilm sheet to avoid evaporation loss.

TH-3195_186151006

The water flux and RSF were calculated by using equation 1 and 3. Moreover, the SRSF was also calculated using equation 4.

The membrane regeneration efficiency was evaluated by flux recovery ratio (FRR%) using the equation 10.

$$FRR\% = \frac{Jv2}{Jv1} * 100 \qquad 10$$

Where, J_{v2} is the water flux obtained after the membrane regeneration and J_{v1} is the water flux of the new membrane.

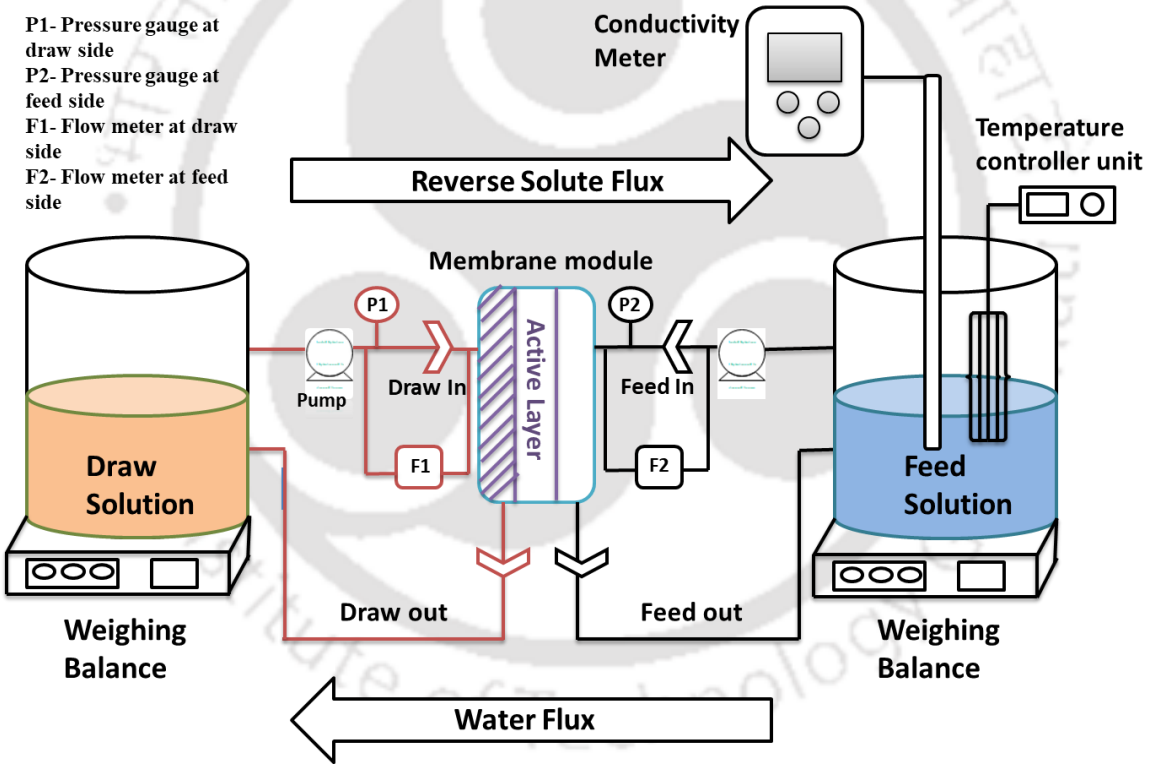

Fig. 16: Schematic of FO setup for evaluating membrane performance for FO applications

4.3.9 Hybrid separation technologies of pharmaceutical effluent

The pharmaceutical effluent was treated with three different separation processes for recovering rifaximin antibiotics. Initially, 2000 ml of effluent was pre-treated using a PP

TH-3195_186151006

hollow fiber MF membrane. The specification of the MF membrane was given in the author's previous work[171]. Due to high turbidity, the Effluent was prefiltered in the batch mode to reduce the turbidity and remove the particulate matter present in the feed effluent. After the UF treatment process, the UF permeate solution was treated with a rotary evaporator to remove the ethanol from the effluent. Out of 2000 ml effluent, 1100 ml of 75% ethanol and 25% water mixture was recovered from the effluent and the balance concentrated 900 ml effluent was further concentrated in the FO process to recover rifaximin. The concentrated effluent was centrifuged in a batch centrifuge (REMI NEYA-12) for 20 mins at 6000 rpm to remove rifaximin crystals. The schematic diagram of the UF treatment process and digital images of rotary evaporator products are shown in Fig. 17a and Fig. 17b, respectively. The properties of raw effluent are given in Table 3.

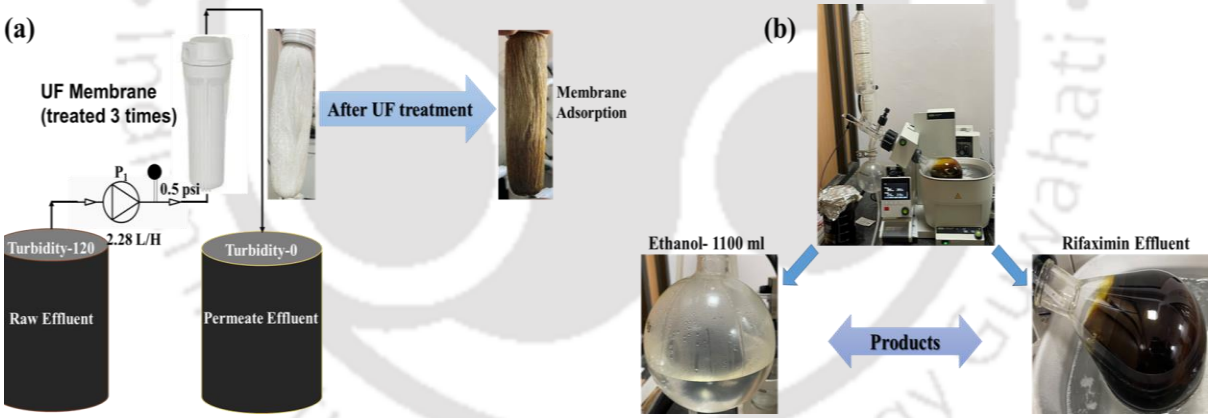

Fig. 17: (a) Schematic diagram of effluent in UF treatment process, (b) digital image of rotary evaporator products

Table 3: Effluent characteristics

Effluent Properties	Units	Values
Turbidity	NTU	114
pH	-	8.5
Ethanol	%	75

TH-3195_186151006

Water	%	25
Rifaximin	g/lit	37.8
Osmotic pressure	bar	125

The best performed FO membrane (i.e., r-GO-S) with the NaCl-DI water system was used to concentrate pharma effluent. Considering low test cell membrane surface area (4 cm^2), the FO process was operated in a batch mode wherein both DS and FS were recirculated for two hrs. In each batch of operation, the water was recovered from the effluent by using 4M NaCl solution as the initial DS concentration. For the FO process, 400 ml of rifaximin solution was taken as feed solution and 4M NaCl in 400 ml was taken as draw solution. To maintain ~45 bar initial osmotic pressure difference across the FO membrane, 4M NaCl (~170 bar) was used as DS. The FS and DS characteristics of all six batches of the FO process along with each batch of operation time were presented in Table 4. Therefore, a sufficient chemical potential gradient should be available to get high water flux through the FO membrane. The water flux was initially measured for every 1 hr interval. Each batch FO cycle was operated for 5 hrs to extract sufficient water from the feed side. In the FO crystallization experiment, the temperature of both DS and FS were maintained at different temperatures (i.e, FS temperature higher than the DS temperature) to achieve high FS saturation concentration, which helps improve the crystallization process. Therefore, the feed effluent and draw solution temperatures were maintained at 40 °C and 25 °C. However, after the end of each FO batch cycle, the feed solution (rifaximin) was cooled down to room temperature (25 °C) to crystalize the rifaximin in the feed solution. After each batch of the FO process, the concentrated FS was centrifuged to recover the rifaximin crystals from FS. However, the used DS was replaced with freshly new DS at each FO batch cycle. The batch centrifuge was operated at 6000 rpm for 20 mins, and the concentrated crystal slurry was dried in an open pan for 24 hrs. The supernatant solution was

TH-3195_186151006

again used as feed solution and the process can be continuous for long term recovery. The extracted crystals from all 6 batches were washed in distilled water to remove NaCl deposition due to RSF. Also, the concentration of rifaximin in DS solution was measured using HPLC for each batch. The continuous FO recovery process can be scaled up for further batch process to recovery maximum rifaximin. The detailed process flow diagram of continuous and integrated batch process for rifaximin recovery is presented in Fig. 18a-b.

Table 4: FS and DS properties for different batches of FO process in both the modes

	ALDS				ALFS			
Properties	Batch 1 (after 5 hrs)				Batch 1 (after 5 hrs)			
	FS		DS		FS		DS	
	Initial	End	Initial	End	Initial	End	Initial	End
Rifaximin (g/L)	15.10	16	0	0.42	14.90	15.35	0	0.22
Volume (ml)	400	365	400	435	400	378	400	422
Pellet Rifaximin (mg)	165				128			
Properties	Batch 2 (after 5 hrs)				Batch 2 (after 5 hrs)			
	FS		DS		FS		DS	

TH-3195_186151006

	Initial	End	Initial	End	Initial	End	Initial	End
Rifaximin (g/L)	15.7	16.3	0	0.32	15	15.3	0	0.16
Volume (ml)	365	340	365	390	375	360	375	390
Pellet Rifaximin (mg)	130				74			
Properties	Batch 3 (after 7 hrs)				Batch 3 (after 7 hrs)			
	FS		DS		FS		DS	
	Initial	End	Initial	End	Initial	End	Initial	End
Rifaximin (g/L)	15.9	16.7	0	0.40	15.15	15.4	0	0.18
Volume (ml)	340	310	340	370	360	343	360	377
Pellet Rifaximin (mg)	142				88			
Properties	Batch 4 (after 5 hrs)				Batch 4 (after 5 hrs)			
	FS		DS		FS		DS	
	Initial	End	Initial	End	Initial	End	Initial	End

TH-3195_186151006

Rifaximin (g/L)	16.36	17.05	0	0.34	15.2	15.53	0	0.16
Volume (ml)	300	275	300	325	340	322	340	360
Pellet Rifaximin (mg)	115				90			
Properties	Batch 5 (after 5 hrs)				Batch 5 (after 5 hrs)			
	FS		DS		FS		DS	
	Initial	End	Initial	End	Initial	End	Initial	End
Rifaximin (g/L)	16.7	17.14	0	0.29	16.35	15.65	0	0.13
Volume (ml)	275	255	270	290	320	305	320	335
Pellet Rifaximin (mg)	90				80			
Properties	Batch 6 (after 5 hrs)				Batch 6 (after 5 hrs)			
	FS		DS		FS		DS	
	Initial	End	Initial	End	Initial	End	Initial	End

TH-3195_186151006

Rifaximin (g/L)	16.87	17.4	0	0.26	15.51	15.8	0	0.11
Volume (ml)	250	232	250	270	305	293	300	312
Pellet Rifaximin (mg)	80				82			

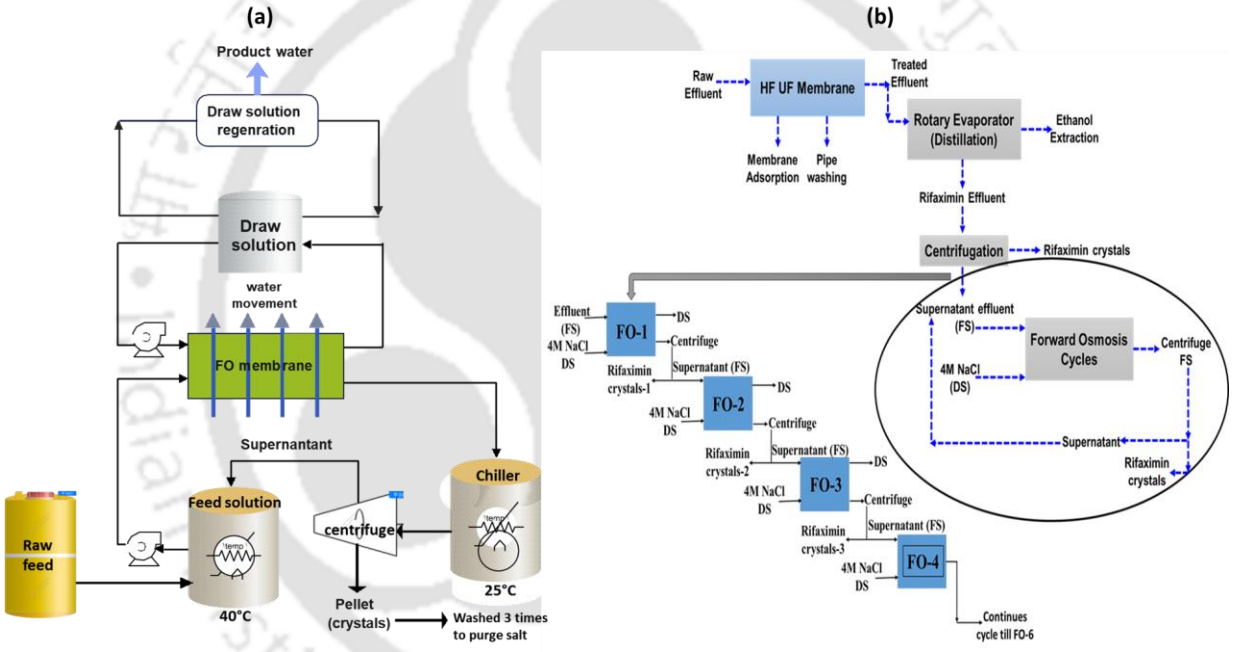

Fig. 18: Schematic flow chart of (a) continuous rifaximin recovery process (b) hybrid batch rifaximin recovery process

4.4 Results and Discussions

4.4.1 Characterization of sericin particles and GO flake

GO flakes and sericin particles used for the coating of commercial nylon membrane were examined under AFM and electron microscope. The AFM analysis revealed the average lateral dimension of the GO flakes to be around 1-2 µm; similarly, the average height of flakes was

TH-3195_186151006

found to be in the range of 4 to 5 nm. Under AFM and electron microscopic investigation, the lateral size and average height of the sericin particles were found to be 0.1-2 µm and ~ 9-10 nm respectively (shown in Fig. 19a-d).

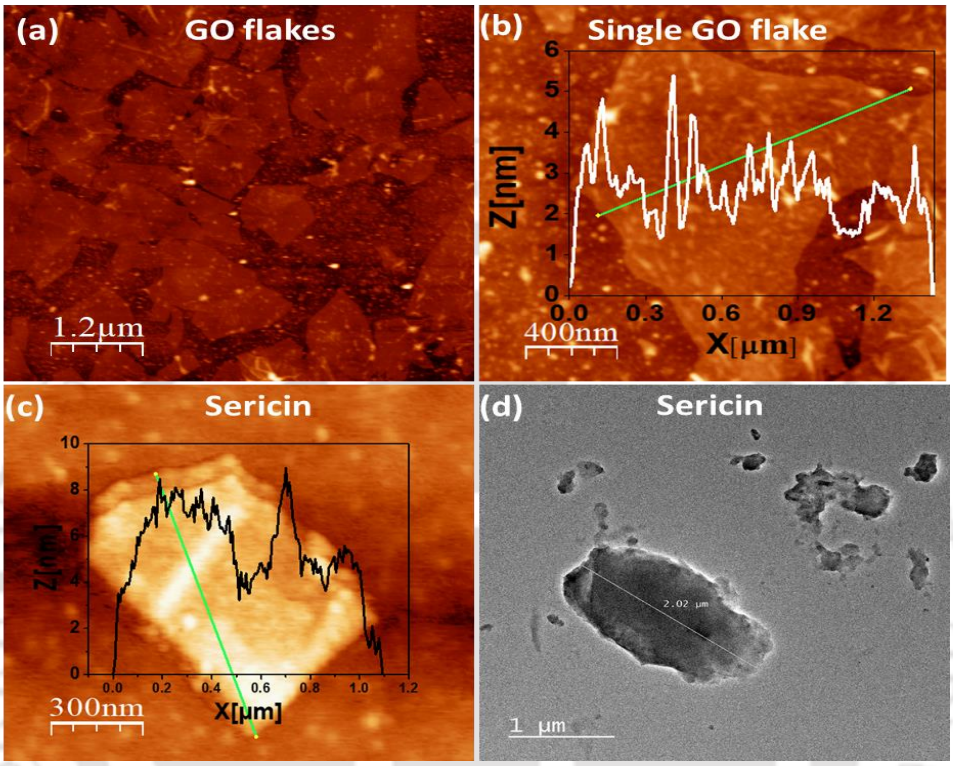

Fig. 19: Representative AFM images along with corresponding height profiles of (a) multiple GO flakes, (b) single GO flake, and (c) single sericin particle. (d) TEM image of the sericin particles.

4.4.2 FESEM analysis of the fabricated membranes

GO and sericin was coated on a porous nylon support through filtration of the respective aqueous dispersions. The pore size distribution and range of pore sizes of different membranes are shown in Fig. 20a and the cross-sectional image of the r-GO membrane shown in Fig. 20b confirms the thickness of the r-GO layer around 1 µm onto the nylon substrate (at higher magnification). The FESEM image of the support layer surface reveals the size of the void space or pores in the range of 0.20 to 0.3 µm, as shown in Fig. 21a. The gravity-induced

TH-3195_186151006

filtration of 30 ml aqueous solution of sericin (20 mg/ml) clogged the large pores of the nylon microfiltration membrane. Under FESEM examination, when sericin was coated on a nylon membrane, the surface appeared to be smooth with partial reduction of pore size due to deposition of sericin which is shown in Fig. 21b. Similarly, vacuum filtration-driven coating of GO flakes on a nylon membrane and annealing it to form r-GO layer created a highly uniform and atomically smooth filtration surface. A FESEM image of the smooth surface of the r-GO coated on nylon membrane is presented in Fig. 21c. When r-GO flakes were deposited on top of the sericin-coated nylon membrane, its macroscopic dents were homogenized and the surface became uniform. The smooth surface of the r-GO-sericin layer is evident from the electron microscopic image in Fig. 21d.

In contrast to the r-GO-S membrane, when sericin was deposited on top of the r-GO coated nylon membrane (S-r-GO), the surface became rough and wrinkled, which is attributed to the non-uniform geometry of the individual sericin particles. The surface morphology of the S-r-GO prepared by depositing sericin (30 ml, 20 mg/ml) on top of the r-GO layer is shown in Fig. 21e. The cross-sectional FESEM image of only the nylon support layer in Fig. 21f revealed a highly porous surface with an inset image showing the pores of nylon in a higher magnification range. In the cross-sectional FESEM image of the r-GO-S/nylon membrane (Fig. 21g), the sericin particles penetrate the pores of the nylon membrane and get deposited in the inner surface of the pores, thus reducing the pore diameters of nylon support which is also evident with the inset image revealing a reduction in pore size of the nylon support when compared to only nylon support. The GO flakes did not penetrate through the sericin-coated pores and got deposited on top of the sericin-coated nylon membrane by producing a thin layer of r-GO of thickness ~1 μm. The coating of sericin particles on both the outer and inner surface of the pores of the nylon membrane is evident from the pore size measurement done by employing a

TH-3195_186151006

porometer instrument. The average pore size of the sericin/nylon membrane (0.15 µm) was measured to be lower than that of the pristine nylon membrane (0.22 µm). This reduction in average pore size supports our hypothesis about the coating of the sericin particles in the inner surface of the pores of commercial nylon membrane. The average pore size of the r-GO-S membrane was found to be further reduced to 0.11 µm after the application of the r-GO coating on top of the sericin/nylon membrane with minimum and maximum pore sizes of 0.08 µm and 0.145 µm, respectively.

The stacking of the sericin and r-GO layer on the commercial nylon membrane is evident from the cross-sectional FESEM image of the S-r-GO membrane in Fig. 21h. In this configuration, the sericin nanostructure did not penetrate the pores of the nylon membrane, as it was blocked by the pre-coated r-GO layer. The higher magnification of the cross-sectional image of the S-r-GO membrane in Fig. 21i revealed layer-by-layer deposition of sericin particles on r-GO coated nylon membrane. The thicknesses of sericin and r-GO layers were measured to be around 150 nm and 850 nm, respectively. Therefore, the sericin particles covered 150 nm thin layer of the r-GO layer. The nylon support layer thickness was around 100 µm which was measured by using an electronic micrometer.

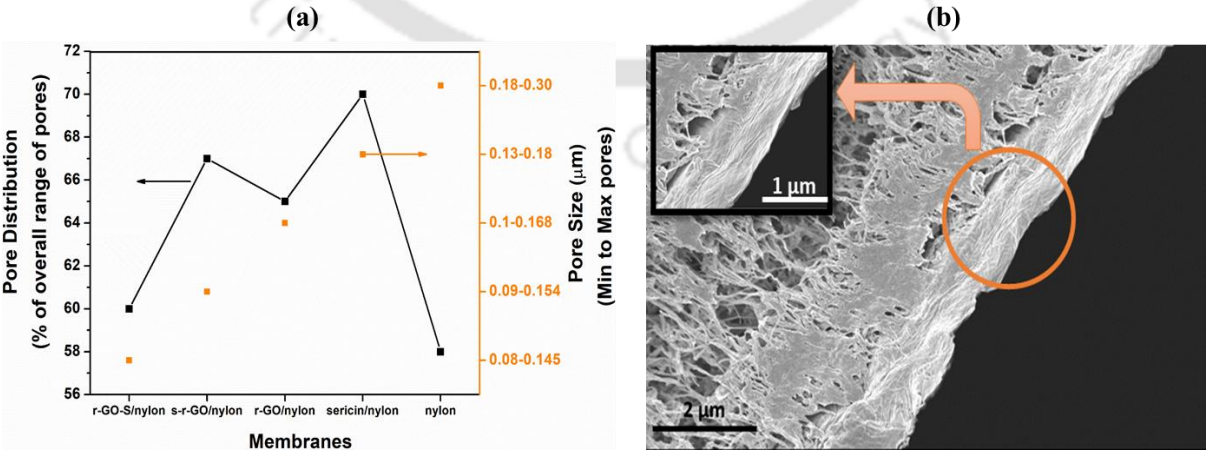

TH-3195_186151006

Fig. 20: (a) Pore size distribution of different membranes, (b) cross-sectional image of r-GO/nylon membrane

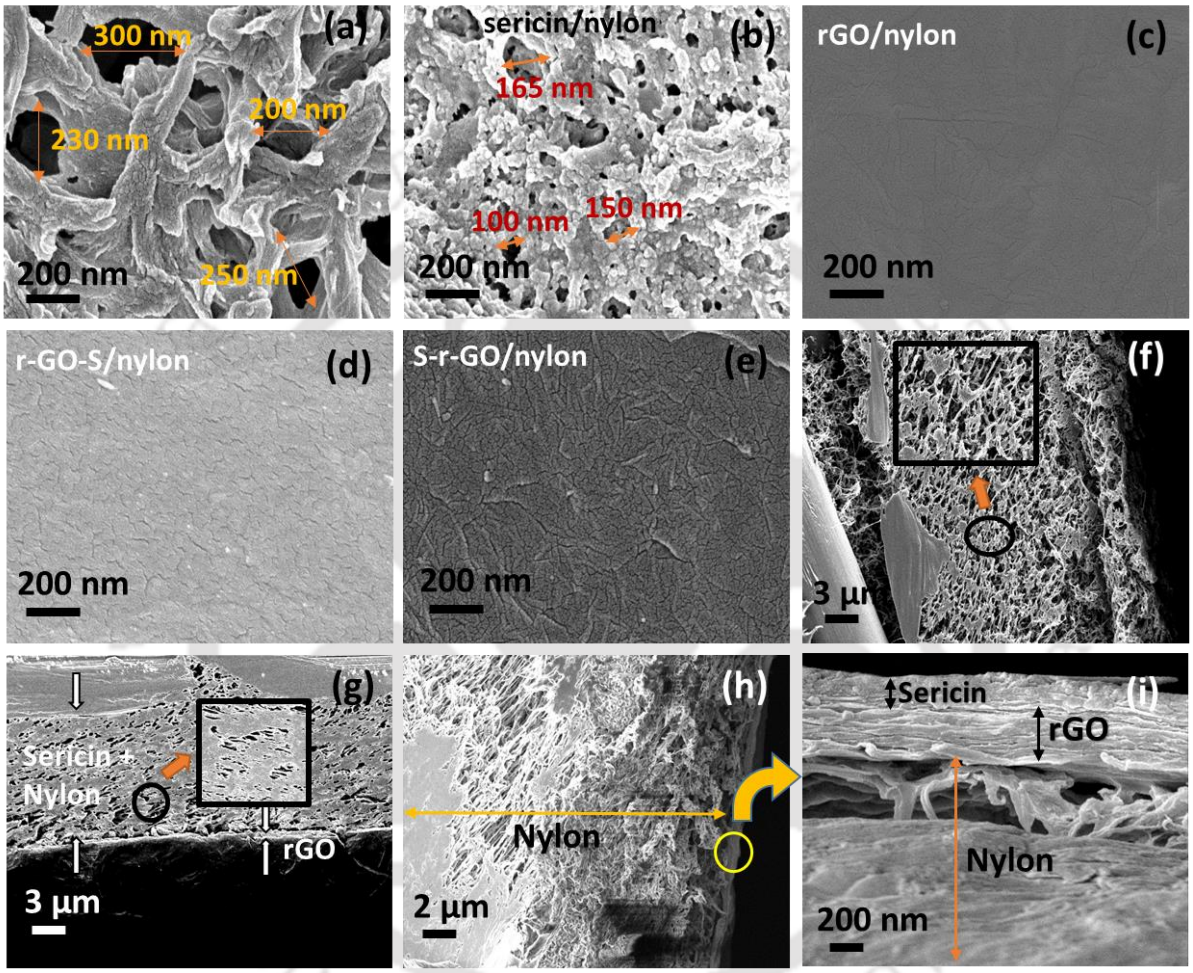

Fig. 21: FESEM analysis of the surface morphology (a) nylon membrane, (b) sericin/nylon membrane, (c) r-GO/nylon membrane, (d) r-GO-sericin/nylon (r-GO-S), (e) sericin-r-GO/nylon (S-r-GO). Cross-sectional FESEM image of (f) only nylon support (inset shows porous nylon support at higher magnification), (g) r-GO-S/nylon membrane (inset shows sericin deposition inside nylon support at higher magnification), (h) S-r-GO/nylon membrane, (i) sericin and r-GO layer of a S-r-GO/nylon membrane at higher magnification..

TH-3195_186151006

4.4.3 EDX analysis of the fabricated membranes

The EDX analyses of the as-prepared membranes are shown in Fig. 22a-d. The C/O ratio of the GO/nylon membrane was observed to be increased from 2.49 to 3.27 in the r-GO/nylon membrane due to partial loss of the oxygen-containing functional groups during the heat treatment process (150 °C for 2 hours). Both GO/nylon and r-GO/nylon membranes have shown the presence of nitrogen contents of about 4.6 wt.% and 5.8 wt.%, respectively, which is attributed to the amine groups present in the nylon membrane. After sericin doping and heat treatment, the nitrogen content was found to be increased to 10 wt.% and 11 wt.% for r-GO-S/nylon and S-r-GO/nylon membranes, respectively. This is attributed to the presence of both nitrogen-containing amide groups in the sericin particles and amine groups of nylon membrane, and this observation further confirmed the co-existence of sericin particles with r-GO. While the oxygen content of the r-GO/nylon membrane was found to be 22.1 wt.%, the oxygen percentage in r-GO-S/nylon and S-r-GO/nylon membranes was found to be 33.8 wt.% and 33.2 wt.%, respectively. The enhancement in oxygen percentage was attributed to the presence of oxygen-containing functional groups (like –OH) in the sericin particles and r-GO together.

TH-3195_186151006

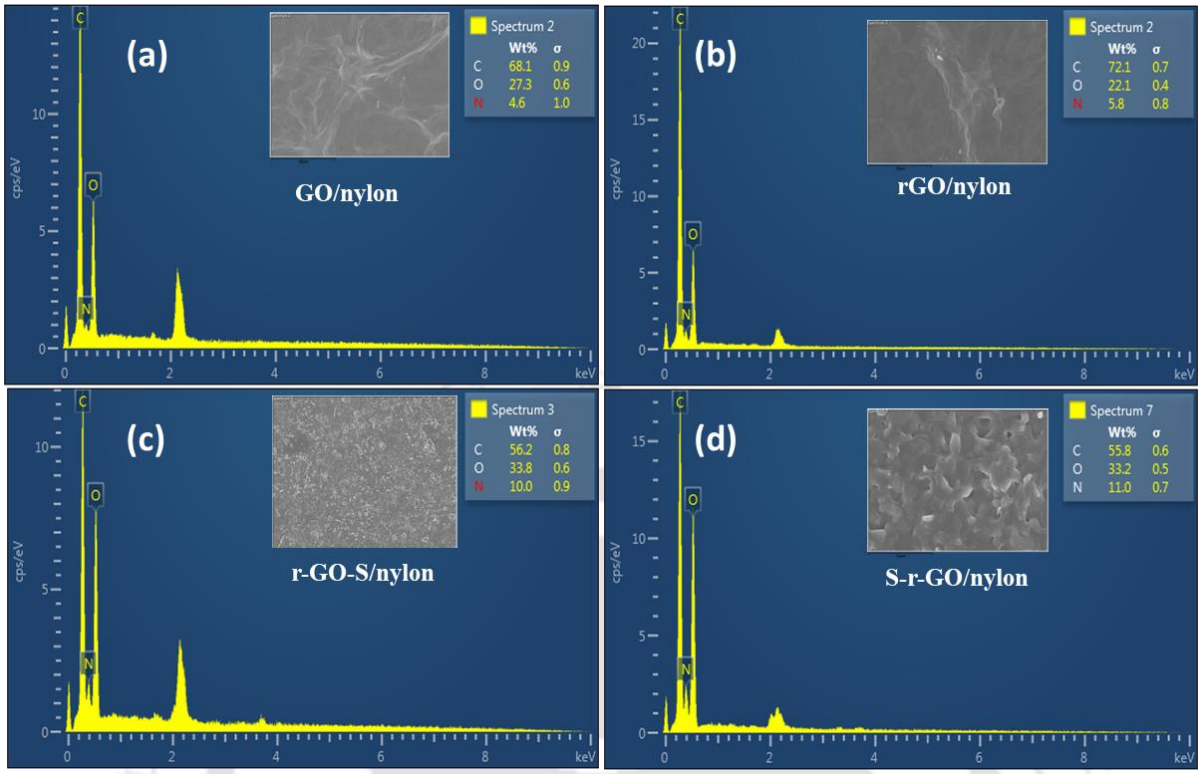

Fig. 22: EDX analysis for membranes (a) GO/nylon, (b) r-GO/nylon (c) r-GO-S/nylon, (d) S-r-GO/nylon membrane with C, O, and N composition

4.4.4 FTIR spectra and XRD of fabricated membrane

Fig. 23a show the FTIR spectra of sericin, GO membrane, S-r-GO membrane, and r-GO membrane. The FTIR spectrum of sericin showed a broad vibrational peak at 3420 cm^{-1}, representing the stretching mode of the hydroxyl group (-OH). The bands that appeared at 1660 cm^{-1} and 1540 cm^{-1} correspond to amide I and amide II groups present in sericin protein. The IR spectrum of GO exhibits peaks at 3400 cm^{-1}, 1720 cm^{-1}, 1620 cm^{-1}, and 1050 cm^{-1} corresponding to -OH, -C=O, -C=C, and –C-O groups, respectively[172]. In the IR spectrum of the r-GO membrane, the broad peak band at the C=O group (1720 cm^{-1}) was removed entirely, while the peak intensity at -OH group (3420 cm^{-1}) was diminished due to the partial removal of oxygen-containing functional groups during the annealing process. The IR spectrum of the S-r-GO membrane suggests that the functionalization with sericin particles and

TH-3195_186151006

the successive annealing process decreased the overall intensity of the band corresponding to the stretching mode of -OH. Furthermore, the disappearance of band representing the -C=O group in the IR spectrum of the S-r-GO membrane confirms the reductive elimination of the oxygen groups. The shifting of the bands (1660 cm^{-1} and 1540 cm^{-1}) of pristine sericin particles to 1653 cm^{-1} and 1534 cm^{-1} at the IR spectrum of both S-r-GO membrane and r-GO-S membrane confirm chemical interactions between the functional groups of GO and sericin[173].

To get further insights into the structure of the membranes, samples were studied through XRD and calculated the interlayer spacing. As shown in Fig. 23b, the GO and r-GO membrane exhibited sharp peaks at 10.2^o and 11.2^o, corresponding to the d-spacing's of 9 Å and 7.7 Å, respectively. The interlayer spacing obtained as such is in good agreement with our previous reports as well as with the reports of other authors[174]. The XRD pattern of sericin displayed a broad peak centred at 2θ=21.5^o, corresponding to the d-spacing of 4.1 Å[175]. However, S-r-GO membrane displayed left shift of prominent reflection in the 2θ=5.5 value corresponding to interlayer d-spacing of 15.8 Å, along with a small hump of very low intensity reflections at 2θ=19.2^o, corresponding to d-spacing of 4.8 Å which might be due to sericin. The increase in d-spacing can be attributed to the incorporation of sericin molecules between GO sheets due to nucleophilic interaction between epoxy group of rGO and -OH groups of sericin.

TH-3195_186151006

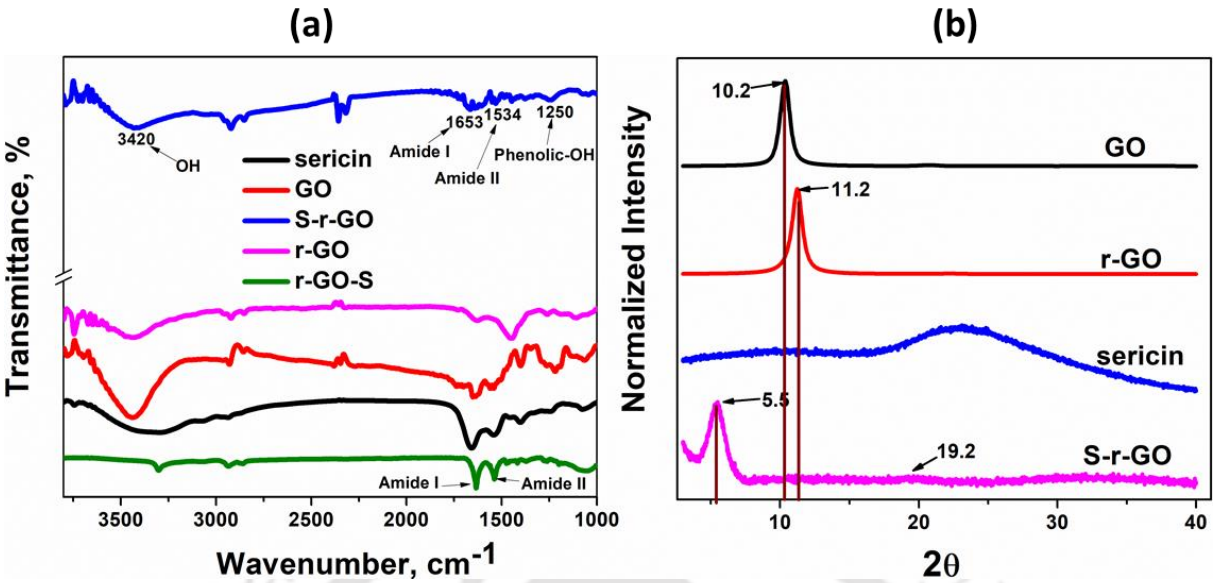

Fig. 23: (a) FTIR spectra of fabricated membranes; (b) XRD pattern of fabricated membranes

4.4.5 Zeta potential and contact angle analysis of the fabricated membrane

Zeta potential values of the individual components of the membranes were studied to obtain insights into the surface charge of the FO membranes. At the concentration used in this study (20 mg/ml), the zeta potential value of sericin was found to be around -11.8 mV (see Fig. 24a) [176]. For the measurement of zeta potential of the membranes, the active layer was removed from nylon substrate and dispersed in DI water. The zeta potential values of GO (-34.8 mV) and r-GO (-26 mV) at neutral pH were also found to be in the same range as the reported literature[177]. The reduced value of zeta potential for r-GO was attributed to the removal of oxygen-containing functional groups. The zeta potential values of both sericin-r-GO mixture (S-r-GO) and (r-GO-S) were found to be around -28.2 mV and -29 mV, respectively, which was slightly higher than r-GO membranes. The synergetic enhancement in the negative zeta potential values of sericin and r-GO mixture is attributed to the functionalization of sericin protein onto the surface of r-GO improves the solution stability of both sericin particles and r-

TH-3195_186151006

GO flakes. Since the membranes (S-r-GO and r-GO-S) were bilayers of the same materials (and sericin), the zeta potential values were almost similar.

Fig. 24b shows the bar diagrams of the water contact angles of sericin/nylon, GO/nylon, r-GO/nylon, S-r-GO/nylon, and r-GO-S/nylon membranes. The pristine GO membrane exhibits a water contact angle of 48°. The removal of oxygen-containing functional groups decreases the surface energy of the membrane, and hence the contact angle of the r-GO membrane increases to 79°. The water contact angle of sericin (20 mg/ml) coated nylon membrane was found to be 35°, which is consistent with the reported values[178]. The contact angle for the S-r-GO membrane was found to 61°. The drastic reduction in the contact angle of the S-r-GO membrane as compared to that of the r-GO membrane is attributed to the deposition of the hydrophilic sericin layer on top of the r-GO layer. However, the contact angle of the r-GO-S membrane (76°) was a bit higher than the S-r-GO membrane but was less than 90° (in the hydrophilic range). The pre-coated r-GO layer on top of the sericin-coated nylon membrane was attributed to an increase in contact angle.

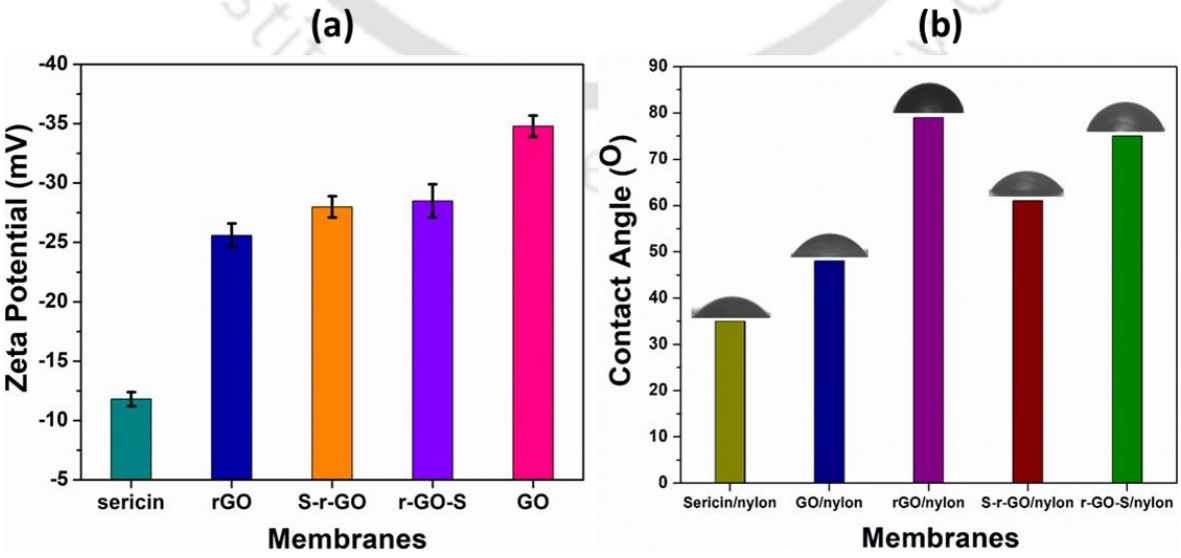

TH-3195_186151006

Fig. 24: (a) zeta potential analysis of different membranes; (b) contact angle analysis of fabricated membranes

4.4.6 Membrane parameter estimation

The model equations for the FO process were solved using the Modelica language in the Dymola software tool. The experimental results at C_{ds} ranging from 0.5 to 2M NaCl provide the basis or parameter estimation followed by validation. The experimental data such as concentrations, flow rates, pressures, and weight change over time of both FS and DS were used to estimate the membrane parameters. The model parameters were estimated by minimizing the error between the model and experimental data. The error function can be defined as the square of absolute error between the experimental and model data as shown in equation 11.

$$Error = \sum_{t=0}^{t}\left[\left(\frac{J_{w,\exp}-J_{w,model}}{J_{w,model}}\right)^2+\left(\frac{J_{s,\exp}-J_{s,model}}{J_{s,model}}\right)^2\right] \quad 11$$

The bound used for model tuning parameters were 0.001 < Lp ($L\ m^{-2}\ h^{-1}\ bar^{-1}$) < 100; 0.0001 < B ($L\ m^{-2}\ h^{-1}$) <10; 1< S ($nm$)< 750000; 0.0001< k_d (m h^{-1}) <100; and 0.0001 <k_f <100.

The estimated pure water permeability ($L_p, L\ m^{-2}h^{-1}bar^{-1}$), solute permeability coefficient ($B, L\ m^{-2}h^{-1}$), structural parameter (S, nm), mass transfer coefficient for DS ($k_d, m\ h^{-1}$) and FS ($k_f, m\ h^{-1}$) were 31.21 ± 0.08, 4.87 ± 0.03, 472500, 18.1 ± 0.53, and 0.28 ± 0.11, respectively for r-GO-S membrane. The above mathematically obtained data for pure water permeability coefficient (L_p) and solute permeability (B) coefficient was almost aligned with the obtained RO experimental result which was around 32.26 $L\ m^{-2}h^{-1}bar^{-1}$ and 3.78 $L\ m^{-2}h^{-1}$, respectively (see Fig. 25c-d) and the corresponding average % error was 1.903. Regarding structural parameter data, Li et al prepared GO incorporated FO membrane and

TH-3195_186151006

found structural parameter (S) to be 452 µm or 452000 nm[179], which was also aligned with our results.

The pure water permeability, solute (NaCl) permeability coefficient, and structural parameter were estimated experimentally, respectively. The estimated membrane parameters were validated using the experimental data. Fig. 25a-b represents the comparison of experimental and model predicted water flux and reverse solute flux for 0.5M to 2M, respectively. From the figures, it can be observed that both water flux and reverse solute fluxes of model and actual experimental data were almost aligning for 0.5M to 2M draw solution concentration with R^2 values around 0.99, thus confirming the validation of experimental results with the model study.

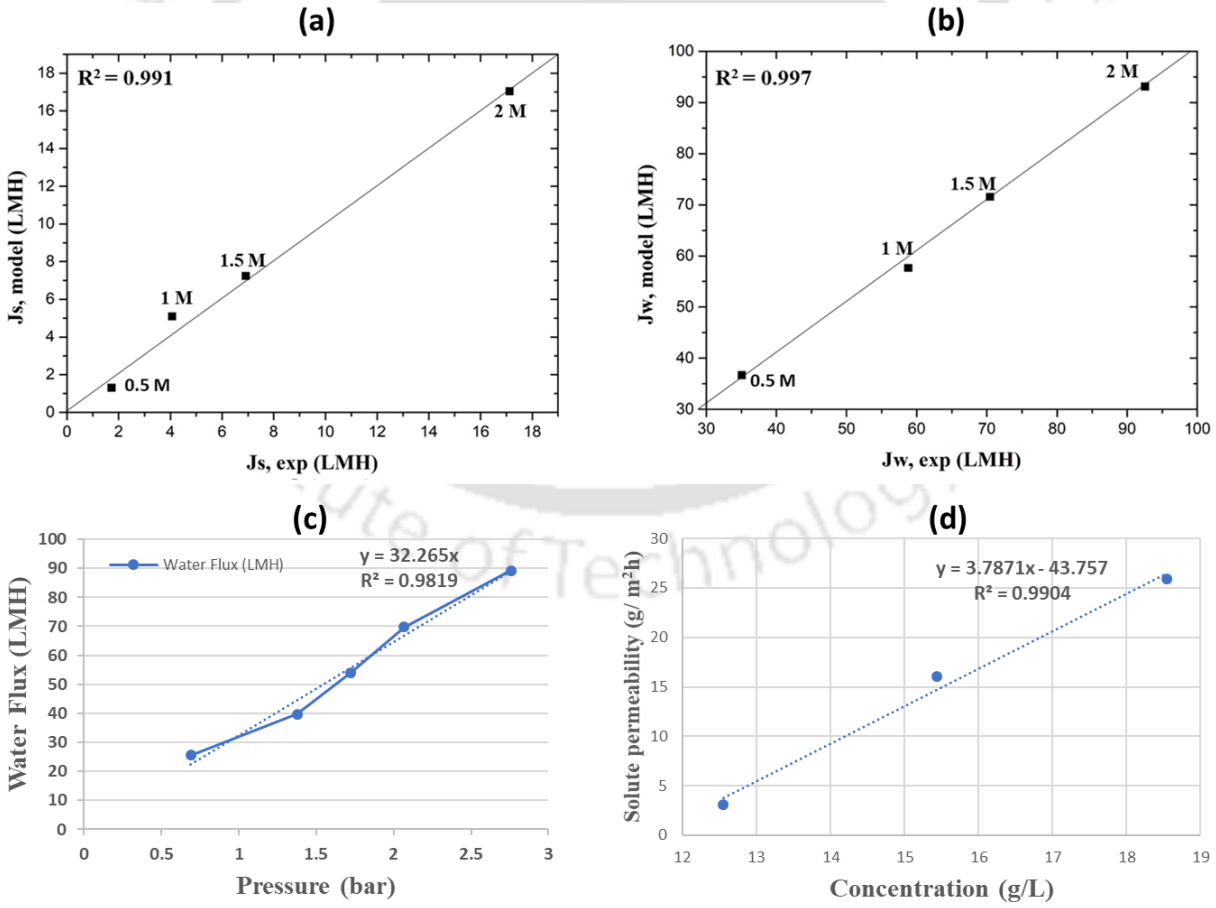

TH-3195_186151006

Fig. 25: Comparison of experimental results and model predictions at different draw solution concentrations (0.5M to 2M) in FO mode for (a) water flux (L m^2 h^{-1}); (b) reverse solute flux (g m^{-2} h^{-1}); Experimental data of r-GO-S membrane in RO mode for (c) water permeability coefficient; (d) solute permeability coefficient

4.4.7 Comparison of membrane performance in forward osmosis

The membrane performance (water flux, RSF, and SRSF) was evaluated using the FO process. The performance of r-GO/nylon, S-r-GO/nylon, r-GO-S/nylon and sericin/nylon membranes was estimated in active layer facing draw solution mode (ALDS) and active layer facing feed solution (ALFS) using a lab-scale cross flow FO system. The GO/nylon membrane cannot withstand the cross-flow system, whereas the r-GO and sericin doped r-GO membranes have attained higher water stability due to the reduction process. The reduction of functional groups reduces the affinity of GO flakes toward water as well as enhances the interlayer π–π attractive force. Moreover, doping agent (sericin) used here comprised functional groups capable of strongly binding with both r-GO laminates and nylon substrate[173]. Fig. 26a-c shows the comparative FO performance of r-GO membrane and sericin doped r-GO membranes with cellulose triacetate (CTA) FO membrane. The highest water flux was observed for the sericin/nylon membrane (78 L m^{-2} h^{-1}) followed by the r-GO-S/nylon membrane (54 L m^{-2} h^{-1}), S-r-GO/nylon (36.8 L m^{-2} h^{-1}) and r-GO/nylon membrane (26 L m^{-2} h^{-1}) and then the CTA FO membrane (8 L m^{-2} h^{-1}) in the ALDS orientation. However, in ALFS orientation, the water fluxes of sericin/nylon (57.7 L m^{-2} h^{-1}), r-GO-S/nylon (38.5 L m^{-2} h^{-1}), S-r-GO/nylon (28 L m^{-2} h^{-1}), r-GO/nylon (15 L m^{-2} h^{-1}), and CTA FO membranes (6.4 L m^{-2} h^{-1}) were lower than ALDS. The resistance offered by the active layer of the membrane induces dilutive ICP across the draw side of the membrane, which significantly reduces the effective osmotic pressure at the interface of the active layer, reducing the water flux to a great extent in ALFS mode. The

TH-3195_186151006

high-water flux for sericin/nylon membrane was due to the presence of hydrophilic sericin particles inside as well as on top of nylon support which will allow more water molecules than NaCl, thus reducing dilutive internal concentration polarization (DICP).

Similarly, the lowest RSF value was observed for the r-GO-S/nylon membrane (6.5 g m^{-2} h^{-1}) followed by the S-r-GO/nylon membrane (7 g m^{-2} h^{-1}), r-GO membrane/nylon (8.2 g m^{-2} h^{-1}) and sericin/nylon (62.8 g m^{-2} h^{-1}) in ALDS orientation. Like water flux in ALFS mode, there was a decline in RSF of all the membranes in ALFS mode. The low water flux of the r-GO/nylon membrane was observed due to the annealing-induced narrowing of inter-layer spacing between GO nanosheets. The sericin doped r-GO membranes showed 2 and 1.4 times increment of water flux for r-GO-S/nylon and S-r-GO/nylon membranes, respectively, compared to the r-GO/nylon membrane in ALDS mode. The reason for higher water flux in the r-GO-S/nylon membrane is due to the presence of sericin particles inside the porous nylon support, resulting in driving more water molecules from the feed solution than salt ions from draw solution since sericin is more hydrophilic than r-GO and the corresponding conceptual mechanism for higher water flux is shown in Fig. 26d. The presence of hydrophilic groups in r-GO and sericin together is attributed to enhancing the overall water flux. However, the water flux of the S-r-GO/nylon membrane was lower than the r-GO-S membrane in ALDS mode because the sericin particles were not coated inside the porous nylon support, which resulted in less water flux from the feed side as the support layer was facing towards feed side, unlike the r-GO-S membrane. Moreover, the area of sericin deposition inside the nylon membrane was high, resulting in more water flux than the S-r-GO/nylon membrane. The movement of water molecules in the S-r-GO/nylon membrane increases compared to the r-GO membrane due to larger d-spacing of 15.8 Å along with sericin particles deposition onto the r-GO layer, which is evident from FESEM analysis, resulting in obtaining an overall higher water flux. In

TH-3195_186151006

ALFS mode, S-r-GO/nylon membrane showed lower water flux than r-GO-S/nylon despite showing lower contact angle due to the occurrence of severe DICP than r-GO-S/nylon membrane inside the nylon support. As sericin was generally reported to have higher chlorine resistance[180], deposition of salt ions inside the pores of S-r-GO/nylon will be higher compared to r-GO-S/nylon membrane as sericin was not penetrated inside the pores of S-r-GO/nylon membrane. The permeate water from feed side would dilute the solute at the interior surface of active layer, thus leading to severe DICP in S-r-GO/nylon membrane. Due to this reason, the net osmotic driving pressure was reduced across the membrane, thus leading to lower water flux in S-r-GO/nylon membrane compared to r-GO-S/nylon membrane. Moreover, in r-GO-S/nylon membrane, sericin particles are seen penetrating inside the sericin-coated nylon membrane which will allow more water molecules than NaCl. This will lead to alleviating the DICP inside the pores. Hence, in r-GO-S/nylon membrane, the sericin molecules improved the performance of both support as well as active layers. Therefore, the overall water flux was higher than S-r-GO membrane in ALFS mode. The high RSF of sericin/nylon membrane was due to non-uniform sericin coating on nylon substrate which facilitated the passes of salt ions easily from draw side, as can be seen in Fig. 26e. Since, the sericin particle are smaller compared to r-GO sheets and absence of r-GO layer in sericin/nylon membrane also facilitated in higher RSF. The low RSF of overall sericin doped r-GO membranes compared to the r-GO/nylon membrane and sericin/nylon is attributed to the higher surface negative charge of both sericin and r-GO layers, resulting in a stronger repulsive force between Cl^- ions and the negatively charged membrane surface by Donnan exclusion[181]. The effect of sericin particles on the r-GO layer had a significant effect as the sericin peak intensity dominates over r-GO intensity, which is evident from the XRD analysis. With the addition of sericin, the SRSF of r-GO-S/nylon and S-r-GO/nylon membranes decreased from 0.28 g/L of

TH-3195_186151006

r-GO/nylon membrane to 0.12 g/L and 0.18 g/L, with a percentage decrease of 57.1% and 35.7%, respectively, in ALDS mode. However, the SRSF values in the ALDS mode were slightly less than in the ALFS mode due to the higher water flux obtained in the ALDS mode. Membranes with lower SRSF values were suitable for FO applications.

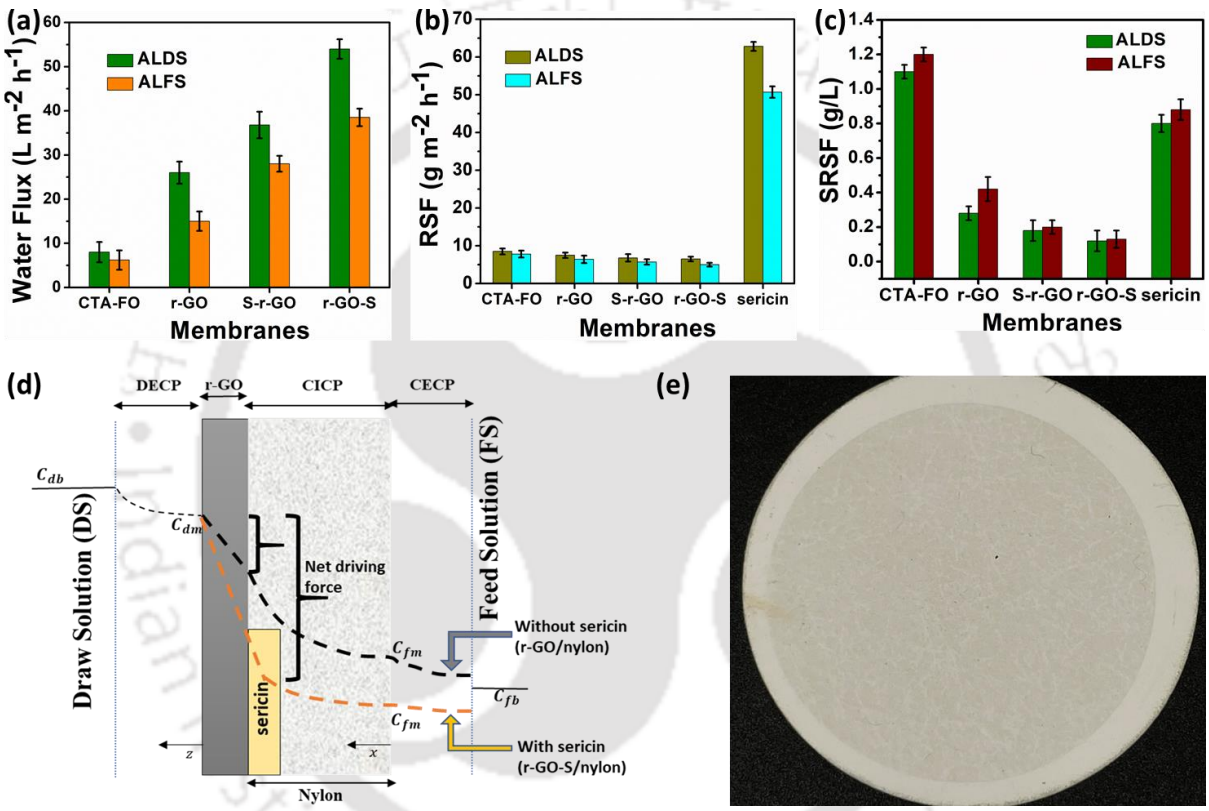

Fig. 26: Comparative FO performance of CTA-FO, r-GO/nylon, S-r-GO/nylon, r-GO-S/nylon and sericin/nylon membranes (a) water flux, (b) RSF, (c) SRSF with 1M NaCl as draw solution and DI water as feed solution in ALDS and ALFS orientation; (d) Conceptual mechanism of water flux of r-GO/nylon and r-GO-S/nylon membrane, (e) Digital image of sericin/nylon membrane (30 ml, 20 mg/ml)

TH-3195_186151006

4.4.8 Long-term stability test

The long-term stability test was conducted for the optimized r-GO-S membrane, and the same was compared with the r-GO membrane. The operating condition was 1M NaCl as draw solution and DI water as feed solution with ALDS orientation. Fig. 27a shows water flux for both r-GO-S and r-GO membranes for 30 long hours. It was observed that for the initial 2 hours of operation the water fluxes of r-GO-S and r-GO membranes were 54 L m^{-2} h^{-1} and 26 L m^{-2} h^{-1}, respectively. With time, the water flux decreases and was saturated at 38 L m^{-2} h^{-1} and 12.2 L m^{-2} h^{-1} for the r-GO-S and r-GO membrane, respectively. It was found that the rate at which the water flux was decreasing was less in the r-GO-S membrane compared to the r-GO membrane. This might be due to the presence of sericin particles inside the substrate which was strongly bonded with nylon substrate as nylon membrane has high protein binding properties. After doing the FO experiment for some hours, both draw and feed sides were thoroughly cleaned with DI water to remove the NaCl and osmotic backwashing was also performed to remove salts from inside the pores of the support layer. This was done to remove the salts completely from both sides and again establishing initial conditions. The water flux of the r-GO-S membrane increased to 45.8 L m^{-2} h^{-1}, while for the r-GO membrane, the water flux increased to 18.5 L m^{-2} h^{-1}. The FRR% of the r-GO-S membrane was 84% whereas for the r-GO membrane it was 70%. The higher FRR% in the r-GO-S membrane was due to the presence of hydrophilic sericin particles present inside the pores, which helped in mitigating internal concentration polarization (ICP) by avoiding the deposition of salt ions inside the pores. As sericin exhibits higher chlorine resistance, the deposition of NaCl inside the pores of nylon will be less as sericin particles were already deposited inside the pores which will ultimately lead to low ICP. Due to low ICP occurrence, after washing with DI water, the r-GO-S membrane produced higher FRR% than r-GO membrane. Similarly, the RSF of the r-GO-S

TH-3195_186151006

membrane was 6.6 g m^{-2} h^{-1} for an initial 2 hours shown in Fig. 27b. With time the RSF value for both the r-GO-S membrane and r-GO membrane was also increased. However, the rate of increment in RSF value for the r-GO-S membrane was less compared to the r-GO membrane because of the more negatively charged r-GO-S membrane. Due to the enhanced negative charges, there is a high electrostatic repulsive force between Cl^- ions and the r-GO-S membrane surface compared to the r-GO surface, and hence, the overall RSF value was less than the r-GO membrane. Moreover, the leaching of r-GO layers after prolonged use also resulted in penetration of salt ions at a faster rate as compared to the r-GO-S membrane where the leaching of the dense layer is not seen in inset of Fig. 27a. The nylon membrane had high protein binding properties which resulted in strong π-π stacking process between the layers along with hydrogen bond network between hydroxyl and epoxy groups of r-GO and polar amino acid residues of sericin, thus increasing the binding force between sericin and r-GO layers[182]. Due to these reasons, the leaching of r-GO-S from the nylon membrane was prevented to a great extent. Fig. 27c shows the leachability of sericin for both draw and feed solutions. It was found to have no traces of sericin in both the solutions. Another reason for the lower RSF of the r-GO-S membrane was due to dilutive external concentration polarization (ECP) at the draw side as higher water flux was obtained for the r-GO-S membrane which diluted the draw solution at a faster rate compared to the r-GO membrane, thus reducing the NaCl concentration difference across the separation layer which resulted in lowering the RSF to a greater extend[116]. Due to this reason, after cleaning the membrane surfaces, the RSF value was observed to be less for the r-GO-S membrane (9 g m^{-2} h^{-1}) than the r-GO membrane (14 g m^{-2} h^{-1}).

TH-3195_186151006

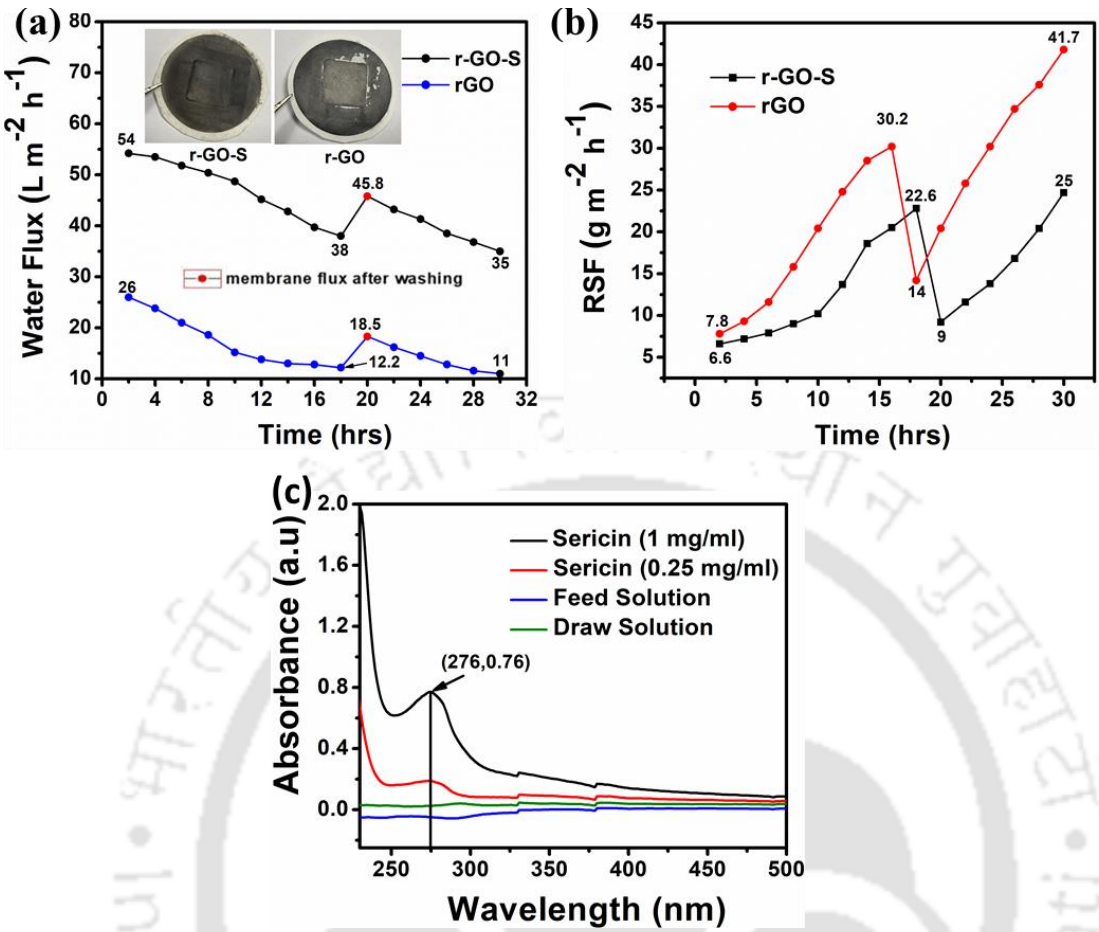

Fig. 27: Comparative long-term stability study of r-GO-S/nylon membrane and r-GO/nylon membrane (inset shows the images of respective membranes) for (a) water flux, (b) RSF with 1M NaCl as draw solution, and DI water as feed solution in ALDS mode, (c) leachability test of sericin in r-GO-S membrane for both draw and feed solutions

4.4.9 Performance of hybrid separation processes of effluent and membrane fouling study

As described in section 4.2.9, downstream of the fermenter was treated through UF, rotary evaporator, FO, centrifuge, and crystallization processes to produce rifaximin crystals. The performance of the membrane was studied by performing multiple FO cycles of batch operation to concentrate rifaximin in an ethanol-water mixer.

TH-3195_186151006

The long-term stability of the r-GO-S membrane in real-time FO experiments for both ALDS and ALFS orientations was investigated. Fig. 28a show the water flux of the r-GO-S membrane. For the initial 2 hours operation, the water fluxes in ALDS and ALFS orientations obtained were 28.6 L m^{-2} h^{-1} and 17.1 L m^{-2} h^{-1}, respectively. With time, the water fluxes decreased and reached 10 L m^{-2} h^{-1} and 7.6 L m^{-2} h^{-1} for ALDS and ALFS modes, respectively, after the 3rd FO cycle due to the deposition of rifaximin crystals nucleate on the membrane support layer, which resulted in fouling and eventually decreased the water flux. During the long-term operation, it was observed that the water flux attenuation in the ALDS mode was high compared to the ALFS mode. This is because the foulant was adsorbed at a faster rate on the support surface compared to the active layer which is negatively charged, thus preventing the foulant to get adsorbed. Moreover, the water flux from the feed to the draw side was concentrated in the feed solution at each FO cycle, which resulted in the increment in the average sizes of rifaximin crystals, thus causing fouling on the membrane surface. Therefore, the membrane and pipes were first flushed with water and then with ethanol (as rifaximin antibiotics were soluble in ethanol only).

Further, to remove foulants in the membrane surface and dense layer, the osmotic backwash was performed by swiping the membrane as described in patent[183]. After cleaning, the FO process was again conducted with the same membrane and the water fluxes in ALDS and ALFS modes were found to be recovered to 21.5 L m^{-2} h^{-1} (74%) and 14.5 L m^{-2} h^{-1} (84%), respectively. The hydrophilic nature of sericin particles build a thin water boundary layer onto the membrane surface through hydrogen bonding that weakens the hydrophobic interaction between rifaximin foulants and membrane surface resulting in smoothed surface that prevents settlement of rifaximin foulants on the membrane surface[184]. Due to the above properties, the rifaximin particles can be removed from the surface by osmotic backwashed and cleaned

TH-3195_186151006

with ethanol (as rifaximin was soluble in ethanol). As a result of better resistance to fouling, the water flux can be recovered to a great extent, thus increasing the FRR. Furthermore, since the r-GO-S membrane was negatively charged, the higher electrostatic repulsion between effluent (-70 mV) and r-GO-S membrane resulted in lesser adsorption of rifaximin in ALFS mode than in the AFDS mode which resulted in less fouling tendency, thus increasing the FRR% of (~ 84%) for ALFS mode compared to FRR% of (~74%) for ALDS mode.

Similarly, like water flux, the forward rifaximin flux (FRF) also showed a decreasing trend with the increasing operating time. After operating for initial 16 hrs, the FRF value decreased from 0.42 g/h to 0.25 g/h and from 0.22 g/h to 0.13 g/h for ALDS mode and ALFS mode, respectively shown in Fig. 28b. This was due to the deposition of the rifaximin crystals on the membrane support layer surface (ALDS) as well as an active layer (ALFS) for a prolonged time (shown in the digital image in Fig. 28d) resulting in the decrease in water flux which simultaneously decreased the rifaximin flux in draw side with time. The deposition of rifaximin foulants on the active and support layer of the membrane is shown in the FESEM image of Fig. A1a-b. However, after ethanol cleaning and osmotic backwashing of the membrane, the FRF value increased to 0.34 g/h and 0.18 g/h for ALDS and ALFS modes. This was mainly due to the removal of rifaximin crystals deposited on the porous nylon support (ALDS) and active layer (ALFS) as well as the inner region, which paved the way for water molecules to pass easily across the separation layer, thus simultaneously increasing both water flux and FRF values. The RSF values shown in Fig. 28c revealed that with increasing operating time, both Na^+ and Cl^- ions from the draw solution were increasing with concentration. However, the RSF_{NaCl} in ALDS (6.8 g m^{-2} h^{-1}) was a little high compared to ALFS (4.2 g m^{-2} h^{-1}). This was due to the higher water flux obtained in ALDS compared to ALFS mode resulting in concentrated ICP in ALDS mode, whereas it was dilutive ICP in ALFS mode. Also, during the

TH-3195_186151006

long-term stability operation, the overall RSF_{NaCl} in ALFS mode was less compared to the ALDS mode due to the Donnan exclusion theory. The digital images of the GO and S-GO membranes along with GO dispersion and sericin solution are shown in Fig. 28e. Fig. A1c-d show the EDX spectra of the r-GO-S membrane before and after the FO process. The high traces of Cl^- ions are visible on the membrane surface after the FO process compared to low traces of Na^+ ions due to penetration of Na^+ ions through the membrane as the surface charge of the membrane is negative. Hence, the rejection of Cl^- ions was higher than Na^+, resulting in deposition on the membrane surface. It was revealed after long-term FO operation (32 hrs for FO process), the coating layer was not leaching out from the nylon membrane, which confirms better durability and satisfactory stability performance. Moreover, to confirm the durability of the fabricated membranes, stress vs stain curves were recorded for different membranes, shown in Fig. A1e. From the stress-strain curve, the maximum tensile stress of both sericin doped r-GO membranes were found to be highest for r-GO-S/nylon (14 MPa) and S-r-GO/nylon (11 MPa) membranes, which was significantly higher than that of pure nylon membrane (8.5 MPa). The improvements in mechanical properties are attributed to strong hydrogen bonding between the functional groups of rGO and sericin, leading to strong interfacial interaction between the matrix, thus increasing the toughness[185].

TH-3195_186151006

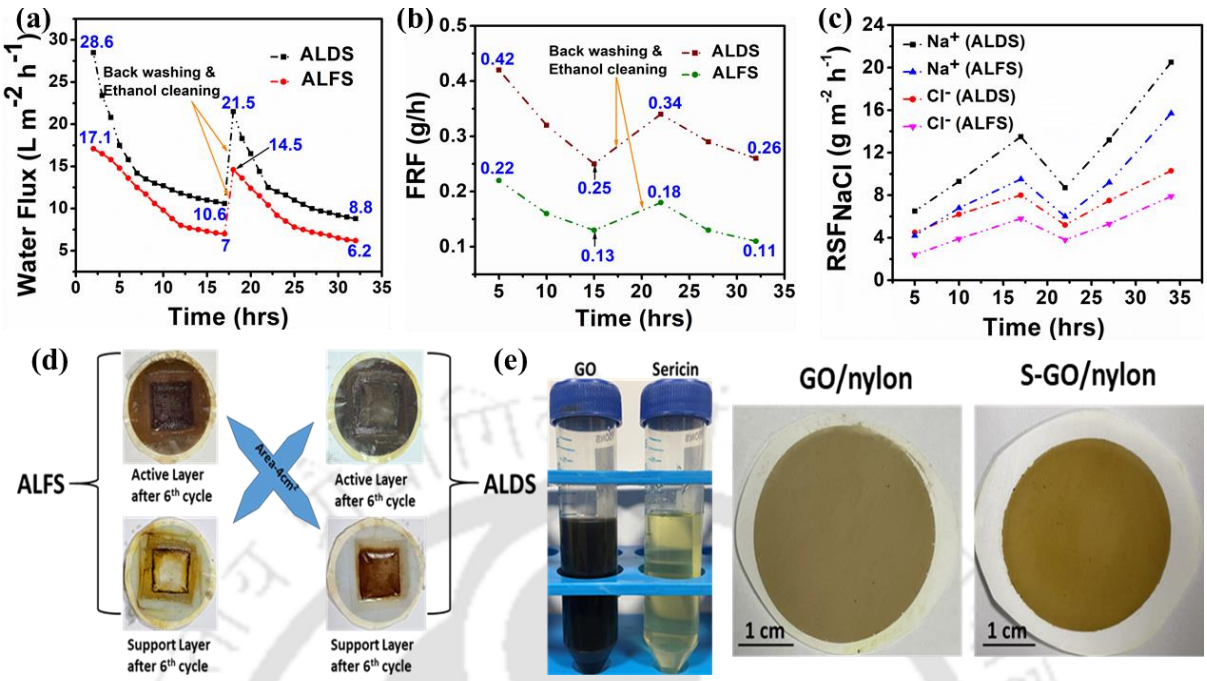

Fig. 28: Long term FO performance of r-GO-S membrane (a) water flux, (b) FRF, (c) RSF with 4M NaCl as draw solution and effluent as feed solution; (d) digital images of r-GO-S membrane used after 6th cycle for ALDS and ALFS modes and corresponding GO dispersion and sericin solution and (e) corresponding GO dispersion and sericin solution along with digital images of GO/nylon and S-GO/nylon membrane

After each FO batch cycle, the concentrated feed solution was centrifuged for 20 mins at 6000 rpm and the supernatant solution was again recycled for subsequent FO cycles. So due to these reasons, there was a decrement of feed volume as the batch cycle increases. Moreover, parafilm sheets were used to seal both draw and feed sides to prevent evaporation loss. The average sizes of supernatant solution were small compared to pellet solution, subsequent FO cycles of supernatant solution would again increase the sizes, thus recovering more rifaximin amount. The pellet solution recovered was vacuum filtered through a PTFE membrane (0.1 µm pore size) and dried in a desiccator. The rifaximin powder crystals recovered were thoroughly washed with DI water 2 times to purge salt ions present inside the crystals. The amount of

TH-3195_186151006

rifaximin powder crystals recovered after successive batches of the FO cycle is shown in Fig. 29a. As the concentration of the feed side was increased slightly due to water removal, the average rifaximin sizes were also increased, resulting in pellet formation after the centrifugation process. It was found that the recovered rifaximin amount in the FO-3 cycle was slightly higher than the FO-2 cycle due to a higher operation run (7 hours) compared to the FO-2 cycle (5 hours), resulting in the extraction of more water which concentrated the feed solution more than FO-2 cycle. However, the average rifaximin sizes in ALFS mode were observed to be lower than in ALDS mode. This may be due to the following two phenomena occurring at the support and dense layer surface (i) high internal concentrative CP of rifaximin with high water flux in ALDS mode and (ii) low external concentrative CP of rifaximin with low water flux in ALFS model. Therefore, in ALDS mode the rifaximin concentration at the dense layer surface was expected to be higher than in the ALFS mode. The high localized concentration of rifaximin can enable better crystal growth. The average rifaximin sizes before and after each batch FO cycle are shown in Fig. 29b. The digital images of rifaximin powder recovered at different stages of FO cycles are shown in Fig. 29c. The characterizations of powder from effluent solution shown in Fig. A2a-c confirm the validation of powder crystal as rifaximin antibiotics which are consistent with reported literature[186]. The XRD analysis of rifaximin powder crystal shows numerous peaks which confirms its crystalline nature of it, whereas the FTIR spectra reveal the presence of functional groups like OH group, ketone group, etc. The FESEM image clearly shows the crystal formation of rifaximin with a size ranging from 0.1 µm to 4 µm and the same validation was done with Delsa nano also.

TH-3195_186151006

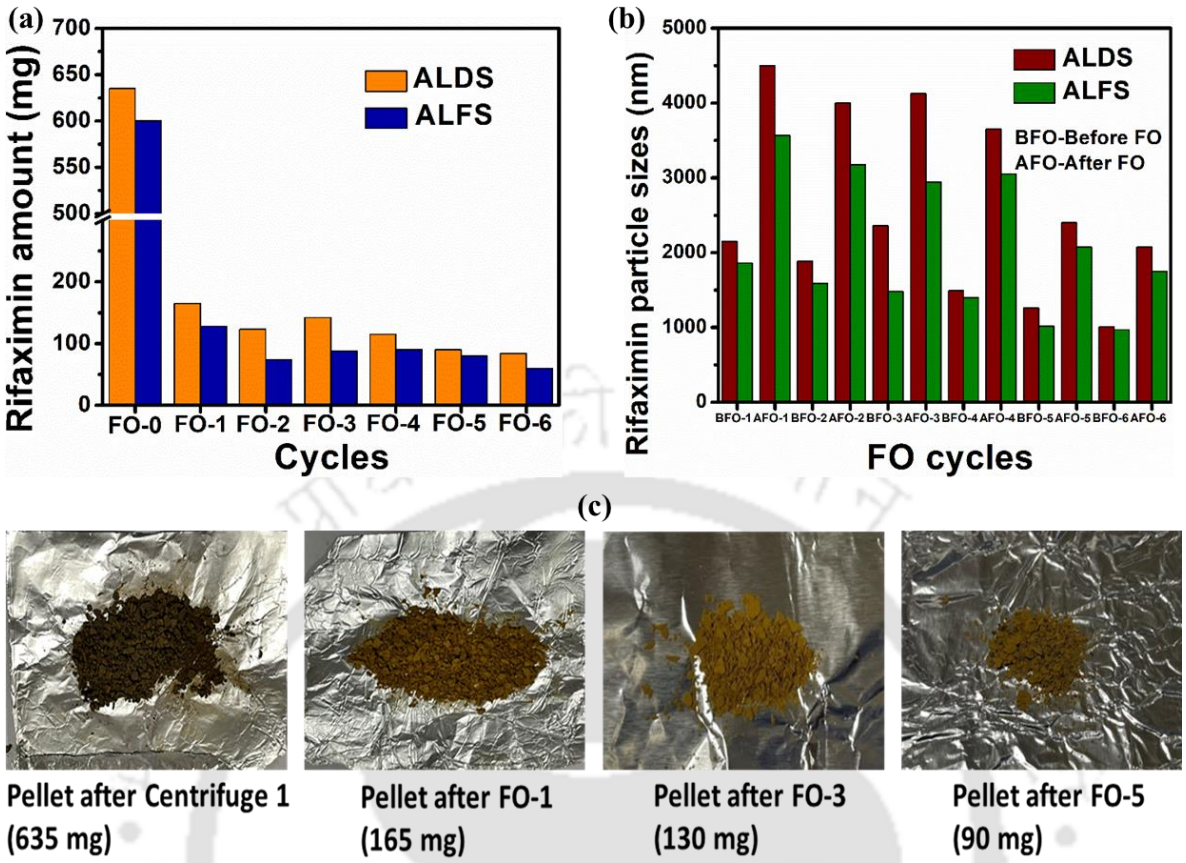

Fig. 29: (a) Amount of rifaximin recovered after each batch of FO cycle; (b) Average rifaximin sizes before and after each cycle; (c) Digital images of recovered rifaximin powder at different stages of FO cycle

Moreover, the comparative fouling studies of r-GO-S/nylon membrane and literature reported sericin doped membranes are shown in Table 5.

Table 5: Comparative fouling studies of the r-GO-S/nylon membrane with literature reported sericin doped membranes

Membrane	Mode	Foulant	FRR%	References
r-GO-S/nylon	FO	Effluent	84%	This work

TH-3195_186151006

r-GO-S/nylon	PRO	Effluent	74%	This work
S-PA	RO	BSA	70.8%	[180]
S-TFC PA	RO	BSA	80%	[187]
S-TMC PSf	NF	BSA	86%	[188]
S-PP HF	NF	Greywater	99%	[189]

S-PA= Sericin modified polyamide; S-TFC PA= Sericin modified thin-film composite polyamide; S-TMC PSf= Sericin modified trimesoyl chloride polysulfone; S-PP HF= Sericin modified polypropylene hollow fiber; BSA- Bovine serum albumin, FO- Forward osmosis, RO- Reverse osmosis, NF- Nanofiltration

4.5 Summary

This study explored the effect of sericin doping on r-GO laminates for higher performance in the FO process. We fabricated sericin doped r-GO membranes by two facile methods including vacuum filtration on a porous nylon support layer and annealing it for final membrane formation. With the addition of hydrophilic sericin on the r-GO layer and vice versa, the membrane properties were further enhanced with surface smoothening, and higher negative surface energy, which improves the membrane performance. The optimized r-GO-S/nylon membrane exhibited excellent water flux (54 L m^{-2} h^{-1}) and better SRSF (0.12 g/L) than the pristine r-GO membrane (0.28 g/L) and commercial membranes (0.4-0.5 g/L). The sericin when combined with r-GO laminates induces higher negative surface energy on the membrane, resulting in the formation of electrostatic repulsion force between Cl^- ions and membrane surface, thus increasing the overall salt rejection capacity. The long-term stability test showed

TH-3195_186151006

higher FO performance for the r-GO-S membrane compared to the r-GO membrane without leaching the coating layer. The membrane regeneration properties of combined sericin and r-GO layers resulted in excellent FRR% of 84% in ALFS mode and 74% in ALDS mode, thus revealing better durability and long-term stability of the membrane. Finally, our results can provide a breakthrough in the modification of FO membranes and can be a potential candidate for various water-related applications. Furthermore, the combination of FO with other membrane processes like UF and vacuum distillation would enable fouling resistant energy-efficient operation and achieve high effective antibiotic recovery from pharmaceutical effluent using a cost-effective strategy.

TH-3195_186151006

TH-3195_186151006

CHAPTER 5

5 Energy recovery from forward osmosis process using amorphous silicon oxide crosslinked vanadium pentoxide-reduced graphene oxide membrane

Abstract: This chapter reports an innovative approach to minimize the energy consumption by transforming the reverse solute flux into sustainable electricity by the application of a novel FO membrane fabricated with two-dimensional flakes of vanadium pentoxide (VO) and reduced graphene oxide (r-GO) and cross-linked with amorphous silicon oxide (aSiO).

This part of the thesis is published in Chemical Engineering Journal. 469 (2023) 143964 (https://doi.org/https://doi.org/10.1016/j.cej.2023.143964).

TH-3195_186151006

5.1 Introduction

Sustainable energy harvesting system became pivotal for meeting today's technological advances. The salinity gradient energy is one of the most predictable and stable energy resources that can produce clean energy due to its abundant reserves and wide distribution[190]. This clean energy resource can be captured through membrane technologies, such as pressure retarded osmosis (PRO) or reverse electrodialysis (RED)[191]. One of the emerging technologies for producing clean water and clean energy in a sustainable way is forward osmosis process (FO)[192]. The FO process is gaining tremendous attention for applications such as concentrations of high-value products and wastewater treatment[193]. However, difficulties and expensive regeneration process of draw solution (DS) is making FO an energy-intensive method for producing low-cost end products. Moreover, the techno-economic studies and financial payback time of any FO process depend on the water flux of the FO membrane[194]. The higher water flux can lead to lower payback time, reducing the system's overall cost and energy consumption. The utilization of commercial FO membranes and polymer-based membranes is hindered by their lower water flux, increased reverse solute flux (RSF), proneness to fouling, and elevated costs, thus restricting their applicability[195]. Additionally, recent statistics indicate that existing technologies require substantial energy and incur high expenses[196,197]. Therefore, the development of tightly arranged permselective nanofluidic membranes, formed by assembling two-dimensional nanomaterials, offers promising prospects for cost reduction by concurrently enhancing water flux and decreasing reverse solute flux.

Scattered research efforts addressing the entangled issues of water and energy as a whole were explored in some literatures. For example, the bio-electrochemical reactions of microorganisms in microbial cells shown to produce energy and pure water simultaneously[198]. However,

TH-3195_186151006

maintaining the pace of such enzymatic processes is a nontrivial task. Park et al. showcased the potential of ion-selective membranes in the reverse osmosis (RO) process, enabling the recovery of approximately 50% of the pumping energy while simultaneously producing water and energy[32]. However, preserving the integrity of electrode-membrane assemblies within high-pressure systems remains a formidable obstacle, particularly in fields such as fuel cells and electrolyzer[199,200]. Therefore, the search is on for alternative systems or methods along with fabrication of novel membranes that could simultaneously address the issues of water and energy.

The salinity gradient driven energy harvesting process, namely pressure retarded osmosis (PRO)[46], RED[201], and capacitive mixing (CM)[202] were extensively studied for standalone energy generation applications, considering the viability of producing more than 15% of the total global energy by mixing river and seawater. However, the unavailability of suitable membranes hinders the progress in longer run. Moreover, the fabrication of membranes for these processes requires exotic techniques, which were not widely available until recently. However, the recent escalation in the research related to the fabrication of novel membranes/materials uncovered several new ways of preparing well-packed perm-selective nanofluidic channels in high density. These new developments in membrane technology were leading to a resurgence in the concentration gradient-driven energy harvesting processes.

5.2 Scope of this investigation

The concentration gradient-driven energy harvesting process involves the transport of ions across a selective membrane from a higher concentration to a lower concentration chamber, while the FO process involves the transport of water molecules across a semi-permeable membrane from a lower concentration to a higher concentration chamber[203]. The basic requirements of the membrane for both these processes are different, for example, a FO

TH-3195_186151006

membrane needs to have high water flux and low salt permeability, while a RED membrane requires to have high ion selectivity and low resistance to ionic transport for the concentration gradient energy generation process. However, features like permselectivity, high porosity, high charge density, and higher stability are desired in both kinds of membranes[204]. Due to their non-ion-specific transport properties, commercial FO membranes are not suitable for electrochemical-based energy harvesting processes. Hence, coating of nanomaterials on conventional FO membranes is found to enhance the water flux and ion selectivity by increasing the charge density, and such coated membranes can be applicable for both FO and energy generation processes. Among different 2D material-based membranes, vanadium pentoxide (VO) possesses the highest surface charge and lowest resistance to ionic transport[205]. Similarly, reduced graphene oxide (rGO) based membranes are known to possess superior stability, selectivity and anti-fouling properties in an aqueous medium[206]. The optimized membrane can exhibit higher water flux and low reverse solute flux (RSF) and simultaneously can generate electrical energy to compensate for the energy consumption during the FO process.

In the present study, we demonstrated the possibility of simultaneous energy generation and FO-based concentrating process by employing a hybrid bi-layer membrane of aSiO crosslinked r-GO and VO nanosheets. Remarkably, the coating of modified VO and rGO nanosheets drastically enhanced the water flux and decreased the RSF while simultaneously generating electrical energy for prolonged operational hours. Additionally, the study also explored energy-recovering possibilities and crystal production in realistic scenarios using different concentrations of tea as the feed solutions Moreover, the robust coating of 2D nanomaterials showed excellent stability (for more than 90 days) in DI water as well as in acidic and basic mediums. The results of this work not only address the critical gap in the efficient use of energy

TH-3195_186151006

in the FO process but also provide a significant breakthrough towards sustainable and efficient water treatment technologies with integrated energy recovery systems.

5.3 Experimental sections

5.3.1 Materials

Sigma Aldrich-India, supplied sulphuric acid (H_2SO_4), graphite powder, hydrogen peroxide (H_2O_2), hydrochloric acid (HCl), sodium chloride (NaCl), potassium chloride (KCl), potassium dihydrogen phosphate (KH_2PO_4), potassium permanganate ($KMnO_4$), vanadium pentoxide (V_2O_5) and bis[3-(triethoxysilyl) propyl] tetrasulfide (Bis) (MW: 538.95 g/mol). Nylon membrane (0.22 µm pore size) was purchased from Sterlitech Corporation, USA. Tea dust was purchased from local market.

5.3.2 Synthesis of GO nanosheets

GO sample was prepared by following modified Hummer's method. Typically, 1 g of graphite and 6 g of $KMnO_4$ were slowly added into 50 ml of H_2SO_4 solution in an ice bath under continuous stirring conditions. The solution was then transferred into a water bath maintained at 35 $^{\circ}$C. After 2 hours, the solution was transferred back to the ice bath and 100 ml of deionized (DI) water was added very slowly, maintaining the temperature below 30 $^{\circ}$C which was followed by dropwise addition of H_2O_2 solution (8 ml). The addition of H_2O_2 changed the colour of the solution from black to light yellow. The resultant solution was repeatedly washed with HCl solution (20 wt.%, 500 ml) through centrifugation and filtration process. After washing with HCl, the GO sample was dried in a desiccator followed by washing with excess acetone. An aqueous dispersion of the prepared GO (1 mg/ml) was centrifuged for 10 minutes (at 2000 rpm) to separate the large aggregates and the supernatant solution was preserved for further experiments.

TH-3195_186151006

5.3.3 Synthesis of VO dispersion and VO-aSiO membrane

The VO nanosheets were synthesized by stirring VO powder with H_2O_2 in ice-cold conditions (5-10 °C)[207]. Typically, 2.4 g VO powder was dispersed in 25 ml deionized (DI) water, followed by the addition of 25 ml of 50 % H_2O_2. The addition of H_2O_2 produced vigorous bubbling, yielding dark-brown precipitation, which slowly turned into a thick gel. The gel was diluted with DI water to prepare dispersions of required concentrations.

For the preparation of VO-aSiO membrane, 40 µl bis[3-(triethoxysilyl) propyl] tetrasulfide (Bis) was stirred with 25 ml ethanol for 1 h and 13 ml of VO dispersion (15 mg/ml) was mixed with Bis solution and heated at 80 °C for 3 h under refluxed conditions. After reacting with Bis, the dark brownish-coloured VO dispersion turned into dark greenish coloured aSiO-VO dispersion. Finally, the solution was filtered through a PTFE membrane of 0.1 µm pore size and dried in ambient conditions to obtain the freestanding VO-aSiO membrane. The digital images of the dispersions and respective membranes are shown in Fig. 30.

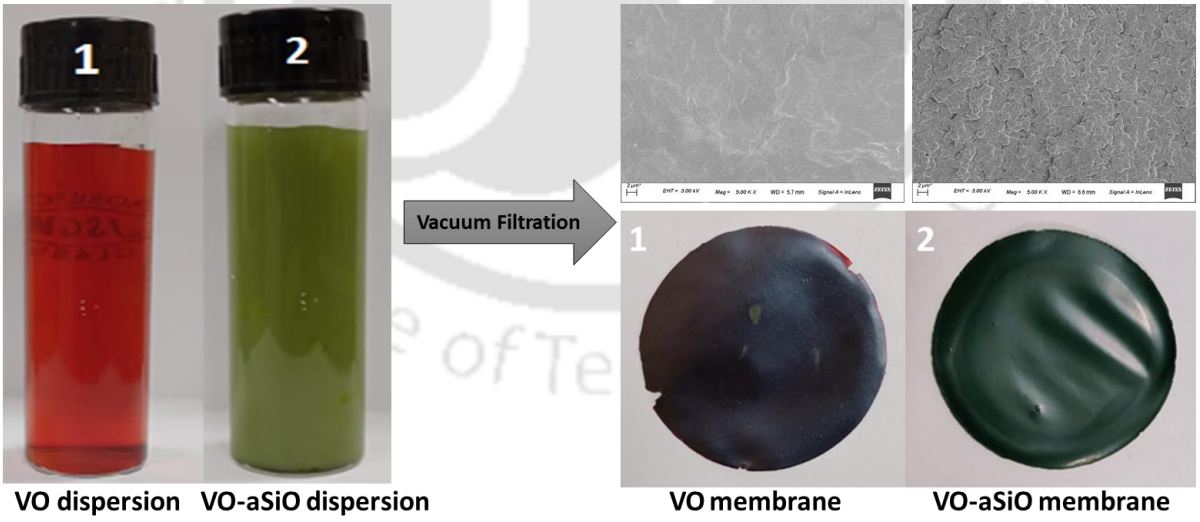

Fig. 30 Digital image of VO and VO-aSiO dispersion and their respective membranes and FESEM images

TH-3195_186151006

5.3.4 Fabrication of VO-aSiO-rGO membrane

Typically, a thin layer of GO flakes was coated on top of a nylon support membrane via vacuum filtering 30 ml aqueous dispersion of graphene oxide (GO) (0.033 mg/ml). The VO-aSiO dispersion (4 ml of 1 mg/ml) was vacuum filtered through the GO-coated nylon membrane. The tri-layered membrane was then dried inside a desiccator for 24 h, followed by heating under vacuum at 150 °C for 2 h. Digital images of thus prepared membranes (VO-aSiO-rGO) and GO membranes are shown in Fig. 31.

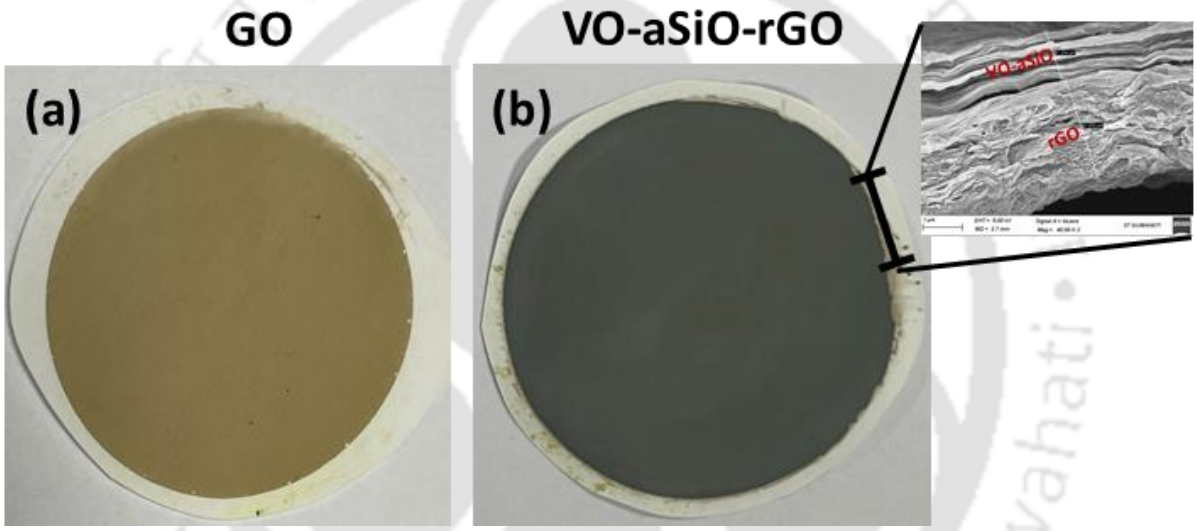

Fig. 31: Digital images of (a) GO, (b) VO-aSiO-rGO membranes (inset FESEM cross-section image)

5.3.5 Generation of electricity from concentration gradient

The VO-aSiO-rGO/nylon membrane was placed as a separator between two chambers of an electrochemical device. Two Ag/AgCl electrodes connected to a Keithley-2450 sourcemeter instrument were dipped in the reservoir solutions. The output voltage and current values were recorded using Keithley-2450 digital sourcemeter, by filling one of the chambers with an aqueous solution of 10^{-6} M KCl, and the KCl concentration of other chambers was varied from

TH-3195_186151006

10^{-5} M to 1 M. The current-voltage (I-V), and current-time (I-T) graphs were recorded under each salinity gradient and correspondingly power density was calculated by using Equation 12.

$$P = V * I/A \quad 12$$

Where V was the output voltage in Volt (V), I was the output current in Ampere (A) and A was the membrane area in m^2.

5.3.6 Membrane parameter estimation

The water flux and reverse solute flux across the membrane for increasing draw solution concentration is represented by solution diffusion (SD) model in equation 5 and equation 6. where, the L_p, B, P_d, and P_f represents the pure water permeability coefficient ($L\ m^{-2}\ h^{-1} bar^{-1}$), solute (NaCl) permeability coefficient ($L\ m^{-2}\ h^{-1}$), and transmembrane pressure (bar) between DS and FS, respectively. The π_{dm}, π_{fm}, $C_{dm}$and C_{fm} represents the osmotic pressure and concentration at the active layer of the membrane surface on the draw and feed sides, respectively.

5.3.7 Membrane performance evaluation

The performance of fabricated rGO, VO-aSiO and VO-aSiO-rGO membranes was investigated in a lab-scale FO set-up (effective area of 4 cm^2) under a controlled environment. The draw solution (DS) and feed solution (FS) tanks were circulated through the FO test cell with a definite flow rate using plunger pumps. The water flux was calculated by measuring the change the DS weight change using a weighing balance (model-XD/XR) with accuracy of ±0.01 g. The reverse solute flux (RSF) of different salt concentrations was measured by using the Hanna conductivity meter (model H15321). Two copper wires were inserted on either side of the membrane and connected to the sourcemeter. The schematic of the FO setup coupled with the sourcemeter is shown in Fig. 32.

TH-3195_186151006

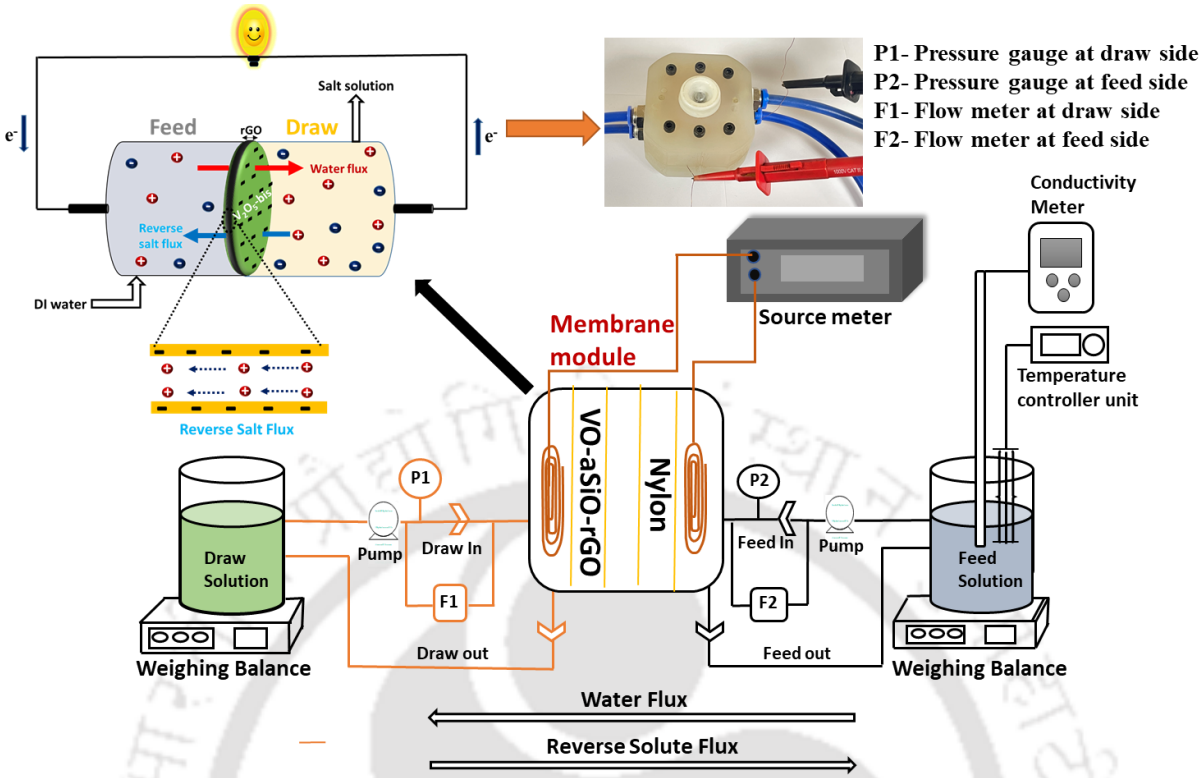

Fig. 32: Schematic of FO setup used for simultaneous energy harvesting and forward osmosis

5.4 Results and Discussions

5.4.1 Characterization of GO and VO nanosheet and their respective membranes

The bi-layer nanoporous membrane was prepared by coating commercial nylon membranes with aSiO crosslinked 2D sheets VO and GO (VO-aSiO-GO). While GO was prepared through the modified hammer method, VO sheets were exfoliated from bulk powder by treating them with ice-cold H_2O_2 at 5-10 °C[208,209]. The EDX spectra of the VO-aSiO-rGO membrane reveal the presence of silicon and sulphur, whereas the XRD spectra shows peaks of both VO-aSiO and rGO for VO-aSiO-rGO membrane. Moreover, the contact angle of VO-aSiO-rGO membrane shows drastic reduction (50°) as compared to rGO membrane (80°) due to the presence of hydrophilic VO-aSiO laminates, as shown in Fig. 33A. The lateral dimensions of GO were in the range of 500 to 2000 nm, and that of VO varies between 300 and 800 nm, see AFM images in Fig. 33B(a-b). The average height of GO, and VO flakes were ~ 5 nm and 6

TH-3195_186151006

nm, respectively. The zeta potentials of both GO and VO were negative with a magnitude of 31 mV and 45 mV, respectively, consistent with the earlier reports. The large negative zeta potentials values indicate the existence of high-density negative charges on the surface of the 2D sheets.

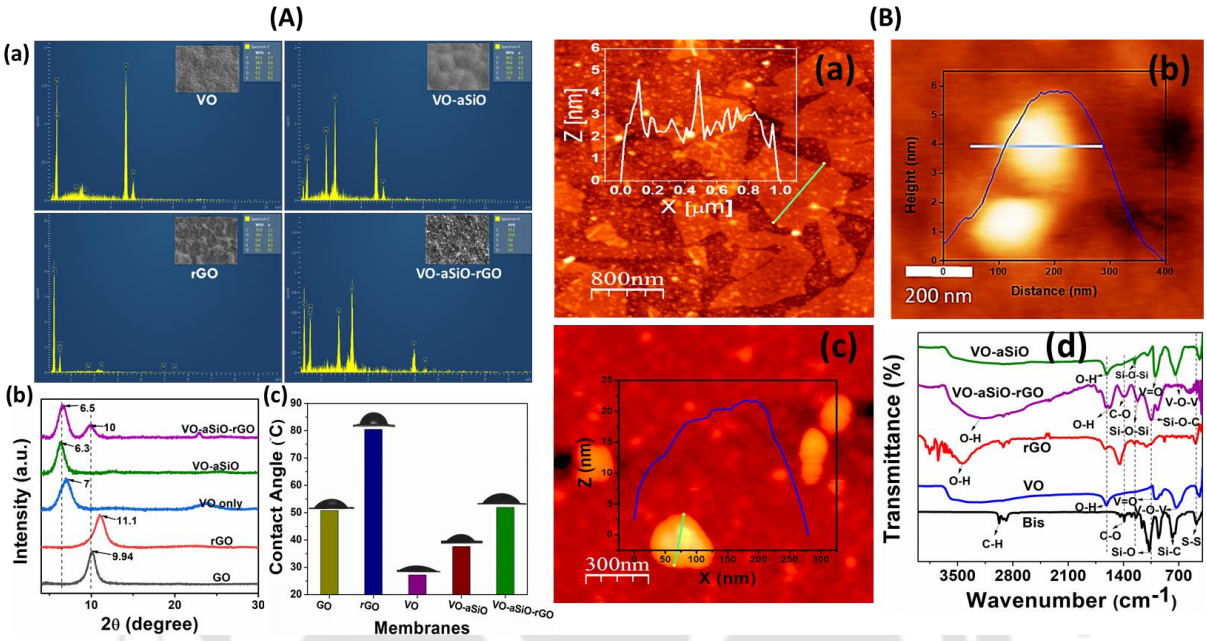

Fig. 33: (A) (a) EDX spectra along with (b) XRD and (c) contact angle of VO, VO-aSiO, r-GO, VO-aSiO-rGO and GO membranes, (B) AFM images of (a) GO, (b)VO nanosheets, (c) VO-aSiO nanosheets and (d) FTIR spectra of VO-aSiO, VO-aSiO-rGO, r-GO, and VO membranes were compared with that of Bis

As illustrated in Fig. 34a, pristine VO nanosheets were functionalized with aSiO crosslinker by reacting the same with Bis molecules at 80 ˚C. After the aSiO coating, the magnitude of the zeta potential of VO was found to decrease from - 45 mV to - 34 mV. The reduction in zeta potential is attributed to the consumption of free surface hydroxyl groups for binding with aSiO linkers generated from the decomposition of Bis molecule. A similar observation was reported by Cheng et al with kaolinite clay [210]. Before heating at 80 ºC, the X–ray photoelectron

TH-3195_186151006

spectrum (XPS) of the VO and Bis mixture showed a doublet energy peak of S 2p centred at 164 eV and 168 eV originating from the S-S group[211]. However, it disappeared after the heat treatment process, suggesting the decomposition of the Bis-molecule, shown in Fig. 34b. The Bis-molecule decomposes by releasing ethanol and the S-S group leaving behind amorphous SiO[210]. The release of the S-S group and formation of aSiO was also supported by the FTIR analysis. The band centred at 472 cm^{-1} (S-S bond) and 780 cm^{-1} (Si-C group) of the Bis molecule[212] disappeared after the heat treatment process, indicating the release of the S-S group and breakage of the Si-C linkage, respectively. A new peak centred at 1256 cm^{-1} appeared in the IR spectrum of the VO-aSiO membrane that represents the Si-O-Si linkage which proves the successful grafting of SiO moieties onto the surface of VO nanosheets via chemical bonding[213], see Fig. 34c. The dark patches of the VO-aSiO sample observed in the FETEM examination also indicate the deposition of aSiO on the VO surface shown in Fig. 34d. Moreover, the surface morphology of the VO-aSiO membrane in FESEM shows a rough and fluffy-like surface (see Fig. 34e), indicating the formation of agglomerated nanospheres of amorphous oxides of silicon after decomposition of Bis molecules.

The VO-aSiO-rGO membrane was prepared by vacuum filtering VO-aSiO dispersion through GO coated nylon membranes followed by heating at 150 °C. The annealing process reduces oxygenated functional groups of GO and helps to strengthen the membrane through π-π interactions between the graphitic regions of adjacent rGO nanosheets[214]. During the vacuum filtration and heating process, the crosslinking of aSiO also extends to rGO layers via bonding between the terminal -Si-OH group of VO-aSiO and oxygen functional groups of rGO through hydrolysis, which is evident from the Si-O-C band at 1050 cm^{-1} in the IR spectrum of VO-aSiO-rGO in Fig. 33B(d). A similar mechanism was reported by Zhang et al, where the hydrolysis of tetra-ethyl-ortho-silicate (TEOS) led to the formation of silica nanoparticles,

TH-3195_186151006

which interacted with GO nanosheets through the conversion of C=O bonds on GO to Si-O-C bonds upon reaction with TEOS[215]. The existence of crosslinking and π-π interactions in the VO-aSiO-rGO membrane was also indicated by the outstanding stability of the membrane in aqueous environments. Soaking in water for more than 60 days did not deteriorate its mechanical and chemical integrity. Under similar conditions, both pristine GO and rGO membranes started breaking down within 10 days. The stability of the VO-aSiO-rGO membrane was also studied under acidic and basic conditions, as shown in Fig. A3a-b. It was seen that even after 90 days of soaking in 10^{-3} M and 10^{-4} M HCl and 10^{-3} M and 10^{-4} M NaOH solution, the membrane's structural integrity was intact without deteriorating its mechanical strength.

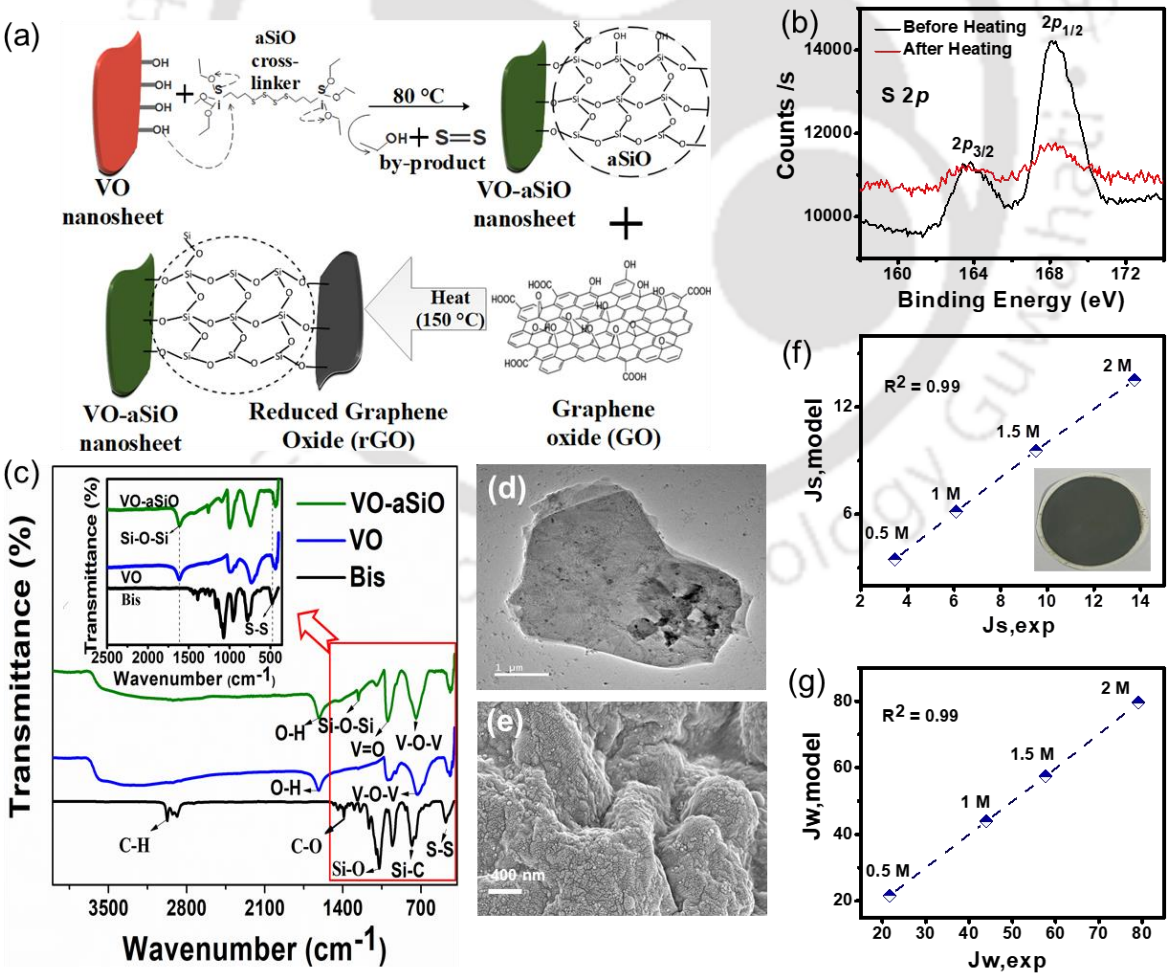

TH-3195_186151006

Fig. 34: Basic characterizations of membranes: (a) Schematic illustration of the VO-aSiO-rGO membrane fabrication process. (b) XPS peak of sulphur 2p in VO-Bis mixture before and after heating at 80 ºC. (c) FTIR spectra of VO-aSiO, VO and Bis samples. (d) FETEM image of VO-aSiO nanosheet, and (e) FESEM surface morphology of VO-aSiO membrane. The intrinsic parameters of the VO-aSiO-rGO membrane: (f) reverse solute flux (g m^{-2} h^{-1}) (inset image shows VO-aSiO-rGO membrane), (g) water flux (L m^{-2} h^{-1}) with DS of different concentrations (0.5M-2M) with DI water as the FS

The intrinsic parameters like water permeability (L_p), solute permeability (B) and structural parameter (S) for optimized VO-aSiO-rGO membrane were estimated in the active layer facing draw solution (ALDS) mode of the FO process[216]. The pure water permeability (L_p, L/m^2.h.bar), solute permeability coefficient (B, L/m^2.h), structural parameter (S, nm), and mass transfer coefficient for DS and FS (K_d, m.h^{-1}) of VO-aSiO-rGO membrane were estimated to be 39.9 ±0.004, 6.57 ±0.065, 472500, 0.74 ±0.008 and 18.02 ±0.043, respectively. The pure water permeability, solute (NaCl) permeability coefficient and structural parameters were also determined experimentally. Fig. 34f and Fig. 34g compares experimentally and model predicted water flux and reverse solute flux for 0.5M-2M draw solution concentration. It can be observed that both water flux and reverse solute fluxes of the model and experimental data were aligned with R^2 values of around 0.99 confirming the validation of experimental results with the model study.

To understand the transport characteristics of the VO-aSiO-rGO membrane, a rectangular piece of the same was mounted in between two compartments of an electrochemical device. Ionic conductivities of the membrane were measured by filling the compartments with aqueous KCl solutions. The linear current vs voltage (I-V) curves going through the origin indicate the presence of fluidic channels in the VO-aSiO-rGO membrane that interconnect the electrolyte

TH-3195_186151006

chambers. The conductivity vs KCl concentration plot shown in Fig. 35a displays two distinct regimes, for bulk-like conductivity and surface-charged-governed conductivity. The occurrence of surface-charged-governed conductivity and XRD reflections in the 2Θ values at 6.5Å and 10Å suggest the existence of molecularly thin 2D nanofluidic channels in the VO-aSiO-rGO membrane as shown in the Fig. 33A(b).

5.4.2 Concentration gradient-driven electricity generation

The developed membrane consists of tiny nanofluidic channels that can selectively transport ions and molecules based on their size and charge, providing an ideal means for separating and purifying substances. The fabricated membrane generated electrical energy from a concentration gradient established in the compartments of an electrochemical device (shown in the inset image of Fig. 35b) and was separated by a VO-aSiO-rGO membrane. The low concentration side was fixed at 10^{-6} M aqueous KCl solution and the high concentration side was varied from 10^{-5} M to 1M. As expected, the VO-aSiO-rGO membrane generated different open circuit voltage (V_{oc}) and short-circuit current (I_{sc}) from the varying concentration gradients. The system could generate a V_{oc} of 293.3 mV and I_{sc} of 32.2 µA at the maximum concentration gradient. The V_{oc} and I_{sc} vs time curve is shown in Fig. 35c. The declining trend of current can be attributed to the change in the concentration gradient across the chambers (due to the water flux and RSF), and concentration polarization near the membrane. The V_{oc} (at I = 0) and I_{sc} (at V = 0) obtained from I-V curves were found to be increasing with the increasing concentration gradient, as shown in Fig. 35d. The power density was found to be increasing with the increasing concentration gradients, and the highest power density of 4.72 $W.m^{-2}$ was measured at a concentration gradient of 10^6 fold, as shown in Fig. 36a . In Table 6, the output energy performance of VO-aSiO-rGO membrane is compared with other systems reported in recent years.

TH-3195_186151006

Table 6: Comparative energy performance of our membrane and other reported literatures

Membrane	**Salinity gradient**	**Power density ($W.m^{-2}$)**	**Voltage (mV)**	**Reference**
PEI@GO/CNFs	50 fold	5	158	[217]
MS/AAO	1µM – 3M	4.5	96	[218]
TOBC/GO	0.5 – 0.01 M	0.96	121	[219]
CoAl LDH	10^3 fold	0.7	165	[220]
ANFs@MMT	10^4 fold	5.16	197.45	[221]
WS_2/CNF	0.5 – 0.01 M	1.99	55.81	[222]
$Ti_3C_2T_X$	10 µM – 3M	7.89	280	[223]
VO-aSiO-rGO	10^6 fold	4.75	293	This work

PEI@GO/CNFs = Carbon nanofibers membrane bridged with grapheme nanosheet and hyperbranched polymer, MS/AAO = Mesoporous silica-alumina heterostructure membrane, TOBC/GO = TEMPO oxidized cellulose nanofiber, CoAl LDH= Cobalt Aluminium layer double hydroxide, ANFs@MMT = Aramid nanofibres were intercalated into lamellar montmorillonite membrane, WS_2/CNF = Metallic phase WS_2/ cellulose nanofibre composite membrane, $Ti_3C_2T_X$ = Layered titanium carbide membrane

TH-3195_186151006

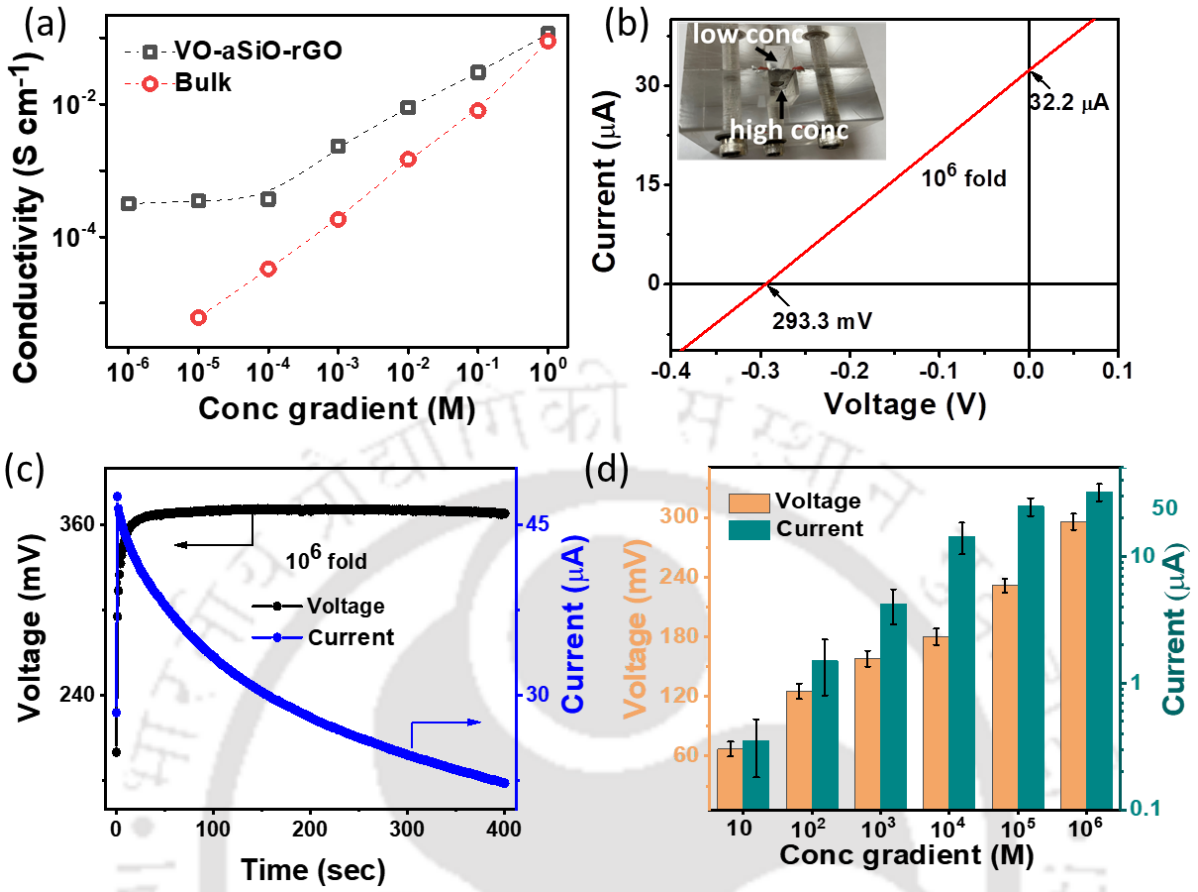

Fig. 35: Generation of electricity from concentration gradients: (a) Surface charge governed ionic conductivity plot, and (b) I-V graph of VO-aSiO-rGO membrane with 10^6 fold concentration gradient of KCl (inset image shows a digital image of an electrochemical device). (c) Output voltage and current as a function of time with 10^6 fold concentration gradient. (d) Comparison of output voltage and current at different concentration gradients

The V_{oc} obtained in the previous experiment comprises two components, (a) the redox potential due to potential drop at the electrode-electrolyte surface (V_{redox}), and (b) voltage due to selective diffusion of ions (V_{osm})[224]. Similarly, the I_{sc} values obtained as such have contributions from both ion selective diffusion and V_{redox}. V_{osm} was obtained by subtracting the contribution of V_{redox} from V_{oc} ($V_{osm} = V_{oc} - V_{red}$), and I_{diff} was obtained from $I_{diff} = V_{diff} \times$

TH-3195_186151006

G, where G was the conductance of the membrane. Transport numbers of cations calculated under each salinity gradient were shown in Table 7.

Table 7: Data extracted from experimental measurements under different salt gradients

C_{max}/C_{min}	V_{meas} (I=0) (mV)	V_{redox} (mV)	$V_{osm} = V_{meas} - V_{red}$ (mV)	I_{meas} (V=0) (µA)	G (µA/V)	$I_{red} = G \times V_{red}$ (µA)	$I_{osm} = I_{meas} - I_{red}$ (µA)	t_+
10	67.6	56	11.6	0.312	4.47	0.25	0.062	0.598
10^2	124	110.5	13.5	1.5	12.4	1.37	0.13	0.557
10^3	158	142	16	4.1	26.7	3.79	0.31	0.545
10^4	180	162	18	14.4	82.4	13.35	1.05	0.538
10^5	235.7	204	31.7	24.8	110	22.44	2.36	0.554
10^6	293	190	103	32.2	91.3	17.34	14.86	0.645

The V_{redox} itself was measured by using a pair of Ag/AgCl electrodes across the nylon support membrane without having a coating on it. In low-concentration gradients, the experimental V_{redox} values were increasing linearly. However, at higher concentration gradients, it deviates linearly with a reduced slope, as shown in the Fig. 36b. Similar behaviour was also reported by other authors [225,226] which can be attributed to the following factors. The large pore sizes of nylon support membrane (without coating), due to which, at higher concentration gradient,

TH-3195_186151006

the ions quickly travel across the chambers minimizing the concentration difference, and inefficiency of Ag electrodes to convert large ionic signals into electrical signals in such a short time. The related I-V graph for other individual membranes (rGO, VO-aSiO) at 10^4 fold is shown in Fig. 36c, represents lower V_{oc} and I_{sc} as compared to VO-aSiO-rGO membrane. This disparity can be ascribed to the lower surface charged density exhibited by the rGO and VO-aSiO membranes.

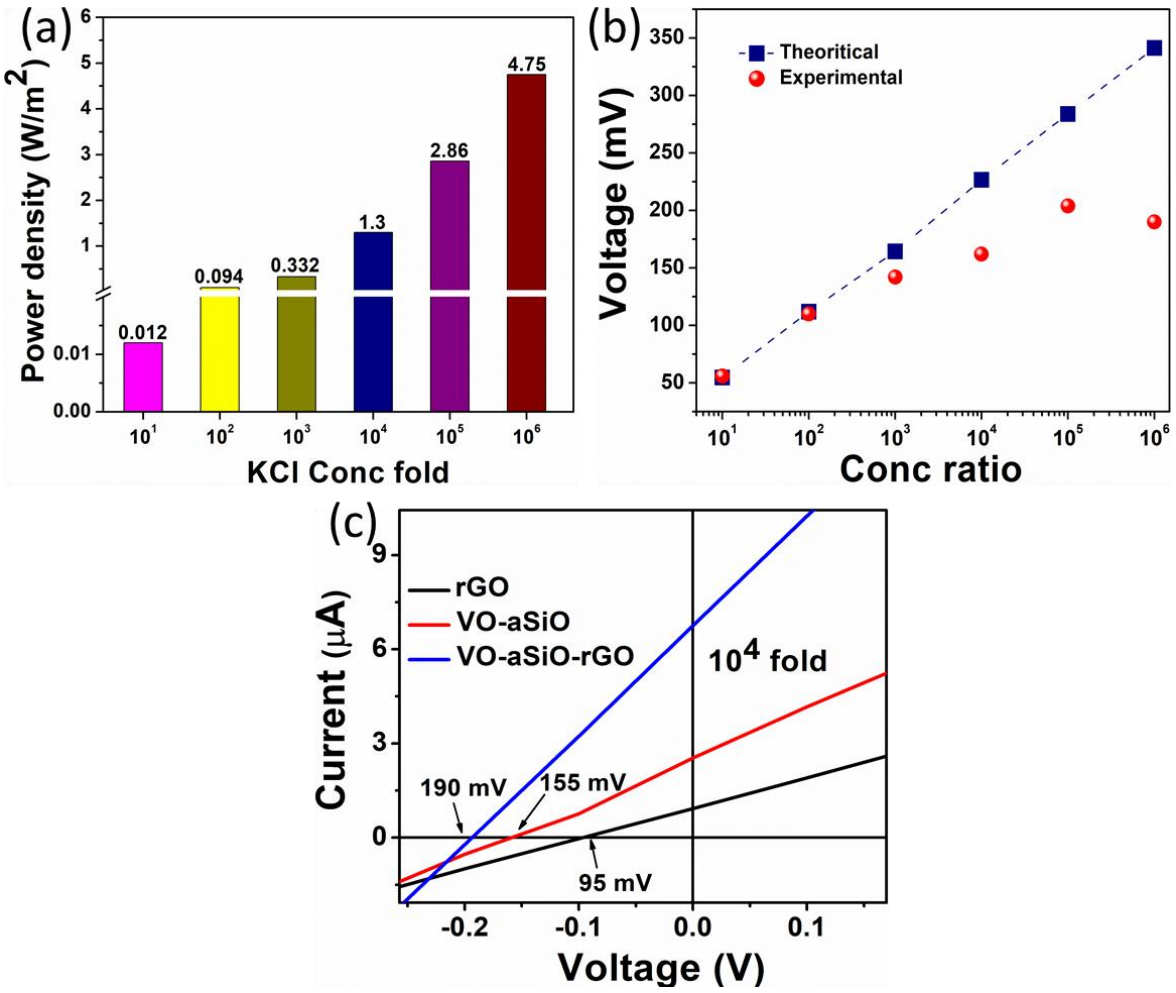

Fig. 36: (a) Power density with respect to KCl concentration gradient, (b) Comparison of calculated and experimental output voltages of uncoated nylon membrane at different concentrations, (c) I-V graph of different membranes at 10^4 fold concentration gradient

TH-3195_186151006

5.4.3 Performance of membranes in the FO process

The membrane performance (water flux and RSF) was evaluated using forward osmosis process using lab scale FO set-up, as shown in Fig. 32. The performance of all the membranes was estimated in active layer facing draw solution mode (ALDS) using lab-scale cross flow FO system. The GO/nylon and VO/nylon membranes could not withstand the cross-flow system, whereas rGO/nylon, VO-aSiO/nylon and VO-aSiO-rGO/nylon membranes have attained higher stability due to cross-linking of Bis-derivatives. Fig. 37a-b shows the comparative FO performance of VO-aSiO/nylon membranes with different amount of VO-aSiO loading (4mg to 20mg). The highest water flux (135 L m^{-2} h^{-1}) and RSF (200 g m^{-2} h^{-1}) were observed for VO-aSiO/nylon membrane with 4 mg loading. The water flux and RSF were found to be inversely proportional to the increasing VO-aSiO loading. At higher loading (20 mg), the water flux and RSF were calculated to be 32 L m^{-2} h^{-1} and 26 g m^{-2} h^{-1}, respectively. The higher water flux of all the VO-aSiO coated membranes can also be attributed to lower contact angle (38°) as well as enlarged inter-layer d-spacing (14 Å), which facilitates the transfer of water molecules at a faster rate, as shown in Fig. 33A(c).

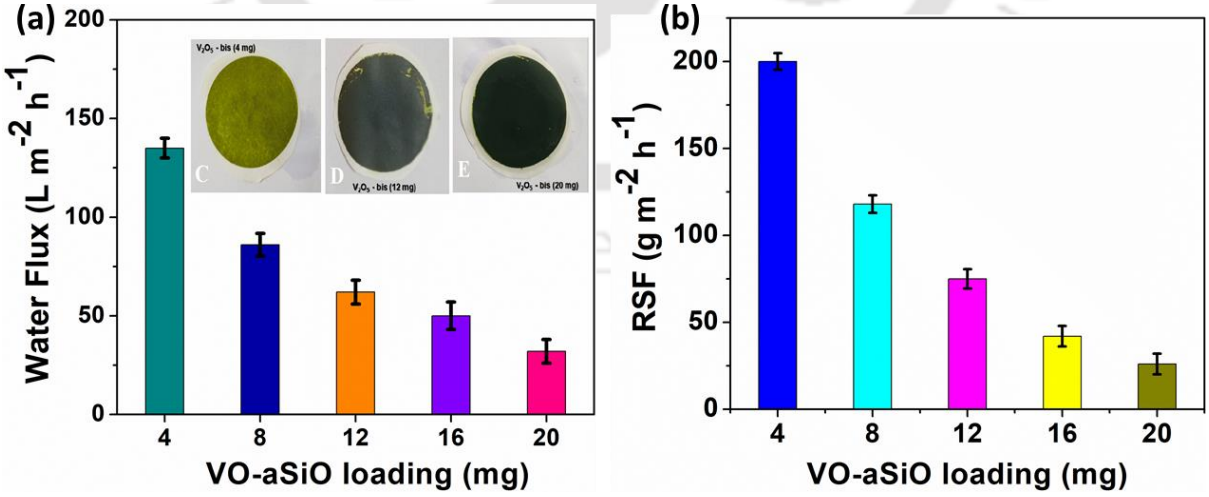

Fig. 37: Membrane performance of VO-aSiO membrane with respect to increasing loading amount for (a) water flux, (b) RSF

TH-3195_186151006

To reduce the effect of RSF, constant amount of GO was coated on nylon substrate and then different amount of VO-aSiO was coated on top of the GO/nylon membrane to form bi-layer membrane. Fig. 38 shows the performance of VO-aSiO-rGO/nylon bilayer membrane in forward osmosis process. Initially, constant 0.25 mg GO was coated on nylon substrate followed by different amount of VO-aSiO loading. Due to the pre-coated GO layer, the water flux and RSF drastically reduced to 80 L m^{-2} h^{-1} and 70 g m^{-2} h^{-1}, respectively for 4 mg VO-aSiO loading. As the VO-aSiO loading was increased to 12 mg, the water flux (38 L m^{-2} h^{-1}) and RSF (25 g m^{-2} h^{-1}) also shown a decreasing trend due to stacking of more VO-aSiO layers along with pre-coated GO layer, which provided higher resistance to water molecules and salt ions. With increased amount of GO layers from 0.25 mg to 0.5 mg and 1 mg, the water flux and RSF correspondingly decreased due to uniform coating of VO-aSiO-rGO/nylon membrane. The RSF of VO-aSiO-rGO/nylon membrane was found to be almost similar to that of rGO/nylon membrane. Finally, with 1 mg GO loading and 4 mg VO-aSiO loading, the optimized water flux and RSF was found to be (45 L m^{-2} h^{-1}) and (6.1 g m^{-2} h^{-1}), respectively. Membrane with this composition was used for most of the applications (unless mentioned otherwise), including long-term stability test and simultaneous energy-water experiments.

TH-3195_186151006

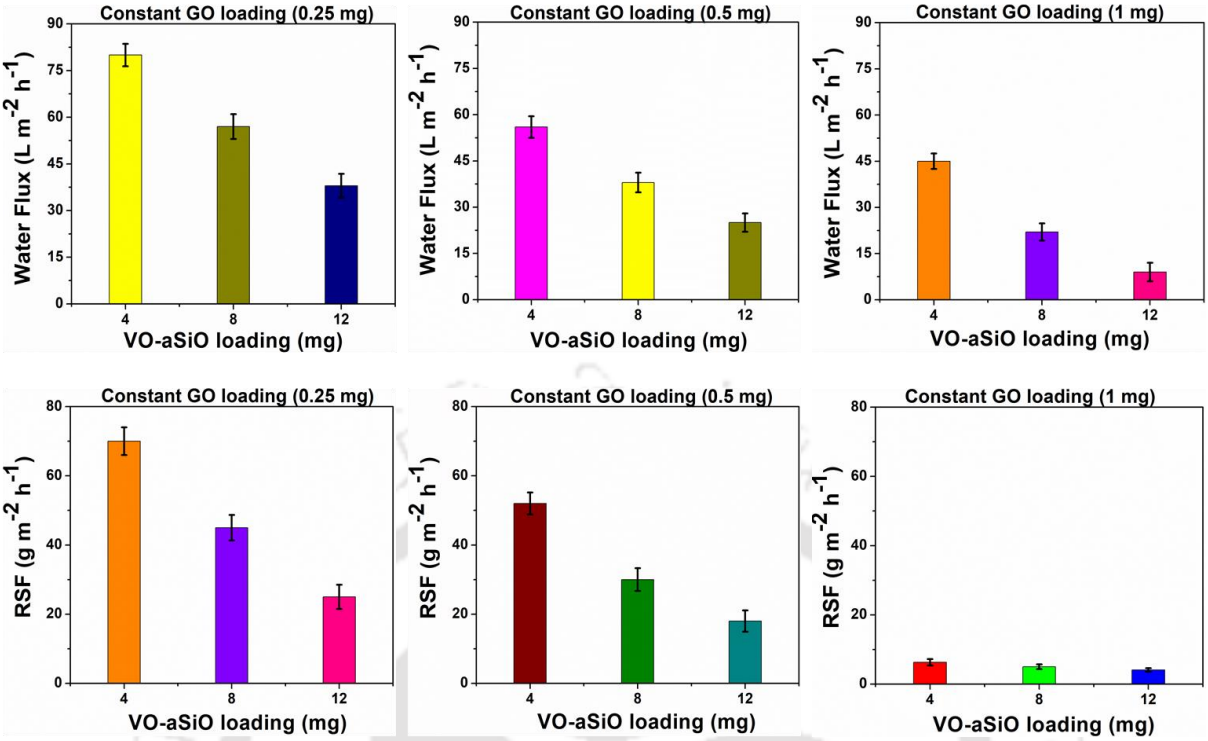

Fig. 38: FO performance of VO-aSiO-rGO membranes fabricated with different VO-aSiO and GO loadings

5.4.4 Comparative performance analysis and stability test

A commercial CTA-FO, r-GO/nylon, and PSS-doped rGO membrane from our previous study [174] were also operated under conditions similar to that of the VO-aSiO-rGO membrane. The water flux of VO-aSiO-rGO (45 L m^{-2} h^{-1}) was found to be 6, 1.8 and 1.3 times higher than CTA-FO (7.8 L m^{-2} h^{-1}), rGO/nylon (26 L m^{-2} h^{-1}) and PSS-rGO/nylon (34 L m^{-2} h^{-1}) membrane, respectively, as shown in Fig. 39a. The higher water flux of VO-aSiO-rGO membrane was attributed to a lower contact angle (51° vs 80° of rGO membrane) and enlarged inter-layer d-spacing (13.6 Å vs 8 Å) of rGO membrane. Moreover, the RSF values of the VO-aSiO-rGO membrane (6.1 g m^{-2} h^{-1}) were found to be lower than that of similar membranes like CTA-FO (8.7 g m^{-2} h^{-1}), rGO/nylon (7 g m^{-2} h^{-1}) and PSS-rGO/nylon (6.5 g m^{-2} h^{-1}), as shown in Fig. 39b. The low RSF of the VO-aSiO-rGO membrane was attributed to the higher

TH-3195_186151006

negative surface charges of both VO-aSiO (-34 mV) and rGO (-26 mV) layers, resulting in a stronger repulsive force between Cl^- ion and negatively charged membrane by Donnan exclusion[181]. With the addition of VO-aSiO to rGO/nylon membrane (VO-aSiO-rGO), the SRSF of VO-aSiO-rGO decreased by 51.8% from 0.27 g/L of rGO/nylon membrane to 0.13 g/L, shown in Fig. 39c.

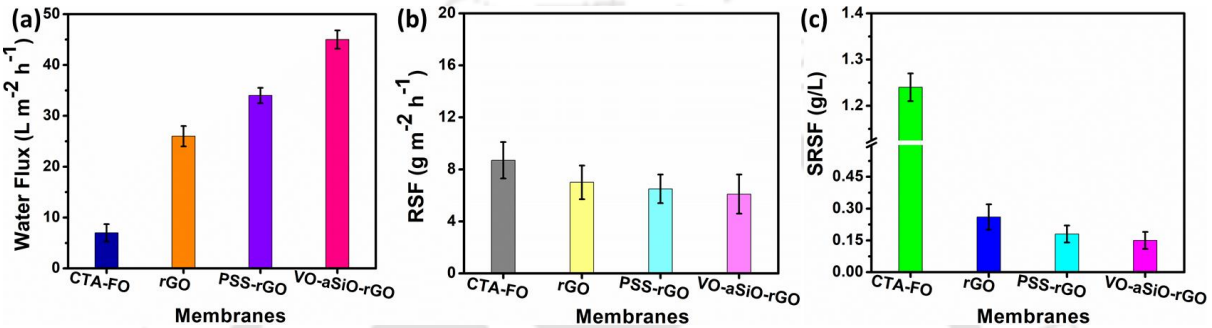

Fig. 39: Comparative FO performance: (a) Water flux, (b) RSF, and (c) SRSF values of CTA-FO, rGO, PSS-rGO and VO-aSiO-rGO membranes coated on nylon substrate measured under identical FO conditions

An experiment to evaluate the long-term stability of the VO-aSiO-rGO membrane was conducted with 1M NaCl as DS and DI water as FS in the ALDS mode. Fig. 40a compares the water flux of the VO-aSiO-rGO membrane with that of the rGO membrane for 40 h. During the initial period (first 2 h), rGO and VO-aSiO-rGO membranes exhibited water fluxes of 25 L m^{-2} h^{-1} and 45 L m^{-2} h^{-1}, respectively. Though declining trends were observed in the water fluxes of both membranes, the VO-aSiO-rGO membrane maintained a stable water flux of 28.5 L m^{-2} h^{-1} after a day of continuous operation. Moreover, the rate of decrease in the water flux was observed to be lower in the VO-aSiO-rGO membrane as compared to that of the rGO membrane. After conducting the FO experiment for 25 h, both the draw and feed sides were thoroughly cleaned with DI water and osmotic backwashing. After cleaning, the water flux of

TH-3195_186151006

the VO-aSiO-rGO membrane was increased to 38.5 L m^{-2} h^{-1}, while that of the r-GO membrane was increased to 16.3 L m^{-2} h^{-1}. The flux recovery ratio (FRR%) of the VO-aSiO-rGO and rGO membranes was calculated to be 85.5% and 65.2%, respectively. The higher FRR% in the VO-aSiO-rGO membrane was attributed to hydrophilic VO-aSiO coating on the rGO layer, which helped in preventing salt penetration from the draw side and mitigating internal concentration polarization (ICP)[116].

Similarly, the RSF values for both VO-aSiO-rGO and r-GO membranes were increased with increasing time, but the rate of increment in the VO-aSiO-rGO membrane was found to be lower than that of the r-GO membrane (Fig. 40b), which was again attributed to the higher negative charge of VO-aSiO (-34 mV) flakes as compared to that of rGO (-26 mV) flakes. Another possible reason for the lower RSF of the VO-aSiO-rGO membrane may be due to reduced dilutive external concentration polarization (DECP) with high water flux, i.e. at higher water flux with VO-aSiO-rGO membrane, the draw solution was highly diluted (compared to r-GO membrane), lowering the concentration gradient across the separation layer, which further help to reduce the RSF[227]. Moreover, after prolonged operation, leaching was observed in the rGO membrane but not in the VO-aSiO-rGO membrane. However, if the membrane was not washed, the water flux reduces as the concentration polarization builds up creating a barrier for permeating water from the feed side to the draw side. However, after a particular duration, the flux reaches a steady state as the effect of concentration polarization gets saturated, as evident from derivative flux value which tends to reach zero. Therefore, after operating for continuous 48 h, the water flux was saturated at 25.7 L m^{-2} h^{-1} as compared to 28.5 L m^{-2} h^{-1} for a day of operation, as shown in Fig. 40c.

TH-3195_186151006

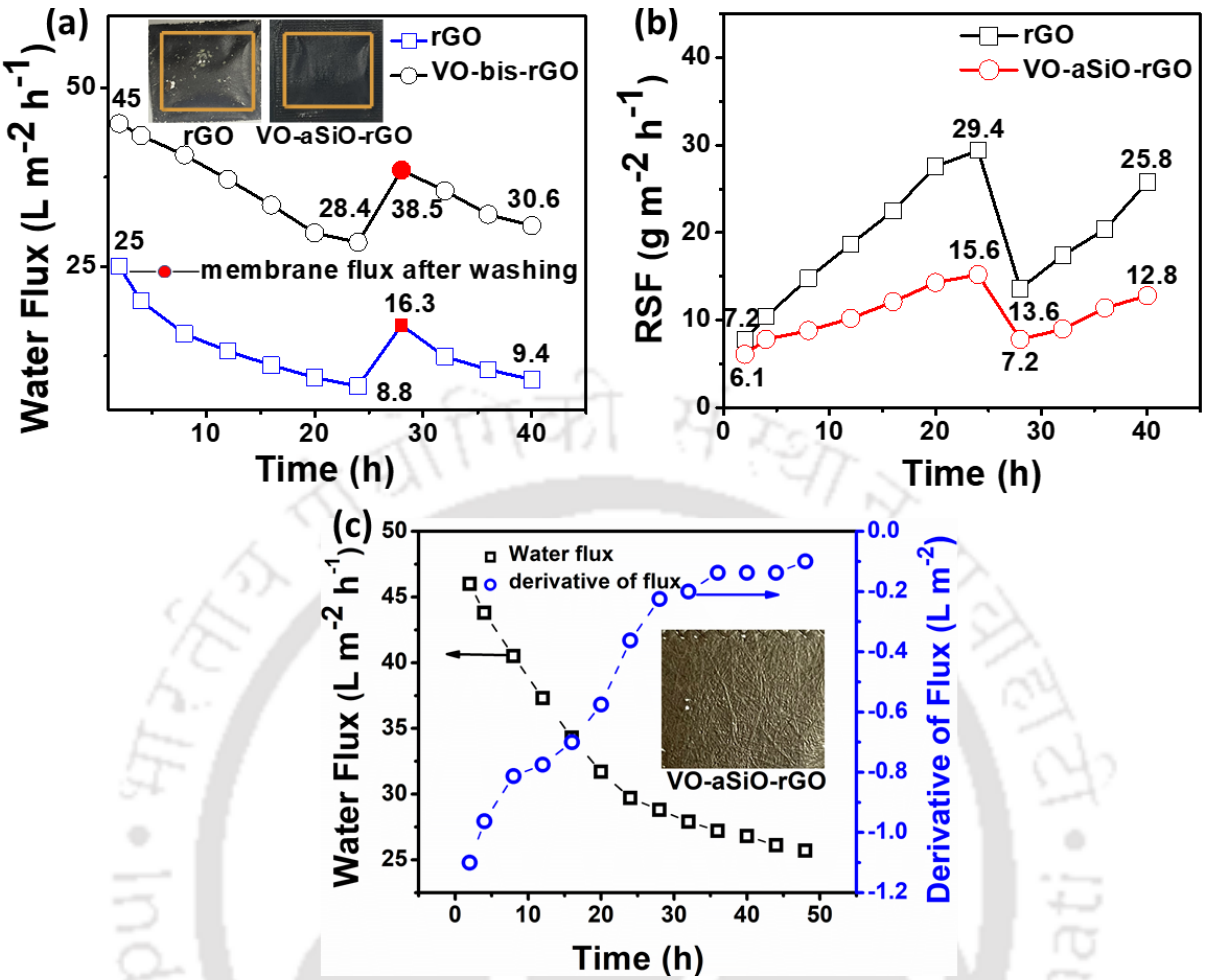

Fig. 40: Long-term stability test of rGO/nylon and VO-aSiO-rGO/nylon membranes with respect to (a) water flux, (b) RSF, (c) long term water flux and derivative flux for 48 h (experiments were performed without washing)

5.4.5 Energy harvesting performance for different membranes in FO process

The previous sections demonstrated that the VO-aSiO-rGO membrane exhibits remarkable performance in the FO process. In this section, the effect of different membrane materials on the energy performance was investigated. In the FO test cell, two Ag wires (connected to the sourcemeter through Cu wires) were placed in the FO test cell on either side of the membrane (active layer and support layer) to study the simultaneous electricity harvesting and FO process in ALDS mode. It can be observed in Fig. 41a-b that the VO-aSiO-rGO membrane exhibited

TH-3195_186151006

higher output voltage and current as compared to standalone rGO and VO-aSiO membranes. The magnitudes of trans-membrane voltage and osmotic current was found to be increasing with increase in the zeta potential values of the different membrane materials, rGO (-26 mV), VO-aSiO (-34 mV), VO-aSiO-rGO (-40 mV). This was because with higher surface charge density, the permselective nature will be higher, which can increase the transport number, thus exhibiting higher output voltage and current[228]. Hence, the highest saturated voltage (285 mV) and saturated current output (20 µA) was observed in VO-aSiO-rGO membrane. Since, higher output voltage and current was found for VO-aSiO-rGO membrane, all the future experiments were performed with VO-aSiO-rGO membrane only.

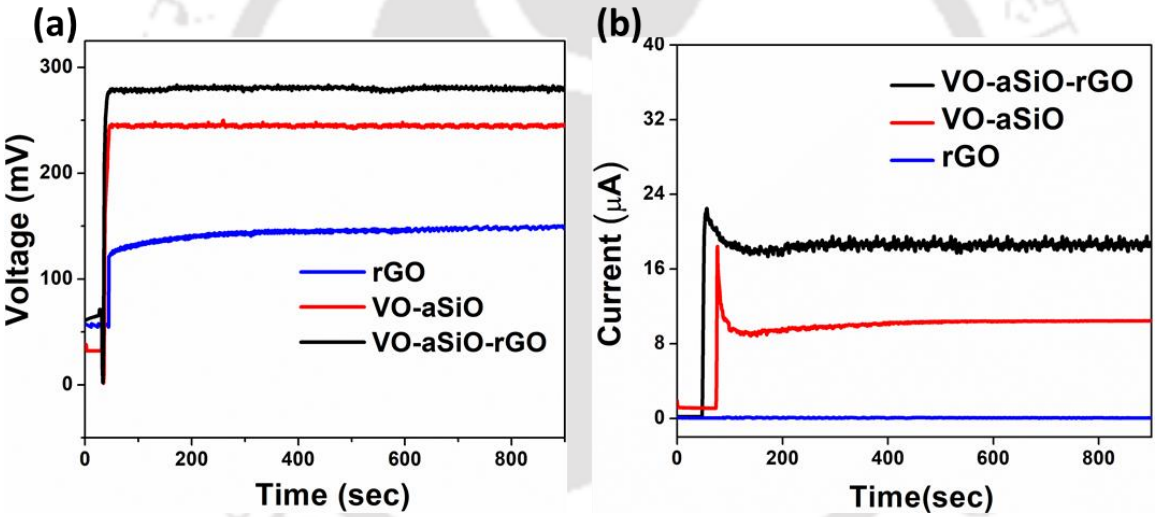

Fig. 41: Output (a) voltage, and (b) current of rGO, VO-aSiO and VO-aSiO-rGO membranes as a function of time during FO process.

5.4.6 Energy harvesting performance for different draw solutions and with increasing KCl molarity concentration in FO process

In this section, the effect of different draw solute concentration on the energy performance was also investigated with the optimized VO-aSiO-rGO membrane. It can be observed in Fig. 42a-b, the output voltage and current for 1M KCl electrolyte solution was highest followed by NaCl, $MgCl_2$ and KH_2PO_4. This can be attributed to the highest diffusion coefficient of K^+ ion

TH-3195_186151006

compared to other cations due to its smaller hydration radius[229]. This faster cation diffusion can provide efficient charge separation which can increase the output voltage and current[230]. Moreover, the effect of increasing DS concentration with respect to energy performance was also investigated, as shown in Fig. 42c-d. When the molarity of KCl concentration was increased from 1M to 3M, the change in output voltage was enhanced from 296 mV to 380 mV with an increment of 28.8%. However, there was 72% increment in output current (from 36 µA to 62 µA). This was because at higher concentration gradient, the mobility of K^+ and Cl^- ions are higher than the water molecules, leading to significant ion flux and hence output current.

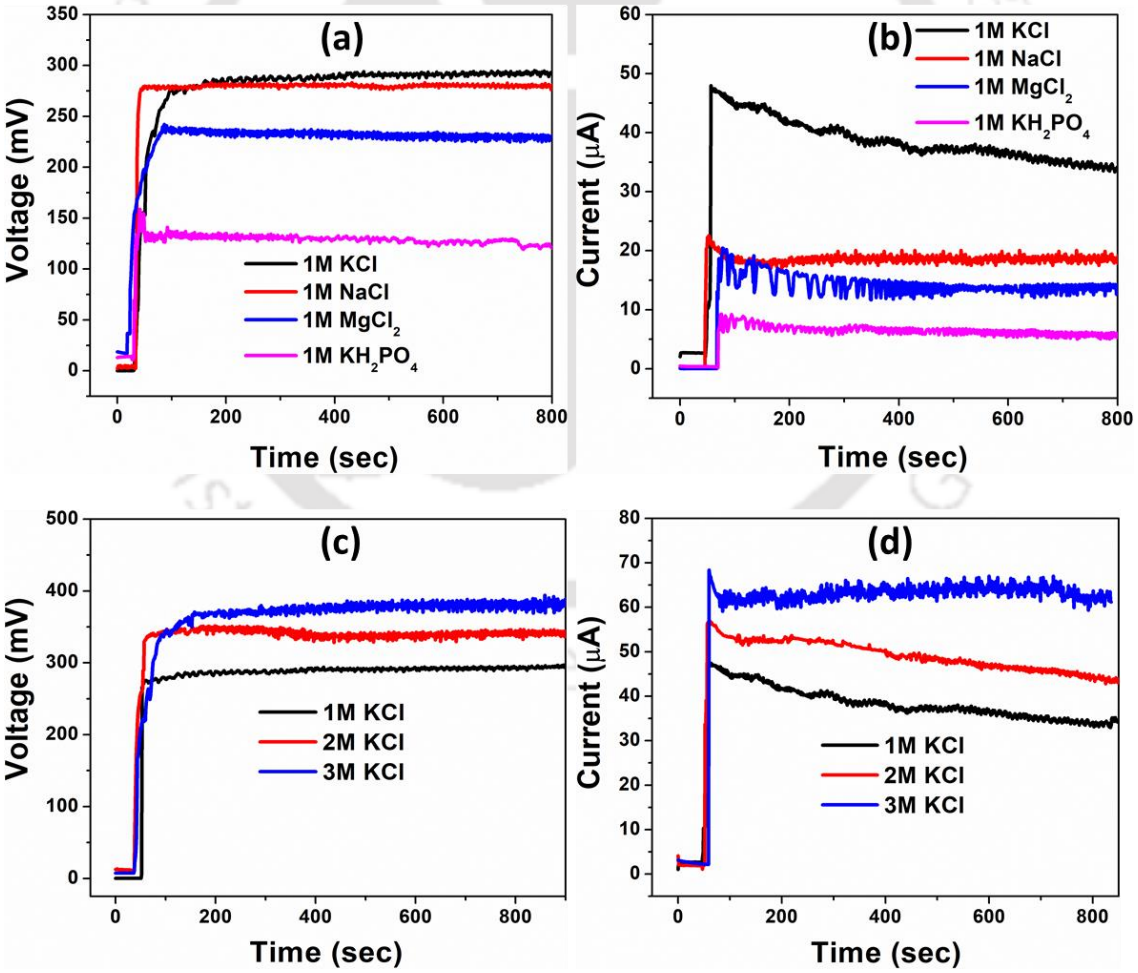

TH-3195_186151006

Fig. 42: Output (a) voltage, and (b) current with different DS; Output (c) voltage, and (d) current with increasing KCl molarity concentration. In all the experiment, flowrates of both DS and FS were maintained at 0.5 L/h and DI water as FS

5.4.7 Energy harvesting performance at zero flow rate and increasing flow rates in FO process

In this experiment as shown in Fig. 43a-b, initially when the pump was switched on, the output voltage and current peaked at value 320 mV and 30 µA, respectively. But as soon as both the pumps were switched off, the output voltage and current drastically decreased due to the disruption of flow. However, even after the initial decrease, there may still be some residual osmotic pressure difference and ion concentration gradient across the membrane. This can be due to the presence of the dissolved solutes in the feed and draw solutions that did not fully mix, or due to ion diffusion across the membrane. As a result, the system generated stable output voltage and current of 240 mV and 24 µA, respectively. With the increasing time, the voltage and current depleted and saturated at 50 mV and 7 µA, respectively. This could be due to the reduction in concentration gradient below the threshold limit which led to the overall decrease in both voltage and current.

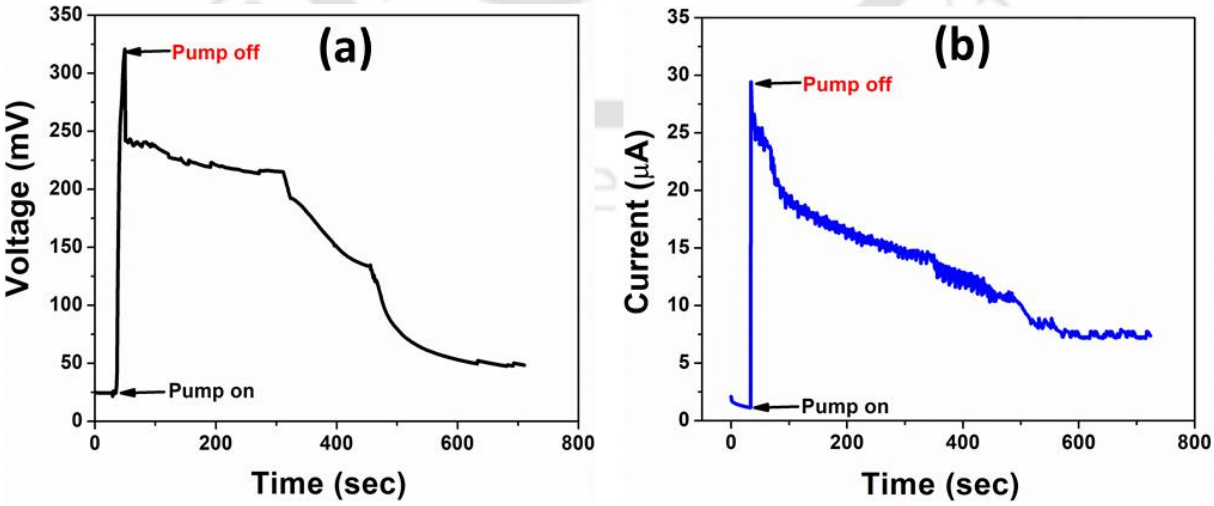

Fig. 43: Output (a) voltage, (b) current at zero flow rate

TH-3195_186151006

5.4.8 Simultaneous energy recovery and FO process

The previous sections demonstrated that the VO-aSiO-rGO membrane exhibits remarkable performance in both concentration gradient-driven energy harvesting and the FO process. Fig. 44a-b shows the output voltage and output current as a function of time with 1 M KCl as DS and DI water as the FS. With equal DS and FS flow rate of 2 L/h, the constant output voltage of 290 mV was measured wherein the current was reduced from 30 µA to 27.8 µA during 2.4 h of continuous operation. The decrease in current over time can be attributed to factors such as accumulation of ions across the membrane and membrane clogging. The open-circuit voltage mainly depends on the permselectivity and concentration difference[32]. Since, the draw and feed solution concentrations were almost constant (in continuous mode), the open-circuit voltage exhibited a constant output throughout the experiment.

The comparison analysis of the energy and forward osmosis performance at different flow rates was also investigated. At a lower flow rate (0.5 L/h), the output voltage and current were 296 mV and 36 µA and simultaneously the water flux and RSF was measured to be around 12.8 L m^{-2} h^{-1} and 3.4 g m^{-2} h^{-1}, respectively. From the saturated voltage and current values (296 mV and 36 µA, respectively) the power output was calculated to be 0.026 $W.m^{-2}$. The energy consumption for pumping was calculated to be 0.100 $W.m^{-2}$ by using the following equation 13.

$$P = (f * Q * \Delta P)/\eta * A \quad (13)$$

Where Q was the flow rate (0.5 L/h), ΔP was the differential pressure measured to be 0.05 Psi, A was the membrane area, η was the pump efficiency ~ 0.7 and f was the conversion value ($11.2*10^{-4}$)[32,231]. Based on the above parameters, overall energy saving in the FO process through concentration-driven electricity was calculated to be ~ 26 %.

TH-3195_186151006

To gain further insights into the synchronized energy harvesting and forward osmosis process, the flow rates of both the DS and FS sides were increased simultaneously. While both the flow rates (DS and FS sides) increased, the water flux and RSF increased from 12.8 L m^{-2} h^{-1} to 43.6 L m^{-2} h^{-1} and 3.4 g m^{-2} h^{-1} to 15.3 g m^{-2} h^{-1}, respectively. The observed variations in the water flux and RSF can be explained through variations in DECP and concentrative internal concentration polarization (CICP) with respect to DS and FS flow rate. The DECP at the active layer of the membrane reduces with an increase in DS flow rate and then will increase the DS concentration at the membrane surface[232]. Similarly, the CICP at the support layer reduces with an increase in FS flow rate, and that will reduce both DS and FS solute concentration at the interface between the support and separation layer and that will increase both water flux and RSF[233]. Even though, the RSF and water flux were increasing with flow rate, the output voltage and current were decreasing when flow rates were increased and this phenomenon was observed due to reduced residence time of ions near the membrane surface, (refer Fig. 44c-d). Further similar response observed while increasing DS flow rate alone (refer Fig. 45a) confirms that DS resistance time was critical parameter to achieve optimum power output. As DI water was taken as FS, no CICP occurred at the support layer [232], but DS solute at interface between support and separation layer will be reduced with increase FS flow rate. The CICP on the support layer may have lighter effect on water flux and RSF, but the DECP on the active layer determines the output voltage and current values. Therefore, the output voltage and current values were found to be proportional to the salt rejection ability [32].

The effect of water flux and RSF on the output voltage and current in ALDS mode and batch mode was also studied for the VO-aSiO-rGO membrane by using 1M KCl and 1M KH_2PO_4 as the DS and DI water as the FS at constant DS and FS flow rates of 10 L/h and 15 L/h, respectively. As can be seen from Fig. 44e-f, the water flux of KCl was found to be higher than

TH-3195_186151006

KH_2PO_4 due to the higher osmotic concentration gradient of KCl across the membrane surface [234]. Regarding the energy performance, the output voltage decreases with the decreasing water flux and increasing RSF for both KCl and KH_2PO_4. Similarly, the current values also decreased with decreasing water flux and increasing RSF, see Fig. 44g-h. The above observation suggests that good selectivity and permeability of membrane support both FO and electricity generation process. As mentioned earlier, detailed understandings of the interdependence of FO and concentration gradient-driven electricity harvesting process under the conditions of flowing electrolytes across the electrodes and membrane surfaces demand further theoretical studies. Since, the experiment was performed in batch mode, the osmotic pressure across the membrane decreased with DS dilution that decreased the water flux and increased the RSF value with time. As a result, both voltage and current decreased with time[235].

TH-3195_186151006

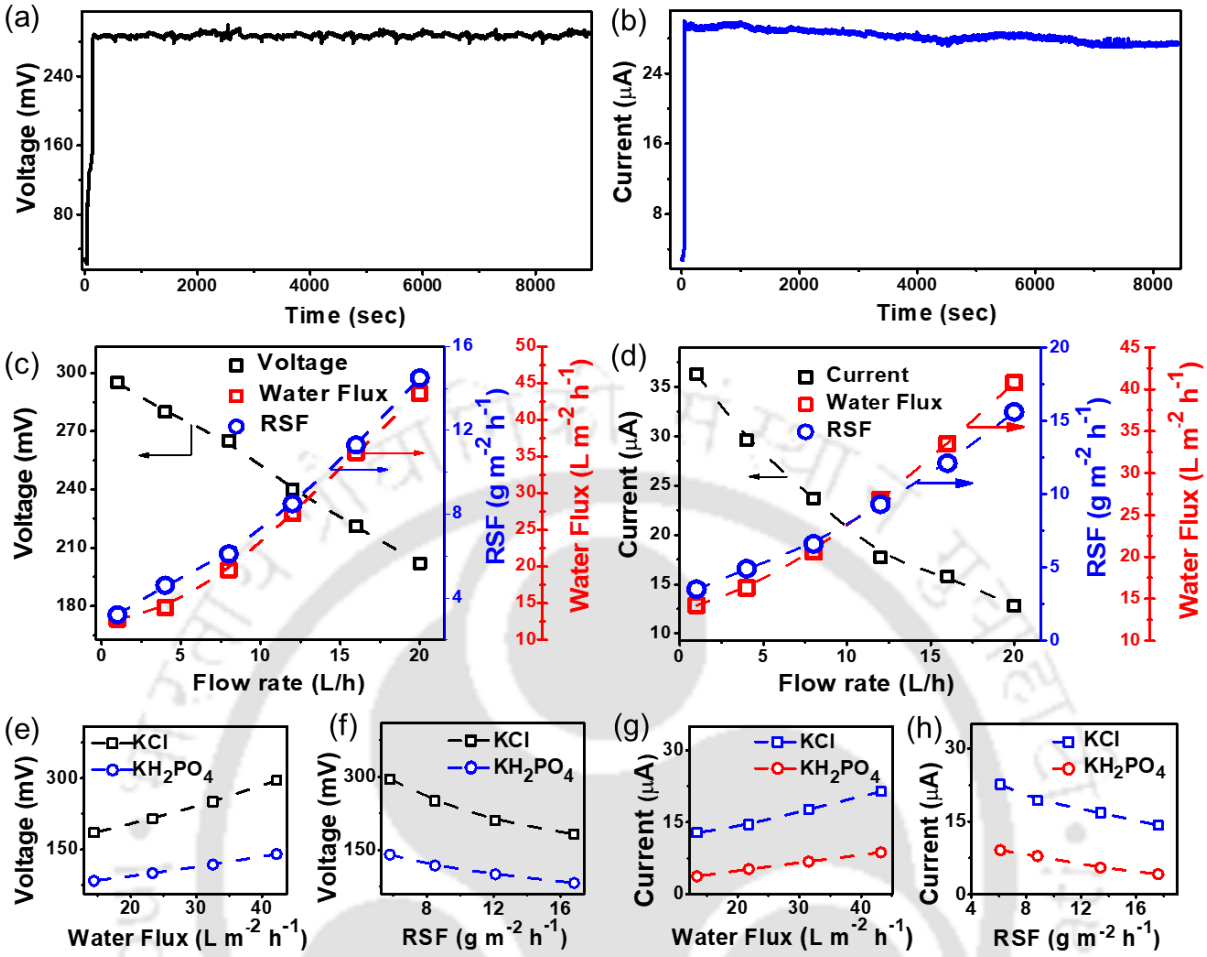

Fig. 44: Energy recovering in the FO process: Output (a) voltage, and (b) current of VO-aSiO-rGO membrane in continuous FO process (flow rate 2 L/h for both DS and FS). Comparison of (c) voltage, and (d) current with different FO parameters at different flowrate in batch mode. 1M KCl and DI water were used as DS and FS, respectively. Simultaneous energy harvesting and FO application with 1M KCl and 1M KH_2PO_4 as the DS in batch mode, (e) voltage vs water flux, (f) voltage vs RSF, (g) current vs water flux, and (h) current vs RSF, DI water was used as the FS

The effect of different flow rates of DS (at a constant flow rate of FS) and FS (at a constant flow rate of DS) on energy performance was also investigated in the ALDS mode. As can be seen from Fig. 45a, with increasing DS flow rates (by maintaining a constant FS flow rate), both output voltage and current decreased. This was because, at higher DS flowrates, the DECP

TH-3195_186151006

and residence time will be reducing that will disrupt the ion equilibrium at the membrane surface, which in turn, reduces the ion transport through the membrane. This reduces the effective driving force of the draw solution and hence reduce both output voltage and current[117]. In contrast, when the FS flow rates were increased with a constant DS flow rate (refer Fig. 45b), both output voltage and current increased. This was because, at higher FS flow rates, the CICP has negligible effect, since DI water was used as FS. This improves the effective ionic transport through the membrane and reduces the RSF value to a great extent, thus maintaining the osmotic pressure across the membrane which will let to increase in both output voltage and current.

The realistic scenario of tea concentrating through FO process was also explored for simultaneous energy recovering. Tea solutions of different concentrations (10 mg/ml and 20 mg/ml concentrations) were used as the FS, the optimized VO-aSiO-rGO was used as the FO membrane with 1M KCl as the DS. The experiment was performed in the ALDS mode. Fig. 45c-d show the output voltage and current as a function of time with flow rates of DS and FS maintained at 0.5 L/h. The output saturated voltage (240 mV and 205 mV) and current (17 µA, and 13.5 µA) obtained with 10 and 20 mg/ml tea solutions as FS was found to be lower than that of DI water as the FS (296 mV and 36 µA). This was because the inorganic ions present in the tea solution could neutralize the concentration gradient-driven permselective movements of ions. Moreover, at higher feed concentration compared to DI water, the mass transfer coefficient decreases due to the effect of CICP, which in turn decreases the net osmotic pressure across the membrane[118]. By emphasizing the application of the membrane in tea concentration and energy generation, we aim to showcase its potential for use in industries related to tea processing and potentially in other applications that require concentration processes and energy harvesting.

TH-3195_186151006

Finally, to check the applicability in real application scenario, the fabricated membrane was explored for tea concentration and energy recovery in the FO process near its saturation point. Long term water flux performance was studied by using 1M KCl as DS and tea solution (20 mg/ml) as the FS, flow rates were maintained at 10 L/h and 15 L/h, respectively. The membrane exhibited a water flux of 30 L m^{-2} h^{-1} for 2 h which gradually decreased with time and saturated at 12.5 L m^{-2} h^{-1} after 20 h continuous operation, thus increasing the tea concentration over time. The decreased water flux was attributed to the accumulation of tea molecules on the membrane surface (fouling) decreasing the mass transfer coefficient. The FO-based concentrating process leads to nucleation of tea crystals near the membrane [140,236], as shown in Fig. 45e-f.

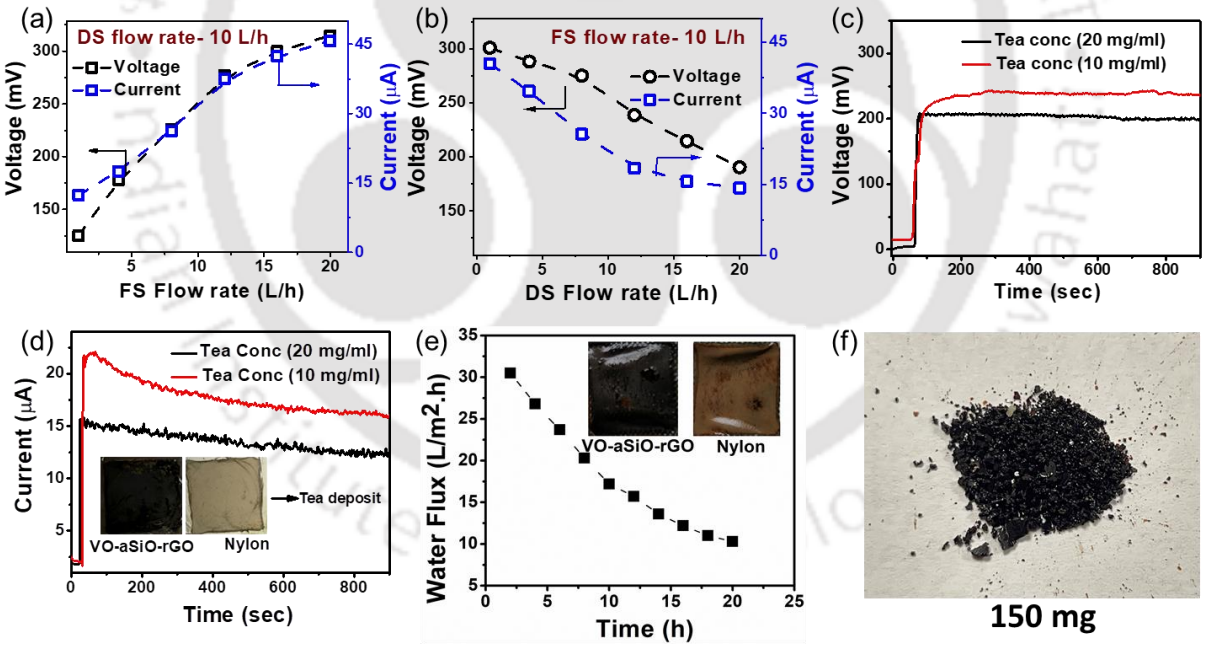

Fig. 45: Energy performance of VO-aSiO-rGO membrane: Effect of (a) varying DS flowrates with constant FS flowrates of 10 L/h, and (b) varying FS flowrates with constant DS flowrates of 10 L/h on current and voltage output. Output (c) voltage, and (d) current with 10 mg/ml and 20 mg/ml tea solutions used as the FS, 1M KCl is used as the DS, (flowrate = 0.5 L/h on both

TH-3195_186151006

sides), (e) long term water flux for tea crystallization in FO process, (f) tea crystals recovered after FO experiment

The comparison of energy efficiency for different DS solutions at lowest flow rate is shown in Table 8.

Table 8: Comparison of energy efficiency for different DS solutions at the lowest flow rate.

Molarity (M)	**DS/FS flow rates (L/h)**	**Voltage (mV)**	**Current (µA)**	**Extracted Power ($W.m^{-2}$)**	**Pumping Power ($W.m^{-2}$)**	**Saving Energy (%)**
1M KCl	0.5	295	35	0.0258	0.10	25.8
2M KCl	0.5	340	48.5	0.041	0.10	41
3M KCl	0.5	380	62	0.0589	0.10	58.9
1M NaCl	0.5	280	20	0.014	0.10	14
1M $MgCl_2$	0.5	240	13.5	0.0081	0.10	8.1
1M KH_2PO_4	0.5	135	8.5	0.00286	0.10	2.86

TH-3195_186151006

5.5 Summary

In conclusion, we demonstrated the possibility of synchronized energy harvesting in the FO process with an overall energy saving of ~ 26 %. The robust nanofluidic FO membrane fabricated by crosslinking 2D flakes of VO and rGO extracted electrical power (up to 4.72 $W.m^{-2}$) from the concentration gradient. The FO performance of the VO-aSiO-rGO membrane (45 L m^{-2} h^{-1}) was found to be better than that of both the pristine rGO membrane (26 L m^{-2} h^{-1}) and commercial CTA-FO membrane (7.8 L m^{-2} h^{-1}). The membrane reported here showed outstanding long-term stability in both acidic and basic mediums (for more than 90 days of soaking) as well as during prolonged operational 40 h of the FO without showing any sign of leaching. The possibility of extracting electrical energy from realistic FO processes was demonstrated by using DI water and tea solutions as the FS. It was observed that in the continuous FO mode, the system is able to generate constant output voltage (290 mV) and current (28 µA) for prolonged operational 2.4 h. Moreover, in batch mode, the system was able to generate highest output voltage and current of 296 mV and 36 µA, respectively while simultaneously producing water flux of 12.8 L m^{-2} h^{-1} and RSF of 3.4 g m^{-2} h^{-1} at 0.5 L/h flow rates. Finally, the FO system is able to produce tea crystals and generate electrical output voltage and current with different tea concentrations. Considering the ease of coupling between FO and concentration gradient-driven energy harvesting process, this study could lead to a novel platform for studying or handling the highly entangled issues water-energy nexus and creating a self-sustaining system that can operate independently of external energy sources.

TH-3195_186151006

TH-3195_186151006

CHAPTER 6

6 Summary and scope for the future work

6.1 Summary

The studies involved the investigation of the potential of 2D nanomaterials as a coating material for FO membrane with an enhancement of surface properties explored in this work. MF flat nylon sheet membrane was used as a support material for the FO membrane, and it is tested for various applications like aqueous solution concentration, resource recovery and energy generation. In the first phase of the thesis work, one of the most common 2D nanomaterials, GO and its derivative rGO, were used as a coating material for the fabrication of the FO membrane. The coating process was performed using a vacuum filtration setup. The physiochemical properties of GO and thermally rGO were studied along with the bonding mechanism with nylon MF membrane. The study revealed that GO swells in an aqueous solution and delaminated from the substrate, thus confirming the instability in the FO process. Therefore, its binding ability with the substrate was analysed at different operating conditions (temperature and heating time). It is found that at high temperature with longer duration of heating, the rGO membrane becomes more stable in an aqueous solution. However, the water flux drastically decreases with increasing temperature and heating time due to the reduction in inter-layer spacing between the nanosheets. Therefore, it is found that the optimum heating condition required for the fabrication of the rGO membrane is 150 °C for 2 hours. All future experiments are conducted with the optimized condition membranes.

After determining the optimal conditions for creating an rGO membrane for FO, the GO flakes were classified into three categories: large, medium, and small. This was achieved through the process of centrifugation and sonication. Additionally, the impact of varying the thickness of

TH-3195_186151006

the GO loading on rGO membranes was explored. The outcome of the FO process showed that membranes created using larger GO flakes displayed lower water flux and reverse solute flux (RSF) when compared to their smaller counterparts, where both the water flux and RSF were noticeably higher. Similarly, the membranes with thicker coating exhibit lower water flux and RSF as compared to thinner coating. Therefore, the rGO membrane fabricated with medium flake size and 1 µm thickness is found to be the optimized FO membrane. Since thermally rGO membrane alleviates the water flux, the incorporation of hydrophilic doping material is introduced to enhance the FO performance. One such hydrophilic polymer is polystyrene sulfonic acid (PSS) which is doped onto rGO laminates to improve the water flux. The physical adsorption followed by the chemical linking and thermal fixation of PSS-rGO membrane was demonstrated during the fabrication process. The PSS-rGO membrane increased the surface hydrophilicity and surface charge density, which enhanced the water flux while simultaneously maintaining the RSF, thus solving the trade-off between permeability and selectivity of the FO membrane. The optimized PSS-rGO membrane is experimented for long-term stability and compared its performance with rGO and CTA-FO membrane for 25 hours. The results showed higher water flux and lower RSF for the PSS-rGO membrane than the rGO membrane throughout the long-term experiment, indicating the effect of PSS on the rGO membrane.

Based on the rGO membrane's stability performance in the aqueous solution, the stable rGO membrane was doped with hydrophilic sericin protein via two facile methods for enhancement of surface properties of rGO membrane for high water flux, low RSF and high anti-fouling properties in pharmaceutical effluent. The study revealed that the sericin-doped rGO membranes (rGO-S and S-rGO) increased the water flux up to 54 L m^{-2} h^{-1} and 36 L m^{-2} h^{-1} and decreased the SRSF up to 0.12 g/L and 0.18 g/L, respectively, as compared to the rGO membrane (26 L m^{-2} h^{-1} and 0.25 g/L). Subsequently, the optimized rGO-S membrane

TH-3195_186151006

exhibited a stable water flux of 28 L m^{-2} h^{-1} for 20 hours while maintaining low RSF. Regarding the anti-fouling test using pharmaceutical effluent as the FS, the rGO-S membrane regeneration properties resulted in excellent FRR% of 84% and 74% in ALDS and ALFS modes, respectively, thus revealing better durability and long-term stability of FO membranes. Finally, the hybrid batch FO process of the pharmaceutical effluent resulted in the recovery of continuous rifaximin antibiotic crystals, thus enabling simultaneous fouling resistant energy-efficient operation and high effective antibiotic recovery from pharmaceutical effluent using a cost-effective strategy.

Another application of the FO process was explored using a novel FO membrane fabricated with two-dimensional flakes of VO and rGO crosslinked with aSiO to form a VO-aSiO-rGO membrane. The optimized VO-aSiO-rGO membrane exhibited a superior water flux of 45 L m^{-2} h^{-1} and low SRSF of 0.13 g/L, thus outperforming the existing commercial FO and standalone rGO membranes. These outstanding characteristics demonstrated the membrane's superior separation efficiency, making it ideal for concentration applications. Furthermore, the study explored the membrane's potential to generate electricity by producing output voltage and current values up to 293 mV and 32.2 µA, respectively, when subjected to a 10^6 fold salinity gradient. This remarkable result led to a power density of approximately 4.72 $W.m^{-2}$. Finally, the possibility of extracting electrical energy from realistic FO processes was demonstrated by using DI water and tea solutions as the FS. The system was able to generate the highest output voltage and current of 296 mV and 36 µA, respectively, while simultaneously producing a water flux of 12.8 L m^{-2} h^{-1} and RSF of 3.4 g m^{-2} h^{-1} at the lowest 0.5 L/h flow rates. Moreover, the FO system could also produce tea crystals and generate electrical output voltage and current with different tea concentrations. This new approach addresses the urgent need for energy-efficient water treatment and lays the foundation for

TH-3195_186151006

sustainable, high-efficiency water treatment technologies integrated with energy recuperation mechanisms.

Overall, these results demonstrated the fabrication of novel FO membranes using 2D nanomaterials to modify the surface properties of polymeric membranes and apply those fabricated membranes for various applications demonstrated in this thesis work.

6.2 Recommendation of future research

In this thesis work, the fabrication of flat sheet FO membrane was explored for various applications. Further investigations into the scalability of large area flat sheet FO membrane with other 2D nanomaterials are recommended. The materials performance found in one section can be applied into other sections as well. However, due to COVID lockdown which led to time constraints, the experiments were not able to perform. Therefore, in the future research work, the same materials can be studied for the different applications as well. Moreover, new ideas on the fabrication techniques of continuous flat sheet FO membrane with different 2D nanomaterials may be a good option to improve the FO process's performance and economic feasibility.

Further investigation on the potential use of 2D nanomaterials for coating on different membrane modules like ceramic and hollow fibre membranes is recommended. Hollow fiber membranes have a significantly higher effective surface area compared to flat sheet membranes. The bundled configuration of multiple fibres allows for a larger surface area per unit volume, which enhances the overall separation efficiency. This scalability makes them suitable for a wide range of applications, from small-scale laboratory setups to large-scale industrial systems.

TH-3195_186151006

7 References

[1] Z. Li, R.V. Linares, S. Sarp, G. Amy, Chapter 9 - Direct and Indirect Seawater Desalination by Forward Osmosis, in: S. Sarp, N.B.T.-M.-B.S.G.P. for W.T. and P.G. Hilal (Eds.), Elsevier, 2018: pp. 245–272. https://doi.org/https://doi.org/10.1016/B978-0-444-63961-5.00009-2.

[2] I.G. Wenten, K. Khoiruddin, R. Reynard, G. Lugito, H. Julian, Advancement of forward osmosis (FO) membrane for fruit juice concentration, Journal of Food Engineering. 290 (2021) 110216. https://doi.org/https://doi.org/10.1016/j.jfoodeng.2020.110216.

[3] J.Y. Law, A.W. Mohammad, Z.K. Tee, N.K. Zaman, J.M. Jahim, J. Santanaraj, M.S. Sajab, Recovery of succinic acid from fermentation broth by forward osmosis-assisted crystallization process, Journal of Membrane Science. 583 (2019) 139–151. https://doi.org/https://doi.org/10.1016/j.memsci.2019.04.036.

[4] B.L. Pangarkar, M.G. Sane, M. Guddad, Reverse Osmosis and Membrane Distillation for Desalination of Groundwater: A Review, ISRN Materials Science. 2011 (2011) 523124. https://doi.org/10.5402/2011/523124.

[5] D.M. Warsinger, J. Swaminathan, E. Guillen-Burrieza, H.A. Arafat, J.H. Lienhard V, Scaling and fouling in membrane distillation for desalination applications: A review, Desalination. 356 (2015) 294–313. https://doi.org/https://doi.org/10.1016/j.desal.2014.06.031.

[6] A. Bardhan, S. Subbiah, K. Mohanty, I. Ibrar, A. Altaee, Feasibility of Poly (Vinyl Alcohol)/Poly (Diallyldimethylammonium Chloride) Polymeric Network Hydrogel as Draw Solute for Forward Osmosis Process, Membranes. 12 (2022). https://doi.org/10.3390/membranes12111097.

[7] M. Yasukawa, Y. Tanaka, T. Takahashi, M. Shibuya, S. Mishima, H. Matsuyama, Effect of Molecular Weight of Draw Solute on Water Permeation in Forward Osmosis Process, Industrial & Engineering Chemistry Research. 54 (2015) 8239–8246. https://doi.org/10.1021/acs.iecr.5b01960.

[8] T.Y. Cath, A.E. Childress, M. Elimelech, Forward osmosis: Principles, applications, and recent developments, Journal of Membrane Science. 281 (2006) 70–87. https://doi.org/https://doi.org/10.1016/j.memsci.2006.05.048.

[9] J.-J. Qin, W.C.L. Lay, K.A. Kekre, Recent developments and future challenges of forward osmosis for desalination: a review, Desalination and Water Treatment. 39 (2012) 123–136. https://doi.org/10.1080/19443994.2012.669167.

[10] K. Lutchmiah, A.R.D. Verliefde, K. Roest, L.C. Rietveld, E.R. Cornelissen, Forward osmosis for application in wastewater treatment: A review, Water Research. 58 (2014) 179–197. https://doi.org/https://doi.org/10.1016/j.watres.2014.03.045.

[11] N. Akther, A. Sodiq, A. Giwa, S. Daer, H.A. Arafat, S.W. Hasan, Recent advancements in forward osmosis desalination: A review, Chemical Engineering Journal. 281 (2015) 502–522. https://doi.org/https://doi.org/10.1016/j.cej.2015.05.080.

[12] J.R. McCutcheon, R.L. McGinnis, M. Elimelech, A novel ammonia—carbon dioxide

TH-3195_186151006

forward (direct) osmosis desalination process, Desalination. 174 (2005) 1–11. https://doi.org/https://doi.org/10.1016/j.desal.2004.11.002.

[13] A. Altaee, A. Sharif, Pressure retarded osmosis: advancement in the process applications for power generation and desalination, Desalination. 356 (2015) 31–46. https://doi.org/https://doi.org/10.1016/j.desal.2014.09.028.

[14] E. Butler, A. Silva, K. Horton, Z. Rom, M. Chwatko, A. Havasov, J.R. McCutcheon, Point of use water treatment with forward osmosis for emergency relief, Desalination. 312 (2013) 23–30. https://doi.org/https://doi.org/10.1016/j.desal.2012.12.013.

[15] T.-S. Chung, S. Zhang, K.Y. Wang, J. Su, M.M. Ling, Forward osmosis processes: Yesterday, today and tomorrow, Desalination. 287 (2012) 78–81. https://doi.org/https://doi.org/10.1016/j.desal.2010.12.019.

[16] Q. She, R. Wang, A.G. Fane, C.Y. Tang, Membrane fouling in osmotically driven membrane processes: A review, Journal of Membrane Science. 499 (2016) 201–233. https://doi.org/https://doi.org/10.1016/j.memsci.2015.10.040.

[17] L. Chekli, S. Phuntsho, H.K. Shon, S. Vigneswaran, J. Kandasamy, A. Chanan, A review of draw solutes in forward osmosis process and their use in modern applications, Desalination and Water Treatment. 43 (2012) 167–184. https://doi.org/10.1080/19443994.2012.672168.

[18] D. Li, Y. Yan, H. Wang, Recent advances in polymer and polymer composite membranes for reverse and forward osmosis processes, Progress in Polymer Science. 61 (2016) 104–155. https://doi.org/https://doi.org/10.1016/j.progpolymsci.2016.03.003.

[19] P.S. Goh, A.F. Ismail, B.C. Ng, M.S. Abdullah, Recent Progresses of Forward Osmosis Membranes Formulation and Design for Wastewater Treatment, Water. 11 (2019). https://doi.org/10.3390/w11102043.

[20] M. Kumar, M. Grzelakowski, J. Zilles, M. Clark, W. Meier, Highly permeable polymeric membranes based on the incorporation of the functional water channel protein Aquaporin Z, Proceedings of the National Academy of Sciences. 104 (2007) 20719–20724. https://doi.org/10.1073/pnas.0708762104.

[21] B.J. Hinds, N. Chopra, T. Rantell, R. Andrews, V. Gavalas, L.G. Bachas, Aligned Multiwalled Carbon Nanotube Membranes, Science. 303 (2004) 62–65. https://doi.org/10.1126/science.1092048.

[22] R.R. Nair, H.A. Wu, P.N. Jayaram, I. V Grigorieva, A.K. Geim, Unimpeded Permeation of Water Through Helium-Leak–Tight Graphene-Based Membranes, Science. 335 (2012) 442 LP – 444. https://doi.org/10.1126/science.1211694.

[23] S. Dervin, D.D. Dionysiou, S.C. Pillai, 2D nanostructures for water purification: graphene and beyond, Nanoscale. 8 (2016) 15115–15131. https://doi.org/10.1039/C6NR04508A.

[24] S. Zhang, G. Lian, H. Si, J. Wang, X. Zhang, Q. Wang, D. Cui, Ultrathin BN nanosheets with zigzag edge: one-step chemical synthesis, applications in wastewater treatment and preparation of highly thermal-conductive BN–polymer composites, Journal of Materials Chemistry A. 1 (2013) 5105–5112. https://doi.org/10.1039/C3TA01597A.

TH-3195_186151006

[25] G. Liu, W. Jin, N. Xu, Two-Dimensional-Material Membranes: A New Family of High-Performance Separation Membranes, Angewandte Chemie International Edition. 55 (2016) 13384–13397. https://doi.org/https://doi.org/10.1002/anie.201600438.

[26] H.M. Hegab, L. Zou, Graphene oxide-assisted membranes: Fabrication and potential applications in desalination and water purification, Journal of Membrane Science. 484 (2015) 95–106. https://doi.org/10.1016/j.memsci.2015.03.011.

[27] Y. Liu, Y. Zhao, X. Zhang, X. Huang, W. Liao, Y. Zhao, MoS2-based membranes in water treatment and purification, Chemical Engineering Journal. 422 (2021) 130082. https://doi.org/https://doi.org/10.1016/j.cej.2021.130082.

[28] Y.A.J. Al-Hamadani, B.-M. Jun, M. Yoon, N. Taheri-Qazvini, S.A. Snyder, M. Jang, J. Heo, Y. Yoon, Applications of MXene-based membranes in water purification: A review, Chemosphere. 254 (2020) 126821. https://doi.org/https://doi.org/10.1016/j.chemosphere.2020.126821.

[29] B. Arora, P. Attri, Carbon Nanotubes (CNTs): A Potential Nanomaterial for Water Purification, Journal of Composites Science. 4 (2020). https://doi.org/10.3390/jcs4030135.

[30] P. Gao, M.H. Tai, D.D. Sun, Hierarchical TiO2/V2O5 Multifunctional Membrane for Water Purification, ChemPlusChem. 78 (2013) 1475–1482. https://doi.org/https://doi.org/10.1002/cplu.201300264.

[31] J. Zhu, J. Hou, A. Uliana, Y. Zhang, M. Tian, B. Van der Bruggen, The rapid emergence of two-dimensional nanomaterials for high-performance separation membranes, Journal of Materials Chemistry A. 6 (2018) 3773–3792. https://doi.org/10.1039/C7TA10814A.

[32] C.H. Park, O. Choi, Electrochemical energy-generating desalination system using a pressure-driven ion-selective nanomembrane, Nano Energy. 94 (2022) 106939. https://doi.org/https://doi.org/10.1016/j.nanoen.2022.106939.

[33] A. Achilli, T.Y. Cath, A.E. Childress, Power generation with pressure retarded osmosis: An experimental and theoretical investigation, Journal of Membrane Science. 343 (2009) 42–52. https://doi.org/https://doi.org/10.1016/j.memsci.2009.07.006.

[34] P. Długołęcki, A. Gambier, K. Nijmeijer, M. Wessling, Practical Potential of Reverse Electrodialysis As Process for Sustainable Energy Generation, Environmental Science & Technology. 43 (2009) 6888–6894. https://doi.org/10.1021/es9009635.

[35] T. Elmakki, S. Zavahir, M. Gulied, H. Qiblawey, B. Hammadi, M. Khraisheh, H.K. Shon, H. Park, D.S. Han, Potential application of hybrid reverse electrodialysis (RED)-forward osmosis (FO) system to fertilizer-producing industrial plant for efficient water reuse, Desalination. 550 (2023) 116374. https://doi.org/https://doi.org/10.1016/j.desal.2023.116374.

[36] Y. Fan, L. Wei, X. Meng, W. Zhang, N. Yang, Y. Jin, X. Wang, M. Zhao, S. Liu, An unprecedented high-temperature-tolerance 2D laminar MXene membrane for ultrafast hydrogen sieving, Journal of Membrane Science. 569 (2019) 117–123. https://doi.org/https://doi.org/10.1016/j.memsci.2018.10.017.

[37] A. Shahzad, J.-M. Oh, M. Azam, J. Iqbal, S. Hussain, W. Miran, K. Rasool, Advances

TH-3195_186151006

in the Synthesis and Application of Anti-Fouling Membranes Using Two-Dimensional Nanomaterials, Membranes. 11 (2021). https://doi.org/10.3390/membranes11080605.

[38] R. Sui, J.M.H. Lo, C.B. Lavery, C.E. Deering, K.G. Wynnyk, N. Chou, R.A. Marriott, Sol–Gel-Derived 2D Nanostructures of Aluminum Hydroxide Acetate: Toward the Understanding of Nanostructure Formation, The Journal of Physical Chemistry C. 122 (2018) 5141–5150. https://doi.org/10.1021/acs.jpcc.7b12490.

[39] F. La Mantia, M. Pasta, H.D. Deshazer, B.E. Logan, Y. Cui, Batteries for Efficient Energy Extraction from a Water Salinity Difference, Nano Letters. 11 (2011) 1810–1813. https://doi.org/10.1021/nl200500s.

[40] H. Wang, Y. Zhang, S. Ren, J. Pei, Z. Li, Athermal concentration of apple juice by forward osmosis: Process performance and membrane fouling propensity, Chemical Engineering Research and Design. 177 (2022) 569–577. https://doi.org/https://doi.org/10.1016/j.cherd.2021.11.023.

[41] Y. Cui, T.-S. Chung, Pharmaceutical concentration using organic solvent forward osmosis for solvent recovery, Nature Communications. 9 (2018). https://doi.org/10.1038/s41467-018-03612-2.

[42] A. Bardhan, S. Subbiah, K. Mohanty, Modelling and experimental validation of osmotic driven energy efficient process for tea solution concentration, Environmental Technology & Innovation. 20 (2020) 101065. https://doi.org/10.1016/j.eti.2020.101065.

[43] X. Wu, J. Tanner, D. Ng, D. Acharya, Z. Xie, Sewage concentration via a graphene oxide modified thin-film nanocomposite forward osmosis membrane: Enhanced performance and mitigated fouling, Chemical Engineering Journal. 420 (2021) 127718. https://doi.org/https://doi.org/10.1016/j.cej.2020.127718.

[44] M. Madhumala, S. Moulik, T. Sankarshana, S. Sridhar, Forward-osmosis-aided concentration of fructose sugar through hydrophilized polyamide membrane: Molecular modeling and economic estimation, Journal of Applied Polymer Science. 134 (2017). https://doi.org/https://doi.org/10.1002/app.44649.

[45] S.E. Skilhagen, J.E. Dugstad, R.J. Aaberg, Osmotic power — power production based on the osmotic pressure difference between waters with varying salt gradients, Desalination. 220 (2008) 476–482. https://doi.org/https://doi.org/10.1016/j.desal.2007.02.045.

[46] N.Y. Yip, A. Tiraferri, W.A. Phillip, J.D. Schiffman, L.A. Hoover, Y.C. Kim, M. Elimelech, Thin-Film Composite Pressure Retarded Osmosis Membranes for Sustainable Power Generation from Salinity Gradients, Environmental Science & Technology. 45 (2011) 4360–4369. https://doi.org/10.1021/es104325z.

[47] R.R. Gonzales, M.J. Park, T.-H. Bae, Y. Yang, A. Abdel-Wahab, S. Phuntsho, H.K. Shon, Melamine-based covalent organic framework-incorporated thin film nanocomposite membrane for enhanced osmotic power generation, Desalination. 459 (2019) 10–19. https://doi.org/https://doi.org/10.1016/j.desal.2019.02.013.

[48] Q. She, J. Wei, N. Ma, V. Sim, A.G. Fane, R. Wang, C.Y. Tang, Fabrication and characterization of fabric-reinforced pressure retarded osmosis membranes for osmotic power harvesting, Journal of Membrane Science. 504 (2016) 75–88.

TH-3195_186151006

https://doi.org/https://doi.org/10.1016/j.memsci.2016.01.004.

[49] M. Son, H. Park, L. Liu, H. Choi, J.H. Kim, H. Choi, Thin-film nanocomposite membrane with CNT positioning in support layer for energy harvesting from saline water, Chemical Engineering Journal. 284 (2016) 68–77. https://doi.org/https://doi.org/10.1016/j.cej.2015.08.134.

[50] F.-J. Fu, S. Zhang, S.-P. Sun, K.-Y. Wang, T.-S. Chung, POSS-containing delamination-free dual-layer hollow fiber membranes for forward osmosis and osmotic power generation, Journal of Membrane Science. 443 (2013) 144–155. https://doi.org/https://doi.org/10.1016/j.memsci.2013.04.050.

[51] D.A. Vermaas, D. Kunteng, M. Saakes, K. Nijmeijer, Fouling in reverse electrodialysis under natural conditions, Water Research. 47 (2013) 1289–1298. https://doi.org/https://doi.org/10.1016/j.watres.2012.11.053.

[52] J. Moreno, S. Grasman, R. van Engelen, K. Nijmeijer, Upscaling Reverse Electrodialysis, Environmental Science & Technology. 52 (2018) 10856–10863. https://doi.org/10.1021/acs.est.8b01886.

[53] M. Tedesco, E. Brauns, A. Cipollina, G. Micale, P. Modica, G. Russo, J. Helsen, Reverse electrodialysis with saline waters and concentrated brines: A laboratory investigation towards technology scale-up, Journal of Membrane Science. 492 (2015) 9–20. https://doi.org/https://doi.org/10.1016/j.memsci.2015.05.020.

[54] D. Brogioli, R. Ziano, R.A. Rica, D. Salerno, F. Mantegazza, Capacitive mixing for the extraction of energy from salinity differences: Survey of experimental results and electrochemical models, Journal of Colloid and Interface Science. 407 (2013) 457–466. https://doi.org/https://doi.org/10.1016/j.jcis.2013.06.050.

[55] W. Chen, Q. Zhang, Y. Qian, W. Xin, D. Hao, X. Zhao, C. Zhu, X.-Y. Kong, B. Lu, L. Jiang, L. Wen, Improved Ion Transport in Hydrogel-Based Nanofluidics for Osmotic Energy Conversion, ACS Central Science. 6 (2020) 2097–2104. https://doi.org/10.1021/acscentsci.0c01054.

[56] F. Zangrando, A simple method to establish salt gradient solar ponds, Solar Energy. 25 (1980) 467–470. https://doi.org/https://doi.org/10.1016/0038-092X(80)90456-9.

[57] R.L. McGinnis, M. Elimelech, Global Challenges in Energy and Water Supply: The Promise of Engineered Osmosis, Environmental Science & Technology. 42 (2008) 8625–8629. https://doi.org/10.1021/es800812m.

[58] J.W. Post, H.V.M. Hamelers, C.J.N. Buisman, Energy Recovery from Controlled Mixing Salt and Fresh Water with a Reverse Electrodialysis System, Environmental Science & Technology. 42 (2008) 5785–5790. https://doi.org/10.1021/es8004317.

[59] A. Al-Mamun, W. Ahmad, M.S. Baawain, M. Khadem, B.R. Dhar, A review of microbial desalination cell technology: Configurations, optimization and applications, Journal of Cleaner Production. 183 (2018) 458–480. https://doi.org/https://doi.org/10.1016/j.jclepro.2018.02.054.

[60] T. Jafary, A. Al-Mamun, H. Alhimali, M.S. Baawain, M.S. Rahman, S. Rahman, B.R. Dhar, M. Aghbashlo, M. Tabatabaei, Enhanced power generation and desalination rate

TH-3195_186151006

in a novel quadruple microbial desalination cell with a single desalination chamber, Renewable and Sustainable Energy Reviews. 127 (2020) 109855. https://doi.org/https://doi.org/10.1016/j.rser.2020.109855.

[61] T. Jafary, A. Al-Mamun, H. Alhimali, M.S. Baawain, S. Rahman, W.A. Tarpeh, B.R. Dhar, B.H. Kim, Novel two-chamber tubular microbial desalination cell for bioelectricity production, wastewater treatment and desalination with a focus on self-generated pH control, Desalination. 481 (2020) 114358. https://doi.org/https://doi.org/10.1016/j.desal.2020.114358.

[62] T. Shivakumar, V. Razaviarani, An integrated approach to enhance the desalination process: coupling reverse osmosis process with microbial desalination cells in the UAE, Water Supply. 21 (2020) 1127–1143. https://doi.org/10.2166/ws.2020.375.

[63] M. Khazraee Zamanpour, H.-R. Kariminia, M. Vosoughi, Electricity generation, desalination and microalgae cultivation in a biocathode-microbial desalination cell, Journal of Environmental Chemical Engineering. 5 (2017) 843–848. https://doi.org/https://doi.org/10.1016/j.jece.2016.12.045.

[64] F. Meng, J. Jiang, Q. Zhao, K. Wang, G. Zhang, Q. Fan, L. Wei, J. Ding, Z. Zheng, Bioelectrochemical desalination and electricity generation in microbial desalination cell with dewatered sludge as fuel, Bioresource Technology. 157 (2014) 120–126. https://doi.org/https://doi.org/10.1016/j.biortech.2014.01.056.

[65] A.Z. Imoro, M. Mensah, R. Buamah, Developments in the microbial desalination cell technology: A review, Water-Energy Nexus. 4 (2021) 76–87. https://doi.org/https://doi.org/10.1016/j.wen.2021.04.002.

[66] W.A. Suwaileh, D.J. Johnson, S. Sarp, N. Hilal, Advances in forward osmosis membranes: Altering the sub-layer structure via recent fabrication and chemical modification approaches, Desalination. 436 (2018) 176–201. https://doi.org/10.1016/j.desal.2018.01.035.

[67] R.R. Gonzales, M.J. Park, L. Tijing, D.S. Han, S. Phuntsho, H.K. Shon, Modification of Nanofiber Support Layer for Thin Film Composite Forward Osmosis Membranes via Layer-by-Layer Polyelectrolyte Deposition, Membranes. 8 (2018). https://doi.org/10.3390/membranes8030070.

[68] N. Widjojo, T.-S. Chung, M. Weber, C. Maletzko, V. Warzelhan, The role of sulphonated polymer and macrovoid-free structure in the support layer for thin-film composite (TFC) forward osmosis (FO) membranes, Journal of Membrane Science. 383 (2011) 214–223. https://doi.org/https://doi.org/10.1016/j.memsci.2011.08.041.

[69] M.R. Chowdhury, L. Huang, J.R. McCutcheon, Thin Film Composite Membranes for Forward Osmosis Supported by Commercial Nanofiber Nonwovens, Industrial & Engineering Chemistry Research. 56 (2017) 1057–1063. https://doi.org/10.1021/acs.iecr.6b04256.

[70] M. Sairam, E. Sereewatthanawut, K. Li, A. Bismarck, A.G. Livingston, Method for the preparation of cellulose acetate flat sheet composite membranes for forward osmosis—Desalination using MgSO4 draw solution, Desalination. 273 (2011) 299–307. https://doi.org/https://doi.org/10.1016/j.desal.2011.01.050.

TH-3195_186151006

[71] K.Y. Wang, R.C. Ong, T.-S. Chung, Double-Skinned Forward Osmosis Membranes for Reducing Internal Concentration Polarization within the Porous Sublayer, Industrial & Engineering Chemistry Research. 49 (2010) 4824–4831. https://doi.org/10.1021/ie901592d.

[72] J. Su, Q. Yang, J.F. Teo, T.-S. Chung, Cellulose acetate nanofiltration hollow fiber membranes for forward osmosis processes, Journal of Membrane Science. 355 (2010) 36–44. https://doi.org/https://doi.org/10.1016/j.memsci.2010.03.003.

[73] P. Lu 逯鹏, Y. Gao, A. Umar, T. Zhou, J. Wang, Z. Zhang, L. Huang, Q. Wang, Recent Advances in Cellulose-Based Forward Osmosis Membrane, Science of Advanced Materials. 7 (2015) 2182–2192. https://doi.org/10.1166/sam.2015.2269.

[74] Y. He, X. Lin, J. Chen, H. Zhan, Fabricating novel high-performance thin-film composite forward osmosis membrane with designed sulfonated covalent organic frameworks as interlayer, Journal of Membrane Science. 635 (2021) 119476. https://doi.org/https://doi.org/10.1016/j.memsci.2021.119476.

[75] M. Tian, Y.-N. Wang, R. Wang, A.G. Fane, Synthesis and characterization of thin film nanocomposite forward osmosis membranes supported by silica nanoparticle incorporated nanofibrous substrate, Desalination. 401 (2017) 142–150. https://doi.org/https://doi.org/10.1016/j.desal.2016.04.003.

[76] P.-F. Sun, Z. Yang, X. Song, J.H. Lee, C.Y. Tang, H.-D. Park, Interlayered Forward Osmosis Membranes with Ti3C2Tx MXene and Carbon Nanotubes for Enhanced Municipal Wastewater Concentration, Environmental Science & Technology. 55 (2021) 13219–13230. https://doi.org/10.1021/acs.est.1c01968.

[77] A.F. Faria, C. Liu, M. Xie, F. Perreault, L.D. Nghiem, J. Ma, M. Elimelech, Thin-film composite forward osmosis membranes functionalized with graphene oxide–silver nanocomposites for biofouling control, Journal of Membrane Science. 525 (2017) 146–156. https://doi.org/https://doi.org/10.1016/j.memsci.2016.10.040.

[78] N. Yanar, M. Son, E. Yang, Y. Kim, H. Park, S.-E. Nam, H. Choi, Investigation of the performance behavior of a forward osmosis membrane system using various feed spacer materials fabricated by 3D printing technique, Chemosphere. 202 (2018) 708–715. https://doi.org/https://doi.org/10.1016/j.chemosphere.2018.03.147.

[79] T.P.N. Nguyen, E.-T. Yun, I.-C. Kim, Y.-N. Kwon, Preparation of cellulose triacetate/cellulose acetate (CTA/CA)-based membranes for forward osmosis, Journal of Membrane Science. 433 (2013) 49–59. https://doi.org/https://doi.org/10.1016/j.memsci.2013.01.027.

[80] L. Xia, M.F. Andersen, C. Hélix-Nielsen, J.R. McCutcheon, Novel Commercial Aquaporin Flat-Sheet Membrane for Forward Osmosis, Industrial & Engineering Chemistry Research. 56 (2017) 11919–11925. https://doi.org/10.1021/acs.iecr.7b02368.

[81] J. Ren, J.R. McCutcheon, A new commercial biomimetic hollow fiber membrane for forward osmosis, Desalination. 442 (2018) 44–50. https://doi.org/https://doi.org/10.1016/j.desal.2018.04.015.

[82] J.T. Arena, S.S. Manickam, K.K. Reimund, P. Brodskiy, J.R. McCutcheon,

TH-3195_186151006

Characterization and Performance Relationships for a Commercial Thin Film Composite Membrane in Forward Osmosis Desalination and Pressure Retarded Osmosis, Industrial & Engineering Chemistry Research. 54 (2015) 11393–11403. https://doi.org/10.1021/acs.iecr.5b02309.

[83] Y. Li, Y. Yang, C. Li, L. Hou, Comparison of performance and biofouling resistance of thin- fi lm composite forward osmosis membranes with substrate / active layer modi fi ed by graphene oxide †, (2019) 6502–6509. https://doi.org/10.1039/c8ra08838a.

[84] H. Kang, W. Wang, J. Shi, Z. Xu, H. Lv, X. Qian, L. Liu, M. Jing, F. Li, J. Niu, Interlamination restrictive effect of carbon nanotubes for graphene oxide forward osmosis membrane via layer by layer assembly, Applied Surface Science. 465 (2019) 1103–1106. https://doi.org/https://doi.org/10.1016/j.apsusc.2018.09.255.

[85] H. Choi, A.A. Shah, S.-E. Nam, Y.-I. Park, H. Park, Thin-film composite membranes comprising ultrathin hydrophilic polydopamine interlayer with graphene oxide for forward osmosis, Desalination. 449 (2019) 41–49. https://doi.org/https://doi.org/10.1016/j.desal.2018.10.012.

[86] E. Yang, A.B. Alayande, C.-M. Kim, J. Song, I.S. Kim, Laminar reduced graphene oxide membrane modified with silver nanoparticle-polydopamine for water/ion separation and biofouling resistance enhancement, Desalination. 426 (2018) 21–31. https://doi.org/https://doi.org/10.1016/j.desal.2017.10.023.

[87] C. Du, X. Zhang, C. Wu, Chitosan-modified graphene oxide as a modifier for improving the structure and performance of forward osmosis membranes, (2019) 1–10. https://doi.org/10.1002/pat.4816.

[88] W. Zhao, H. Liu, Y. Liu, M. Jian, L. Gao, H. Wang, X. Zhang, Thin-Film Nanocomposite Forward-Osmosis Membranes on Hydrophilic Microfiltration Support with an Intermediate Layer of Graphene Oxide and Multiwall Carbon Nanotube, ACS Applied Materials and Interfaces. 10 (2018) 34464–34474. https://doi.org/10.1021/acsami.8b10550.

[89] M. Bagherzadeh, M. Nikkhoo, M.M. Ahadian, M. Amini, Novel Thin-Film Nanocomposite Forward Osmosis Membranes Modified with WS2/CuAl LDH Nanocomposite to Enhance Desalination and Anti-fouling Performance, Journal of Inorganic and Organometallic Polymers and Materials. 33 (2023) 956–968. https://doi.org/10.1007/s10904-023-02547-6.

[90] T. Luo, S. Abdu, M. Wessling, Selectivity of ion exchange membranes: A review, Journal of Membrane Science. 555 (2018) 429–454. https://doi.org/https://doi.org/10.1016/j.memsci.2018.03.051.

[91] A.M. Samsudin, M. Roschger, S. Wolf, V. Hacker, Preparation and Characterization of QPVA/PDDA Electrospun Nanofiber Anion Exchange Membranes for Alkaline Fuel Cells, Nanomaterials. 12 (2022). https://doi.org/10.3390/nano12223965.

[92] B. Zhang, Z. He, Improving water desalination by hydraulically coupling an osmotic microbial fuel cell with a microbial desalination cell, Journal of Membrane Science. 441 (2013) 18–24. https://doi.org/https://doi.org/10.1016/j.memsci.2013.04.005.

[93] J.G. Hong, W. Zhang, J. Luo, Y. Chen, Modeling of power generation from the mixing

TH-3195_186151006

of simulated saline and freshwater with a reverse electrodialysis system: The effect of monovalent and multivalent ions, Applied Energy. 110 (2013) 244–251. https://doi.org/https://doi.org/10.1016/j.apenergy.2013.04.015.

[94] M. Rahimnejad, A.A. Ghoreyshi, G. Najafpour, T. Jafary, Power generation from organic substrate in batch and continuous flow microbial fuel cell operations, Applied Energy. 88 (2011) 3999–4004. https://doi.org/https://doi.org/10.1016/j.apenergy.2011.04.017.

[95] J.-S. Jang, Y. Lim, H. Shin, J. Kim, T.G. Yun, Bidirectional Water-Stream Behavior on a Multifunctional Membrane for Simultaneous Energy Generation and Water Purification, Advanced Materials. 35 (2023) 2209076. https://doi.org/https://doi.org/10.1002/adma.202209076.

[96] G. Yang, Q. Yijun, D. Liu, L. Wang, Y. Ma, J. Sun, Y. Su, K. Jarvis, X. Wang, W. Lei, Simultaneous Electrokinetic Energy Conversion and Organic Molecular Sieving by Two-dimensional Confined Nanochannels, Chemical Engineering Journal. 446 (2022) 136870. https://doi.org/10.1016/j.cej.2022.136870.

[97] Z. Li, Y. Guo, X. Wang, P. Li, W. Ying, D. Chen, X. Ma, Z. Deng, X. Peng, Simultaneous Recovery of Metal Ions and Electricity Harvesting via K-Carrageenan@ZIF-8 Membrane, ACS Applied Materials & Interfaces. 11 (2019) 34039–34045. https://doi.org/10.1021/acsami.9b12501.

[98] A. Ghaffar, Q. Imran, M. Hassan, M. Usman, M.U. Khan, Simultaneous solar water desalination and energy generation by high efficient graphene oxide-melanin photothermal membrane, Journal of Environmental Chemical Engineering. 10 (2022) 108424. https://doi.org/https://doi.org/10.1016/j.jece.2022.108424.

[99] D. Ma, Y. Tian, T. He, X. Zhu, Preparation of novel magnetic nanoparticles as draw solutes in forward osmosis desalination, Chinese Journal of Chemical Engineering. 46 (2022) 223–230. https://doi.org/https://doi.org/10.1016/j.cjche.2021.07.013.

[100] A. Achilli, T.Y. Cath, A.E. Childress, Selection of inorganic-based draw solutions for forward osmosis applications, Journal of Membrane Science. 364 (2010) 233–241. https://doi.org/https://doi.org/10.1016/j.memsci.2010.08.010.

[101] Q. She, X. Jin, Q. Li, C.Y. Tang, Relating reverse and forward solute diffusion to membrane fouling in osmotically driven membrane processes, Water Research. 46 (2012) 2478–2486. https://doi.org/https://doi.org/10.1016/j.watres.2012.02.024.

[102] N.T. Hancock, T.Y. Cath, Solute Coupled Diffusion in Osmotically Driven Membrane Processes, Environmental Science & Technology. 43 (2009) 6769–6775. https://doi.org/10.1021/es901132x.

[103] Q. Long, Y. Jia, J. Li, J. Yang, F. Liu, J. Zheng, B. Yu, Recent Advance on Draw Solutes Development in Forward Osmosis, Processes . 6 (2018). https://doi.org/10.3390/pr6090165.

[104] S. Zhao, L. Zou, Effects of working temperature on separation performance, membrane scaling and cleaning in forward osmosis desalination, Desalination. 278 (2011) 157–164. https://doi.org/https://doi.org/10.1016/j.desal.2011.05.018.

TH-3195_186151006

[105] S. Lee, Exploring the Operation Factors that Influence Performance of a Spiral-Wound Forward Osmosis Membrane Process for Scale-up Design, Membranes. 10 (2020). https://doi.org/10.3390/membranes10030053.

[106] M. Kahrizi, R.R. Gonzales, L. Kong, H. Matsuyama, P. Lu, J. Lin, S. Zhao, Significant roles of substrate properties in forward osmosis membrane performance: A review, Desalination. 528 (2022) 115615. https://doi.org/https://doi.org/10.1016/j.desal.2022.115615.

[107] B.M. Ibraheem, S.A. Aani, A.A. Alsarayreh, Q.F. Alsalhy, I.K. Salih, Forward Osmosis Membrane: Review of Fabrication, Modification, Challenges and Potential, Membranes. 13 (2023). https://doi.org/10.3390/membranes13040379.

[108] N. Ma, J. Wei, S. Qi, Y. Zhao, Y. Gao, C.Y. Tang, Nanocomposite substrates for controlling internal concentration polarization in forward osmosis membranes, Journal of Membrane Science. 441 (2013) 54–62. https://doi.org/https://doi.org/10.1016/j.memsci.2013.04.004.

[109] W. Wang, Y. Guo, M. Liu, X. Song, J. Duan, Porous nano-hydroxyapatites doped into substrate for thin film composite forward osmosis membrane to show high performance, Korean Journal of Chemical Engineering. 37 (2020) 1573–1584. https://doi.org/10.1007/s11814-020-0554-x.

[110] F. Niu, M. Huang, T. Cai, L. Meng, Effect of Membrane Thickness on Properties of FO Membranes with Nanofibrous Substrate, IOP Conference Series: Earth and Environmental Science. 170 (2018) 52005. https://doi.org/10.1088/1755-1315/170/5/052005.

[111] C. Suh, S. Lee, Modeling reverse draw solute flux in forward osmosis with external concentration polarization in both sides of the draw and feed solution, Journal of Membrane Science. 427 (2013) 365–374. https://doi.org/https://doi.org/10.1016/j.memsci.2012.08.033.

[112] S. Zhao, L. Zou, D. Mulcahy, Effects of membrane orientation on process performance in forward osmosis applications, Journal of Membrane Science. 382 (2011) 308–315. https://doi.org/https://doi.org/10.1016/j.memsci.2011.08.020.

[113] E.O. Ezugbe, E. Kweinor Tetteh, S. Rathilal, D. Asante-Sackey, Assessment of Forward Osmosis in PRO Mode during Desalination of a Local Oil Refinery Effluent, Membranes. 11 (2021). https://doi.org/10.3390/membranes11110801.

[114] S.S. Sablani, M.F.A. Goosen, R. Al-Belushi, M. Wilf, Concentration polarization in ultrafiltration and reverse osmosis: a critical review, Desalination. 141 (2001) 269–289. https://doi.org/https://doi.org/10.1016/S0011-9164(01)85005-0.

[115] C. Klaysom, T.Y. Cath, T. Depuydt, I.F.J. Vankelecom, Forward and pressure retarded osmosis: potential solutions for global challenges in energy and water supply, Chemical Society Reviews. 42 (2013) 6959–6989. https://doi.org/10.1039/C3CS60051C.

[116] A. Bhinder, S. Shabani, M. Sadrzadeh, Effect of Internal and External Concentration Polarizations on the Performance of Forward Osmosis Process, Osmotically Driven Membrane Processes - Approach, Development and Current Status. (2018). https://doi.org/10.5772/intechopen.71343.

TH-3195_186151006

[117] J.R. McCutcheon, M. Elimelech, Influence of concentrative and dilutive internal concentration polarization on flux behavior in forward osmosis, Journal of Membrane Science. 284 (2006) 237–247. https://doi.org/https://doi.org/10.1016/j.memsci.2006.07.049.

[118] S. Phuntsho, S. Sahebi, T. Majeed, F. Lotfi, J.E. Kim, H.K. Shon, Assessing the major factors affecting the performances of forward osmosis and its implications on the desalination process, Chemical Engineering Journal. 231 (2013) 484–496. https://doi.org/https://doi.org/10.1016/j.cej.2013.07.058.

[119] J.R. McCutcheon, R.L. McGinnis, M. Elimelech, Desalination by ammonia–carbon dioxide forward osmosis: Influence of draw and feed solution concentrations on process performance, Journal of Membrane Science. 278 (2006) 114–123. https://doi.org/https://doi.org/10.1016/j.memsci.2005.10.048.

[120] H. Zhou, D.W. Smith, Advanced technologies in water and wastewater treatment, Journal of Environmental Engineering and Science. 1 (2002) 247–264. https://doi.org/10.1139/s02-020.

[121] S.B. Sadr Ghayeni, P.J. Beatson, R.P. Schneider, A.G. Fane, Water reclamation from municipal wastewater using combined microfiltration-reverse osmosis (ME-RO): Preliminary performance data and microbiological aspects of system operation, Desalination. 116 (1998) 65–80. https://doi.org/https://doi.org/10.1016/S0011-9164(98)00058-7.

[122] Y.-F. Huang, S.-L. Lo, 19 - Utilization of rice hull and straw, in: J.B.T.-R. (Fourth E. Bao (Ed.), AACC International Press, 2019: pp. 627–661. https://doi.org/https://doi.org/10.1016/B978-0-12-811508-4.00019-8.

[123] Y. Chun, D. Mulcahy, L. Zou, I.S. Kim, A Short Review of Membrane Fouling in Forward Osmosis Processes, Membranes. 7 (2017). https://doi.org/10.3390/membranes7020030.

[124] C.Y. Tang, Q. She, W.C.L. Lay, R. Wang, A.G. Fane, Coupled effects of internal concentration polarization and fouling on flux behavior of forward osmosis membranes during humic acid filtration, Journal of Membrane Science. 354 (2010) 123–133. https://doi.org/https://doi.org/10.1016/j.memsci.2010.02.059.

[125] Q. She, Y.K.W. Wong, S. Zhao, C.Y. Tang, Organic fouling in pressure retarded osmosis: Experiments, mechanisms and implications, Journal of Membrane Science. 428 (2013) 181–189. https://doi.org/https://doi.org/10.1016/j.memsci.2012.10.045.

[126] J. Zhang, W.L.C. Loong, S. Chou, C. Tang, R. Wang, A.G. Fane, Membrane biofouling and scaling in forward osmosis membrane bioreactor, Journal of Membrane Science. 403–404 (2012) 8–14. https://doi.org/https://doi.org/10.1016/j.memsci.2012.01.032.

[127] S. Zou, Y.-N. Wang, F. Wicaksana, T. Aung, P.C.Y. Wong, A.G. Fane, C.Y. Tang, Direct microscopic observation of forward osmosis membrane fouling by microalgae: Critical flux and the role of operational conditions, Journal of Membrane Science. 436 (2013) 174–185. https://doi.org/https://doi.org/10.1016/j.memsci.2013.02.030.

[128] B. Mi, M. Elimelech, Organic fouling of forward osmosis membranes: Fouling reversibility and cleaning without chemical reagents, Journal of Membrane Science. 348

TH-3195_186151006

(2010) 337–345. https://doi.org/https://doi.org/10.1016/j.memsci.2009.11.021.

[129] C. Boo, M. Elimelech, S. Hong, Fouling control in a forward osmosis process integrating seawater desalination and wastewater reclamation, Journal of Membrane Science. 444 (2013) 148–156. https://doi.org/https://doi.org/10.1016/j.memsci.2013.05.004.

[130] Z.L. Cheng, X. Li, T.-S. Chung, The forward osmosis-pressure retarded osmosis (FO-PRO) hybrid system: A new process to mitigate membrane fouling for sustainable osmotic power generation, Journal of Membrane Science. 559 (2018) 63–74. https://doi.org/https://doi.org/10.1016/j.memsci.2018.04.036.

[131] Z.-X. Low, J. Ji, D. Blumenstock, Y.-M. Chew, D. Wolverson, D. Mattia, Fouling resistant 2D boron nitride nanosheet – PES nanofiltration membranes, Journal of Membrane Science. 563 (2018) 949–956. https://doi.org/https://doi.org/10.1016/j.memsci.2018.07.003.

[132] L. Loske, K. Nakagawa, T. Yoshioka, H. Matsuyama, 2D Nanocomposite Membranes: Water Purification and Fouling Mitigation, Membranes. 10 (2020). https://doi.org/10.3390/membranes10100295.

[133] M. Qiu, C. He, Novel zwitterion-silver nanocomposite modified thin-film composite forward osmosis membrane with simultaneous improved water flux and biofouling resistance property, Applied Surface Science. 455 (2018) 492–501. https://doi.org/https://doi.org/10.1016/j.apsusc.2018.06.020.

[134] F. Li, Q. Cheng, Q. Tian, B. Yang, Q. Chen, Biofouling behavior and performance of forward osmosis membranes with bioinspired surface modification in osmotic membrane bioreactor, Bioresource Technology. 211 (2016) 751–758. https://doi.org/https://doi.org/10.1016/j.biortech.2016.03.169.

[135] K.L. Lee, R.W. Baker, H.K. Lonsdale, Membranes for power generation by pressure-retarded osmosis, Journal of Membrane Science. 8 (1981) 141–171. https://doi.org/https://doi.org/10.1016/S0376-7388(00)82088-8.

[136] R. Thiruvenkatachari, M. Francis, M. Cunnington, S. Su, Application of integrated forward and reverse osmosis for coal mine wastewater desalination, Separation and Purification Technology. 163 (2016) 181–188. https://doi.org/https://doi.org/10.1016/j.seppur.2016.02.034.

[137] J. Zhang, Q. She, V.W.C. Chang, C.Y. Tang, R.D. Webster, Mining Nutrients (N, K, P) from Urban Source-Separated Urine by Forward Osmosis Dewatering, Environmental Science & Technology. 48 (2014) 3386–3394. https://doi.org/10.1021/es405266d.

[138] K. Lutchmiah, A.R.D. Verliefde, K. Roest, L.C. Rietveld, E.R. Cornelissen, Forward osmosis for application in wastewater treatment: A review, Water Research. 58 (2014) 179–197. https://doi.org/https://doi.org/10.1016/j.watres.2014.03.045.

[139] R.E. WROLSTAD, M.R. MCDANIEL, R.W. DURST, N. MICHEALS, K.A. LAMPI, E.G. BEAUDRY, Composition and Sensory Characterization of Red Raspberry Juice Concentrated by Direct-Osmosis or Evaporation, Journal of Food Science. 58 (1993) 633–637. https://doi.org/https://doi.org/10.1111/j.1365-2621.1993.tb04344.x.

[140] A. Bardhan, S. Subbiah, K. Mohanty, Modeling and Experimental Validation for the

TH-3195_186151006

Preparation of Concentrated Tea Extract Using a Forward Osmosis Process Using a Food-Grade Inorganic Draw Solute, Industrial & Engineering Chemistry Research. 62 (2023) 3315–3326. https://doi.org/10.1021/acs.iecr.2c04219.

[141] R. Singh, Chapter 1 - Introduction to Membrane Technology, in: R.B.T.-M.T. and E. for W.P. (Second E. Singh (Ed.), Butterworth-Heinemann, Oxford, 2015: pp. 1–80. https://doi.org/https://doi.org/10.1016/B978-0-444-63362-0.00001-X.

[142] J. Webley, Technology developments in forward osmosis to address water purification, Desalination and Water Treatment. 55 (2015) 2612–2617. https://doi.org/10.1080/19443994.2014.991568.

[143] N. Akther, S. Phuntsho, Y. Chen, N. Ghaffour, H.K. Shon, Recent advances in nanomaterial-modified polyamide thin-film composite membranes for forward osmosis processes, Journal of Membrane Science. 584 (2019) 20–45. https://doi.org/https://doi.org/10.1016/j.memsci.2019.04.064.

[144] X. Wu, R.W. Field, J.J. Wu, K. Zhang, Polyvinylpyrrolidone modified graphene oxide as a modifier for thin film composite forward osmosis membranes, Journal of Membrane Science. 540 (2017) 251–260. https://doi.org/https://doi.org/10.1016/j.memsci.2017.06.070.

[145] K. Khan, M. Irfan, N.U. Amin, H. Jiang, S. Gul, Synthesis and characterization of porous reduced graphene oxide based geopolymeric membrane with titanium dioxide coating for forward osmosis application, Chemosphere. 313 (2023) 137480. https://doi.org/https://doi.org/10.1016/j.chemosphere.2022.137480.

[146] Y. Wang, R. Ou, Q. Ge, H. Wang, T. Xu, Preparation of polyethersulfone/carbon nanotube substrate for high-performance forward osmosis membrane, Desalination. 330 (2013) 70–78. https://doi.org/https://doi.org/10.1016/j.desal.2013.09.028.

[147] D.R. Dreyer, S. Park, C.W. Bielawski, R.S. Ruoff, The chemistry of graphene oxide, Chemical Society Reviews. 39 (2010) 228–240. https://doi.org/10.1039/B917103G.

[148] J. Pei, X. Zhang, L. Huang, H. Jiang, X. Hu, Fabrication of reduced graphene oxide membranes for highly efficient water desalination, RSC Adv. 6 (2016) 101948–101952. https://doi.org/10.1039/C6RA22711B.

[149] B. Li, X.-X. Ke, L.-B. Zhong, R.-X. Wu, Z.-H. Yuan, J.-J. Fan, Y.-M. Zheng, Super-hydrophilic nanofiber substrate supported forward osmosis membrane with less polyamide layer defects by polydopamine-graphene oxide modification for high salinity desulfurization wastewater desalination, Journal of Membrane Science. 659 (2022) 120767. https://doi.org/https://doi.org/10.1016/j.memsci.2022.120767.

[150] B.M. Ganesh, A.M. Isloor, A.F. Ismail, Enhanced hydrophilicity and salt rejection study of graphene oxide-polysulfone mixed matrix membrane, Desalination. 313 (2013) 199–207. https://doi.org/https://doi.org/10.1016/j.desal.2012.11.037.

[151] Y. Li, Y. Zhao, E. Tian, Y. Ren, Preparation and characterization of novel forward osmosis membrane incorporated with sulfonated carbon nanotubes, RSC Advances. 8 (2018) 41032–41039. https://doi.org/10.1039/C8RA08900K.

[152] D.C. Marcano, D. V Kosynkin, J.M. Berlin, A. Sinitskii, Z. Sun, A.S. Slesarev, L.B.

TH-3195_186151006

Alemany, W. Lu, J.M. Tour, Correction to Improved Synthesis of Graphene Oxide, ACS Nano. 12 (2018) 2078. https://doi.org/10.1021/acsnano.8b00128.

[153] H.-K. Jeong, Y.P. Lee, M.H. Jin, E.S. Kim, J.J. Bae, Y.H. Lee, Thermal stability of graphite oxide, Chemical Physics Letters. 470 (2009) 255–258. https://doi.org/https://doi.org/10.1016/j.cplett.2009.01.050.

[154] C.N. Yeh, K. Raidongia, J. Shao, Q.H. Yang, J. Huang, On the origin of the stability of graphene oxide membranes in water, Nature Chemistry. 7 (2015) 166–170. https://doi.org/10.1038/nchem.2145.

[155] G. Wang, B. Wang, J. Park, J. Yang, X. Shen, J. Yao, Synthesis of enhanced hydrophilic and hydrophobic graphene oxide nanosheets by a solvothermal method, Carbon. 47 (2009) 68–72. https://doi.org/https://doi.org/10.1016/j.carbon.2008.09.002.

[156] H. Hou, X. Hu, X. Liu, W. Hu, R. Meng, L. Li, Sulfonated graphene oxide with improved ionic performances, Ionics. 21 (2015) 1919–1923. https://doi.org/10.1007/s11581-014-1355-1.

[157] S. Ayyaru, Y. Ahn, Application of sulfonic acid group functionalized graphene oxide to improve hydrophilicity , permeability , and antifouling of PVDF nanocomposite ultra fi ltration membranes, Journal of Membrane Science. 525 (2017) 210–219. https://doi.org/10.1016/j.memsci.2016.10.048.

[158] H. Huang, Z. Song, N. Wei, L. Shi, Y. Mao, Y. Ying, L. Sun, Z. Xu, X. Peng, Ultrafast viscous water flow through nanostrand-channelled graphene oxide membranes, Nature Communications. 4 (2013) 2979. https://doi.org/10.1038/ncomms3979.

[159] R. Kumar, M. Mamlouk, K. Scott, Sulfonated polyether ether ketone – sulfonated graphene oxide composite membranes for polymer electrolyte fuel cells, RSC Advances. 4 (2014) 617–623. https://doi.org/10.1039/C3RA42390E.

[160] G. Yang, Z. Xie, M. Cran, D. Ng, C.D. Easton, M. Ding, H. Xu, S. Gray, Functionalizing graphene oxide framework membranes with sulfonic acid groups for superior aqueous mixture separation, Journal of Materials Chemistry A. 7 (2019) 19682–19690. https://doi.org/10.1039/C9TA04031E.

[161] M.H. Khan, H. Bae, J.-Y. Jung, Tetracycline degradation by ozonation in the aqueous phase: Proposed degradation intermediates and pathway, Journal of Hazardous Materials. 181 (2010) 659–665. https://doi.org/https://doi.org/10.1016/j.jhazmat.2010.05.063.

[162] A. Alves, A. Morão, J. Cardoso, Isolation of antibiotics from industrial fermentation broths using membrane technology, Desalination. 148 (2002) 181–186. https://doi.org/10.1016/S0011-9164(02)00695-1.

[163] K.S. Hong, J.S. Kim, Rifaximin for the treatment of acute infectious diarrhea, Therapeutic Advances in Gastroenterology. 4 (2011) 227–235. https://doi.org/10.1177/1756283X11398734.

[164] S. Jeong, K.G. Song, J. Kim, J. Shin, S.K. Maeng, J. Park, Feasibility of membrane distillation process for potable water reuse: A barrier for dissolved organic matters and pharmaceuticals, Journal of Hazardous Materials. 409 (2021).

TH-3195_186151006

https://doi.org/10.1016/j.jhazmat.2020.124499.

[165] M. Shibuya, M. Yasukawa, T. Takahashi, T. Miyoshi, M. Higa, H. Matsuyama, Effect of operating conditions on osmotic-driven membrane performances of cellulose triacetate forward osmosis hollow fiber membrane, Desalination. 362 (2015) 34–42. https://doi.org/https://doi.org/10.1016/j.desal.2015.01.031.

[166] W. Xu, Q. Chen, Q. Ge, Recent advances in forward osmosis (FO) membrane: Chemical modifications on membranes for FO processes, Desalination. 419 (2017) 101–116. https://doi.org/https://doi.org/10.1016/j.desal.2017.06.007.

[167] H.M. Hegab, A. ElMekawy, T.G. Barclay, A. Michelmore, L. Zou, C.P. Saint, M. Ginic-Markovic, Effective in-situ chemical surface modification of forward osmosis membranes with polydopamine-induced graphene oxide for biofouling mitigation, Desalination. 385 (2016) 126–137. https://doi.org/https://doi.org/10.1016/j.desal.2016.02.021.

[168] W. Ding, Y. Li, M. Bao, J. Zhang, C. Zhang, J. Lu, Highly permeable and stable forward osmosis (FO) membrane based on the incorporation of Al2O3 nanoparticles into both substrate and polyamide active layer, RSC Advances. 7 (2017) 40311–40320. https://doi.org/10.1039/C7RA04046F.

[169] F. Mouhat, F.-X. Coudert, M.-L. Bocquet, Structure and chemistry of graphene oxide in liquid water from first principles, Nature Communications. 11 (2020) 1566. https://doi.org/10.1038/s41467-020-15381-y.

[170] H. Teklu, D.K. Gautam, S. Subbiah, Axial flow hollow fiber forward osmosis module analysis for optimum design and operating conditions in desalination applications, Chemical Engineering Science. 216 (2020) 115494. https://doi.org/https://doi.org/10.1016/j.ces.2020.115494.

[171] V.K. Verma, S. Subbiah, Sericin-coated polymeric microfiltration membrane for removal of drug-based micropollutants, Journal of Chemical Technology & Biotechnology. 94 (2019) 3625–3636. https://doi.org/10.1002/jctb.6168.

[172] G. Wang, B. Wang, J. Park, J. Yang, X. Shen, J. Yao, Synthesis of enhanced hydrophilic and hydrophobic graphene oxide nanosheets by a solvothermal method, 7 (2008) 6–10. https://doi.org/10.1016/j.carbon.2008.09.002.

[173] S.B. Maddinedi, J. Sonamuthu, S. SuzuK Yildiz, G. Han, Y. Cai, J. Gao, Q. Ni, J. Yao, Silk sericin induced fabrication of reduced graphene oxide and its in-vitro cytotoxicity, photothermal evaluation, Journal of Photochemistry and Photobiology B: Biology. 186 (2018) 189–196. https://doi.org/https://doi.org/10.1016/j.jphotobiol.2018.07.020.

[174] P. Deka, V.K. Verma, B. Yurembam, A.B. Neog, K. Raidongia, S. Subbiah, Performance evaluation of reduced graphene oxide membrane doped with polystyrene sulfonic acid for forward osmosis process, Sustainable Energy Technologies and Assessments. 44 (2021) 101093. https://doi.org/https://doi.org/10.1016/j.seta.2021.101093.

[175] V.R. Silva, F. Hamerski, T.A. Weschenfelder, M. Ribani, M.L. Gimenes, A.P. Scheer, Equilibrium, kinetic, and thermodynamic studies on the biosorption of Bordeaux S dye by sericin powder derived from cocoons of the silkworm Bombyx mori, Desalination

TH-3195_186151006

and Water Treatment. 57 (2016) 5119–5129. https://doi.org/10.1080/19443994.2014.996776.

[176] D. Bhuyan, G.W. Greene, R.K. Das, Dataset on the synthesis and physicochemical characterization of blank and curcumin encapsulated sericin nanoparticles obtained from Philosamia ricini silkworm cocoons, Data in Brief. 26 (2019) 104359. https://doi.org/https://doi.org/10.1016/j.dib.2019.104359.

[177] M. Li, C. Liu, Y. Xie, H. Cao, H. Zhao, Y. Zhang, The evolution of surface charge on graphene oxide during the reduction and its application in electroanalysis, Carbon. 66 (2014) 302–311. https://doi.org/https://doi.org/10.1016/j.carbon.2013.09.004.

[178] V.K. Verma, S. Subbiah, Fouling resistant sericin-coated polymeric microfiltration membrane, Journal of Chemical Technology & Biotechnology. 94 (2019) 3637–3649. https://doi.org/https://doi.org/10.1002/jctb.6169.

[179] Z. Li, Y. Wang, M. Han, D. Wang, S. Han, Z. Liu, N. Zhou, R. Shang, C. Xie, Graphene Oxide Incorporated Forward Osmosis Membranes With Enhanced Desalination Performance and Chlorine Resistance , Frontiers in Chemistry . 7 (2020) 877. https://www.frontiersin.org/article/10.3389/fchem.2019.00877.

[180] R. Xu, P. Jiang, C. Wei, Z. Lü, S. Yu, M. Liu, C. Gao, Depositing sericin on partially degraded polyamide reverse osmosis membrane for restored salt rejection and simultaneously enhanced resistance to both fouling and chlorine, Journal of Membrane Science. 545 (2018) 196–203. https://doi.org/https://doi.org/10.1016/j.memsci.2017.09.073.

[181] D.R. Paul, Reformulation of the solution-diffusion theory of reverse osmosis, Journal of Membrane Science. 241 (2004) 371–386. https://doi.org/https://doi.org/10.1016/j.memsci.2004.05.026.

[182] S.W. Vedakumari, S.J. Veda Jancy, Y.R. Pravin, J. Bhoopathy, K. Iyswariya, S. Thomas, R. Rubiya, L. Prabakaran, C. Kumar, P. Prabu, R. Murugesan, Facile synthesis of sericin modified graphene oxide nanocomposites for treating ischemic diseases, Environmental Research. 209 (2022) 112925. https://doi.org/https://doi.org/10.1016/j.envres.2022.112925.

[183] M.S. Senthilmurugan S, Method and a system for monitoring and control of fouling and optimization thereof of two side membrane fouling process, US9737858B2, 2013. https://patents.google.com/patent/US9737858.

[184] L. Shen, S. Xiong, Y. Wang, Graphene oxide incorporated thin-film composite membranes for forward osmosis applications, Chemical Engineering Science. 143 (2016) 194–205. https://doi.org/https://doi.org/10.1016/j.ces.2015.12.029.

[185] H. Yun, M.K. Kim, H.W. Kwak, J.Y. Lee, M.H. Kim, E.H. Kim, K.H. Lee, Preparation and characterization of silk sericin/glycerol/graphene oxide nanocomposite film, Fibers and Polymers. 14 (2013) 2111–2116. https://doi.org/10.1007/s12221-013-2111-2.

[186] S.A. Algharib, A. Dawood, K. Zhou, D. Chen, C. Li, K. Meng, M.K. Maa, S. Ahmed, L. Huang, S. Xie, Designing, structural determination and biological effects of rifaximin loaded chitosan- carboxymethyl chitosan nanogel, Carbohydrate Polymers. 248 (2020) 116782. https://doi.org/https://doi.org/10.1016/j.carbpol.2020.116782.

TH-3195_186151006

[187] S. Yu, G. Yao, B. Dong, H. Zhu, X. Peng, J. Liu, M. Liu, C. Gao, Improving fouling resistance of thin-film composite polyamide reverse osmosis membrane by coating natural hydrophilic polymer sericin, Separation and Purification Technology. 118 (2013) 285–293. https://doi.org/https://doi.org/10.1016/j.seppur.2013.07.018.

[188] C. Zhou, Y. Shi, C. Sun, S. Yu, M. Liu, C. Gao, Thin-film composite membranes formed by interfacial polymerization with natural material sericin and trimesoyl chloride for nanofiltration, Journal of Membrane Science. 471 (2014) 381–391. https://doi.org/10.1016/j.memsci.2014.08.033.

[189] V.K. Verma, S. Subbiah, Fouling resistant sericin-coated polymeric microfiltration membrane, Journal of Chemical Technology & Biotechnology. 94 (2019) 3637–3649. https://doi.org/10.1002/jctb.6169.

[190] Y. Xu, Y. Song, F. Xu, TEMPO oxidized cellulose nanofibers-based heterogenous membrane employed for concentration-gradient-driven energy harvesting, Nano Energy. 79 (2021) 105468. https://doi.org/https://doi.org/10.1016/j.nanoen.2020.105468.

[191] B.E. Logan, M. Elimelech, Membrane-based processes for sustainable power generation using water, Nature. 488 (2012) 313–319. https://doi.org/10.1038/nature11477.

[192] T.-S. Chung, L. Luo, C.F. Wan, Y. Cui, G. Amy, What is next for forward osmosis (FO) and pressure retarded osmosis (PRO), Separation and Purification Technology. 156 (2015) 856–860. https://doi.org/https://doi.org/10.1016/j.seppur.2015.10.063.

[193] W.L. Ang, A. Wahab Mohammad, D. Johnson, N. Hilal, Forward osmosis research trends in desalination and wastewater treatment: A review of research trends over the past decade, Journal of Water Process Engineering. 31 (2019) 100886. https://doi.org/https://doi.org/10.1016/j.jwpe.2019.100886.

[194] M. Szczygiełda, M. Krajewska, A. Andrzejewski, L. Zheng, L.D. Nghiem, P. Oleskowicz-Popiel, D. Szymanowska, K. Prochaska, Dewatering fermentation broth for keto carboxylic acid enrichment by forward osmosis: A techno-economic analysis, Journal of Membrane Science. 679 (2023) 121699. https://doi.org/https://doi.org/10.1016/j.memsci.2023.121699.

[195] N. Akther, A. Sodiq, A. Giwa, S. Daer, H.A. Arafat, S.W. Hasan, Recent advancements in forward osmosis desalination: A review, Chemical Engineering Journal. 281 (2015) 502–522. https://doi.org/https://doi.org/10.1016/j.cej.2015.05.080.

[196] S.K. Singh, C. Sharma, A. Maiti, A comprehensive review of standalone and hybrid forward osmosis for water treatment: Membranes and recovery strategies of draw solutions, Journal of Environmental Chemical Engineering. 9 (2021) 105473. https://doi.org/https://doi.org/10.1016/j.jece.2021.105473.

[197] N.K. Rastogi, Opportunities and Challenges in Application of Forward Osmosis in Food Processing, Critical Reviews in Food Science and Nutrition. 56 (2016) 266–291. https://doi.org/10.1080/10408398.2012.724734.

[198] T. Cai, N. Jiang, G. Zhen, L. Meng, J. Song, G. Chen, Y. Liu, M. Huang, Simultaneous energy harvest and nitrogen removal using a supercapacitor microbial fuel cell, Environmental Pollution. 266 (2020) 115154.

TH-3195_186151006

https://doi.org/https://doi.org/10.1016/j.envpol.2020.115154.

[199] A.M. Dafalla, L. Wei, B.T. Habte, J. Guo, F. Jiang, Membrane Electrode Assembly Degradation Modeling of Proton Exchange Membrane Fuel Cells: A Review, Energies. 15 (2022). https://doi.org/10.3390/en15239247.

[200] G. Wei, Y. Wang, C. Huang, Q. Gao, Z. Wang, L. Xu, The stability of MEA in SPE water electrolysis for hydrogen production, International Journal of Hydrogen Energy. 35 (2010) 3951–3957. https://doi.org/https://doi.org/10.1016/j.ijhydene.2010.01.153.

[201] J.G. Hong, B. Zhang, S. Glabman, N. Uzal, X. Dou, H. Zhang, X. Wei, Y. Chen, Potential ion exchange membranes and system performance in reverse electrodialysis for power generation: A review, Journal of Membrane Science. 486 (2015) 71–88. https://doi.org/https://doi.org/10.1016/j.memsci.2015.02.039.

[202] B. Yang, J. Yu, T. Ma, A charge-free and membrane-free hybrid capacitive mixing system for salinity gradient energy harvesting, Journal of Materials Chemistry A. (2023). https://doi.org/10.1039/D2TA08213F.

[203] M. Sharma, P.P. Das, A. Chakraborty, M.K. Purkait, Clean energy from salinity gradients using pressure retarded osmosis and reverse electrodialysis: A review, Sustainable Energy Technologies and Assessments. 49 (2022) 101687. https://doi.org/https://doi.org/10.1016/j.seta.2021.101687.

[204] E. Güler, R. Elizen, D.A. Vermaas, M. Saakes, K. Nijmeijer, Performance-determining membrane properties in reverse electrodialysis, Journal of Membrane Science. 446 (2013) 266–276. https://doi.org/https://doi.org/10.1016/j.memsci.2013.06.045.

[205] R.K. Gogoi, A.B. Neog, T.J. Konch, N. Sarmah, K. Raidongia, A two-dimensional ion-pump of a vanadium pentoxide nanofluidic membrane, Journal of Materials Chemistry A. 7 (2019) 10552–10560. https://doi.org/10.1039/C8TA11233A.

[206] Z. Zhao, S. Ni, X. Su, Y. Gao, X. Sun, Thermally Reduced Graphene Oxide Membrane with Ultrahigh Rejection of Metal Ions' Separation from Water, ACS Sustainable Chemistry & Engineering. 7 (2019) 14874–14882. https://doi.org/10.1021/acssuschemeng.9b02972.

[207] C.J. Fontenot, J.W. Wiench, M. Pruski, G.L. Schrader, Vanadia Gel Synthesis via Peroxovanadate Precursors. 1. In Situ Laser Raman and 51V NMR Characterization of the Gelation Process, The Journal of Physical Chemistry B. 104 (2000) 11622–11631. https://doi.org/10.1021/jp0021897.

[208] J. Deka, K. Saha, R. Gogoi, G.K. Dutta, K. Raidongia, Fabrication of Pressure-Responsive Energy Device from Nanofluidic Vanadium Pentoxide and Polymeric Hydrogel, ACS Applied Electronic Materials. 3 (2021) 277–284. https://doi.org/10.1021/acsaelm.0c00849.

[209] W.S. Hummers, R.E. Offeman, Preparation of Graphitic Oxide, Journal of the American Chemical Society. 80 (1958) 1339. https://doi.org/10.1021/ja01539a017.

[210] H. Cheng, Y. Zhou, Y. Feng, W. Geng, Q. Liu, W. Guo, L. Jiang, Electrokinetic Energy Conversion in Self-Assembled 2D Nanofluidic Channels with Janus Nanobuilding Blocks, Advanced Materials. 29 (2017) 1700177.

TH-3195_186151006

https://doi.org/https://doi.org/10.1002/adma.201700177.

[211] M. Fantauzzi, B. Elsener, D. Atzei, A. Rigoldi, A. Rossi, Exploiting XPS for the identification of sulfides and polysulfides, RSC Advances. 5 (2015) 75953–75963. https://doi.org/10.1039/C5RA14915K.

[212] M. Marrone, T. Montanari, G. Busca, L. Conzatti, G. Costa, M. Castellano, A. Turturro, A Fourier Transform Infrared (FTIR) Study of the Reaction of Triethoxysilane (TES) and Bis[3-triethoxysilylpropyl]tetrasulfane (TESPT) with the Surface of Amorphous Silica, The Journal of Physical Chemistry B. 108 (2004) 3563–3572. https://doi.org/10.1021/jp036148x.

[213] Q. Tian, Y. Tang, T. Ding, X. Li, Z. Zhang, Effect of nano-silica surface-capped by bis[3-(triethoxysilyl)propyl] tetrasulfide on the mechanical properties of styrene-butadiene rubber/butadiene rubber nanocomposites, Composites Communications. 10 (2018) 190–193. https://doi.org/https://doi.org/10.1016/j.coco.2018.10.005.

[214] Y.-H. Xi, J.-Q. Hu, Z. Liu, R. Xie, X.-J. Ju, W. Wang, L.-Y. Chu, Graphene Oxide Membranes with Strong Stability in Aqueous Solutions and Controllable Lamellar Spacing, ACS Applied Materials & Interfaces. 8 (2016). https://doi.org/10.1021/acsami.6b00928.

[215] W.L. Zhang, H.J. Choi, Silica-Graphene Oxide Hybrid Composite Particles and Their Electroresponsive Characteristics, Langmuir. 28 (2012) 7055–7062. https://doi.org/10.1021/la3009283.

[216] B. Kim, G. Gwak, S. Hong, Review on methodology for determining forward osmosis (FO) membrane characteristics: Water permeability (A), solute permeability (B), and structural parameter (S), Desalination. 422 (2017) 5–16. https://doi.org/https://doi.org/10.1016/j.desal.2017.08.006.

[217] W. Wang, J. Hao, Q. Sun, M. Zhao, H. Liu, C. Li, X. Sui, Carbon nanofibers membrane bridged with graphene nanosheet and hyperbranched polymer for high-performance osmotic energy harvesting, Nano Research. 16 (2023) 1205–1211. https://doi.org/10.1007/s12274-022-4634-6.

[218] S. Zhou, L. Xie, L. Zhang, L. Wen, J. Tang, J. Zeng, T. Liu, D. Peng, M. Yan, B. Qiu, Q. Liang, K. Liang, L. Jiang, B. Kong, Interfacial Super-Assembly of Ordered Mesoporous Silica–Alumina Heterostructure Membranes with pH-Sensitive Properties for Osmotic Energy Harvesting, ACS Applied Materials & Interfaces. 13 (2021) 8782–8793. https://doi.org/10.1021/acsami.0c21661.

[219] N. Sheng, S. Chen, M. Zhang, Z. Wu, Q. Liang, P. Ji, H. Wang, TEMPO-Oxidized Bacterial Cellulose Nanofibers/Graphene Oxide Fibers for Osmotic Energy Conversion, ACS Applied Materials & Interfaces. 13 (2021) 22416–22425. https://doi.org/10.1021/acsami.1c03192.

[220] T.J. Konch, T. Dutta, A.B. Neog, R. Gogoi, K. Raidongia, Uphill Anion Pumping through Triangular Nanofluidic Device of Reconstructed Layered Double Hydroxide, The Journal of Physical Chemistry C. 125 (2021) 17939–17949. https://doi.org/10.1021/acs.jpcc.1c03118.

[221] R. Qin, J. Tang, C. Wu, Q. Zhang, T. Xiao, Z. Liu, Y. Jin, J. Liu, H. Wang, Nanofiber-

TH-3195_186151006

reinforced clay-based 2D nanofluidics for highly efficient osmotic energy harvesting, Nano Energy. 100 (2022) 107526. https://doi.org/https://doi.org/10.1016/j.nanoen.2022.107526.

[222] Z. Gao, J. Zhang, M. Ahmad, B. Jiang, Z. Sun, S. Wang, Y. Jin, Design of metallic phase WS2/cellulose nanofibers composite membranes for light-boosted osmotic energy conversion, Carbohydrate Polymers. 296 (2022) 119847. https://doi.org/https://doi.org/10.1016/j.carbpol.2022.119847.

[223] P. Liu, Y. Sun, C. Zhu, B. Niu, X. Huang, X.-Y. Kong, L. Jiang, L. Wen, Neutralization Reaction Assisted Chemical-Potential-Driven Ion Transport through Layered Titanium Carbides Membrane for Energy Harvesting, Nano Letters. 20 (2020) 3593–3601. https://doi.org/10.1021/acs.nanolett.0c00526.

[224] J. Gao, W. Guo, D. Feng, H. Wang, D. Zhao, L. Jiang, High-Performance Ionic Diode Membrane for Salinity Gradient Power Generation, Journal of the American Chemical Society. 136 (2014) 12265–12272. https://doi.org/10.1021/ja503692z.

[225] P. Jia, X. Du, R. Chen, J. Zhou, M. Agostini, J. Sun, L. Xiao, The Combination of 2D Layered Graphene Oxide and 3D Porous Cellulose Heterogeneous Membranes for Nanofluidic Osmotic Power Generation, Molecules. 26 (2021). https://doi.org/10.3390/molecules26175343.

[226] J. Feng, M. Graf, K. Liu, D. Ovchinnikov, D. Dumcenco, M. Heiranian, V. Nandigana, N.R. Aluru, A. Kis, A. Radenovic, Single-layer MoS2 nanopores as nanopower generators, Nature. 536 (2016) 197–200. https://doi.org/10.1038/nature18593.

[227] A. Bhinder, S. Shabani, M. Sadrzadeh, Effect of Internal and External Concentration Polarizations on the Performance of Forward Osmosis Process, in: 2018. https://doi.org/10.5772/intechopen.71343.

[228] J.-P. Hsu, T.-C. Su, P.-H. Peng, S.-C. Hsu, M.-J. Zheng, L.-H. Yeh, Unraveling the Anomalous Surface-Charge-Dependent Osmotic Power Using a Single Funnel-Shaped Nanochannel, ACS Nano. 13 (2019) 13374–13381. https://doi.org/10.1021/acsnano.9b06774.

[229] E.R.J. Nightingale, Phenomenological Theory of Ion Solvation. Effective Radii of Hydrated Ions, The Journal of Physical Chemistry. 63 (1959) 1381–1387. https://doi.org/10.1021/j150579a011.

[230] Y. Wang, H. Zhang, Y. Kang, Y. Zhu, G.P. Simon, H. Wang, Voltage-Gated Ion Transport in Two-Dimensional Sub-1 nm Nanofluidic Channels, ACS Nano. 13 (2019) 11793–11799. https://doi.org/10.1021/acsnano.9b05758.

[231] T.M. Mansour, T.M. Ismail, K. Ramzy, M. Abd El-Salam, Energy recovery system in small reverse osmosis desalination plant: Experimental and theoretical investigations, Alexandria Engineering Journal. 59 (2020) 3741–3753. https://doi.org/https://doi.org/10.1016/j.aej.2020.06.030.

[232] G.T. Gray, J.R. McCutcheon, M. Elimelech, Internal concentration polarization in forward osmosis: role of membrane orientation, Desalination. 197 (2006) 1–8. https://doi.org/https://doi.org/10.1016/j.desal.2006.02.003.

TH-3195_186151006

[233] D. Dsilva Winfred Rufuss, E. Hosseinipour, S. Arulvel, P.A. Davies, Complete parametric investigation of a forward osmosis process using sodium chloride draw solution, Desalination. 547 (2023) 116218. https://doi.org/https://doi.org/10.1016/j.desal.2022.116218.

[234] D. Bai, B. Kruczek, Effect of Membrane Orientation and Concentration of Draw Solution on the Behavior of Commercial Osmotic Membrane in a Novel Dynamic Forward Osmosis Tests, Membranes. 12 (2022). https://doi.org/10.3390/membranes12040385.

[235] Y.C. Kim, Y. Kim, D. Oh, K.H. Lee, Experimental Investigation of a Spiral-Wound Pressure-Retarded Osmosis Membrane Module for Osmotic Power Generation, Environmental Science & Technology. 47 (2013) 2966–2973. https://doi.org/10.1021/es304060d.

[236] P. Deka, V.K. Verma, A. Chandrasekaran, A.B. Neog, A. Bardhan, K. Raidongia, S. Subbiah, Performance of novel sericin doped reduced graphene oxide membrane for FO based membrane crystallization application, Journal of Membrane Science. 660 (2022) 120884. https://doi.org/https://doi.org/10.1016/j.memsci.2022.120884.

TH-3195_186151006

Appendix A1: Characterization of r-GO-S membrane after fouling test

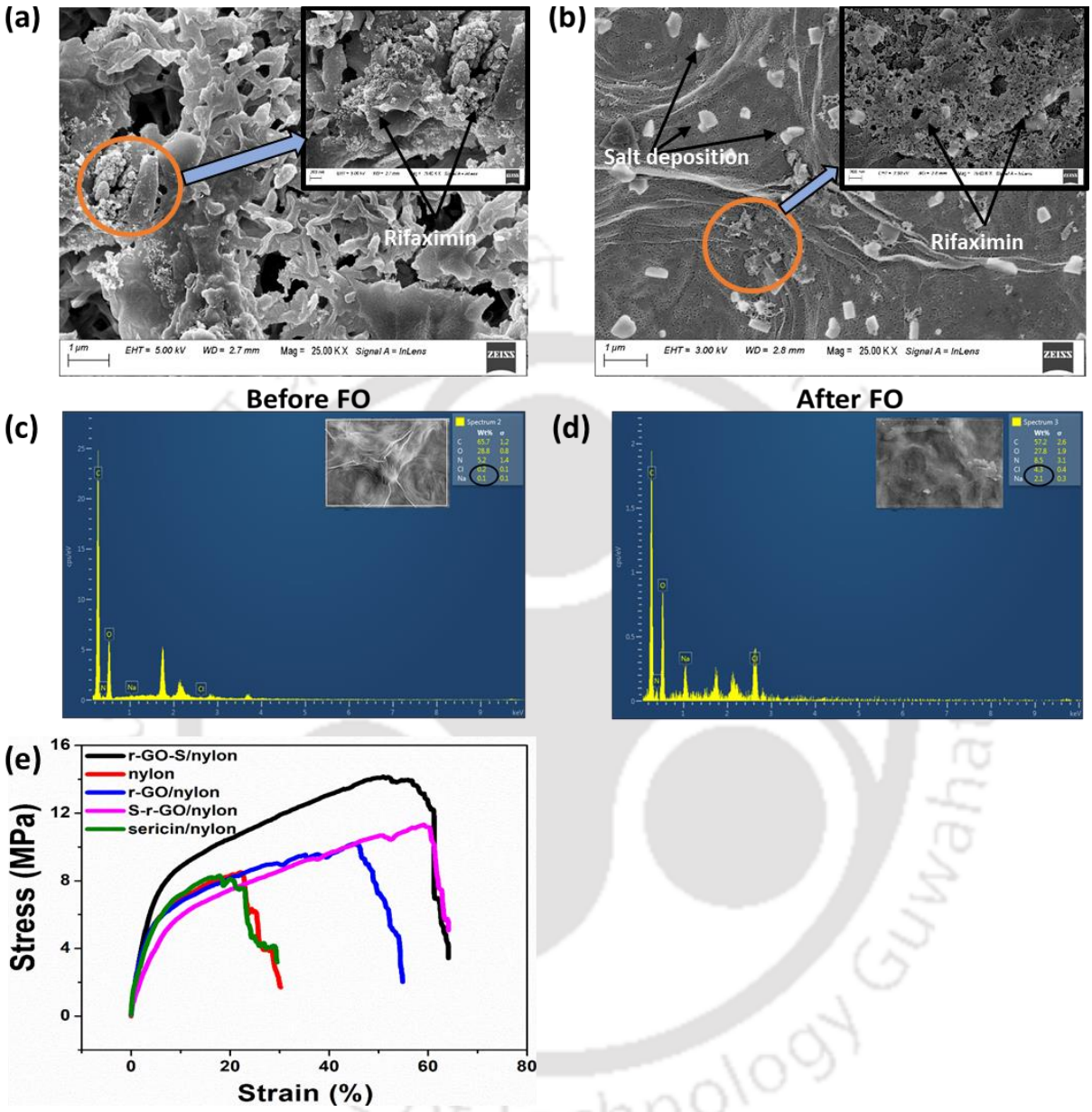

Fig. A1: (a) FESEM image of nylon support in ALDS mode (inset shows magnified image), (b) FESEM image of r-GO-S layer in ALFS mode (inset shows magnified image), (c) EDX spectra and mapping of r-GO-S membrane before and after FO process, (e) stress-strain curve of all the fabricated membranes

TH-3195_186151006

Appendix A2: Characterizations of Rifaximin crystals

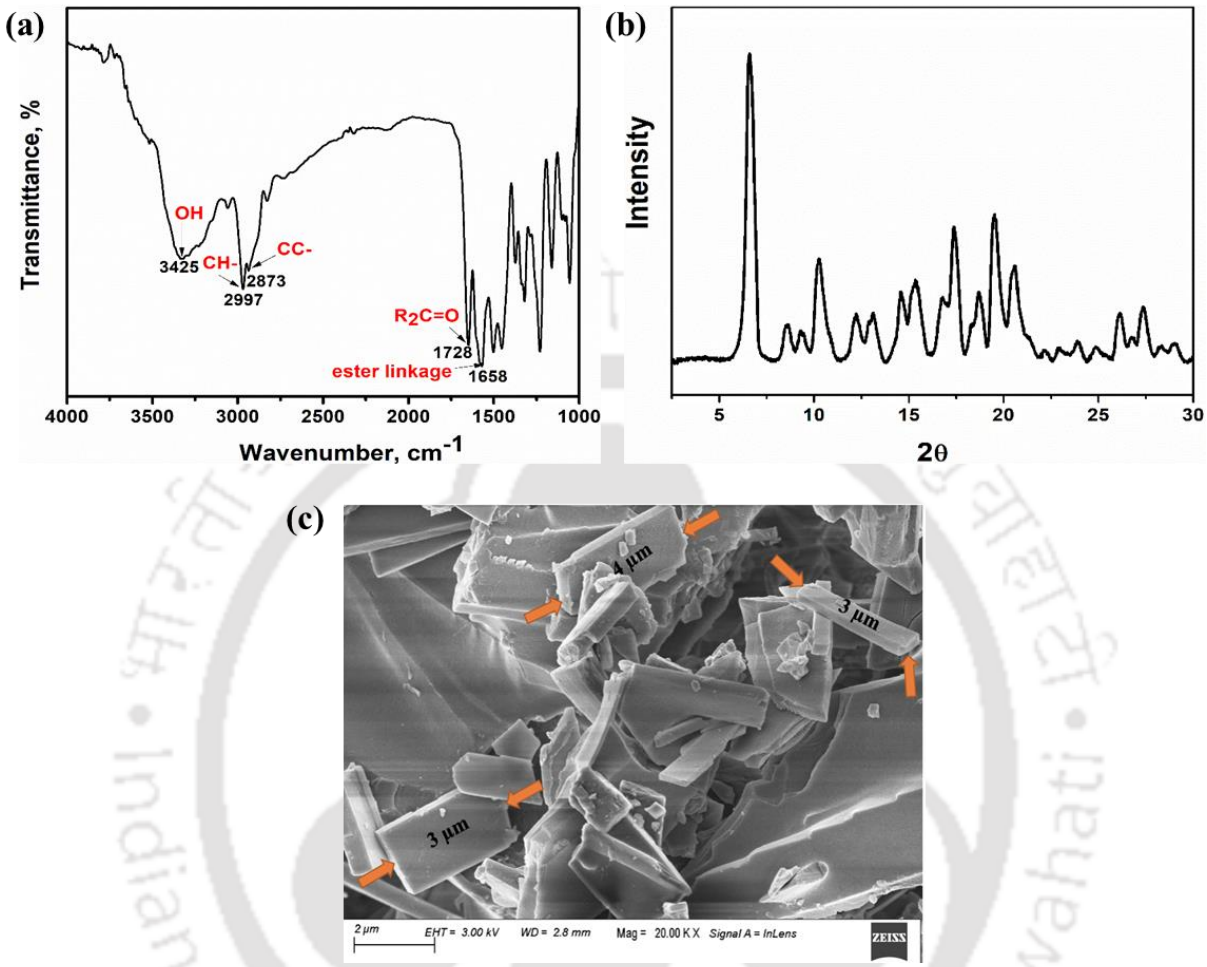

Fig. A2: (a) FTIR spectra of rifaximin crystals, (b) XRD peaks of rifaximin crystals, (c) FESEM image of rifaximin crystal

TH-3195_186151006

Appendix A3: Membrane stability performance data

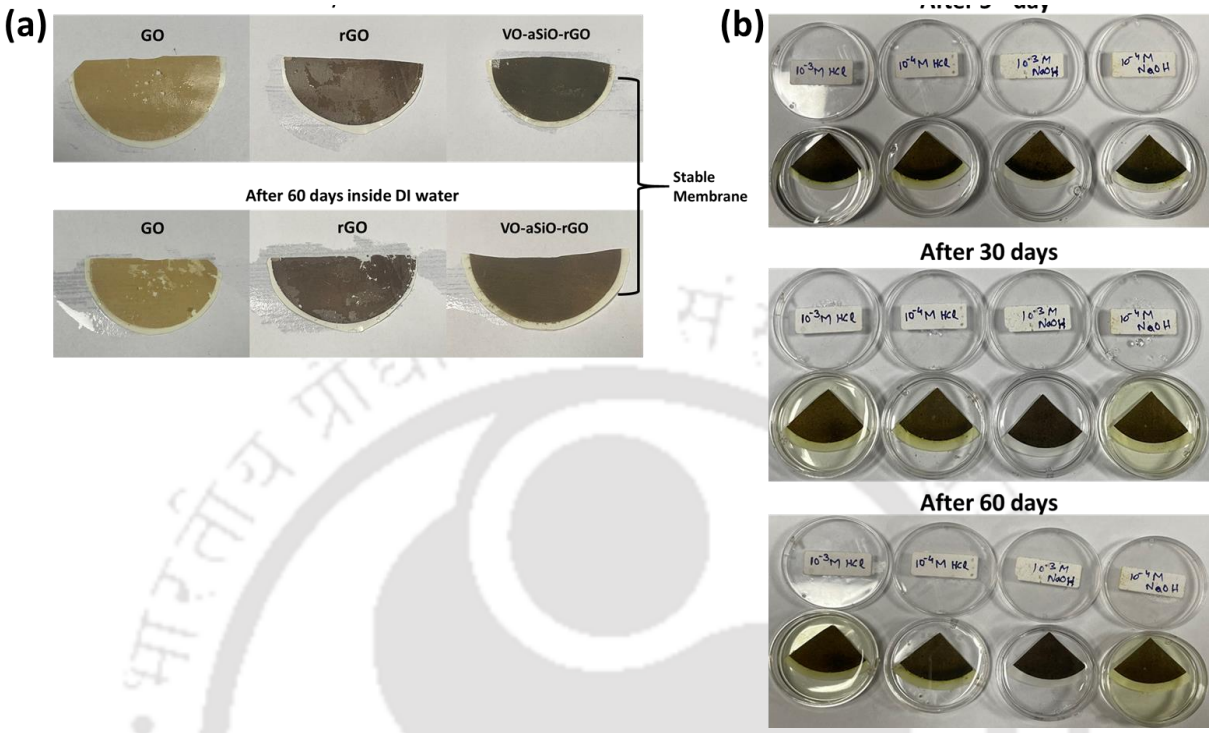

Fig. A3: Membrane stability test of VO-aSiO-rGO membrane in (a) DI water, (b) acidic and basic mediums for more than 60 days

TH-3195_186151006

List of publications during the PhD tenure

❖ ***Journals***

1. **P. Deka**, V.K. Verma, B. Yurembam, A.B. Neog, K. Raidongia, S. Subbiah, Performance evaluation of reduced graphene oxide membrane doped with polystyrene sulfonic acid for forward osmosis process, Sustainable Energy Technologies and Assessments. 44 (2021) 101093
2. A.B. Neog, R.K. Gogoi, **P. Deka**, T.J. Konch, B.R. Bora, K. Raidongia, Application of reduced graphene oxide-based actuators for real-time chemical sensing of liquid and vapour phase contaminants, New Journal of Chemistry. 45 (2021) 16883–16891.
3. **P. Deka**, V.K. Verma, A. Chandrasekaran, A.B. Neog, A. Bardhan, K. Raidongia, S. Subbiah, Performance of novel sericin doped reduced graphene oxide membrane for FO based membrane crystallization application, Journal of Membrane Science. 660 (2022) 120884
4. A. Khan, S. Yadav, I. Ibrar, R.A. Al Juboori, S.A. Razzak, **P. Deka**, S. Subbiah, S. Shah, Fouling and Performance Investigation of Membrane Distillation at Elevated Recoveries for Seawater Desalination and Wastewater Reclamation, Membranes. 12 (2022).
5. I. Ibrar, S. Yadav, A. Altaee, J. Safaei, A.K. Samal, S. Subbiah, G. Millar, **P. Deka**, J. Zhou, Sodium docusate as a cleaning agent for forward osmosis membranes fouled by landfill leachate wastewater, Chemosphere. 308 (2022) 136237.
6. A. Khan, I. Ibrar, A. Mirdad, R.A. Al-Juboori, **P. Deka**, S. Subbiah, A. Altaee, Novel Approach to Landfill Wastewater Treatment Fouling Mitigation: Air Gap Membrane Distillation with Tin Sulfide-Coated PTFE Membrane, Membranes. 13 (2023).

TH-3195_186151006

7. R. Gogoi, A. Ghosh, **P. Deka**, K.K.R. Datta, K. Raidongia, Application of lamellar nickel hydroxide membrane as a tunable platform for ionic thermoelectric studies, Materials Horizons. (2023).
8. **P. Deka**, S. Roy, T. Jyoti Konch, B. Rani Bora, R. Gogoi, A. Bikash Neog, K. Sundararajan, S. Subbiah, K. Raidongia, Recovering electrical energy from forward osmosis process through amorphous silicon oxide crosslinked vanadium pentoxide-reduced graphene oxide membrane, Chemical Engineering Journal. 469 (2023) 143964

❖ ***Patents filed***

1. **Priyamjeet Deka**, Vishal Kumar Verma, Senthilmurugan Subbiah, Kalyan Raidongia, Rakesh Kejriwal, *A Sericin doped graphene oxide membrane for forward osmosis and a process of preparation thereof* (Application No- 202031025232)
2. **Priyamjeet Deka**, Arunkumar Chandrasekaran, Nivedhitha Swaminathan, Neelam Dutta, Bharat Singh, Kalyan Raidongia, Senthilmurugan Subbiah, *A method for recovering antibiotics from pharmaceutical effluent by the combination of membrane technological systems* (Application No-202131015728)
3. Kalyan Raidongia, **Priyamjeet Deka**, Senthilmurugan Subbiah, Sonali Roy, *A hybrid multi-layered nanofluidic FO membrane and a method of preparation thereof* (Application No-202331038876)

TH-3195_186151006

❖ ***Conferences***

1. **Priyamjeet Deka**, Kalyan Raidongia, Senthilmurugan Subbiah, Performance of variable sized graphene oxide composite membranes in forward osmosis desalination- National conference on Recent Advances in Chemistry (RAC) - 2019, NIT Meghalaya
2. **Priyamjeet Deka**, Kalyan Raidongia, Senthilmurugan Subbiah, Performance of variable sized graphene oxide composite membranes in forward osmosis desalination- International conference on Emerging Trends in Chemical Science (ETCS) - 2020, Guwahati University
3. **Priyamjeet Deka**, Kalyan Raidongia, Senthilmurugan Subbiah, Performance of novel sericin doped reduced graphene oxide membrane for FO based membrane crystallization application- International conference on Recent Advances in Materials Chemistry and Catalysis (RAMCC-2023), Dibrugarh university

TH-3195_186151006